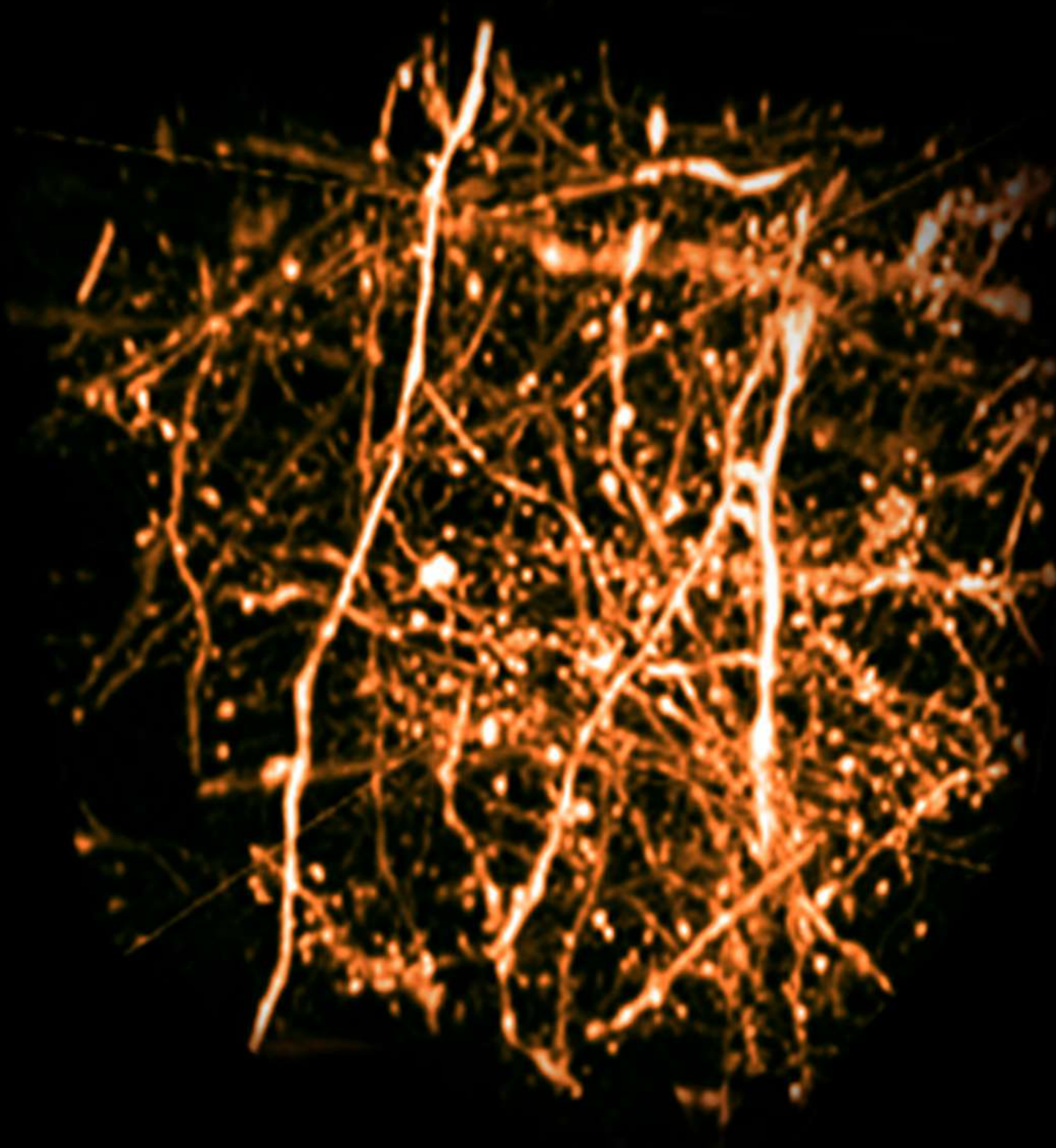


Reprint Compendium

Bio-protocol Selections | 2020 Neuroscience



Free access to more than 4000 high-quality protocols

- Contributed by 10,000+ scientists
- Each validated in at least one primary publication
- >91% reproducibility (2018 survey of Bio-protocol users)
- ~1000 videos of key procedural steps

Foreword

We are pleased to launch Bio-protocol first series of reprint collections, which consist of most widely used protocols published in 2018 and 2019, and reprint them as “Protocol Selections” highlighting a given research area or application. In this series, it is Protocol Selections focusing on neuroscience.

Established in 2011 by a group of Stanford scientists, Bio-protocol’s mission is to improve research reproducibility and usability through the publication of high quality step-by-step peer-reviewed life science protocols. One primary method for Bio-protocol to publish this content is to invite contributions from authors that have published methods in brief that are used in results-oriented literature (called “Original research article” in the Protocol Selections) but not described in sufficient detail for others to replicate. Our survey carried out in 2018 showed that over 91% of users (2166 users) who tried their downloaded bio-protocols were able to successfully reproduce the experiment. This users’ feedback indicates that indeed most of bio-protocols (if not all) are highly reproducible.

In this reprint collection, we have selected 16 of the most-used neuroscience protocols based on published dates (published in last 2 years) as well as some metrics such as view number, download number and citations. We have to admit that the measurement of the “most-used” protocols is not absolutely accurate, in particular, given the fact that it would take time to cite a relatively new published protocol. That said, we believe this Protocol Selections well represents a collection of high-quality protocols contributed by outstanding researchers in the community.

Hopefully, you will find this collection intriguing and visit www.bio-protocol.org to check out the entire collection of protocols. Please feel free to email us (eb@bio-protocol.org) your feedback. Also, look forward to your contribution of protocols to Bio-protocol in the future.

The Bio-protocol Editorial Team

Original research article: *J Cell Biol.* 197 (1): 45–57.

**The RiboPuromycylation Method (RPM):
an Immunofluorescence Technique to
Map Translation Sites at the Sub-cellular
Level**

6

Amandine Bastide, Jonathan W. Yewdell
and Alexandre David

Original research article: *Nat Neurosci.* 20(8):1085–95

**Assaying Mechanonociceptive Behavior
in *Drosophila* Larvae**

35

Nina Hoyer, Meike Petersen, Federico
Tenedini and Peter Soba

Original research article: *Nat Neurosci.* 20(8):1122–32

**Spared Nerve Injury Model of
Neuropathic Pain in Mice**

59

Joseph Cichon, Linlin Sun and Guang
Yang

Original research article: *eLife* 6:e29378

**Magnetic Resonance Imaging and
Histopathological Visualization of Human
Dural Lymphatic Vessels**

84

Seung-Kwon Ha, Govind Nair, Martina
Absinta, Nicholas J. Luciano and Daniel S.
Reich

Original research article: *J Neurosci.* 38(2):484–97

**Measurement of Dopamine Using Fast
Scan Cyclic Voltammetry in Rodent
Brain Slices**

120

Madelyn I. Mauterer, Paige M. Estave,
Katherine M. Holleran and Sara R. Jones

Original research article: *Neuron.* 94(4):840–54

23

Obtaining Acute Brain Slices

Thomas Papouin and Philip G. Haydon

Original research article: *J Neurosci.* 35(46):15326–38

48

**Barnes Maze Procedure for Spatial
Learning and Memory in Mice**

Matthew W. Pitts

Original research article: *eLife* 6:e21629

66

**Measuring Spatiotemporal Dynamics of
Odor Gradient for Small Animals by Gas
Chromatography**

Akiko Yamazoe-Umemoto, Yuishi Iwasaki
and Koutarou D. Kimura

Original research article: *Cell Rep.* 8(6):1870–8

97

**Preparation of Cerebellum Granule
Neurons from Mouse or Rat Pups and
Evaluation of Clostridial Neurotoxin
Activity and Their Inhibitors by Western
Blot and Immunohistochemistry**

Domenico Azarnia Tehran and Marco
Pirazzini

<i>Original research article:</i> Cell Rep. 14(11):2718-32	144	Optical Clearing and Index Matching of Tissue Samples for High-resolution Fluorescence Imaging Using SeeDB2	<i>Original research article:</i> eLife 6:e21629	157	Estimation of the Readily Releasable Synaptic Vesicle Pool at the Drosophila Larval Neuromuscular Junction
Meng-Tsen Ke and Takeshi Imai			Pragya Goel, Xiling Li and Dion Dickman		
<i>Original research article:</i> Neurosci Lett. 682:1-9	172	Analysis of the Mitochondrial Membrane Potential Using the Cationic JC-1 Dye as a Sensitive Fluorescent Probe	<i>Original research article:</i> J Neurosci. 38(25):5807-25	185	A Mouse Model of Postoperative Pain
Farzane Sivandzade, Aditya Bhalerao and Luca Cucullo			Ashley M. Cowie and Cheryl L. Stucky		
<i>Original research article:</i> Nat Commun. 9(1):4724	196	Protocol to Quantitatively Assess the Structural Integrity of Perineuronal Nets <i>ex vivo</i>	<i>Original research article:</i> Nat Commun. 9(1):5211	208	Construction of Viral Vectors for Cell Type-specific CRISPR Gene Editing in the Adult Mouse Brain
Bhanu P. Tewari and Harald Sontheimer			Hiroshi Yamaguchi and Luis de Lecea		
<i>Original research article:</i> Development. 146(3):dev172106	219	Explant Culture of the Embryonic Mouse Spinal Cord and Gene Transfer by <i>ex vivo</i> Electroporation			
Mariko Kinoshita-Kawada, Hiroshi Hasegawa, Tsunaki Hongu, Shigeru Yanagi, Yasunori Kanaho, Ichiro Masai, Takayasu Mishima, Xiaoping Chen, Yoshio Tsuboi, Yi Rao, Junichi Yuasa-Kawada and Jane Y. Wu					

On the Cover:



Image from protocol "Optical Clearing and Index Matching of Tissue Samples for High-resolution Fluorescence Imaging Using SeeDB2"

Authors

China					
Yi Rao	Peking University	Junichi Yuasa-Kawada		Jane Y. Wu	Northwestern University Feinberg School of Medicine
		Mariko Kinoshita-Kawada	Fukuoka University	Xiaoping Chen	
		Takayasu Mishima		Hiroshi Yamaguchi	Stanford University
		Yoshio Tsuboi		Luis de Lecea	
Jonathan W. Yewdell	National Institute of Allergy and Infectious Diseases	Ichiro Masai	Okinawa Institute of Science and Technology Graduate University	Aditya Bhalerao	Texas Tech University Health Sciences Center
Thomas Papouin	Tufts University School of Medicine	Meng-Tsen Ke	RIKEN Center for Developmental Biology	Farzane Sivandzade	
		Takeshi Imai		Luca Cucullo	
		Shigeru Yanagi	Tokyo University of Pharmacy and Life Sciences	Philip G. Haydon	Tufts University School of Medicine
Federico Tenedini	University Medical Campus Hamburg-Eppendorf	Hiroshi Hasegawa	University of Tsukuba	Thomas Papouin	
Meike Petersen		Tsunaki Hongu		Matthew W. Pitts	University of Hawaii
Nina Hoyer		Yasunori Kanaho		Joseph Cichon	University of Pennsylvania
Peter Soba				Dion Dickman	University of Southern California
				Pragya Goel	
Domenico Azarnia	University of Padova	Daniel S. Reich	National Institute of Neurological Disorders and Stroke (NINDS)	Xiling Li	
Tehran		Govind Nair		Katherine M. Holleran	Winston Salem North Carolina
Marco Pirazzini		Martina Absinta		Madelyn I. Mauterer	
		Nicholas J. Luciano		Paige M. Estave	
		Seung-Kwon Ha		Sara R. Jones	
		Guang Yang	New York University		
Akiko Yamazoe-Umemoto	Osaka University	Marco Pirazzini			
Koutarou D. Kimura					
Yuishi Iwasaki	Ibaraki University				

Editors

Alessandro Didonna	<i>University of California, San Francisco, USA</i>	Andrea Puhar	<i>Umea University, Sweden</i>	Arnaud Busquets-Garcia	<i>French Institute of Health and Medical Research, France</i>
Giusy Tornillo	<i>Cardiff University, UK</i>	Neelanjan Bose	<i>Emery Pharma, USA</i>	Oneil Girish Bhalala	<i>Baker Institute, Australia</i>
Pengpeng Li	<i>Boston Children's Hospital, USA</i>	Soyun Kim	<i>University of California, Irvine, USA</i>	Xiaoyi Zheng	<i>Stanford University, USA</i>
Zinan Zhou	<i>Boston Children's Hospital, USA</i>				

Reviewers

Arnaud Busquets-Garcia	<i>French Institute of Health and Medical Research, France</i>	Carola Staedele	<i>University of California, Los Angeles, USA</i>	Deanna Benson	<i>Icahn School of Medicine at Mount Sinai, USA</i>
Di Wang	<i>Jilin University, China</i>	Emma Puighermanal	<i>Weill Cornell Medical College, USA</i>	Fan-Yan Wei	<i>Tohoku University, Japan</i>
Fereshteh Azedi	<i>Iran University of Medical Sciences, Iran</i>	Gary Liu	<i>Baylor College of Medicine, USA</i>	Geoffrey C. Y. Lau	<i>City University of Hong Kong, China</i>
Jackeline Moraes Malheiros	<i>Universidade Federal de São Paulo, Brazil</i>	Jay Z Parrish	<i>University of Washington, USA</i>	Jeremy Ferrier	<i>Iconeus, France</i>
Jerneja Stare	<i>University of Windsor, Canada</i>	Jingli Cao	<i>Duke University, USA</i>	José M. Dias	<i>Karolinska Institutet, USA</i>
Joshua Brumberg	<i>City University of New York, USA</i>	Junjie Luo	<i>Tsinghua University, China</i>	Karthik Krishnamurthy	<i>Thomas Jefferson University, USA</i>
Manuel Lopez	<i>Stanford University, USA</i>	Marc-Antoine Sani	<i>University of Melbourne, Australia</i>	Marta Miquel	<i>Universitat Jaume I, Spain</i>
Qiuyu Martin Zhu	<i>Broad Institute, USA</i>	Ross Wilson	<i>University of California, Berkeley, USA</i>	Sabine Pellett	<i>University of Wisconsin, USA</i>
Salome Botelho	<i>Stanford University, USA</i>	Sanjib Guha	<i>Buck Institute for Research on Aging, USA</i>	Shaarika Sarasija	<i>Albany Medical College, USA</i>
Valeria B Fernandez Vallone	<i>Charité - Universitätsmedizin Berlin, Germany</i>	Xiaoliang Zhao	<i>Max Planck Florida Institute for Neuroscience, USA</i>	Xuecai Ge	<i>University of California, Merced, USA</i>

The RiboPuromycylation Method (RPM): an Immunofluorescence Technique to Map Translation Sites at the Sub-cellular Level

Amandine Bastide¹, Jonathan W. Yewdell² and Alexandre David^{1,*}

¹IGF, CNRS, INSERM, Univ. Montpellier, F-34094 Montpellier, France; ²Laboratory of Viral Diseases, National Institute of Allergy and Infectious Diseases, Bethesda, USA

*For correspondence: adavid@igf.cnrs.fr



[Abstract] While isotopic labeling of amino acids remains the reference method in the field for quantifying translation rate, it does not provide any information on spatial localization of translation sites. The rationale behind developing the ribopuromycylation method (RPM) was primarily to map translation sites at the sub-cellular level while avoiding detection of newly synthesized proteins released from ribosomes. RPM visualizes actively translating ribosomes in cells via standard immunofluorescence microscopy in fixed and permeabilized cells using a puromycin-specific monoclonal antibody to detect puromycylated nascent chains trapped on ribosomes treated with a chain elongation inhibitor.

Keywords: Translation site, Puromycin, Ribopuromycylation, Ribosome, Nascent chain

[Background] For decades, isotopic labeling of amino acids has been considered as the gold standard for studying protein translation. Though this method has proven to be remarkably accurate for evaluating translation rates, it provides no information on the location of translating ribosomes. More recently, amino acids analogs have enabled fluorescent detection nascent chains (Dieterich *et al.*, 2007). Nevertheless, nearly all of the detected signal comes from polypeptides released from ribosome. Our initial idea was to develop a method to label nascent chains while still tethered to translating ribosomes.

Puromycin (PMY) is an aminoglycoside antibiotic that mimics charged tRNA^{Tyr} and incorporates into the ribosome A site. Consequently, PMY triggers premature translation termination by ribosome catalyzed-covalent incorporation into the nascent chain COOH-terminus (Pestka, 1971) followed by release of PMY-peptide. Polyclonal antibodies (Abs) to PMY were initially generated (Eggers *et al.*, 1997) to detect puromycylated nascent chains released from ribosomes by immunoblotting and immunoprecipitation. Subsequently, fluorescent PMY was used to label nascent chains by microscopy (Starck *et al.*, 2004). Schmidt *et al.* (2009) found that cells exposed to PMY generate a sufficient amount of PMY-terminated cell surface proteins to enable detection by live cell flow cytometry using a monoclonal Ab (mAb), providing a measure of translation rates. Importantly, none of these methods discriminate between ribosome-attached or released PMY-peptides and are all hindered to some extent as measures of translation by degradation of released proteins.

Having found that chain elongation inhibitors, such as cycloheximide (CHX) or emetine, prevent the release of PMY-nascent chain from ribosomes, we developed the ribopuromycylation method (RPM)

that enables immunofluorescent detection of translation sites at the sub-cellular level (Figure 1) (David *et al.*, 2011 and 2012b). This method has been used by our labs and many other labs to study translation in neurons (Biever *et al.*, 2015; Perry *et al.*, 2016; Williams *et al.*, 2016), migrating cells (Willett *et al.*, 2011), immune cells (Seedhom *et al.*, 2016) and stressed or infected cells (Kedersha *et al.*, 2016; Emmott *et al.*, 2017; Roth *et al.*, 2017).

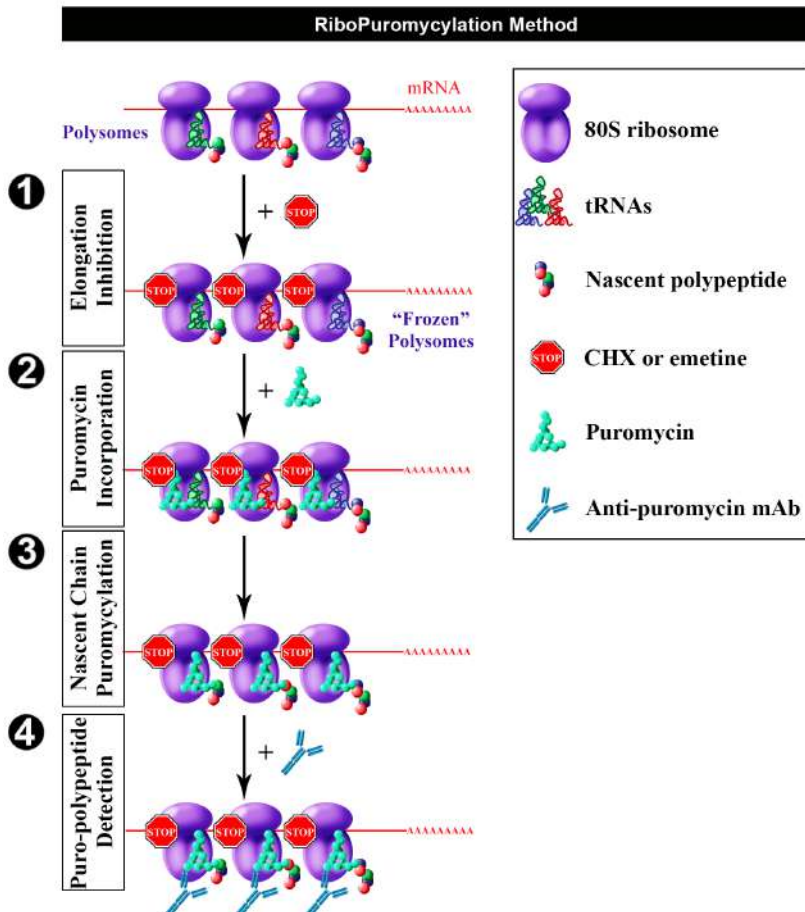


Figure 1. Schematic representation of RPM (from David *et al.*, 2012b). Following freezing of polysome with an elongation inhibitor (step 1), PMY is added (step 2) to living cells and nascent chains become puromycylated through ribosome catalysis (step 3). Anti-PMY monoclonal antibodies detect puromycylated nascent chains via indirect immunofluorescence (step 4). Reproduced from David *et al.* (2012b) with permission of the publisher and of Dr. Yewdell.

Materials and Reagents

1. Materials
 - a. 6-well and 24-well plates (Corning, Costar®, catalog numbers: 3506, 3524)
 - b. High quality glass coverslips, 12 mm diameter, #1 thickness (Glaswarenfabrik Karl Hecht, Assistent, catalog number: 1001/12)

Note: Either autoclave or sterilize with 70% ethanol before use.

- c. Microscope slides (Thermo Fisher Scientific, Thermo Scientific™, catalog number: J1800AMNZ)
- d. Whatman paper (GE Healthcare, catalog number: 3030-917)
- e. Parafilm (Bemis, catalog number: 701606)
- f. Petri dishes (Corning, catalog number: 430591)
- g. Aluminum foil (Sigma-Aldrich, catalog number: Z691569)
Manufacturer: Heathrow Scientific, catalog number: HD23534A.
- h. Plastic tips

2. Cell line(s)

The described procedure and associated figure (Figure 2) uses HeLa cells (ATCC, catalog number: CCL-2.1)

Note: Though this procedure was originally designed for HeLa cells, it can be easily adapted for other adherent cell lines (Graber et al., 2013). However, controls with several inhibitors are needed to validate any adjustment (e.g., Digitonin concentration) of any kind. For non-adherent cells, we describe an alternate protocol (Procedure D).

3. Reagents

- a. Alcian blue (Sigma-Aldrich, catalog number: A5268)
- b. 70% ethanol (Thermo Fisher Scientific, Thermo Scientific™, catalog number: R40135)
- c. Hoechst 33258 (Thermo Fisher Scientific, Invitrogen™, catalog number: H1398)
- d. Fluoromount-G (SouthernBiotech, catalog number: 0100-01)
- e. Potassium phosphate monobasic (KH_2PO_4)
- f. Sodium chloride (NaCl)
- g. $\text{Na}_2\text{HPO}_4 \cdot 7\text{H}_2\text{O}$
- h. Dulbecco's modified Eagle medium (DMEM) (Thermo Fisher Scientific, Gibco™, catalog number: 41966029)
- i. Glutamine (Thermo Fisher Scientific, Gibco™, catalog number: 25030081)
- j. Penicillin/streptomycin (Thermo Fisher Scientific, Gibco™, catalog number: 10378016)
- k. Fetal bovine serum (FBS) (Eurobio, catalog number: CVFSVF0101)
- l. Digitonin (Wako Pure Chemical Industries, catalog number: 043-21376)
- m. Tris-HCl pH 7.5 (Thermo Fisher Scientific, Invitrogen™, catalog number: 15567027)
- n. Magnesium chloride hexahydrate ($\text{MgCl}_2 \cdot 6\text{H}_2\text{O}$) (Sigma-Aldrich, catalog number: M0250)
- o. Potassium chloride (KCl) (Sigma-Aldrich, catalog number: P9541)
- p. Complete Mini EDTA-free protease inhibitor tablets (Sigma-Aldrich, Roche Diagnostics, catalog number: 11836170001)
- q. RNase Out (Life Technologies, catalog number: 100000840; or Thermo Fisher Scientific, Invitrogen™, catalog number: 10777019)
- r. DEPC treated water (Thermo Fisher Scientific, Invitrogen™, catalog number: 750023)
- s. 16% paraformaldehyde (PFA) (Electron Microscopy Sciences, catalog number: 15710)

- t. Sucrose (Sigma-Aldrich, catalog number: 84097)
 - u. Saponin (Sigma-Aldrich, catalog number: 84510)
 - v. Glycine (Sigma-Aldrich, catalog number: G7126)
4. Protein synthesis inhibitors (see Table 1)
- a. Anisomycin (Sigma-Aldrich, catalog number: A9789)
 - b. Cycloheximide (CHX) (Sigma-Aldrich, catalog number: C7698)
 - c. Emetine dihydrochloride (Sigma-Aldrich, catalog number: E2375)
 - d. Harringtonine (Santa Cruz Biotechnology, catalog number: sc-204771)
 - e. Puromycin (PMY) (Sigma-Aldrich, catalog number: P7255)
 - f. Sodium arsenite (NaAsO_2) (Sigma-Aldrich, catalog number: S7400)
5. Antibodies
- a. Primary antibodies
 - i. Anti-PMY mouse monoclonal antibodies: We tested 3 mouse mAbs from different hybridoma clones 12D10, 2A4, 5B12. Clone 12D10 was generated by the Pierre laboratory (Schmidt *et al.*, 2009), and is commercially available (Merck, catalog number: MABE343). We generated 2A4 and 5B12. 2A4 cells and supernatant are freely available to the scientific community from the Developmental Studies Hybridoma Bank <http://dshb.biology.uiowa.edu/PMY-2A4>
 - ii. Anti-ribosomal P antibody: human polyclonal autoimmune antiserum (from lupus patients) which recognizes three proteins of the 60S ribosomal subunit, RPLP0, P1 and P2 (Immunovision, catalog number: HPO-0100)
 - iii. Anti-lysyl-tRNA synthetase (KRS) antibody: rabbit polyclonal serum which recognizes KRS enzyme (Abcam, catalog number: ab31532)
 - b. Secondary antibodies
 - i. Donkey anti-mouse Alexa Fluor 488 (Jackson ImmunoResearch, catalog number: 715-545-150)
 - ii. Donkey anti-rabbit Alexa Fluor 594 (Jackson ImmunoResearch, catalog number: 711-585-152)
 - iii. Donkey anti-human Cy5 (Jackson ImmunoResearch, catalog number: 709-175-149)
6. Solutions (see Recipes)
- a. Anisomycin stock solution (1,000x)
 - b. Cycloheximide (CHX) stock solution (1,000x)
 - c. Emetine dihydrochloride stock solution (1,000x)
 - d. Harringtonine stock solution (1,000x)
 - e. PMY stock solution (1,000x)
 - f. Sodium arsenite stock solution (1,000x)
 - g. Phosphate buffered saline (PBS)
 - h. Growth medium
 - i. Labeling medium

- j. Labeling control medium
- k. Extraction buffer
- l. Wash buffer
- m. 3% PFA
- n. Co-extraction/fixation buffer
- o. Staining buffer (SB)

Equipment

- 1. Ice bucket
 - 2. 37 °C water bath (JULABO, model: TW20)
 - 3. Class II laminar flow hood (FASTER, model: SafeFAST Elite)
 - 4. Microscopy ultrafine tweezers (Electron Microscopy Sciences, catalog number: 78522-7)
 - 5. PIPETMAN 1-20 µl (Sartorius, model: Proline® Plus, catalog number: 728030)
 - 6. PIPETMAN 20-200 µl (Sartorius, model: Proline® Plus, catalog number: 728060)
 - 7. PIPETMAN 100-1,000 µl (Sartorius, model: Proline® Plus, catalog number: 728070)
 - 8. Slide tray (Glaswarenfabrik Karl Hecht, Assistent, catalog number: 2700/10)
 - 9. Cell Incubator (Heraeus, model: HERACell)
 - 10. Centrifuge (Eppendorf, model: 5415 R)
 - 11. Microwave
 - 12. Microscopy
- Laser scanning confocal microscope: Leica TCS SP5 (Leica Microsystems, model: Leica TCS SP5) with an HCX PL APO lambda blue 63.0x 1.40 oil UV objective. We used type FF immersion liquid (Cargille-Sacher Laboratories, catalog number: 16212)
- Note: Other comparable systems may be used.*

Software

- 1. LAS AF V2.3.1 software (Leica)
- 2. Imaris (Bitplane) and Huygens Essential Software for image deconvolution using the classical maximum likelihood estimation algorithm (V3.6, Scientific Volume Imaging BV, Hilversum, The Netherlands)
- 3. ImageJ (NIH) <https://imagej.net/Downloads>

Procedure

In the following protocol, we have included controls needed to ensure the specificity of both labeling and staining steps: 3 ‘translation inhibitor controls’ and 1 ‘no PMY’ control. Furthermore, we describe a quadruple staining protocol that permits simultaneous visualization of nuclear translation sites (PMY),

large subunit ribosomal proteins (RPLP0, RPLP1, RPLP2), a component of the multi-synthetase complex (lysyl-tRNA synthetase, KRS) and DNA (Hoechst 33258).

As emphasized in ‘Materials and Regents #3 Solutions’, either emetine or CHX can be used as elongation inhibitors to ‘trap’ PMY in translating ribosomes. **However, emetine has proven to be more efficient for PMY labeling than CHX (David et al., 2012a). Furthermore, being irreversible, emetine, unlike CHX does not have to be maintained in all solutions throughout the procedure.**

Two RPM methods have been developed: the original procedure (Procedure A) and a co-fixation/extraction procedure (Procedure B), easier and more adapted for non-adherent and primary cell cultures. Furthermore, labeling non-adherent cells necessitates an additional step (Procedure C).

A. Procedure A (Original RPM protocol)

Day 1

1. Pre-warm growth medium (see Recipes) in 37 °C water bath. In a cell culture hood, distribute 4 ml of warm growth medium per well in 5 wells of a 6-well plate. In each well, carefully place up to five non-overlapping coverslips using sterile forceps.

Notes:

- a. **Backup plan.** Coverslips are easily broken and ‘accidents’ frequently happen. Moreover, it’s always interesting to perform RPM with multiple Abs. For these reasons, we usually work with 4 coverslips per well.
 - b. **High quality forceps** with extremely sharp tips are recommended to enable easy removal of the coverslips from wells. Practice is required to develop the knack of picking them up from 24-well plates without breaking them.
 - c. **Avoid coverslip overlapping.** In order to be certain that coverslips will not move around in the well and overlap each other: (1) always add the medium first; (2) gently press down the coverslips down to remove any air bubbles between coverslip and the bottom of the well, gently slide the coverslips in order to create an adhesive force.
2. Transfer 1 ml of growth medium containing 0.5×10^6 HeLa cells per ml in each well. Softly shake the plates to distribute cells uniformly in the wells. Incubate for 24 h to allow HeLa cells to attach tightly to the coverslips and spread. Immunofluorescent resolution is maximized when visualizing well spread cells.

Day 2

3. Examine cells using an inverted microscope to ensure they have reached 70%-90% confluence. Several solutions must be prepared, at distinct temperatures.

Warm to 37 °C:

- a. 10 ml of growth medium.
- b. 4 ml of freshly prepared labeling medium (prepared extemporaneously, see Recipes).
- c. 1 ml of labeling control medium (prepared extemporaneously, see Recipes).

Chill on ice:

- a. 40 ml of PBS buffer (see Recipes).

b. 5 ml of extraction buffer (freshly made, see Recipes).

c. 5 ml of wash buffer (freshly made, see Recipes).

Prepare 5 ml of 3% PFA (see Recipes) and maintain at RT.

4. **Optional step:** Ensuring the specificity of PMY labeling necessitates pre-incubation with several translation inhibitors (see Table 1). This step is mandatory when working with new cell lines. The described protocol is designed to accommodate 3 ‘translation inhibitor controls’, preventing PMY labeling in different ways. Dilute each inhibitor in 2 ml of pre-warmed **growth media**. Assign a well for each: aspirate the media and replace it with media containing the corresponding inhibitor. Incubation times vary depending on the nature of the antibiotic and are indicated in Table 1.

Note: Necessary controls. When performing RPM procedure for the first time (or with a new cell line), we recommend using at least 3 control conditions:

- a. *Without ‘active ribosome’, using a translation initiation inhibitor (such as Harringtonine) that results in ribosome run off of mRNA, maximally releasing nascent chains.*
- b. *Without ‘ribosome catalyzed PMY incorporation’, i.e., no PMY.*
- c. *Using a PMY competitor, such as anisomycin, and in the ‘absence of antigen’, i.e., without PMY labeling.*

Table 1. Protein synthesis inhibitors

Translation Inhibitor	Treatment	Reversibility	Mechanism of Action	Effect on Ribosome	Reference
PMY	50 µg/ml 5 min	Reversible	Tyr-tRNA-mimetic enter A-site and associate covalently with nascent chain	Blocks elongation step of translation by inducing premature termination	(Pestka, 1971)
Cycloheximide	100 µg/ml 5 min	Reversible	Binds 60S ribosome subunit	Freezes translation during elongation; stabilizes polysomes	(Pestka, 1971)
Emetine	25 µg/ml 5 min	Irreversible	Binds 40S ribosome subunit	Freezes translation during elongation; stabilizes polysomes	(Jimenez et al., 1977)
Anisomycin	10 µg/ml 15 min	Reversible	Binds A-site, 60S ribosome subunit competes with PMY	Blocks peptidyl-transferase activity; stabilizes polysomes	(Hansen et al., 2003)
Sodium arsenite	65 µg/ml 15 min	Reversible	Oxidative stressor induces eIF2a phosphorylation	Induces stress granule, inhibits polysome formation	(Kedersha et al., 2002)
Harringtonine	2 µg/ml 15 min	Partially Reversible	Prevent peptide bond formation at the initiation complex	Blocks initiation step of translation, inhibits polysome formation	(Fresno et al., 1977)

5. Aspirate media in each well and replace with 900 µl of pre-warmed **labeling medium** (test well + 3 'inhibitor controls' wells) or **labeling control** (in the last well). Incubate for 5 min at 37 °C.

Note: *Co-incubation with PMY and elongation inhibitor.* Because emetine freezes translation instantly, it can be added simultaneously with PMY.

Reversibility. Anisomycin, being a reversible competitor of PMY, we recommend adding anisomycin in the corresponding well during the PMY labeling incubation (to maintain a constant anisomycin concentration).

6. Place the 6-well plate on ice, aspirate the medium and wash with 5 ml of ice-cold PBS.
 7. Aspirate PBS and add 1 ml of ice-cold **extraction buffer** in each well. Incubate for 2 min on ice.

Note: **Be careful with pipetting.** It's crucial from this step to slowly add buffer down the side of the well and avoid detaching the cells.

8. Aspirate **extraction buffer** and extremely gently add 900 µl of ice-cold **wash buffer**.
9. Aspirate gently on the side and extremely gently add 900 µl of freshly made 3% PFA. Incubate for 15 min at RT. Then, replace the fixing solution with 2 ml of ice-cold PBS. Check the wells using an inverted microscope to make sure that cells are still attached.

Note: **Storage prior to staining.** Following PFA fixation, cells may be kept for at least 7 days at 4 °C (in PBS) without noticeably affecting the quality of the RPM staining. Likewise, stained coverslips can be stored for long periods (years, even decades) at -20 °C and retrieved.

10. Proceed to 'immunostaining procedure' (Procedure D).

B. Procedure B (co-extraction/fixation procedure)

1. Follow Steps 1-6 of the 'original RPM procedure' (Procedure A).
2. Aspirate PBS and add 1 ml of ice-cold **Co-extraction/fixation buffer** (see Recipes). Incubate for 20 min on ice.
3. Aspirate **Co-extraction/fixation buffer**.
4. Add 900 µl of freshly made 3% PFA. Incubate for 10 min at RT. Then, replace the fixing solution with 2 ml PBS.
5. Proceed to 'immunostaining procedure' (Procedure D).

C. PMY labeling procedure on non-adherent cells

This procedure should be employed for non-adherent cells such as human peripheral blood monocytes (David *et al.*, 2012b). It permits efficient attachment of cells to coverslips within minutes.

1. 'Alcian blue treated coverslips' must be prepared in advance as followed:
 - a. Prepare a solution of 1% (w/v) Alcian blue (Sigma-Aldrich) in distilled water. This solution lasts for months at RT.
 - b. Completely cover 100-200 coverslips in few ml of this solution in a microwave-safe container.
 - c. Stir manually, making sure that all coverslips are coated with Alcian blue (coverslips tend to stick together).
 - d. Heat for 30 sec to 1 min in the microwave (maximum power intensity, the solution should boil for few seconds).
 - e. Mix again manually, by shaking the container.
 - f. Heat again until boiling.
 - g. Discard Alcian blue solution.
 - h. Wash with distilled water and with a gloved hand dissociate aggregated coverslips.
 - i. Wash with 70% ethanol until only a very light blue shade remains on coverslips.
 - j. Thoroughly wash with water.
 - k. Separate coverslips by hand on a large piece of Whatman paper and let them dry.

- I. Alcian blue coated coverslips can be kept for months at RT.
2. Place one Alcian blue treated coverslip per well of a 24-well plate.
3. Centrifuge cells at $400 \times g$ for 5 min at room temperature, wash cells by resuspending them with 5 ml warm DMEM twice in order to remove any trace of FBS.

Note: *Do not use FBS with Alcian blue coverslips.* Alcian blue binds to negatively charged macromolecules such as glycosaminoglycans. The presence of FBS in the medium would inhibit Alcian blue association with membrane glycoproteins and prevent cell adhesion on coverslip.

4. Resuspend cells in a small volume of DMEM (at least 10^6 cells/ml). Spot one drop of cells (about 50 μ l) per coverslips.
5. Incubate at 37 °C for 5 to 15 min (the more you wait, the better they stretch out).
6. Aspirate the medium and replace it with 1 ml of ice-cold PBS.
7. Proceed to the 'Co-extraction/fixation procedure' (Procedure B), starting with Step B7.

D. Immunostaining procedure

1. Transfer one coverslip of each condition into a 24-well plate (save the others at 4 °C). Then incubate cells with 500 μ l of **staining buffer (SB)** (see Recipes) for 15 min at RT. Meanwhile, dilute primary antibodies in **staining buffer**: anti-PMY mAb (depending on the clone, final concentration varies between 1-4 μ g/ml), anti-KRS Abs (1/200) and anti-ribosomal P Abs (1/5,000). To minimize non-specific binding of secondary antibodies, we usually supplement primary antibodies with 5% serum from the species used to generate the secondary antibodies (typically donkey antibodies from Jackson ImmunoResearch).

Note: *Staining buffer components.* Glycine will quench the fixative properties of PFA. Saponin will facilitate the accessibility of the antibody to some epitopes. FBS can decrease non-specific binding of primary antibodies.

2. Lay down a small piece of Parafilm. If needed, tape it on the bench. Spot 30 μ l of diluted primary antibodies on Parafilm. This step is used to minimize the amount of primary Abs needed for staining. In 24-well plates, 200 μ l is needed to completely cover the coverslip. Staining in 24-well plates will reduce the effort required and minimize errors. While antibodies can be reused, mAbs are generally available in essentially unlimited amounts if you have the hybridoma.
3. Using forceps, carefully remove the coverslip, remove excess **staining buffer** by gently blotting coverslip edge on a Kimwipe and place cells side down on the primary antibody drop on Parafilm. Cover with a Petri dish with a moist paper towel attached to the inner top and incubate at room temperature for 60 min.

Notes:

- a. **Staining with 'precious' antibody.** In order to limit the use of precious antibodies you can spot only 10 μ l. In this case, you definitely need to incubate in a 'moist chamber' to prevent coverslips from drying out.

- b. **When you inadvertently drop the coverslip.** Inevitably, you will drop coverslips and will need to determine the ‘cell side’. This can be done if cells are sufficiently dense by holding up the light and looking for the side with a white film. If unsure, you can scratch the suspected side and see the loss of cells, or place the coverslip on an inverted microscope.
4. Meanwhile, dilute secondary antibodies in **staining buffer**: 1/500 for goat anti-mouse A488, 1/500 for donkey anti-rabbit Alexa Fluor 594, 1/500 for donkey anti-human Cy5.
 5. With forceps, remove coverslips from primary antibody spots, and place in 24-wells plate. Wash three times with 1 ml 1x PBS.
 6. Lay down a small piece of Parafilm. If needed, tape it on the bench. Spot 30 µl of diluted secondary antibodies solution on Parafilm.
 7. Using forceps, carefully remove the coverslip from the plate, remove excess wash buffer by gently blotting coverslip edge on a Kimwipe and place cells side down on the secondary antibody drop on Parafilm, cover Petri dish with aluminum foil (to protect the fluorophore), incubate for 45 min at room temperature.
 8. With forceps, pick up coverslips from secondary antibody spots, and place them in a 24-well plate. Wash twice with 1 ml 1x PBS. Then wash again with 1 ml distilled water. Dilute Hoechst 33258 in distilled water (1 µg/ml).
- Note: PBS does not solubilize Hoechst 33258. For this reason, we recommend using distilled water for washes after this step.*
9. Aspirate distilled water and add 200 µl of diluted Hoechst solution. Incubate for 5 min at RT.
 10. Aspirate and wash twice with distilled water.
 11. Place a drop of Fluoromount-G (5 µl) on slides.

Notes:

- a. **Fluoromount-G.** This mounting solution is quite viscous when cold. To facilitate the pipetting of small volumes (5 µl), we usually warm up the solution at RT for 15 min before using. Another helpful trick: cutting the tip of the plastic tip with a razor or scissor helps.
 - b. **The number of coverslips per slide.** With practice, up to 8 coverslips can be placed on each slide. It is greatly advantageous to minimize the number of slides that have to be manipulated during microscopy which should be performed in the dark to accommodate the eyes and maximize visual acuity. Generally, the focal plane only has to be established one time for each slide, allowing rapid viewing of coverslips on the same slide. Give careful thought to the order of the coverslips on the slide. Put the most important coverslips for comparison with each other as closely as possible on the slide. The most important antibodies should be visualized with colors that can be seen by eye. It is important to form a general impression of staining of as many cells as possible, and this is by far most easily done by eye. Equally important is to write down your conclusions of the staining during or immediately after viewing the slides.
12. Using forceps carefully pry up an edge and remove the coverslip, gently place cell side down on a Kimwipe to remove water and then place cells side down on mounting solution drops.

13. Place slides in a tray and leave them dry overnight at room temperature in a drawer to protect the fluorophore.
Note: Fast dry. If needed, drying may be hastened by incubating slides at 37 °C for 2-3 h. Never examine slides before mountant is dry, as this can damage the extremely expensive oil immersion objectives.
14. Store the tray at 4 °C until analysis. Staining is stable for at least 2 weeks at 4 °C in darkness. For a longer storage we recommend using slide boxes and storing at -20 °C.
15. Analyze with a confocal microscope (Figure 2).

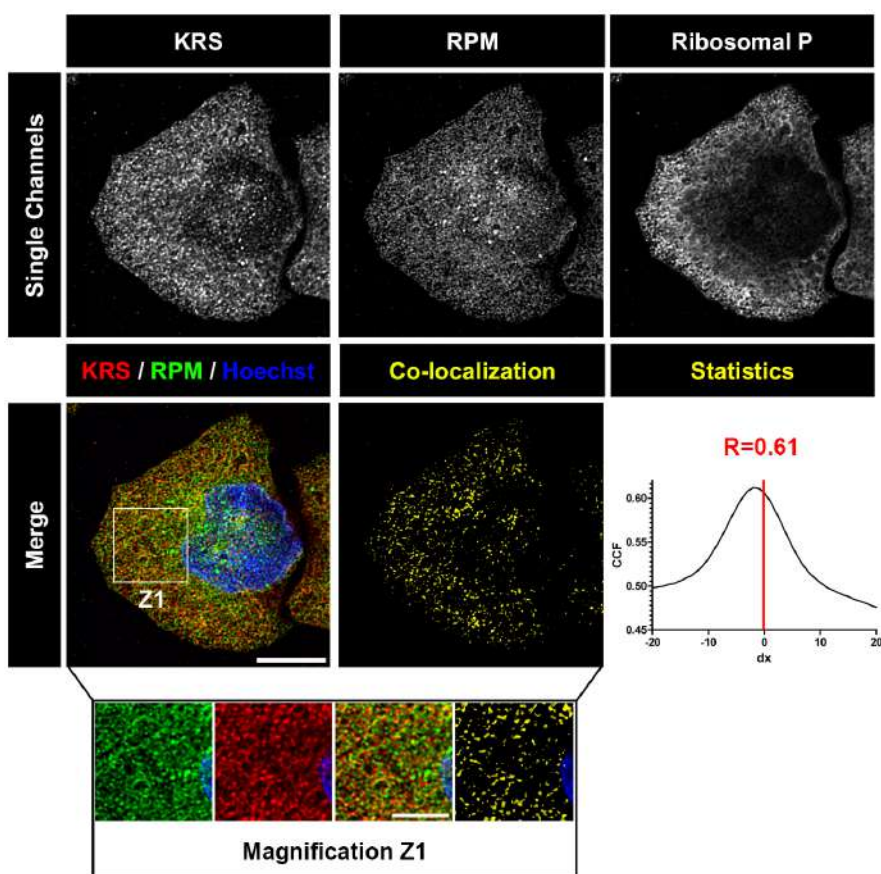


Figure 2. Deconvolved images of HeLa cell labeled with RPM (from David *et al.*, 2011). HeLa cells were pulsed with PMY + CHX to label translating ribosomes and extracted with Dig to remove free PMY and cytosolic components. Cells were then fixed, permeabilized and stained for KRS, PMY or ribosomal P proteins. Co-localization was estimated using ImageJ (NIH) and JACoP plugin that compiles general co-localization indicators such as Pearson's coefficient (Manders *et al.*, 1992) and Van Steensel's CCF (Van Steensel *et al.*, 1996). KRS and RPM demonstrate extensive co-localization as quantitated by Van Steensel's CCF greater than 0.75 and Pearson's coefficient (R) greater than 0.5. Bar scales, 10 μm , 5 μm for Z1. Reproduced from David *et al.*, 2011 with permission of the publisher and of Dr. Yewdell.

Data analysis

Images can be processed using LAS AF software (Leica), Imaris (Bitplane), Huygens Essentials Software (Version 3.6, Scientific Volume Imaging BV), Photoshop CS2 (Adobe), and/or ImageJ. For obvious ethical reasons, gamma function—which connects the numerical value of a pixel with its actual luminance—must not be manipulated. Each set of images for a given experiment must be processed identically to maintain the image intensity ratio. In previous publications (David *et al.*, 2011; 2012a and 2012b; Macari *et al.*, 2015), ImageJ and Prism software were used for quantitation and statistical analysis. Comparing translation activity from different condition necessitates acquisition of multiple fields (at least 6 fields per condition for statistical significance). In order to normalize each field, the mean fluorescence ratio of PMY/ribo P staining must be quantitated using ImageJ. Then, values may be plotted (mean \pm SEM). For statistical analysis, we previously used two-tailed unpaired *t*-test. An example is presented in the following paper: David *et al.*, 2012.

Notes

As stated above (methods #4), multiple controls are necessary when applying RPM for the first time or using new cell lines.

Recipes

1. Anisomycin (Calbiochem) stock solution (1,000x)
10 mg/ml (or 37 mM) in 100% ethanol solution
Store at -20 °C
2. Cycloheximide (CHX) stock solution (1,000x)
100 mg/ml (or 355 mM) in 50% ethanol
Store at -20 °C
3. Emetine dihydrochloride stock solution (1,000x)
25 mg/ml (or 45 mM) in 50% ethanol
Store at -20 °C
4. Harringtonine stock solution (1,000x)
2 mg/ml (or 3.7 mM) in 100% ethanol
Store at -20 °C
5. PMY stock solution (1,000x)
50 mg/ml (or 91 mM) in 50% ethanol
Store at -20 °C
6. Sodium arsenite stock solution (1,000x)
65 mg/ml (or 500 mM) in distilled water

Store at 4 °C

7. Phosphate buffered saline (PBS)

210.0 mg/L KH₂PO₄

9,000 mg/L NaCl

726.0 mg/L Na₂HPO₄·7H₂O

8. Growth medium

Dulbecco's modified Eagle's medium with:

Glutamine 2 mM final

1% penicillin/streptomycin

7.5% fetal bovine serum (FBS)

9. Labeling medium

Add 5 µl of PMY stock solution (91 µM final) and either 5 µl of emetine stock solution (45 µM final) or 5 µl of CHX stock solution (355 µM final) to 5 ml growth medium

10. Labeling control medium

Add either 5 µl of emetine stock solution (45 µM final) or 5 µl of CHX stock solution (355 µM final) to 1 ml growth medium

11. Extraction buffer

0.015% (m/v) digitonin

50 mM Tris-HCl pH 7.5

5 mM MgCl₂

25 mM KCl

355 µM CHX

1x EDTA-free protease inhibitors (1 tablet per 10 ml)

10 U/ml RNase Out

DEPC treated water

12. Wash buffer

50 mM Tris-HCl pH 7.5

5 mM MgCl₂

25 mM KCl

355 µM CHX

1x EDTA-free protease inhibitors (1 tablet per 10 ml)

10 U/ml RNase Out

DEPC treated water

13. 3% PFA

Dilute stock solution (16%) in 1x PBS

14. Co-extraction/fixation buffer

0.015% (m/v) digitonin

50 mM Tris-HCl pH 7.5

5 mM MgCl₂

25 mM KCl
0.2 M sucrose
355 µM CHX
1x EDTA-free protease inhibitors (1 tablet per/10 ml)
10 U/ml RNase Out
3% PFA
DEPC treated water
15. Staining buffer (SB)
0.05% saponin
10 mM glycine
5% FBS
1x PBS

Acknowledgments

JWY is generously supported by the Division of Intramural Research, National Institute of Allergy and Infectious Diseases. AD benefits from generous funding from Fondation pour la Recherche Médicale, Ligue contre le Cancer and Cancéropôle GSO. The authors declare no conflicts of interest or competing interests.

References

1. Biever, A., Puighermanal, E., Nishi, A., David, A., Panciatici, C., Longueville, S., Xirodimas, D., Gangarossa, G., Meyuhas, O., Herve, D., Girault, J. A. and Valjent, E. (2015). [PKA-dependent phosphorylation of ribosomal protein S6 does not correlate with translation efficiency in striatonigral and striatopallidal medium-sized spiny neurons](#). *J Neurosci* 35(10): 4113-4130.
2. David, A., Bennink, J. R. and Yewdell, J. W. (2012a). [Emetine optimally facilitates nascent chain puromycylation and potentiates the ribopuromycylation method \(RPM\) applied to inert cells](#). *Histochem Cell Biol* 139(3): 501-504.
3. David, A., Dolan, B. P., Hickman, H. D., Knowlton, J. J., Clavarino, G., Pierre, P., Bennink, J. R. and Yewdell, J. W. (2012b). [Nuclear translation visualized by ribosome-bound nascent chain puromycylation](#). *JCB* 197(1): 45-57.
4. David, A., Netzer, N., Strader, M. B., Das, S. R., Chen, C. Y., Gibbs, J., Pierre, P., Bennink, J. R. and Yewdell, J. W. (2011). [RNA binding targets aminoacyl-tRNA synthetases to translating ribosomes](#). *J Biol Chem* 286(23): 20688-20700.
5. Dieterich, D. C., Lee, J. J., Link, A. J., Graumann, J., Tirrell, D. A. and Schuman, E. M. (2007). [Labeling, detection and identification of newly synthesized proteomes with bioorthogonal non-canonical amino-acid tagging](#). *Nat Protoc* 2(3): 532-540.

6. Eggers, D. K., Welch, W. J. and Hansen, W. J. (1997). [Complexes between nascent polypeptides and their molecular chaperones in the cytosol of mammalian cells.](#) *Mol Biol Cell* 8(8): 1559-1573.
7. Emmott, E., Sorgeloos, F., Caddy, S. L., Vashist, S., Sosnovtsev, S., Lloyd, R., Heesom, K., Locker, N. and Goodfellow, I. (2017). [Norovirus-mediated modification of the translational landscape via virus and host-induced cleavage of translation initiation factors.](#) *Mol Cell Proteomics* 16(4 suppl 1): S215-S229.
8. Fresno, M., Jimenez, A. and Vazquez, D. (1977). [Inhibition of translation in eukaryotic systems by harringtonine.](#) *Eur J Biochem* 72(2): 323-330.
9. Gruber, T. E., Hebert-Seropian, S., Khoutorsky, A., David, A., Yewdell, J. W., Lacaille, J. C. and Sossin, W. S. (2013). [Reactivation of stalled polyribosomes in synaptic plasticity.](#) *Proc Natl Acad Sci U S A* 110(40): 16205-16210.
10. Hansen, J. L., Moore, P. B. and Steitz, T. A. (2003). [Structures of five antibiotics bound at the peptidyl transferase center of the large ribosomal subunit.](#) *J Mol Biol* 330(5): 1061-1075.
11. Jimenez, A., Carrasco, L. and Vazquez, D. (1977). [Enzymic and nonenzymic translocation by yeast polysomes. Site of action of a number of inhibitors.](#) *Biochemistry* 16(21): 4727-4730.
12. Kedersha, N., Chen, S., Gilks, N., Li, W., Miller, I. J., Stahl, J. and Anderson, P. (2002). [Evidence that ternary complex \(eIF2-GTP-tRNA\(i\)\(Met\)\)-deficient preinitiation complexes are core constituents of mammalian stress granules.](#) *Mol Biol Cell* 13(1): 195-210.
13. Kedersha, N., Panas, M. D., Achorn, C. A., Lyons, S., Tisdale, S., Hickman, T., Thomas, M., Lieberman, J., McInerney, G. M., Ivanov, P. and Anderson, P. (2016). [G3BP-Caprin1-USP10 complexes mediate stress granule condensation and associate with 40S subunits.](#) *J Cell Biol* 212(7): 845-860.
14. Macari, F., El-Houfi, Y., Boldina, G., Xu, H., Khouri-Hanna, S., Ollier, J., Yazdani, L., Zheng, G., Bieche, I., Legrand, N., Paulet, D., Durrieu, S., Bystrom, A., Delbecq, S., Lapeyre, B., Bauchet, L., Pannequin, J., Hollande, F., Pan, T., Teichmann, M., Vagner, S., David, A., Choquet, A. and Joubert, D. (2016). [TRM6/61 connects PKC \$\alpha\$ with translational control through tRNAi\(Met\) stabilization: impact on tumorigenesis.](#) *Oncogene* 35(14): 1785-1796.
15. Manders, E., Stap, J., Brakenhoff, G., van Driel, R. and Aten, J. (1992). [Dynamics of three-dimensional replication patterns during the S-phase, analysed by double labelling of DNA and confocal microscopy.](#) *J Cell Sci* 103: 857-862.
16. Perry, R. B., Rishal, I., Doron-Mandel, E., Kalinski, A. L., Medzihradszky, K. F., Terenzio, M., Alber, S., Koley, S., Lin, A., Rozenbaum, M., Yudin, D., Sahoo, P. K., Gomes, C., Shinder, V., Geraisy, W., Huebner, E. A., Woolf, C. J., Yaron, A., Burlingame, A. L., Twiss, J. L. and Fainzilber, M. (2016). [Nucleolin-mediated RNA localization regulates neuron growth and cycling cell size.](#) *Cell Rep* 16(6): 1664-1676.
17. Pestka, S. (1971). [Inhibitors of ribosome functions.](#) *Annu Rev Microbiol* 25: 487-562.

18. Roth, H., Magg, V., Uch, F., Mutz, P., Klein, P., Haneke, K., Lohmann, V., Bartenschlager, R., Fackler, O. T., Locker, N., Stoecklin, G. and Ruggieri, A. (2017). [Flavivirus infection uncouples translation suppression from cellular stress responses.](#) *MBio* 8(1).
19. Schmidt, E. K., Clavarino, G., Ceppi, M. and Pierre, P. (2009). [SUnSET, a nonradioactive method to monitor protein synthesis.](#) *Nat Methods* 6(4): 275-277.
20. Seedhom, M. O., Hickman, H. D., Wei, J., David, A. and Yewdell, J. W. (2016). [Protein translation activity: A new measure of host immune cell activation.](#) *J Immunol* 197(4): 1498-1506.
21. Starck, S. R., Green, H. M., Alberola-Illa, J. and Roberts, R. W. (2004). [A general approach to detect protein expression *in vivo* using fluorescent puromycin conjugates.](#) *Chem Biol* 11(7): 999-1008.
22. Van Steensel, B., van Binnendijk, E., Hornsby, C., van der Voort, H., Krozowski, Z., de Kloet, E. and van Driel, R. (1996). [Partial colocalization of glucocorticoid and mineralocorticoid receptors in discrete compartments in nuclei of rat hippocampus neurons.](#) *J Cell Sci* 109: 787-792.
23. Willett, M., Brocard, M., Davide, A. and Morley, S. J. (2011). [Translation initiation factors and active sites of protein synthesis co-localize at the leading edge of migrating fibroblasts.](#) *Biochem J* 438(1): 217-227.
24. Williams, K. R., McAninch, D. S., Stefanovic, S., Xing, L., Allen, M., Li, W., Feng, Y., Mihailescu, M. R. and Bassell, G. J. (2016). [hnRNP-Q1 represses nascent axon growth in cortical neurons by inhibiting Gap-43 mRNA translation.](#) *Mol Biol Cell* 27(3): 518-534.

Obtaining Acute Brain Slices

Thomas Papouin* and Philip G. Haydon

Department of Neuroscience, Tufts University School of Medicine, Boston, MA, USA

*For correspondence: thomas.papouin@tufts.edu



[Abstract] Obtaining acute brain slices for electrophysiology or amperometric recordings has become a routine procedure in most labs in the field of neuroscience. Yet, protocols describing the step by step process are scarce, in particular for routine acute preparations such as from the mouse hippocampus. Here we provide a detailed protocol for the dissection, extraction and acute slicing of the mouse brain, including tips and list of material required.

Keywords: Acute brain slices, Hippocampus, Dissection, Brain extraction, Electrophysiology, Mouse

[Background] With the democratization of *in vitro* electrophysiology and amperometry recording techniques, obtaining acute slices from rodent brains has become a classic and pivotal procedure in neuroscience research. Yet, the know-how required to achieving this procedure is typically passed on verbally, and most labs have developed home-made recipes and adapted the most important steps to their own needs or region of interest, such that there is a lack of protocols describing how to obtain high-quality acute brain slices in a step by step manner. While some protocols can be found describing particularly challenging preparations, such as acute slicing of adult mouse spinal cord (Garre *et al.*, Bioprotocol 2017: <https://doi.org/10.21769/BioProtoc.2102>), a description of the basic procedure for more routine preparations (e.g., hippocampal slices) is particularly lacking. Aside from the practical aspect, this is a major problem because extracellular field recordings from hippocampal slice have become widely employed, due to their relative simplicity and little equipment-requirement, including by labs without electrophysiology and acute brain slices preparation expertise. Given that the slices' quality is the limiting factor to obtaining reliable electrophysiological recordings, this poses a major challenge for the reproducibility of results within and across labs. In light of these needs and caveats, we here provide a detailed protocol for the dissection, brain extraction and acute slicing of the mouse hippocampus, including tips and list of material required. It will allow beginner and non-experts to obtain acute hippocampal brain slices of the required quality for follow-up studies such as field recordings, patch-clamp recordings or amperometric recordings (Papouin *et al.*, 2017).

Materials and Reagents

Materials

A. For the 'nest beaker'

1. Nylon tights

2. Instant superglue (such as Scotch Super Glue, 3M, catalog number: AD124)
3. 15 ml tubes (such as VWR, catalog number: 89039-670 US, 525-0450 Europe)
4. Disposable 6 cm diameter plastic Petri dish (such as Thermo Fisher Scientific, Thermo Scientific™, catalog number: 123TS1)

B. For dissection

1. Large kitchen scissors or guillotine
2. Straight fine scissors (such as Fine Science Tools, catalog number: 14060-11)
3. Curved spatula (such as Fine Science Tools, catalog number: 10092-12)
4. Scalpel (such as Fine Science Tools, catalog number: 91003-12)
5. Glass disposable Pasteur pipet (such as Fisher Scientific, FisherBrand, catalog number: 13-678-6A)
6. Dropper bulb (such as Fisher Scientific, FisherBrand, catalog number: 03-448-25)
7. Plastic container, about 2.5 cm high and 150 ml, such as the lid of a pipet tip box or a large glass Petri dish (Cole-Parmer Instrument, catalog number: EW-34551-06)
8. Whatman paper (GE Healthcare, Whatman, catalog number: 1001-090)
9. Disposable Razor blade (such as Personna Double Edge Razor Blades [Amazon, PERSONNA, catalog number: BP9020])

Reagents

1. Glucose (Sigma-Aldrich, catalog number: G7021)
2. Sodium chloride (NaCl) (Sigma-Aldrich, catalog number: S7653)
3. Sodium phosphate monobasic anhydrous (VWR, catalog number: 470302-666)
Manufacturer: ALDON, catalog number: SS0756-500GR.
4. Sodium bicarbonate (NaHCO₃) (Sigma-Aldrich, catalog number: S5761)
5. Potassium chloride (KCl) (Sigma-Aldrich, catalog number: P9333)
6. Magnesium chloride solution (1 M) (Sigma-Aldrich, catalog number: 63069)
7. Calcium chloride solution (1 M) (Sigma-Aldrich, catalog number: 21115)
8. Stock artificial cerebrospinal fluid (ACSF) solution (see Recipes)
9. Ice-cold Slicing ACSF solution (see Recipes)
10. Recovery ACSF solution (see Recipes)
11. Experimental ACSF (see Recipes)

Equipment

1. 250 ml Pyrex beaker (such as VWR, catalog number: 10754-952)
2. Straight spring scissors (such as Fine Science Tools, catalog number: 15018-10)
3. Curved fine forceps (such as Fine Science Tools, catalog number: 11152-10)
4. 600 ml Pyrex beaker (such as VWR, catalog number: 10754-956)

5. 95% O₂/5% CO₂ tank (such as AirGas, catalog number: Z02OX9522000043)
6. Vibratome (such as Leica, model: Leica VT 1200 S, catalog number: 14048142066)
7. Bath heater (such as Thermo Fisher Scientific, Thermo Scientific, model: Precision 180, catalog number: 51221073)

Procedure

Before starting:

1. Assemble the ‘nest beaker’ (Figure 1) and a modified Pasteur pipet dropper (Figure 2).
 - a. ‘Nest beaker’ preparation (Figure 1)
 - i. Using nylon tights, a 6 cm plastic Petri dish, a 15 ml tube, superglue and a 250 ml beaker, prepare a ‘nest beaker’ in which slices will be incubated during and after recovery. Using kitchen scissors (or a ‘Dremel’ if you have one) cut out or simply open the base of the Petri dish, preferably without breaking the wall.
 - ii. Stretch the nylon around the open Petri dish to form a firm mesh base, and secure it by tying it or by using elastic bands. Glue the nylon on the outside wall of the Petri dish. Do not use excessive amounts of glue as this can be toxic to slices and would prevent proper drying. Let dry for 24 h.
 - iii. Using a scalpel or fine scissors, cut out the excess nylon. Rinse abundantly and soak in clear water overnight (we had instances where ‘fresh’ glue revealed toxic to slices). Cut and discard the conical end of the 15 ml tube, and cut out a rectangular window near the bottom end.
 - iv. Assemble all three elements as shown. Plastic tubing from the 95% CO₂/5% O₂ tank will be lowered into the 15 ml tube to maintain appropriate pH and oxygenation.



Figure 1. Nest beaker. Using nylon tights, a 6 cm plastic Petri dish, a 15 ml tube, superglue and a 250 ml beaker, prepare a ‘nest beaker’ in which slices will be incubated during and after recovery.

b. Modified Pasteur pipette dropper (Figure 2)



Figure 2. Modifier Pasteur pipette dropper. Break the thinnest end of a Glass disposable Pasteur pipet, and insert that end in a Dropper bulb.

2. Prepare 1 L of ACSF the day prior and store overnight at 4 °C.

Setting up:

1. On the day of the experiment, prepare 300 ml of ice-cold slicing ACSF (see Recipes) in a 600 ml Pyrex beaker (by adding 2 mM of MgCl₂ and 1 mM of CaCl₂ to 300 ml of stock ACSF) and place in a -20 °C freezer for about 20-30 min or until a thin layer of ice on the walls of the beaker and at the surface forms. Agitate vigorously to break the ice into a homogeneous icy solution. Avoid over-freezing as this will drastically change the osmolarity of the solution and reduce the quality of the slices. However, the amount of ice should be enough that the solution remains at 0-1 °C throughout the entire slicing procedure. Therefore it is recommended to adjust the iciness of the solution to your need/speed. We recommend against placing the beaker of slicing ACSF in a -80 °C freezer.
2. While the ice-cold slicing ACSF is in the freezer, prepare 150 ml of recovery ACSF in the ‘nest beaker’ (by adding 1.5 mM of MgCl₂ and 2 mM of CaCl₂ to 150 ml of stock ACSF). Warm up in the heated bath at 33 °C while oxygenating with 95% O₂/5% CO₂ for at least 25 min before to start (Figure 3B).
3. Prepare the vibratome by placing a mix of ice and water in the tray surrounding the slicing chamber. Cut a razor blade in half with the kitchen scissors (or use two blades): place one half in the blade holder of the vibratome and keep the other half for the dissection Procedure B.
4. Familiarize yourself with the Procedures A to C below and prepare your tools accordingly, to optimize the process. Typically, this consists in placing the tools in the following order (right to left but adjust depending on your dominant hand): Large kitchen scissors, scalpel, fine scissors, fine forceps, plastic container or large glass Petri dish with a piece of Whatman paper at the bottom (this will help increasing visual contrast and providing greater surface grip) and the

curved spatula nearby, ready-to-grab second half of the razor blade, vibratome cutting plate and tube of glue, modified Pasteur pipet dropper and spring scissors (Figure 3A).

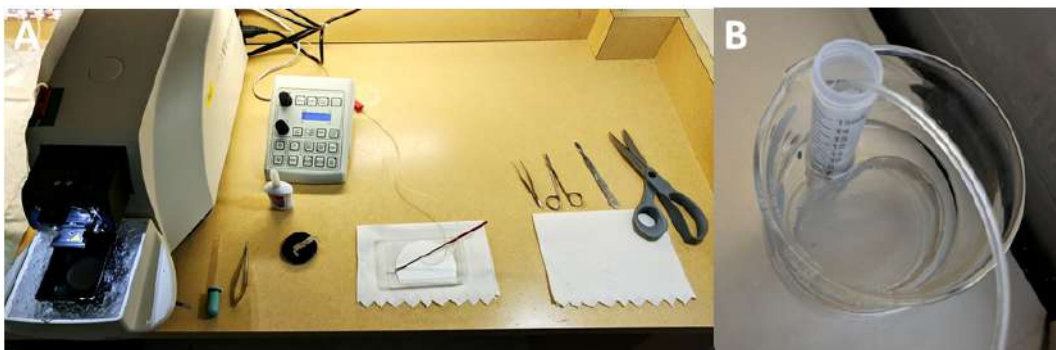


Figure 3. Set-up. A. The tools on the dissection and slicing bench are set up from right to left according to the sequence of steps described in this protocol. B. Close up view of the nest beaker filled with recovery ACSF bubbling with 95%O₂/5%CO₂ and incubating at 33 °C.

A. Quickly extract the brain

1. Pour about half (150 ml) of the ice-cold slicing ACSF into the plastic container or large glass Petri dish and oxygenate.
2. Anesthetize the mouse using isoflurane, check for the absence of reflex upon tail or paw pinching and quickly decapitate the mouse using a small guillotine or large kitchen scissors (Figures 4A and 4B). Expose the skull with a large incision through the skin down the midline (Figure 4C) and cut the auditory conducts on each side (Figures 4D and 4E). Pull the skin toward the nose of the animal to fully expose the skull (Figure 4F). This will also provide a better grip of the head.
3. Place the head in ice-cold oxygenated slicing ACSF. Leave it submerged for 10 sec to chill.
4. While making sure the head remains submerged at all times, with fine scissors, open the back of the skull by making a cut immediately caudal to the cerebellum (Figures 4G and 4H), and then cut the skull open along the midline from the caudal end working your way up to the olfactory bulbs (Figures 4I-4L). Avoid putting pressure on the skull and make sure no damage is made to the brain underneath with the lower scissors tip. We also recommend making a lateral cut at the base of the skull through the jaw bones, this will help to extract the brain (Figure 4M).
5. Using fine forceps grab the open edge of the skull on one side of the midline, hold firmly and open to the side while steadily holding down the head with the other hand (Figures 4N and 4O, ideally, your index and thumb should be on each side of the mouse ‘face’, roughly on the eyes. Having the skin tight under your fingers usually helps).
6. Then proceed to the other side (Figures 4P and 4Q). Using a curved spatula, and being extremely gentle reach under the brain (let the floor of the skull guide you) and gently scoop out the brain, without pulling (Figures 4R-4T). The optic nerve, on the ventral part, and the cranial nerves, caudally, might need to be cut with the fine scissors or directly with the spatula to

completely free the brain. Leave the extracted brain in the ice-cold slicing ACSF (Figure 4U). Make sure you keep the brain submerged in the ice-cold ACSF throughout this entire procedure.

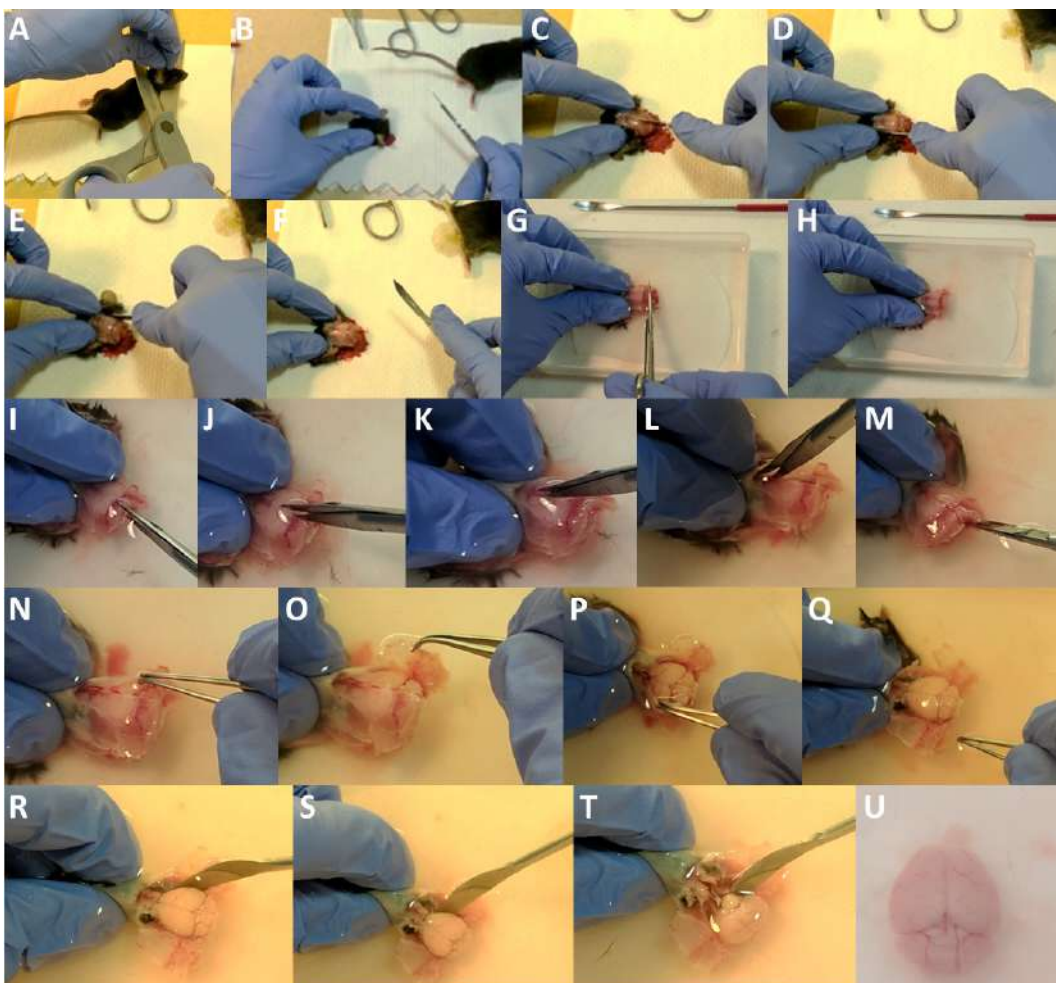


Figure 4. Extracting the brain from the skull. A. Decapitate the anesthetized animal; B-F. Using the scalpel, incise the skin, cut the auditory conducts and pull the skin to expose the skull. G-H. Open the back of the skull by making a cut immediately caudal to the cerebellum. I-L. Using fine scissors, carefully cut through the skull along the midline. Angle the scissors to minimize potential damage by the tip to the brain underneath. M. If animals used are adults, we recommend making a lateral cut at the base of the skull through the jaw bones. N-Q. Using fine tweezers, grab the open edge of the skull on one side, hold firmly and open to the side while firmly holding down the head by the 'nose' with the other hand. Then proceed to the other side. R-U. Using the curved spatula, carefully reach under the brain (let the floor of the skull guide you) and gently scoop out the brain. Cut through the optic chiasma with fine scissors or directly with the spatula (T). For clarity purpose, there is no ice and no bubbling in the solution in Panels G-U.

B. Isolate the region of interest

1. With the razor blade, remove the unwanted parts of the brain, rostral and caudal to the region of interest. In the case of the hippocampus: place the brain ventral side down, locate the superior colliculi, make a transverse cut and discard the caudal part (cerebellum, Figure 5A).
Note: Make sure the cut is perpendicular to the rostro-caudal axis as this face will be glued on the cutting-plate of the vibratome.
2. Then flip the brain ventral side up, locate the optic chiasma and make a transverse cut (Figures 5B and 5D). This should expose the fimbria of the fornix, which is immediately rostral to the hippocampus (*i.e.*, the hippocampus lies under it). Spread just enough glue on the cutting plate (make sure the plate is dry beforehand, Figure 5E).
3. Using the curved spatula and your index and thumb as an abutment (do not grab the brain with your fingers!), pick up the brain rostral side up and ventral side facing you (Figures 5F and 5G). Gently place the bottom of the spatula on a paper towel, to drain the excess of ACSF by capillarity (do not touch the brain with the paper towel). Place the spatula immediately above the glue (without touching it) and gently transfer the brain on the glue in a single motion by pushing it off the spatula with your finger (Figure 5H).

Note: Being slow or hesitant will ‘stretch’ the brain and reduce the quality of the slices. Do not press down on the brain, tap the plate or wait and let the brain dry off, or this will dramatically reduce the quality of the slices as well.

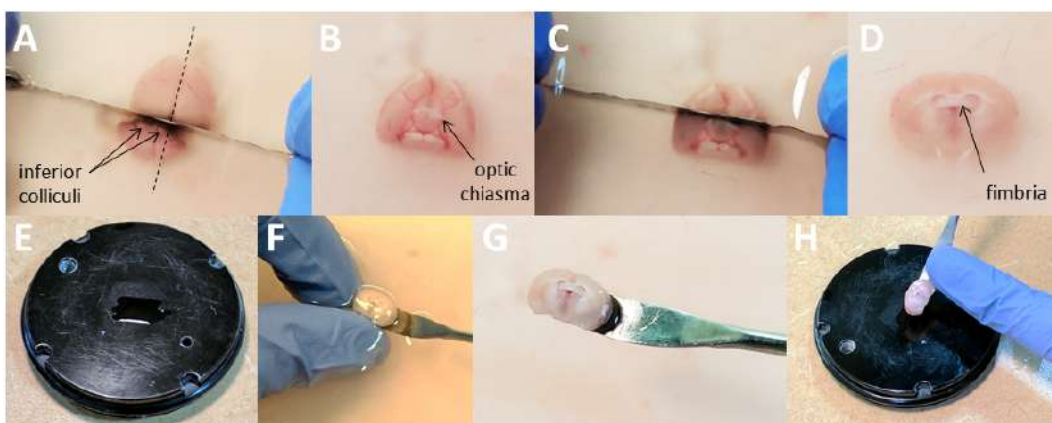


Figure 5. Isolate the region of interest. A. While the brain is dorsal side up, locate the inferior colliculi and, using a razor blade, make a cut immediately above them perpendicular to the rostro-caudal axis. Discard the part containing the cerebellum. B-C. Flip the brain ventral side up, locate the optic chiasma and using the razor blade, make a cut perpendicular to the rostro-caudal axis. Discard the frontal part. This should free the fimbria of the fornix, which lies immediately above the hippocampus. E-H. Apply just the required amount of glue on the vibratome plate. F. Using the curved spatula and your index and thumb as an abutment (do not grab the brain with your fingers!) pick up the brain. Use your finger to push the brain off the

spatula immediately above the glue and delicately ‘drop’ in on the glue in a single motion. For clarity purpose, there is no ice and no bubbling in the solution in Panels A-D and F.

C. Obtain brain slices

1. Immediately transfer the plate into the slicing chamber (Figure 6A), with the ventral part of the brain facing you and the dorsal part (*i.e.*, the surface of cortex) facing the back of the vibratome. Gently pour the rest of the ice-cold oxygenated slicing ACSF (Figure 6B).
2. Lower the blade in the solution and, using the vibratome control panel, set up a fairly narrow yet safe ‘slicing window’ (~2 mm on each side). Lower the blade to the surface of the brain (do not press the blade on the brain) and start the slicing to obtain 300-350 μm hippocampal coronal slice (thickness should be pre-set).

Notes:

- a. *Avoid pouring the ACSF directly onto the brain and be careful not to drop pieces of ice onto the brain. Oxygenate while ensuring that the agitation caused by the bubbling is not excessive as this may be a problem once slices come unattached.*
 - b. *To optimize the quality of the slices and minimize the total duration of the procedure, we recommend adjusting the speed of the vibratome to medium (0.12-0.16 mm/sec on Leica VT1200s) when the blade is not in any region of interest, and to low when the blade is in the hippocampus or region of interest (0.08-0.1 mm/sec on Leica VT1200s).*
 - c. *Once the blade reaches the last ventral micrometers, the optic chiasma or meninges can resist and prevent full detachment of the slice. This can also distort or ‘pull’ the slice before it is entirely freed. In most cases, gently holding the slice onto the blade with the spring scissors without applying any pressure (Figure 6C) will suffice to help the blade cut through the chiasma or meninges. In extreme cases, we recommend quickly but very carefully sniping the meninges or the remaining part of the slice with spring scissors. In any case, be extremely careful not to push on the vibrating blade, on the brain underneath, or to pull the slice while still attached. Any sort of mechanical pressure (‘pulling’) will damage the slice. This could also cause the brain to come unglued.*
3. Once the first slice is freed (Figure 6D), with spring scissors, separate both hemispheres (Figure 6E) and, using the Pasteur pipet dropper, transfer them into the nest beaker containing the recovery ACSF (see Recipes), incubating at 33 °C in the bath heater (Figure 6F).
 4. Repeat until all slices are obtained and all hemi-slices are transferred in the nest beaker containing the recovery ACSF. Incubate at 33 °C for an additional 30 min.
 5. Carefully remove the nest beaker from the heating bath and let recover at room temperature for 45 min.
 6. Slices are now ready to be used for electrophysiology or other procedures such as Bio-protocol ‘D-serine measurement in brain slices or other tissue explants’ (Papouin and Haydon, 2018).

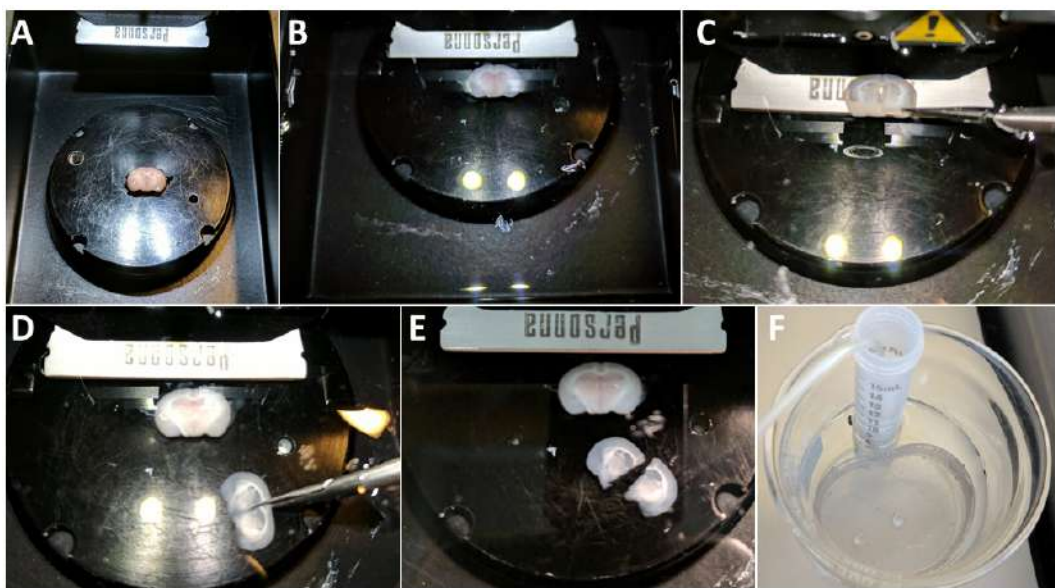


Figure 6. Obtain brain slices. A. Transfer the plate with the glued brain in the slicing chamber of the vibratome and lower the blade holder. B. Pour the remaining of the ice-cold Slicing aCSF. C. If meninges or the optic chiasma are an issue during slicing, gently hold the slice onto the blade with the spring scissors (without applying any pressure) to help cut through. D. Once the slice is freed, separate the two hemispheres with the spring scissors (you can use the fine forceps to hold the bottom of the slice) and transfer to the nest beaker with Recovery ACSF incubating and bubbling at 33 °C. For clarity purpose, there is no ice and no bubbling in the solution in Panels B-E.

Data analysis

The quality of slices (notably hippocampal slices) can be very easily assessed visually with the 5x objective of any given microscope (Figure 7). Typically, healthy slices show stark contrasts and differential coloring across layers and regions. The *stratum oriens* and *radiatum* will have a bright orange color. The *stratum lacunosum molecular* generally appears much darker (deep brown to deep grey). The pyramidal layer, while clear in comparison, will appear thin or ‘compact’ and, depending on the angle of the slicing, can be delineated from the *s. oriens* and *radiatum* by thin dark lines. Unhealthy slices take greyish and uniform tints. The pyramidal layer of an unhealthy slice appears exceedingly white or transparent and usually ‘swollen’.

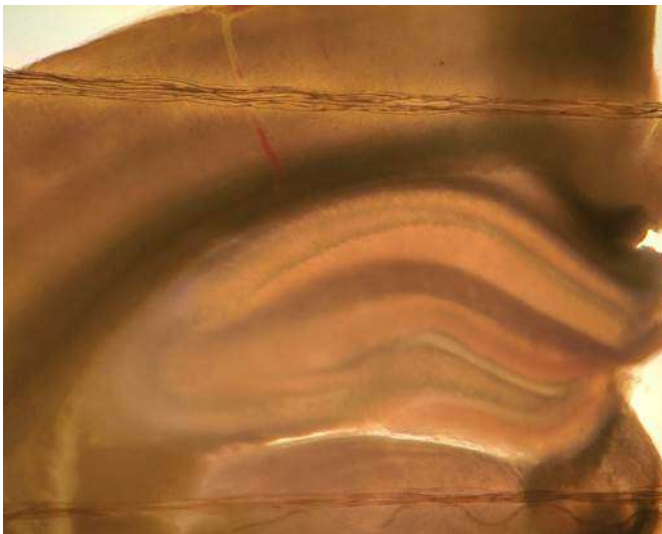


Figure 7. A healthy hippocampal slice. Healthy, brain/hippocampal slices typically show orange coloring with obvious differences in tints and contrasts across layers. Layers are also evident in the cortex.

Note: The two sets of horizontal 'strings' are from the 'harp' system that holds the slice down under the microscope (not described in this protocol).

Notes

1. From our experience, Steps A2 (once the mouse is decapitated) to C4 (when the last slice is extracted) should be achieved within 10 min for optimal brain slices quality. In particular, the complete extraction of the brain should be achieved in less than 2 min, *i.e.*, no more than ~2-3 min should elapse between the decapitation of the animal and the transfer of the brain into the vibratome chamber.
2. Please note that contrary to most of labs or protocols we strongly advice against using a sucrose-based slicing solution. We found that reducing calcium concentration while increasing that of magnesium and ensuring that the procedure is performed rapidly (see above) and in ice-cold ACSF throughout is the most efficient way to reduce excitotoxicity and the best guarantee of good slice quality.
3. Please note that contrary to most of labs or protocols we also strongly advice against using a paint brush to manipulate slices. While they feel soft to the touch of one's finger, at the scale of a 350 μm slice, paint brushes are the equivalent of many small knives bundle together and result in multiple stab wounds to slices.

Recipes

1. Stock artificial cerebrospinal fluid (ACSF) solution (1 L, store at 4 °C)
Glucose 10 mM (1.8 g for 1 L)
Potassium chloride 3.2 mM (0.23 g for 1 L)
Sodium chloride 120 mM (7 g for 1 L)
Sodium phosphate monobasic anhydrous 1 mM (0.119 g for 1 L)
Sodium bicarbonate 26 mM (2.18 g for 1 L)
Make up to 1 L with ddH₂O
Verify and adjust pH to 7.3 and osmolarity to 290-300 mOsm L⁻¹
2. Ice-cold slicing ACSF (~300 ml)
Stock ACSF
2 mM magnesium chloride
1 mM calcium chloride
3. Recovery ACSF (~150 ml)
Stock ACSF
1.5 mM magnesium chloride
2 mM calcium chloride
4. Experimental ACSF (~550 ml) for follow-up electrophysiological or amperometric recordings
Stock ACSF
1.3 mM magnesium chloride
2 mM calcium chloride

Acknowledgments

This work was supported by two Philippe Foundation grants and a Human Frontier Science Program long-term fellowship (LT000010/2013) awarded to T.P., and two NIH/NINDS R01 grants (NS037585 and AA020183) awarded to P.G.H. who is also the founder of GliaCure. Authors declare no conflict of interest. We thank Jaclyn M. Dunphy for her careful proofreading of this protocol.

References

1. Garré, J. M., Yang, G., Bukauskas, F. F. and Bennett, M. V. (2017). [An acute mouse spinal cord slice preparation for studying glial activation ex vivo](#). *Bio-protocol* 7(2): e2102.
2. Papouin, T., Dunphy, J. M., Tolman, M., Dineley, K. T. and Haydon, P. G. (2017). [Septal cholinergic neuromodulation tunes the astrocyte-dependent gating of hippocampal NMDA receptors to wakefulness](#). *Neuron* 94(4): 840-854 e847.

3. Papouin, T and Haydon, P. G. (2018). [D-serine measurements in brain slices or other tissue explants.](#) *Bio-protocol* 8(2): e2698.

Assaying Mechanonociceptive Behavior in *Drosophila* Larvae

Nina Hoyer, Meike Petersen, Federico Tenedini and Peter Soba*

Research Group Neuronal Patterning and Connectivity, Center for Molecular Neurobiology (ZMNH), University Medical Campus Hamburg-Eppendorf, Hamburg, Germany

*For correspondence: peter.soba@zmnh.uni-hamburg.de



[Abstract] *Drosophila melanogaster* larvae have been extensively used as a model to study the molecular and cellular basis of nociception. The larval nociceptors, class IV dendritic arborization (C4da) neurons, line the body wall of the animal and respond to various stimuli including noxious heat and touch. Activation of C4da neurons results in a stereotyped escape behavior, characterized by a 360° rolling response along the body axis followed by locomotion speedup. The genetic accessibility of *Drosophila* has allowed the identification of mechanosensory channels and circuit elements required for nociceptive responses, making it a useful and straightforward readout to understand the cellular and molecular basis of nociceptive function and behavior. We have optimized the protocol to assay mechanonociceptive behavior in *Drosophila* larvae.

Keywords: Nociception, Noxious touch, *Drosophila melanogaster*, Somatosensory network, Mechanosensory

[Background] Nociception, the innate ability to detect and avoid noxious stimuli, is highly conserved across the animal kingdom. *Drosophila melanogaster* larvae are capable to detect and avoid a variety of noxious stimuli including noxious touch, heat and light (Tracey *et al.*, 2003; Hwang *et al.*, 2007; Xiang *et al.*, 2010). Mechanical stimulation above a certain threshold (> 30 mN) elicits a stereotyped rolling escape response at all larval stages (Almeida-Carvalho *et al.*, 2017), which is thought to have evolved to avoid ovipositor injection by parasitic wasps such as *L. boulardi* (Hwang *et al.*, 2007). This escape response is mediated by activation of nociceptive C4da neurons, which possess sensory dendrites covering the entire body wall allowing the animal to detect noxious cues. C4da neurons express several mechanosensory channels belonging to the DEG/ENaC family (pickpocket [ppk], ppk26/balboa) (Zhong *et al.*, 2010; Gorczyca *et al.*, 2014; Guo *et al.*, 2014; Mauthner *et al.*, 2014), a mechanosensitive TrpA1 isoform (Zhong *et al.*, 2012), piezo (Kim *et al.*, 2012) and the Trp channel painless (Tracey *et al.*, 2003), all of which are required for normal mechanonociceptive responses.

The escape response can be assayed by using a von Frey filament exerting a force between 30-120 mN, which activates mechanosensory channels in C4da neurons (Hwang *et al.*, 2007; Kim *et al.*, 2012). Recent work has also shed light on circuit mechanisms required for mechanonociceptive responses. Mechanically induced escape responses require co-activation of class II da (C2da) and class III da (C3da) sensory neurons, as silencing of either subset impaired rolling behavior (Hu *et al.*, 2017). Moreover, this sensory integration is specific for mechanonociception and in addition requires neuropeptide-mediated feedback. We provide a detailed protocol from our recent work (Hu *et al.*, 2017),

which employed a mechanonociception assay based on previously described methods (Hwang *et al.*, 2007; Caldwell and Tracey, 2010; Zhong *et al.*, 2010). We typically use a mechanical force of 45–50 mN, which elicits weak responses after the first stimulus, but enhanced responses after a second subsequent stimulus. This approach allows assaying changes in sensitivity and sensitization of mechanonociceptive responses, which can be coupled with genetic approaches to identify molecular and network components required for normal escape behavior.

Materials and Reagents

1. Drosophila vials (wide, K-Resin) (Dutscher, catalog number: 789002)
2. Flugs® fly plugs, plastic vials (wide) (Dutscher, catalog number: 789035)
3. Omniflex monofilament fishing line Shakespeare (6 lb test, diameter 0.23 mm) (Zebco, Tulsa, USA)
4. Petri dishes (Ø 10 cm) (SARSTEDT, catalog number: 82.1473)
5. Fly stocks
Chromosome, Bloomington stock center No.:
w¹¹¹⁸ (X, BL 6326)
w^{}; ppk-Gal4* (X, 3rd, BL 32079)
w^{}; UAS-TNT^E* (X, 3rd, BL 28997)
w^{}; TrpA1^I* (X, 2nd, BL 36342)
6. Agar Kobe I (Carl Roth, catalog number: 5210.4)
7. Agar plates (see Recipes)
8. Fly food (see Recipes)
 - a. Agar (strings) (Gewürzmühle Brecht, Eggenstein, catalog number: 00262)
 - b. Corn flour (Davert, Newstartcenter, catalog number: 17080)
 - c. Soy flour (Davert, Newstartcenter, catalog number: 46985)
 - d. Brewer's yeast (ground) (Gewürzmühle Brecht, Eggenstein, catalog number: 03462)
 - e. Malt syrup (MeisterMarken–Ulmer Spatz, Bingen am Rhein, catalog number: 728985)
 - f. Treacle (molasses) (Grafschafter Krautfabrik, Meckenheim, catalog number: 01939)
 - g. Nipagin (Methyl 4-hydroxybenzoate) (Sigma-Aldrich, catalog number: 54752-1KG-F)
 - h. Propionic acid (Carl Roth, catalog number: 6026.3)

Equipment

1. Brush (Size 1, Boesner, model: Da Vinci Nova Serie 1570, catalog number: D15701)
2. Forceps (Dumont, #3) (Fine Science Tools, catalog number: 11231-30)
3. Light source (white light) LED Schott KL 1500 LCD (Pulch und Lorenz, catalog number: 150.200)
Manufacturer: SCHOTT, model: KL 1500 LCD.

4. SZX7 stereo microscope (Olympus, model: SZX7)

Software

1. Origin Pro 9.0 (OriginLab, Northampton, USA) or similar for statistical analysis

Procedure

1. All fly stocks were maintained at 25 °C and 70% humidity with a 12 h dark/light cycle on standard fly food. All experiments were performed using 3rd instar larvae at 96 h (hours) after egg laying (AEL). In order to ensure that all larvae were about the same age, the egg laying was restricted to 4-6 h. Experimental crosses were raised on standard fly food at 25 °C with 70% humidity and a 12 h light/12 h dark cycle.
2. Prepare your genetic crosses 2 days before staging with approx. 20-30 virgins and 10-15 males each (more if you are using weak genotypes). After 2 days, transfer flies to a fresh food vial for timed egg-laying for 4-6 h at 25 °C (Figure 1A). Transfer the adult flies to a fresh vial (for another round of staging on the same or next day). The original vial is maintained at 25 °C until 96 ± 3 h AEL. All larvae should be in the third instar (L3) foraging stage and not yet leaving the food (Figure 1B).

Note: Precise staging is important, as nociceptive responses of larvae are reduced after 120 h AEL, likely due to the transition to the wandering stage and preparation for pupariation. The density of larvae in the food will also affect staging: too few animals cannot efficiently process the food, while having too many larvae will result in competition for food, both of which is affecting developmental progression and will broaden the developmental stage of the larval population. In case mutant animals with delayed development are used staging has to be adjusted accordingly (staging either by animal size or molting counting mouth hook teeth).

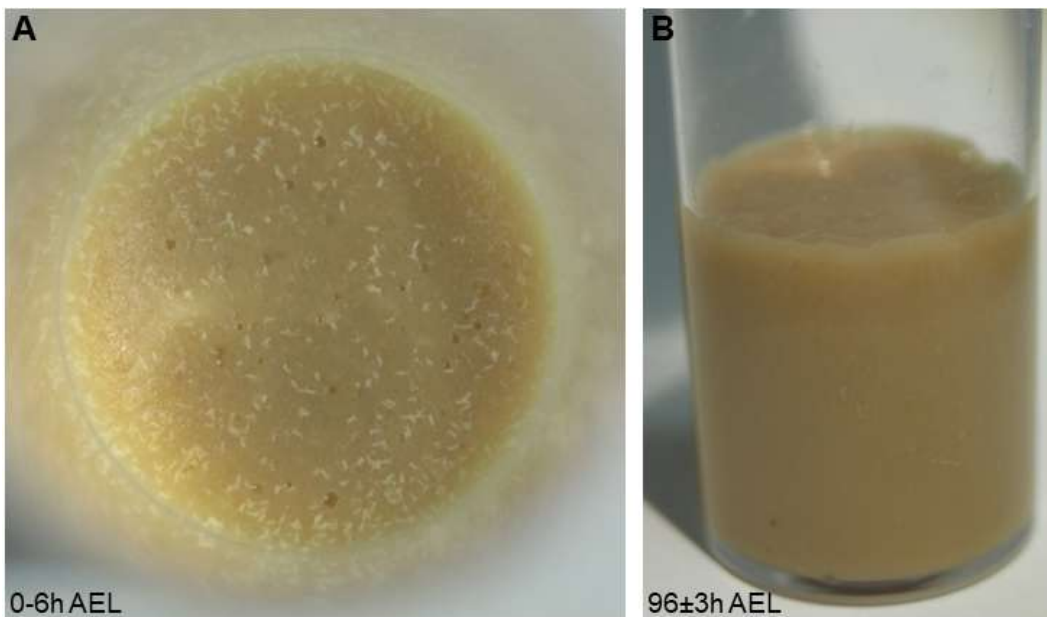


Figure 1. Correct staging and larval density. A. A photograph showing appropriate embryo numbers for the used vial size (approx. 100-150 embryos laid within 4-6 h). B. At 96 h AEL, larvae should have processed the food well and still be in the foraging stage.

3. Tool preparation
 - a. Cut the omniflex monofilament fishing line (Shakespeare, 6 lb test, diameter 0.009 inch [0.23 mm]) to a length of 18 mm. 10 mm is attached to a toothpick such that 8 mm of the fiber protruded from the end of the toothpick (Figure 2A).
 - b. Calibrate the force of the fiber by using it to depress a balance until the fishing line is seen to bend. Record the force (in grams) and convert to milli-Newton (mN) by multiplying the measured grams by a factor of 9.81. Typically, this length of filament results in a force of 45-50 mN (Figures 2B-2D). Varying the filament length will change the mechanical force (the longer, the less the force), which might be desirable if different forces should be tested. The probability of nociceptive responses of larvae increases with the applied force from 30 to 120 mN (Kim *et al.*, 2012; Almeida-Carvalho *et al.*, 2017).
 - c. Examine the filament under a stereoscope and make sure that no sharp edges remain, which might potentially injure the animal. Puncturing the body wall will result in altered behavioral responses.

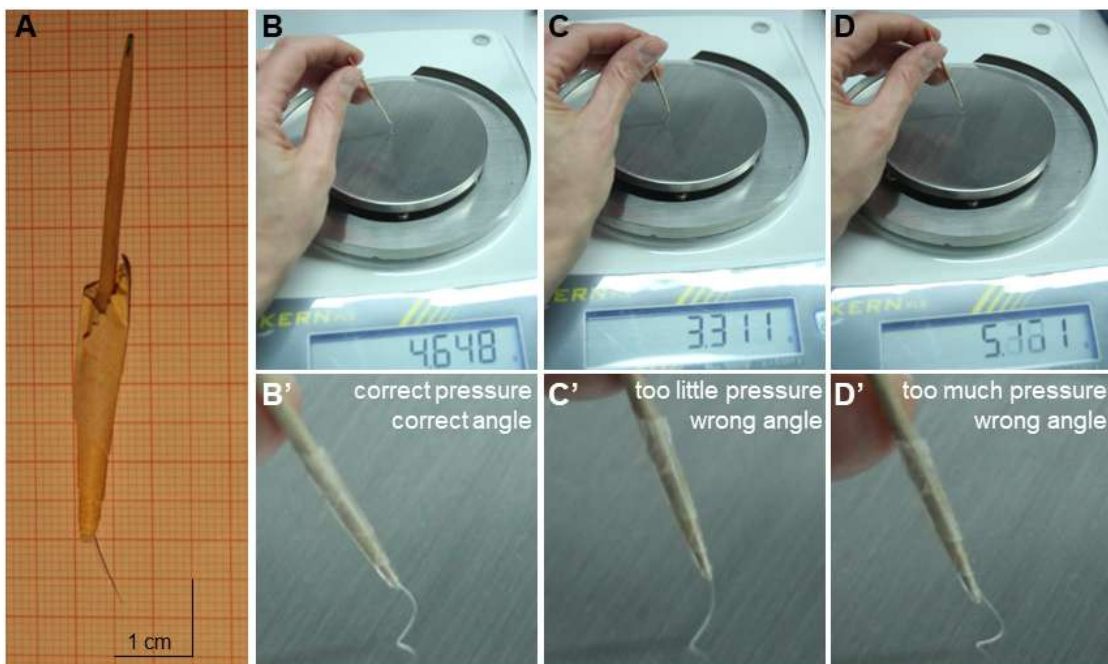


Figure 2. Tool preparation and calibration. A. 8 mm filament attached to toothpick prepared according to instructions above. B-D. Calibrating the filament: the filament should exert a force of 45-50 mN (4.59-5.10 g). B. Repeated depression of the filament should result in comparable forces (here 46 ± 5 mN). B'. Replicable forces are achieved by correct pressure and bending of the filament at the right angle as shown (approx. $45-60^\circ$). C'. Too little pressure and/or wrong angle of deflection result in lower forces. C'. Too much pressure and/or wrong angle of deflection result in too high forces.

4. Distribute 2 ml of dH₂O on a 2% agar plate to create a thin water film, which enables the animals to crawl freely and perform their rolling behavior. Without water, the larvae are not fully mobile and do not display consistent behavioral responses.
5. Prepare 10-20 staged larvae by washing in dH₂O to remove any residual food and place them gently on the agar plate using a brush (Figures 3A-3D).

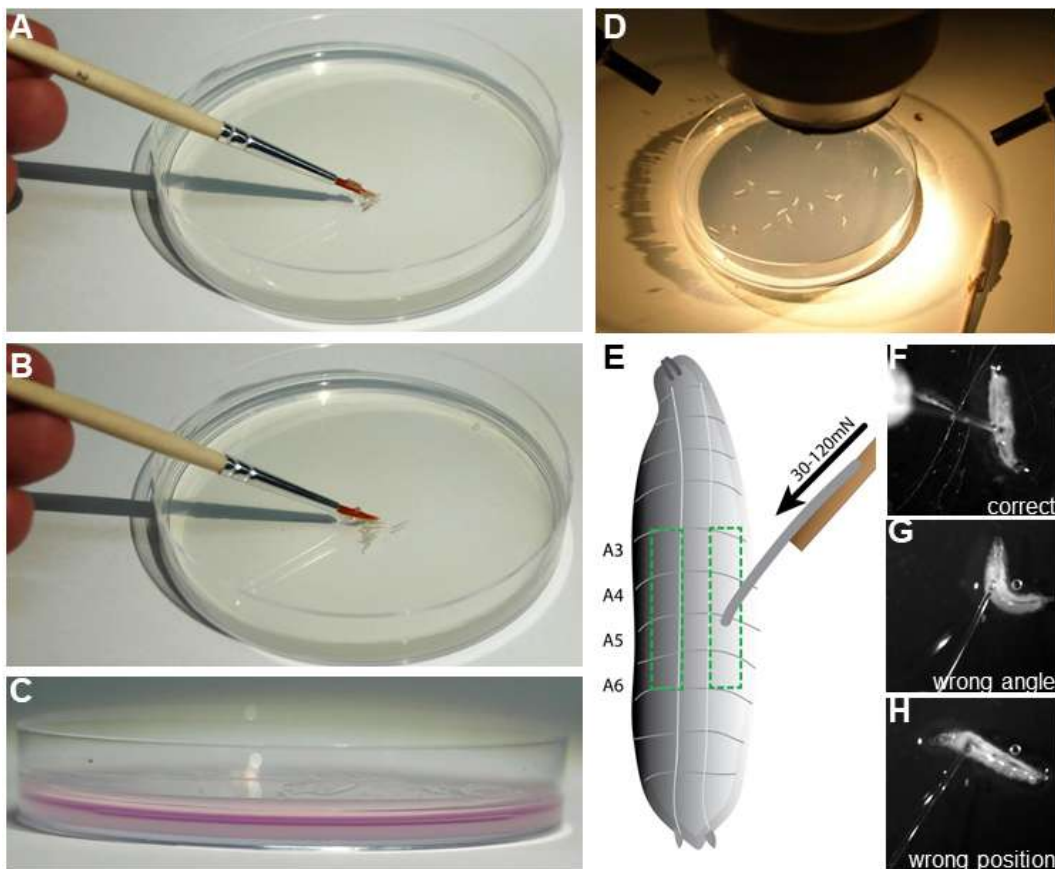


Figure 3. Preparation of mechanonociception assay. A and B. The assay is prepared by gently placing 10-20 staged 3rd instar larvae on a 10 cm 2% agar plate using a brush. C. A thin water film of 2 ml (colored magenta for illustration) is necessary for consistent behavioral responses. D. Agar plate with test animals is placed under a stereoscope with a light source. E. Illustration of a 3rd instar larva. Boxed region indicates the dorsolateral region of abdominal segments A3-A6, which should be targeted with the filament calibrated to the chosen force (30-120 mN). F-H. Examples of correct and incorrect placement of the filament on the larva are shown. F. Correct placement on dorsolateral A3 region. G. Wrong placement with animal moving away from filament resulting in a bad angle for the stimulus. H. Filament placement at an anterior segment which generally does not elicit rolling behavior.

6. Deliver the mechanical stimulus by rapidly depressing the larva with the filament on the dorsal side (abdominal segments four, five, or six) for approximately 1 sec. The quick release allows the larvae to perform escape behavior. Reapply the stimulus to the same larva after a pause of 2-3 sec.
7. Score the response immediately on a scoring sheet according to Hwang *et al.* (2007): no response, stop, stop and turn (non-nociceptive responses), or rolling (nociceptive response); in addition, we introduced bending to score for an incomplete nociceptive response (C-shaped simultaneous convulsive head and tail movements) that did not result in rolling (response classification: 1 = no response, 2 = stop, 3 = stop and turn, 4 = bending, 5 = rolling). A positive

rolling response is scored if at least one 360° rotation along the body axis occurred in response to the mechanical stimulus (Figures 4A-4D; Videos 1 and 2).

Note: To develop and entrain precision in applying the correct force to the animal the experimenter should practice the correct motion on a balance. Hold the toothpick with the filament and depress the filament at a 45-60° angle until it bends, which should result in a consistent force every time. Practicing with control animals will further ensure consistent results. 50-70% of the animals should respond with rolling escape behavior after the 2nd stimulus.

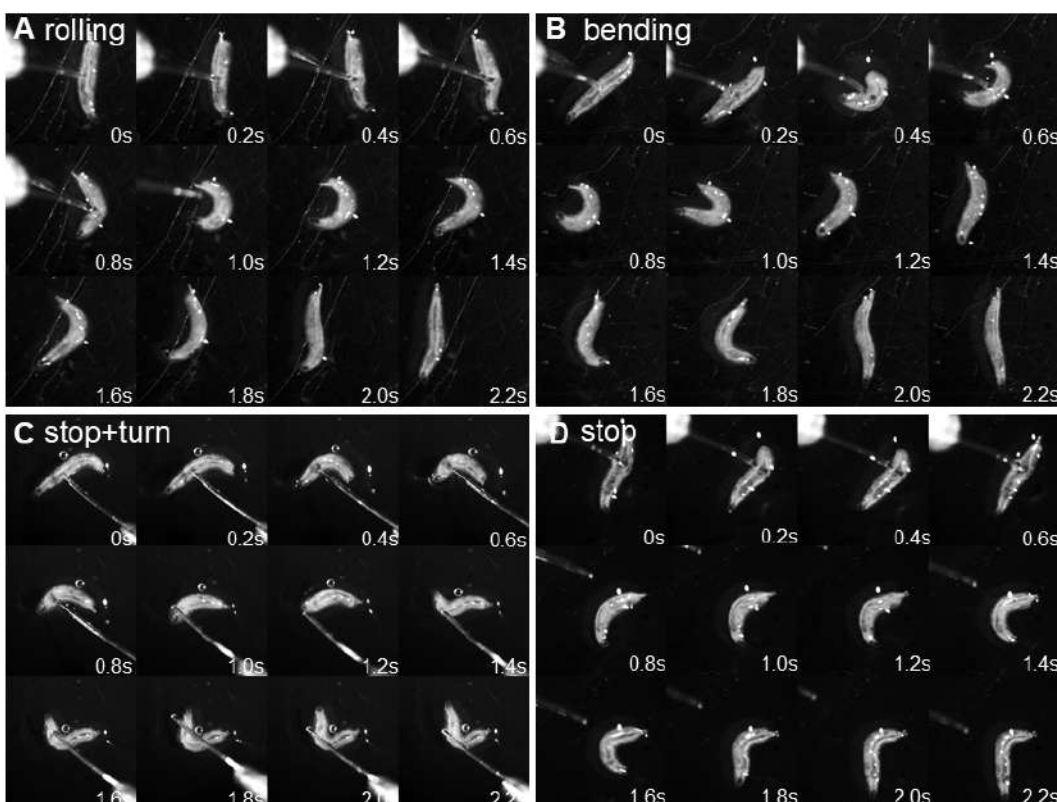
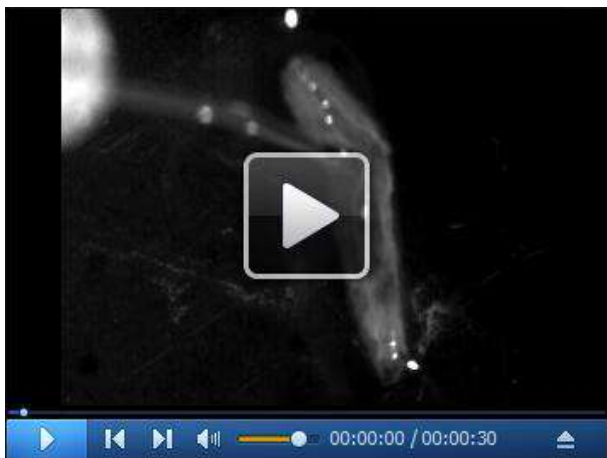


Figure 4. Behavioral responses to mechanonociceptive stimulation. A. Montage of nociceptive rolling response after mechanical stimulation. Note that the larva performs a full 360° roll along the body axis as visible following the main trachea. B. Montage of a partial nociceptive response ('bending') resulting in C-shaped body bending but no full 360° roll. C. Montage of stop and turn response (stop and at least 45° change in direction). D. Montage of stop response (no major change in direction of movement).



Video 1. Behavioral responses to mechanical stimulation using a 50 mN von Frey filament (all 5 categories)



Video 2. Side by side comparison rolling vs. bending

Data analysis

1. Statistical differences in mechanonociceptive responses can be calculated using a χ^2 -test, which allows comparing categorical data between 2 genotypes (e.g., control vs. *TrpA1*¹). Distinguishing only nociceptive and non-nociceptive behaviors allows the use of a 2 x 2 contingency table providing the highest statistical power using a χ^2 -test with 1 degree of freedom. χ^2 can be determined according to the following formula:

$$\chi^2 = \sum_{i=1}^k \frac{(O_i - E_i)^2}{E_i}$$

O: observed values, E: expected value.

The χ^2 -test requires the actual number of animals, as it cannot compute ratios, percentages or frequencies. Most statistics programs (Origin Pro, SigmaPlot, Prism, SAS, Statistica, R) can be used to calculate χ^2 and compute statistical significances.

Note: In cases where more than two genotypes should be compared, appropriate correction for multiple comparisons of statistical significances should be performed, e.g., a Bonferroni correction factor (significant if $p < a/n$, typically with $a = 0.05$ and n being the number of compared hypotheses).

2. At least 60 animals per genotype should be tested to ensure that an effect of 20% or greater is resulting in statistical significance ($P < 0.05$) with sufficient power of the χ^2 -test (> 0.9).

Note: All behavioral experiments should be blinded and randomized to avoid unwanted bias. The genotypes for the mechanonociception assay should be coded (e.g., numbers or letters), with the experimenter being unaware of the genotypes being tested.

Expected results

1. The functionality of the mechanonociception assay can be assessed by inactivation of C4da neurons, either by genetic silencing using Tetanus toxin light chain (*UAS-TnT*), the inward rectifying potassium channel Kir2.1, or genetic mutants of mechano-sensitive channels (e.g., *TrpA1¹*) (Hwang *et al.*, 2007; Zhong *et al.*, 2012; Hu *et al.*, 2017).
2. Performing the mechanonociception assay with *TrpA1¹* mutant larvae showed a decrease in nociceptive responses compared to control *w¹¹¹⁸* larvae (Video 3). After the first stimulation already 76% of control larvae displayed nociceptive responses (bending + rolling behavior) (Figure 5A). In contrast, none of *TrpA1¹* larvae showed nociceptive responses to the mechanical force. Treating the larvae a second time resulted in 85% nociceptive response (50% rolling), whereas only 10% of *TrpA1¹* animals reacted with nociceptive bending but no rolling (Figure 5B).



Video 3. Exemplary behavioral response of *TrpA1¹* animals to mechanical stimulation using a 50 mN von Frey filament

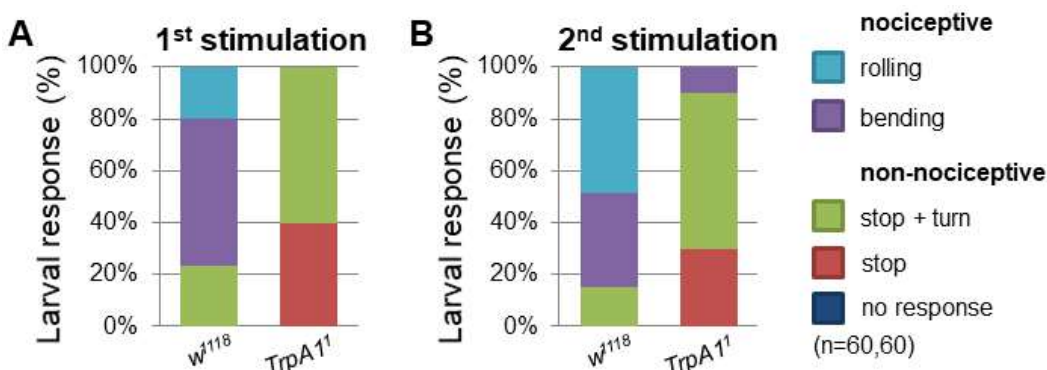


Figure 5. *TrpA1¹* mutant larvae exhibited defects in mechanonociceptive behavior. Response of 3rd instar larvae to a mechanonociceptive stimulus (50 mN). The behavioral response was categorized into nociceptive (rolling, bending) and non-nociceptive responses (stop and turn, stop, no response). Behavioral differences between nociceptive and non-nociceptive behavior of 3rd instar control and *TrpA1¹* larvae after the 2nd stimulation were compared using a χ^2 -test. $P < 0.0001$ (χ^2 -test, 1 degree of freedom, n = 60/genotype).

3. Alternatively, cell type specific genetic manipulation or silencing can be employed to explore circuit function by employing expression of the tetanus toxin light chain (*UAS-TnT*). C4da specific expression of TnT (*ppk-Gal4/UAS-TnT*) resulted in mechanonociceptive defects, displayed by a decrease in nociceptive behavior and an increase in non-nociceptive responses compared to control animals (Figure 6).
4. These results confirmed the experimental design and C4da neuron function in mechanonociception. This approach should allow the identification of genes required for mechanonociception in C4da or downstream neurons of the nociceptive network.

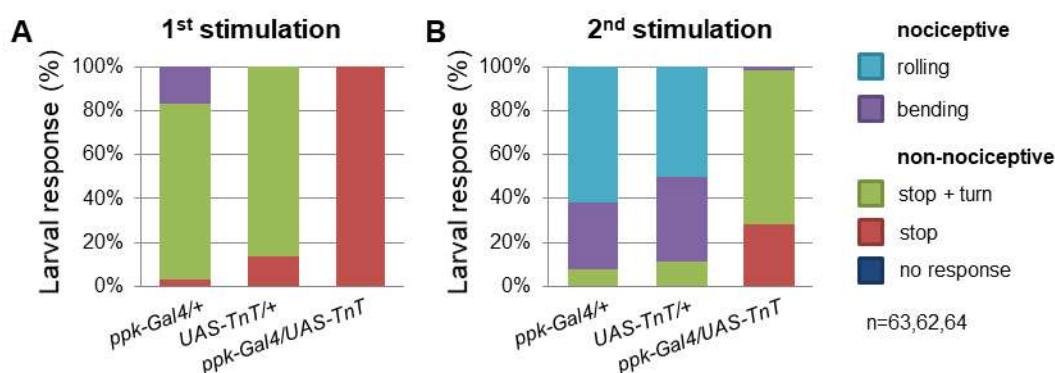


Figure 6. C4da neuron silencing with TnT impairs mechanonociceptive behavior. Percentage of 3rd instar larvae showing categorized responses after mechanonociceptive stimulation (50 mN). Behavioral responses of animals with C4da neuron-specific overexpression of TnT (*ppk-Gal4/UAS-tnt*) and controls were compared. Responses were categorized into nociceptive (rolling, bending) and non-nociceptive responses (stop and turn, stop, no response). Blocking synaptic transmission in C4da neurons by TnT expression

resulted in strong defects in mechanonociceptive responses after the 2nd stimulation. $P < 0.0001^{(\ast\ast\ast)}$ (χ^2 -test, 1 degree of freedom, n = 63, 62, 64).

Notes

Under optimal conditions (proper staging, same filament, etc.) results are highly reproducible between experiments performed on different days and by different trained experimenters. From our experience, tight staging, density-controlled vials and gentle handling of the animals are critical for reproducible results. Behavioral response rates are highly dependent on applying the stimulus consistently and appropriately. Due to the manual procedure it takes practice to be able to consistently stimulate larvae. We recommend practicing with a balance first to ensure that the applied force is constant. Next, practicing with wildtype and mutant larvae displaying impaired mechanonociception (e.g., *TrpA1*¹ mutant larvae) will ensure consistent and reproducible behavioral responses.

Recipes

1. Agar plates

Note: For mechanonociception assays, 2% agar plates were used.

Dissolve Kobe agar I in dH₂O and fill Petri dishes (Ø 10 cm) with a defined volume of 12 ml

2. Fly food

Use the following ingredients for 1 L of standard fly food:

Ingredients for 1 L of standard fly food:

Quantity	Ingredient
8.75 g	Agar (strings)
0.08 g	Corn flour
10 g	Soy flour
25 g	Brewer's yeast (ground)
0.08 g	Malt syrup
21.88 g	Treacle (molasses)
1.88 g	Nipagin (Methyl 4-hydroxybenzoate)
9.38 ml	Propionic acid

Dissolved in 1 L dH₂O

Acknowledgments

This work was supported by the Landesforschungsförderung LFF-FV27 (to P.S.) and the Deutsche Forschungsgemeinschaft priority program SPP1926 (project SO1337/2-1 to P.S.). The authors would like to acknowledge the previous work and effort of several groups developing and applying

mechanonociceptive assays in *Drosophila*, in particular the labs of D. Tracey, A. Patapoutian, Y.N. Jan and Z. Wang. The authors declare that no conflicts of interest or competing interests exist.

References

1. Almeida-Carvalho, M. J., Berh, D., Braun, A., Chen, Y. C., Eichler, K., Eschbach, C., Fritsch, P. M. J., Gerber, B., Hoyer, N., Jiang, X., Kleber, J., Klambt, C., Konig, C., Louis, M., Michels, B., Mirochnikow, A., Mirth, C., Miura, D., Niewalda, T., Otto, N., Paisios, E., Pankratz, M. J., Petersen, M., Ramsperger, N., Randel, N., Risse, B., Saumweber, T., Schlegel, P., Schleyer, M., Soba, P., Sprecher, S. G., Tanimura, T., Thum, A. S., Toshima, N., Truman, J. W., Yarali, A. and Zlatic, M. (2017). [The OI1mpiad: concordance of behavioural faculties of stage 1 and stage 3 *Drosophila* larvae](#). *J Exp Biol* 220(Pt 13): 2452-2475.
2. Caldwell, J. C. and Tracey, W. D. (2010). [Alternatives to mammalian pain models 2: Using *Drosophila* to identify novel genes involved in nociception](#). *Methods Mol Biol* 617: 19-29.
3. Gorczyca, D. A., Younger, S., Meltzer, S., Kim, S. E., Cheng, L., Song, W., Lee, H. Y., Jan, L. Y. and Jan, Y. N. (2014). [Identification of ppk26, a DEG/ENaC channel functioning with Ppk1 in a mutually dependent manner to guide locomotion behavior in *Drosophila*](#). *Cell Rep* 9(4): 1446-1458.
4. Guo, Y., Wang, Y., Wang, Q. and Wang, Z. (2014). [The role of PPK26 in *Drosophila* larval mechanical nociception](#). *Cell Rep* 9(4): 1183-1190.
5. Hu, C., Petersen, M., Hoyer, N., Spitzweck, B., Tenedini, F., Wang, D., Gruschka, A., Burchardt, L. S., Szpotowicz, E., Schweizer, M., Guntur, A. R., Yang, C. H. and Soba, P. (2017). [Sensory integration and neuromodulatory feedback facilitate *Drosophila* mechanonociceptive behavior](#). *Nat Neurosci* 20(8): 1085-1095.
6. Hwang, R. Y., Zhong, L., Xu, Y., Johnson, T., Zhang, F., Deisseroth, K. and Tracey, W. D. (2007). [Nociceptive neurons protect *Drosophila* larvae from parasitoid wasps](#). *Curr Biol* 17(24): 2105-2116.
7. Kim, S. E., Coste, B., Chadha, A., Cook, B. and Patapoutian, A. (2012). [The role of *Drosophila* Piezo in mechanical nociception](#). *Nature* 483(7388): 209-212.
8. Mauthner, S. E., Hwang, R. Y., Lewis, A. H., Xiao, Q., Tsubouchi, A., Wang, Y., Honjo, K., Skene, J. H., Grandl, J. and Tracey, W. D., Jr. (2014). [Balboa binds to pickpocket in vivo and is required for mechanical nociception in *Drosophila* larvae](#). *Curr Biol* 24(24): 2920-2925.
9. Tracey, W. D., Jr., Wilson, R. I., Laurent, G. and Benzer, S. (2003). [Painless, a *Drosophila* gene essential for nociception](#). *Cell* 113(2): 261-273.
10. Xiang, Y., Yuan, Q., Vogt, N., Looger, L. L., Jan, L. Y. and Jan, Y. N. (2010). [Light-avoidance-mediating photoreceptors tile the *Drosophila* larval body wall](#). *Nature* 468(7326): 921-926.
11. Zhong, L., Bellemer, A., Yan, H., Ken, H., Jessica, R., Hwang, R. Y., Pitt, G. S. and Tracey, W. D. (2012). [Thermosensory and nonthermosensory isoforms of *Drosophila melanogaster*](#)

- [TRPA1 reveal heat-sensor domains of a thermoTRP Channel.](#) *Cell Rep* 1(1): 43-55.
12. Zhong, L., Hwang, R. Y. and Tracey, W. D. (2010). [Pickpocket is a DEG/ENaC protein required for mechanical nociception in *Drosophila* larvae.](#) *Curr Biol* 20(5): 429-434.

Barnes Maze Procedure for Spatial Learning and Memory in Mice

Matthew W. Pitts*

Department of Cell and Molecular Biology, John A. Burns School of Medicine, University of Hawaii, Honolulu, HI 96813, USA

*For correspondence: mwpitts@hawaii.edu



[Abstract] The Barnes maze is a dry-land based rodent behavioral paradigm for assessing spatial learning and memory that was originally developed by its namesake, Carol Barnes. It represents a well-established alternative to the more popular Morris Water maze and offers the advantage of being free from the potentially confounding influence of swimming behavior. Herein, the Barnes maze experimental setup and corresponding procedures for testing and analysis in mice are described in detail.

Keywords: Spatial memory, Mouse, Hippocampus, Cognition, Behavior

[Background] The Barnes maze is a dry-land based behavioral test that was originally developed by Carol Barnes to study spatial memory in rats (Barnes, 1979) and later adapted for use in mice (Bach *et al.*, 1995). Conceptually, it is similar to the Morris water maze (MWM) (Morris, 1984), in that it is a hippocampal-dependent task where animals learn the relationship between distal cues in the surrounding environment and a fixed escape location. For mice, the typical Barnes maze setup consists of an elevated circular platform with 40 evenly-spaced holes around the perimeter. An escape tunnel is mounted underneath one hole while the remaining 39 holes are left empty. Both bright light and open spaces are aversive to rodents, thus serve as motivating factors to induce escape behavior. The escape tunnel is maintained at a fixed location for the duration of training, which involves multiple daily trials spread over several days. During the course of training, rodents typically utilize a sequence of three different search strategies (random, serial, spatial) to learn the location of the escape tunnel. Following sufficient acquisition training, the escape tunnel is removed and a probe trial is administered to assess spatial reference memory.

Although the MWM is the dominant model for assessing spatial learning in rodents, the Barnes maze offers several important advantages worth noting. First and foremost, the Barnes maze does not involve swimming and the potential confounding factors associated with it. Swimming is stressful, as detailed in studies documenting that MWM training increases plasma corticosterone levels to a greater extent than that of the Barnes maze (Harrison *et al.*, 2009). In addition, the swim conditions utilized in most MWM protocols elicit reductions in core body temperature that can affect performance (Iivonen *et al.*, 2003). Moreover, rodents often take to floating, which is thought to represent a state of behavioral despair and is considered an index of 'depressive-like' behavior in the widely utilized Porsolt forced swim test (Porsolt *et al.*, 1977). Finally, as noted above, the Barnes maze allows clear delineation of the three possible search strategies used by the mouse during performance of each trial.

Materials and Reagents

1. Tissue paper (Georgia-Pacific Consumer Products, catalog number: 48100)
2. 70% ethanol in a spray bottle
3. C57BL/6J adult male mice (Purchased from Jackson Labs, 3-5 months of age)

Equipment

1. Well-lit (~1,000 lux) testing room with a holding room located nearby (Figure 1A)
2. Barnes maze apparatus (TSE Systems, catalog number: 302050-BM/M), includes:
 - a. Circular PVC platform* (diameter = 122 cm; thickness = 1 cm) containing 40 equally spaced holes (diameter = 5 cm) (Figure 1B)
 - b. Gray PVC start chamber* consisting of a base plate and a cover (Figure 1C)
 - c. PVC escape tunnel* that can be mounted under any of the 40 escape holes (Figure 1D)
 - d. Aluminum support frame* (height = 80 cm) for circular PVC platform (Figure 1E)
3. Overhead camera (Panasonic, catalog number: WV-BP332, Figure 1F)
4. Three distal visual cues (length/width ~30 cm) surrounding the platform (Figure 1G)
5. Loudspeaker for 90 dB white noise (Sony, catalog number: SS-MB150H)
6. Windows-based PC computer (Dell, model: OptiPlex 780) connected to the camera
7. Tally counter

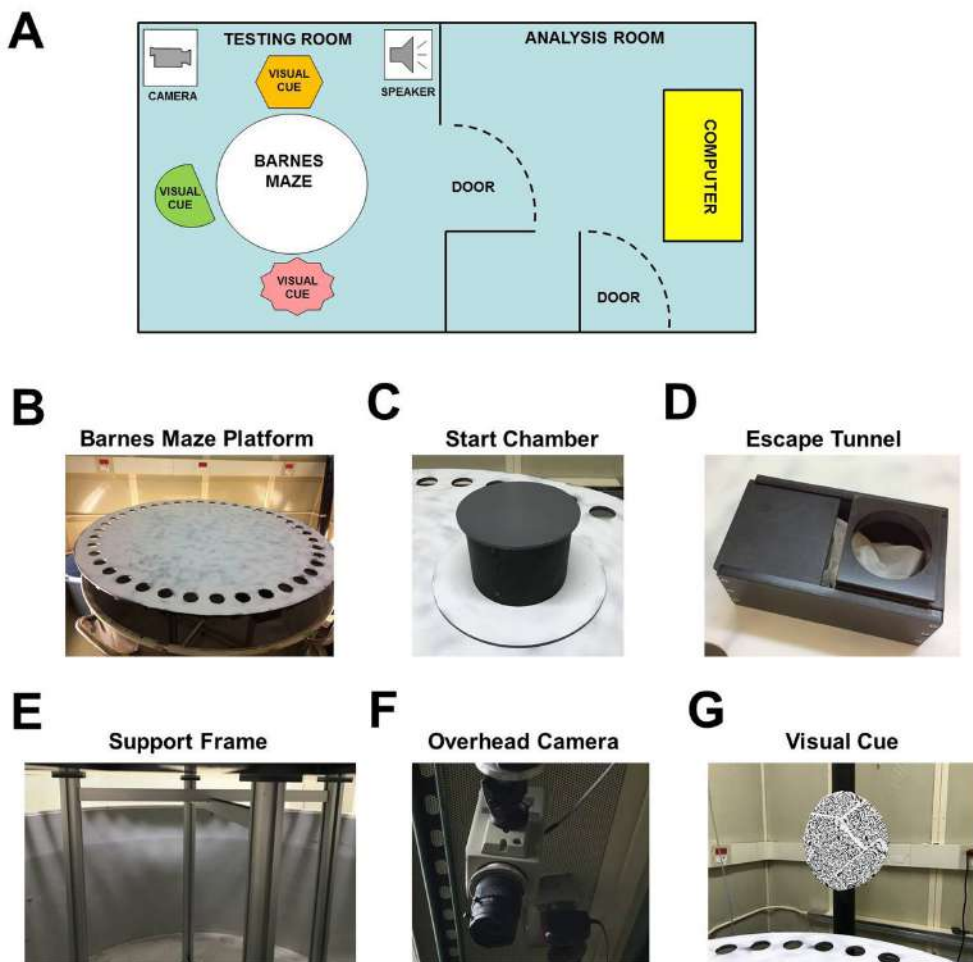


Figure 1. Barnes maze experimental setup. A. Layout of behavioral testing room and adjacent room used for analysis. B-F. Images of the Barnes maze platform (B), start chamber (C), escape tunnel (D), aluminum support frame (E), overhead camera (F), a single visual cue (G).

Software

1. TSE VideoMot2 video tracking software (TSE Systems)
2. GraphPad Prism version 5.0 (GraphPad Software)
3. Microsoft Excel

Procedure

A. Software setup

1. Calibration
 - a. Under the 'Mode' tab located in the upper left corner of VideoMot2 software program, select 'Calibration' (Figure 2).
 - b. Hit the button for 'Calibration'.

- c. Draw a line across the diameter of the Barnes maze platform.
- d. Enter 1,220 mm in the box for 'Real length'. This corresponds to the actual diameter of the Barnes maze.

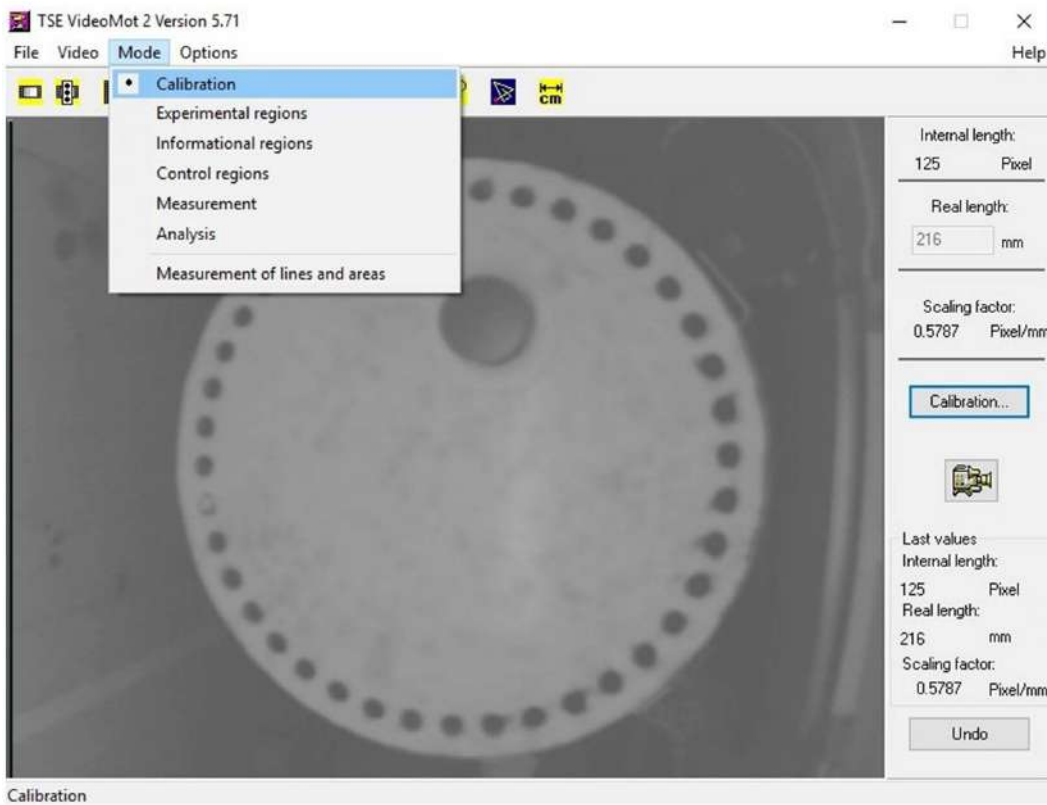


Figure 2. Screenshot of VideoMot2 analysis software

2. Define experimental region
 - a. Under the 'Mode' tab in the VideoMot2 program, select 'Experimental regions'.
 - b. Use the draw tools located at the bottom of the display window to make a circle that covers the entire Barnes platform. This defines the region where the mouse will be tracked by the software.
3. Define informational region
 - a. Under the 'Mode' tab in the VideoMot2 program, select 'Informational regions'.
 - b. Use the draw tools to make a circle around the hole covering the escape tunnel.
4. Measurement
 - a. Select 'Measurement' from the 'Mode' tab.
 - b. Enter 00:03:00 in the white box to the right of the text 'Autostop at'. Make sure that the white box to the left of the 'Autostop at' text is checked off. This will insure that the video tracking software automatically stops each trial after 3 min.
 - c. Click on the 'Start' button located in the lower right corner of the display window.
 - d. Enter relevant study information (Study number, etc.) when prompted.

- e. Click the spacebar once to start the background measurement and then again to conclude it. During the background measurement, make sure that there is no movement or change in lighting in view of the camera.
- f. Enter trial data (Animal #, Group) when prompted.
- g. Click the spacebar once to begin tracking the mouse. In the video display, a cross will be superimposed on the mouse's body and will follow its movements in the maze. Click the spacebar again to end the trial.
- h. To save data for each trial, select 'Save track as' under the 'File' tab located in the upper left corner of the screen.

B. Barnes maze procedure (Figure 3)

1. Habituation (Day 1)
 - a. Attach the escape tunnel to the platform and add one piece of clean tissue paper for each mouse habituation trial. The surrounding visual cues should be in place. These cues should remain unaltered for the habituation, acquisition, and probe trial phases.
 - b. Place mouse in the escape tunnel for 1 min.
 - c. Put mouse in the center of the apparatus. Allow it to explore until it enters the escape tunnel or 5 min elapses.
 - d. Clean the apparatus and escape tunnel with 70% ethanol
2. Acquisition training (Days 1-10)
 - a. Allow an interval of at least 1 h between habituation and the onset of acquisition training. Attach the escape tunnel to the platform at a location different from that used for the habituation trial. The position of the escape tunnel remains at this fixed location relative to spatial cues in the room for the duration of training. Add one piece of clean tissue paper to the escape tunnel for each mouse acquisition trial.
 - b. Training consists of two acquisition trials daily (3 min limit per trial; intertrial interval ~1 h) with the starting location varied pseudorandomly among the four quadrants.
 - c. At the start of each trial, the mouse is placed in a gray PVC start chamber located in the center of one of the four quadrants. After a 15 sec period, the start chamber is lifted (Figure 3B), and the mouse is allowed to explore the maze. During each trial, loud white noise (90 dB) is played through a loudspeaker to induce escape behavior. The trial concludes when the mouse enters the escape tunnel (Figure 3D) or 3 min elapses. If a mouse fails to find the escape tunnel within the 3 min period, it is placed in the tunnel by the researcher and allowed to stay there for 15 sec prior to removal.

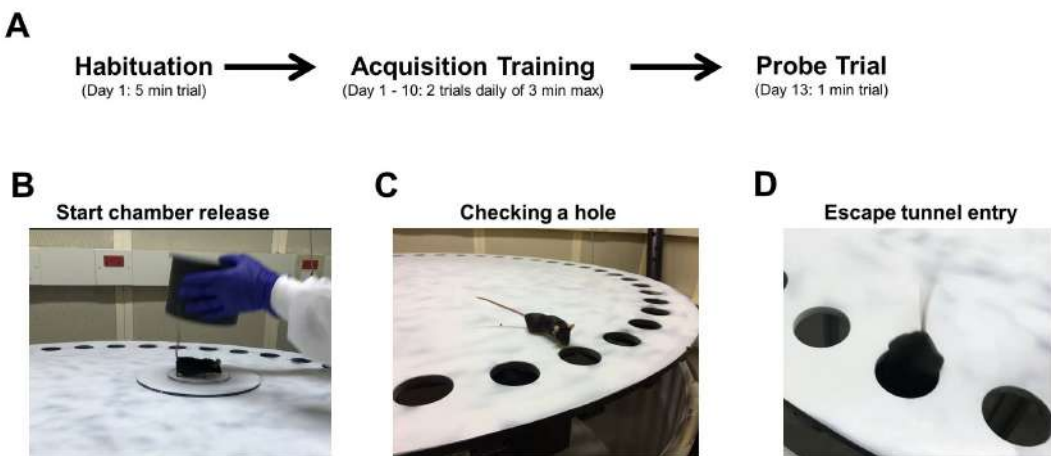


Figure 3. Barnes maze procedure. A. Experimental timeline; B-D. Images of a mouse being released from the start chamber (B), checking a hole (C), and entering the escape tunnel (D).

- d. Following each trial, the maze and escape tunnel are cleaned with 70% ethanol.
 - e. For each trial, a number of parameters are recorded to assess performance. These include the latency to locate (primary latency) and enter (total latency) the escape tunnel, along with the number of incorrect holes checked prior to locating (primary errors) and entering (total errors) the tunnel. Errors are defined as checking any hole that does not contain the escape tunnel and are scored live using a tally counter. The distance traveled (path length) prior to locating the escape tunnel and total distance for each trial are also chronicled. In addition, we also make note of the location of the first hole checked relative to the escape tunnel (primary hole distance) by a given mouse during each trial. For this measure, values range from 0 (target hole) to 20 (directly opposite the target hole). Finally, for each trial, the search strategy is classified as spatial, serial, or random (Figure 4). Trials where mice have scores of 3 or less for both primary errors and primary hole distance are defined as spatial searches (Video 1). Trials in which mice spent the majority of the time on the periphery performing systematic hole searches in a clockwise or counterclockwise manner are classified as a serial searches (Video 2). All other trials are considered random searches, including those in which mice failed to enter the escape tunnel within the 3-min trial period (Video 3).

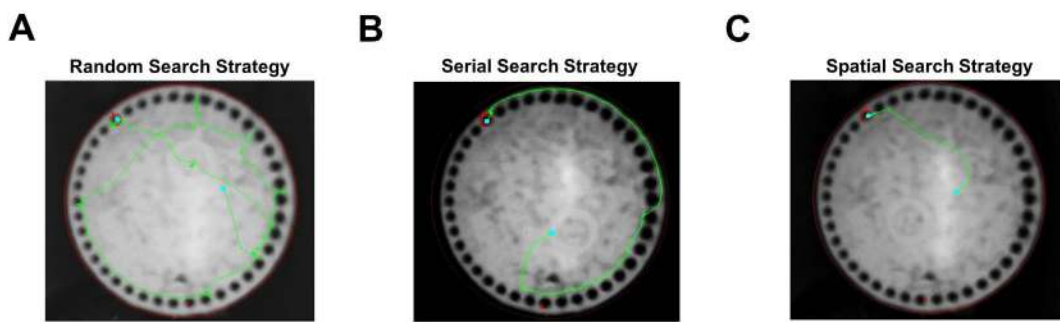


Figure 4. Barnes maze search strategy. A-C. Tracking data from individual trials that were classified as random (A), serial (B), and spatial searches (C).



Video 1. Spatial search strategy



Video 2. Serial search strategy



Video 3. Random search strategy

3. Probe trial
 - a. Three days after the final session of acquisition training, mice undergo a 1 min probe trial in which the escape tunnel is removed from the apparatus.
 - b. The probe trial is administered in a similar manner to the acquisition trials, except that the start chamber is placed in the center of the apparatus, rather than the center of any given quadrant.
 - c. For the probe trial, the latency and distance traveled (path length) prior to reaching to previous escape tunnel location are recorded, along with the primary hole distance, total distance traveled, number of target hole checks, and number of incorrect holes checks.

Data analysis

1. Under the 'Mode' tab in the VideoMot2 program, select 'Analysis'.
2. Under the 'File' tab, select the chosen file to be analyzed.
3. Recorded data can be examined using the video player located in the lower right hand corner of the software program. Here the experimenter can determine and/or review the number of errors and target hole distance as well as classify the search strategy.
4. Click on the 'Protocol' button situated in the lower right hand corner of the software program. This will open a new display that contains data for latency to target (primary latency) and distance traveled.
5. After all relevant data for each trial is tabulated from VideoMot2, it is then consolidated into trial blocks using Microsoft Excel. Each trial block consists of four trials conducted over two consecutive days with one start location in each of the four quadrants. Mean values for each trial block are imported into GraphPad Prism 5.0 to generate graphs and to determine whether statistically significant differences exist between groups.
6. Figure 5 displays graphs for measures of primary latency (A), primary errors (B), and primary hole distance (C) that compare groups of wild-type and knockout mice. Both groups showed

similar decreases in all three measures with increased training, indicating that spatial learning occurred. Other Barnes maze parameters that are often graphed include path length, average speed, percentage of failed trials (3 min without finding escape tunnel), and percentage of trials using a spatial search strategy.

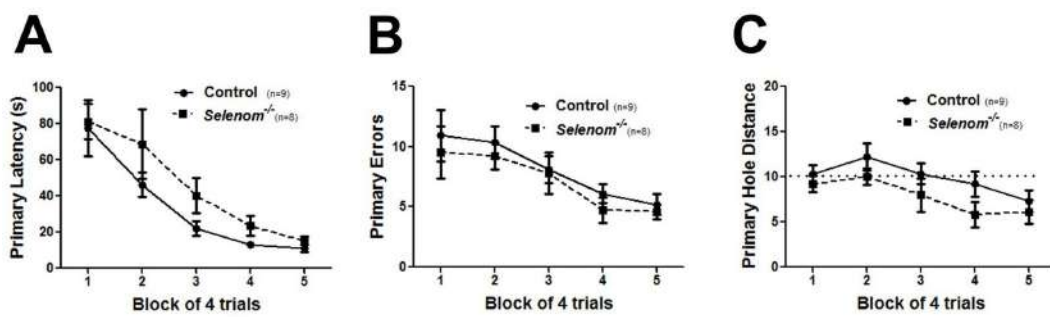


Figure 5. Barnes maze data presentation. A-C. Graphs for measures of primary latency (A), primary errors (B), and primary hole distance (C) that compare performance between groups of wild-type and knockout mice. For primary hole distance, the dotted line indicates random chance performance (score = 10).

Notes

1. One potential drawback of the Barnes maze is that the lack of stressful stimuli can result in slow learning. To provide mild stress and increase motivation for escape, we play 90 dB white noise through a loudspeaker during all trials. Other groups have used buzzer noise in a similar manner to induce escape behavior (Bach *et al.*, 1995; O’Leary and Brown, 2012).
2. It should also be noted that pharmacological and/or genetic manipulations that increase anxiety could act as confounding factors on Barnes maze performance. However, this potential confound appears to be of greater concern for the MWM than the Barnes maze. For example, one study used both the MWM and the Barnes maze to assess spatial learning in neurogranin null mice, a mutant strain with increased anxiety. These mice were unable to reach acquisition criterion on the MWM, but were able to do so for the Barnes maze (Miyakawa *et al.*, 2001). Nevertheless, when testing mice with increased anxiety on the Barnes maze, decreasing the light intensity would be one possible remedy to minimize the confounding influence of anxiety.
3. In addition to the procedure outlined above, we have also used a version with more extensive acquisition training that included 40 trials spread over 20 days (Pitts *et al.*, 2013). In our studies, we have found that wild-type C57BL/6J mice develop a spatial preference after 15-20 acquisition trials, as indicated by primary hole distances significantly less than 10 (random chance). Further training results in decreasing primary hole distances and an increasing percentage of spatial search strategies. However, this additional training can also have a saturating effect, as cognitively impaired mice may eventually catch up with that of normal mice. There is no clear consensus among researchers as to when acquisition training should end. In

the initial paper adapting the Barnes maze for use in mice, researchers kept testing a given mouse until it made 3 errors or less on 7 out of 8 consecutive trials (Bach *et al.*, 1995). For wild-type mice used in this study, the median time to meet this criteria was 22 days on a training regimen of one trial daily. In the published literature since that time, the typical range is 15-30 acquisition trials (Seeger *et al.*, 2004; Patil *et al.*, 2009; O'Leary *et al.*, 2011 and 2012) before administering the probe trial.

4. Our experience with the Barnes maze is limited to the use of young (3-5 months of age) adult C57BL/6J mice. We have found that rates of learning can vary substantially between individual mice within a given group. Due to this variability, we recommend a group size of 10-12 mice (matched for age and gender) in order to accurately compare performance between groups on this task. In terms of gender differences, we have observed that males adopt a spatial search strategy to a greater degree than females as training progresses. Moreover, it also should be noted that other groups have reported significant differences in Barnes maze performance with respect to mouse background strain (O'Leary *et al.*, 2011) and age (Kesby *et al.*, 2015).
5. Following administration of the probe trial, training can be further extended to examine reversal learning (Seeger *et al.*, 2004). For reversal learning, the escape tunnel is moved to a location directly opposite the initial target site. Training proceeds in an analogous manner to that described above for initial acquisition and the same parameters are measured.

Acknowledgments

Our laboratory used this protocol to assess spatial learning in mice in two recent publications (Pitts *et al.*, 2013 and 2015). That work was supported by NIH grants G12 MD007601, R01 DK47320 (Marla J. Berry), and Pilot Project Award funds from G12 MD007601 to M.W.P. The author thanks Ann Hashimoto, Ting Gong, Daniel Torres, and Tessi Sherrin for helping obtain the images and video that accompany this manuscript. The author declares that there are no any conflicting and/or competing interests.

References

1. Bach, M. E., Hawkins, R. D., Osman, M., Kandel, E. R. and Mayford, M. (1995). [Impairment of spatial but not contextual memory in CaMKII mutant mice with a selective loss of hippocampal LTP in the range of the theta frequency](#). *Cell* 81(6): 905-915.
2. Barnes, C. A. (1979). [Memory deficits associated with senescence: a neurophysiological and behavioral study in the rat](#). *J Comp Physiol Psychol* 93(1): 74-104.
3. Harrison, F. E., Hosseini, A. H. and McDonald, M. P. (2009). [Endogenous anxiety and stress responses in water maze and Barnes maze spatial memory tasks](#). *Behav Brain Res* 198(1): 247-251.

4. Kesby, J. P., Kim, J. J., Scadeng, M., Woods, G., Kado, D. M., Olefsky, J. M., Jeste, D. V., Achim, C. L. and Semenova, S. (2015). [Spatial cognition in adult and aged mice exposed to a high-fat diet](#). *PLoS One* 10(10): e0140034.
5. Iivonen, H., Nurminen, L., Harri, M., Tanila, H. and Puolivali, J. (2003). [Hypothermia in mice tested in Morris water maze](#). *Behav Brain Res* 141(2): 207-213.
6. Miyakawa, T., Yared, E., Pak, J. H., Huang, F. L., Huang, K. P. and Crawley, J. N. (2001). [Neurogranin null mutant mice display performance deficits on spatial learning tasks with anxiety related components](#). *Hippocampus* 11(6): 763-75.
7. Morris, R. (1984). [Developments of a water-maze procedure for studying spatial learning in the rat](#). *J Neurosci Methods* 11(1): 47-60.
8. O'Leary, T. P. and Brown, R. E. (2012). [The effects of apparatus design and test procedure on learning and memory performance of C57BL/6J mice on the Barnes maze](#). *J Neurosci Methods* 203(2): 315-324.
9. O'Leary, T. P., Savoie, V. and Brown, R. E. (2011). [Learning, memory and search strategies of inbred mouse strains with different visual abilities on the Barnes maze](#). *Behav Brain Res* 216(2): 531-42.
10. Patil, S. S., Sunyer, B., Hoger, H. and Lubec, G. (2009). [Evaluation of spatial memory of C57BL/6J and CD1 mice in the Barnes maze, the Multiple T-maze, and the Morris water maze](#). *Behav Brain Res* 198(1): 58-68.
11. Pitts, M. W., Kremer, P. M., Hashimoto, A. C., Torres, D. J., Byrns, C. N., Williams, C. S. and Berry, M. J. (2015). [Competition between the brain and testes under selenium-compromised conditions: Insight into sex differences in Selenium metabolism and risk of neurodevelopmental disease](#). *J Neurosci* 35(46):15326-38.
12. Pitts, M. W., Reeves, M. A., Hashimoto, A. C., Ogawa, A., Kremer, P., Seale, L. A. and Berry, M. J. (2013). [Deletion of selenoprotein M leads to obesity without cognitive deficits](#). *J Biol Chem* 288(36): 26121-26134.
13. Porsolt, R. D., Le Pichon, M. and Jalfre, M. (1977). [Depression: a new animal model sensitive to antidepressant treatments](#). *Nature* 266(5604): 730-732.
14. Seeger, T., Fedorova, I., Zheng, F., Miyakawa, T., Koustova, E., Gomeza, J., Basile, A. S., Alzheimer, C. and Wess, J. (2004). [M2 muscarinic acetylcholine receptor knock-out mice show deficits in behavioral flexibility, working memory, and hippocampal plasticity](#). *J Neurosci* 24(45): 10117-10127.

Spared Nerve Injury Model of Neuropathic Pain in Mice

Joseph Cichon¹, Linlin Sun^{2, 3} and Guang Yang^{2, 3, *}

¹Department of Anesthesiology and Critical Care, University of Pennsylvania, Philadelphia, Pennsylvania, USA; ²Department of Anesthesiology, Perioperative Care and Pain Medicine, New York University School of Medicine, New York, New York, USA; ³Neuroscience Institute, New York University School of Medicine, New York, New York, USA

*For correspondence: guang.yang@med.nyu.edu



[Abstract] Experimental models of peripheral nerve injury have been developed to study mechanisms of neuropathic pain in living animals. The spared nerve injury (SNI) model in rodents is a partial denervation model, in which the common peroneal and tibial nerves are injured, producing consistent and reproducible tactile hypersensitivity in the skin territory of the spared, intact sural nerve. SNI-operated mice require less force applied to the affected limb to elicit a withdrawal behavior as compared to sham mice. This effect is observed as early as 2 days after surgery and lasts for at least 1 month. We describe detailed surgical procedures to establish the SNI mouse model that has been widely used for investigating mechanisms of neuropathic pain.

Keywords: Mouse pain model, SNI surgery, Peripheral nerve injury, Sciatic nerve, Neuropathic pain

[Background] Partial nerve injury animal models have been developed for the purpose of studying the molecular, cellular, and circuit mechanisms of neuropathic pain (Bennett and Xie, 1988; Seltzer *et al.*, 1990; Kim and Chung, 1992). A partial denervation model enables researchers to investigate structural and functional changes in diverse groups of neuronal and non-neuronal cells. Studies can be performed during the initiation, progression (also known as acute) and maintenance (chronic) phases of neuropathic pain, as well as at different anatomical sites along the pain pathway including distal vs. proximal peripheral nerve fibers, dorsal root ganglion, spinal cord, subcortical and cortical areas. The spared nerve injury (SNI) model involves partial nerve injury where the common peroneal and tibial nerves are injured, producing consistent and reproducible pain hypersensitivity in the territory of the spared sural nerve (Decosterd and Woolf, 2000; Shields *et al.*, 2003). This model has proved to be robust, demonstrating substantial and prolonged changes in behavioral measures of mechanical sensitivity and thermal responsiveness (Bourquin *et al.*, 2006). These features closely mimic the cardinal symptoms of clinically described neuropathic pain disorders.

Materials and Reagents

1. Cotton-wool applicator
2. Double edge razor blades (Baili, catalog number: BP005)
3. Povidone-Iodine Prep Pad (Dynarex, catalog number: 1108)

4. 6-0 nylon suture (Surgical Specialties, Look, catalog number: 916B)
5. 8-0 nylon suture (Fine Science Tools, catalog number: 12051-08)
6. C57BL/6J male mice, 8-12 weeks of age (THE JACKSON LABORATORY, catalog number: 000664)
7. Sterile Lubricant Eye Ointment (Stye)
8. Ketamine hydrochloride (Ketathesia, NDC 11695-0702-1)
9. Xylazine Sterile Solution (AnaSed, NDC 59399-110-20)
10. Sterile saline
11. Ketamine and xylazine (KX) mixture (see Recipes)

Equipment

1. Stereomicroscope (Olympus, model: SZX10)
2. LED surgical light (Schott ACE light source with EKE lamp, Schott, model: A20500)
3. Dissecting scissors and forceps (Fine Science Tools, catalog numbers: 14094-11, 14084-09, 15000-08, 11150-10)
4. Fine forceps (Fine Science Tools, catalog number: 11253-20)
5. Vannas spring scissors (Fine Science Tools, catalog number: 15000-08)
6. Electronic von Frey Anesthesiometer (IITC Life Science, catalog number: 2392)

Procedure

Note: All procedures in this study were approved by the New York University School of Medicine Institutional Animal Care and Use Committee (IACUC) as consistent with the National Institute of Health (NIH) Guide for the Care and Use of Laboratory Animals to ensure minimal animal use and discomfort.

A. Spared nerve injury surgery

1. Anesthetize mice with a mixture of KX (0.1 ml/20 g mouse, intraperitoneal injection).
Note: Assess depth of anesthesia with hindlimb or tail pinch. An animal deeply anesthetized does not react to stimulus. The mouse should be placed on a heating blanket for the maintenance of normothermia while undergoing anesthesia.
2. Apply ophthalmic ointment to the eyes with a cotton-wool applicator.
3. Shave the skin on the lateral surface of the left thigh using a razor blade (Figure 1A) followed by topical application of povidone-iodine prep pad.
4. Make a single, small skin incision at the mid-thigh level with fine scissors (#14094-11) using the femur as a landmark (Figure 1B) and make blunt dissection using the dull portion of the dissection scissors (# 14084-09) through the biceps femoris muscle (BFM) (Figure 1C). Expose the sciatic nerve and its three branches (Figure 1D).

Note: Perform minimal retraction when exposing the sciatic nerve and its three branches. If there is accidental bleeding from the operation site, apply proper pressure with a cotton bud until coagulation. If bleeding persists, the mouse should not be used for further experiments.

5. For the SNI operation, distal to the trifurcation of the sciatic nerve, ligate the common peroneal and tibial nerves using 8-0 nylon suture (Figures 1E and 1F) and axotomize with Vannas spring scissors (#15000-08), removing a 2-4 mm piece of each distal nerve stump (Figure 1G). Keep the sural nerve intact (Figures 1E-1G). Avoid any stretching or contact with the spared sural nerve. In the sham operation, the aforementioned manipulations of the sciatic nerve and its branches are not performed.
6. Close incisions with muscle and skin sutures (Figure 1H).

Note: The SNI surgery can be performed in both mice and rats for the study of neuropathic pain.

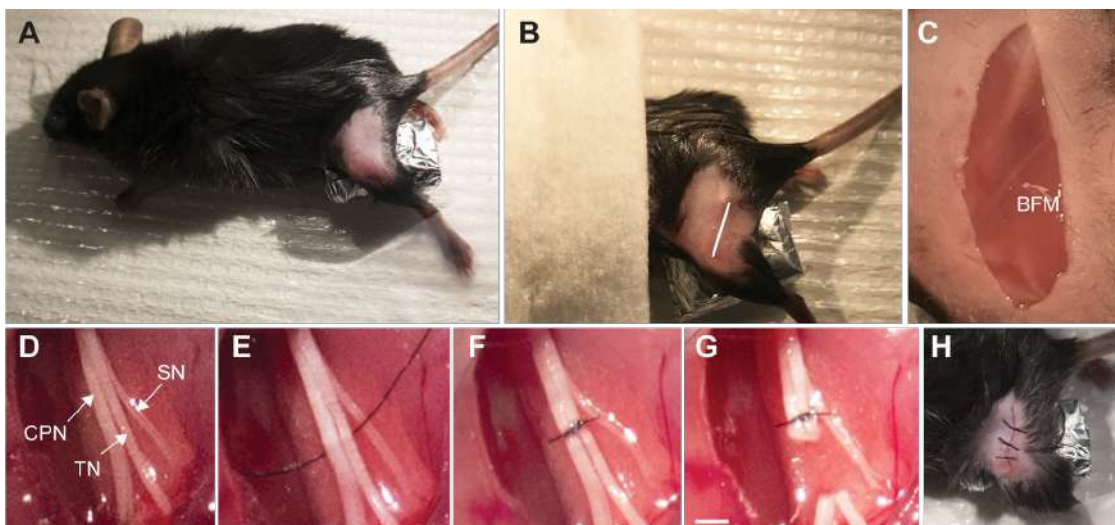


Figure 1. Spared nerve injury surgical procedure to induce neuropathic pain in mice. A. Mouse was anesthetized with KX and positioned prone. Surgical area was then shaved and disinfected. The paw was abducted and elevated from the table. B. White line indicates the incision site on left hindlimb or thigh. C. Following the incision along the white line, the biceps femoris muscle (BFM) was exposed and a careful blunt dissection was made through to expose the trifurcation of the sciatic nerve. D. Exposure of the sciatic nerve and peripheral branches: common peroneal (CPN), tibial (TN) and sural nerves (SN). E. An 8-0 nylon suture was passed under the common peroneal and tibial nerves. F. Ligation of the common peroneal and tibial nerves was performed with a surgical knot. G. The ligated nerves were transected distally and a 2 mm section was removed to prevent nerve regeneration. The surgical steps in panels E-G were not performed in the sham operation. Care was taken to avoid contact with the sural nerve. Scale bar = 2 mm. H. Muscles were reapproximated, followed by overlying skin. The skin was closed with 6-0 nylon suture with at least 3 individual knots along the incision.

7. The SNI-operated animals should have normal food intake, growth, display regular movements, and grooming.

Note: Behavior testing can be performed immediately following recovery from anesthesia.

B. Behavior testing

The von Frey test is used to assess the onset and maintenance of mechanical allodynia over time.

1. Animals were placed in clear plexiglass cages on an elevated mesh floor and tested after 30 min of habituation (Figure 2A).

Note: During the 30-min habituation before behavior testing, place a small amount of food in testing chambers to help the mice readjust to a new environment, which also lessens their general activity.

2. In all animal groups, mechanical paw withdrawal threshold was examined using an electronic von Frey anesthesiometer (Figure 2B) with #8 flexible von Frey hair which delivers force up to 11 g (Figure 2C). The anesthesiometer displays the actual force at which paw withdrawal behavior occurs. To perform measurements, first ensure that von Frey hair is securely attached to the anesthesiometer probe. Second, clear the reading on the anesthesiometer before the measurement. Third, direct the von Frey hair through the mesh floor to the lateral plantar aspect (the sural nerve skin territory) of the hind paw (Figure 2D) and record the force displayed.

3. Three trials of withdrawal per paw were recorded with intervals of 5 min in between measurements. An average was reported for each day tested (as shown in Figure 2E).

Note: The von Frey test should be performed during the light cycle by the same researcher, who should be blinded to the surgery and treatments.

4. After SNI, behavioral tests were performed at designated time points (e.g., 2, 7, 14 and 28 days) after surgery (Figure 2E).

Note: The course of SNI-induced neuropathic pain in mice is usually divided into development (1-7 days) and maintenance (8-14 days) phases. Depending on the purpose of each study, behavior tests should be planned accordingly.

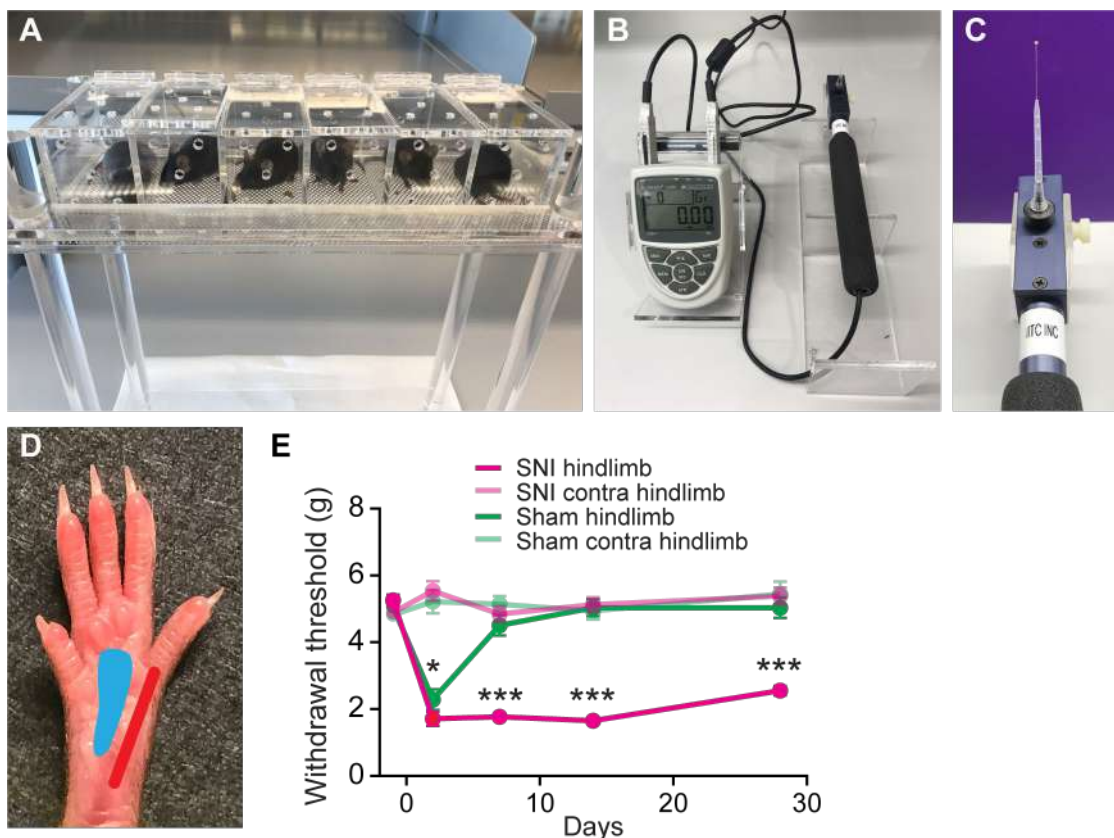


Figure 2. Measuring hindlimb paw withdrawal threshold before and after SNI. A. SNI and sham-operated mice were placed in plexiglass cages on an elevated mesh platform for paw access. B and C. Electronic von Frey anesthesiometer with #8 von Frey hair. D. Plantar view of the left hindlimb paw from a mouse after SNI operation. The red area on the photograph corresponds to the sural nerve skin territory that was tested with the von Frey hair, while the blue area corresponds to the tibial nerve skin territory, which was denervated from SNI surgery and should not be tested during the test. E. Paw withdrawal threshold measured in grams from ipsilateral and contralateral hindlimbs in both SNI and sham-operated mice over 1 month (Two-way ANOVA followed by Tukey's test; 2 day: $P = 0.025$; 7 day: $P < 0.001$; 14 day: $P < 0.001$; 31 day: $P < 0.001$. $n = 17$ in SNI group, and $n = 12$ in sham group) (Cichon *et al.*, 2017).

Data analysis

A complete description of statistics used for analyzing von Frey behavioral experiments is presented in Cichon *et al.* (2017).

Notes

1. Positive aspects: SNI surgery is a simple procedure to carry out and can be performed by researchers with some surgical experience. Also, following SNI surgery, mice reliably display mechanical hypersensitivity as early as 2 days after injury, and develop long-term hypersensitivity for at least 30 days. Sham-operated mice initially show increased mechanical sensitivity (e.g., 2 days after surgery), which could be related to the surgical inflammation, but should return to baseline levels within days (Figure 2E). Cortical neurons in the awake behaving SNI/sham mice could be imaged with two-photon microscopy (Yang *et al.*, 2013; Cichon *et al.*, 2017). Thus, experiments can be performed to study mechanisms for the initiation, progression and maintenance of neuropathic pain.
2. Negative aspects: SNI model induces lesions in the peroneal and tibial nerves, leaving the sural nerve intact. Because the sural nerve innervates the skin on the lateral aspect of the hind paw (Figure 2D), experience and repetitive measurements are required to improve the accuracy and precision of paw withdrawal testing.

Recipes

1. Ketamine and xylazine mixture

To make 50 ml of KX:

10 ml ketamine (100 mg/ml)

7.5 ml xylazine (20 mg/ml)

32.5 ml of sterile saline (0.9% NaCl), mix well

Store it away from light exposure and at room temperature

Acknowledgments

This protocol is adapted from the previously published paper (Cichon *et al.*, 2017). This work was supported by National Institutes of Health grants R01GM107469 and R21NS106469 to G.Y. The authors have nothing to disclose.

References

1. Bennett, G. J. and Xie, Y. K. (1988). [A peripheral mononeuropathy in rat that produces disorders of pain sensation like those seen in man](#). *Pain* 33(1): 87-107.
2. Bourquin, A. F., Suveges, M., Pertin, M., Gilliard, N., Sardy, S., Davison, A. C., Spahn, D. R. and Decosterd, I. (2006). [Assessment and analysis of mechanical allodynia-like behavior induced by spared nerve injury \(SNI\) in the mouse](#). *Pain* 122(1-2): 14 e11-14.

3. Cichon, J., Blanck, T. J. J., Gan, W. B. and Yang, G. (2017). [Activation of cortical somatostatin interneurons prevents the development of neuropathic pain.](#) *Nat Neurosci* 20(8): 1122-1132.
4. Decosterd, I. and Woolf, C. J. (2000). [Spared nerve injury: an animal model of persistent peripheral neuropathic pain.](#) *Pain* 87(2): 149-158.
5. Kim, S. H. and Chung, J. M. (1992). [An experimental model for peripheral neuropathy produced by segmental spinal nerve ligation in the rat.](#) *Pain* 50(3): 355-363.
6. Seltzer, Z., Dubner, R. and Shir, Y. (1990). [A novel behavioral model of neuropathic pain disorders produced in rats by partial sciatic nerve injury.](#) *Pain* 43(2): 205-218.
7. Shields, S. D., Eckert, W. A., 3rd and Basbaum, A. I. (2003). [Spared nerve injury model of neuropathic pain in the mouse: a behavioral and anatomic analysis.](#) *J Pain* 4: 465-470.
8. Yang, G., Pan, F., Chang, P. C., Gooden, F. and Gan, W. B. (2013). [Transcranial two-photon imaging of synaptic structures in the cortex of awake head-restrained mice.](#) *Methods Mol Biol* 1010: 35-43.

Measuring Spatiotemporal Dynamics of Odor Gradient for Small Animals by Gas Chromatography

Akiko Yamazoe-Umemoto¹, Yuishi Iwasaki² and Koutarou D. Kimura^{1,*}

¹Department of Biological Sciences, Graduate School of Science, Osaka University, Toyonaka, Osaka, Japan; ²Department of Intelligent Systems Engineering, Ibaraki University, Hitachi, Ibaraki, Japan

*For correspondence: kokimura-lab@umin.ac.jp or kokimura@bio.sci.osaka-u.ac.jp



[Abstract] Odor is the most fundamental chemical stimulus that delivers information regarding food, mating partners, enemies, and danger in the surrounding environment. Research on odor response in animals is widespread, although studies on experimental systems in which the gradient of odor concentration is quantitatively measured has been quite limited. Here, we describe a method for measuring a gradient of odor concentration established by volatilization and diffusion in a relatively small enclosed space, which has been used widely in laboratories to analyze small model animals such as the nematode *Caenorhabditis elegans* and the fruit fly *Drosophila melanogaster*. We first vaporized known amounts of a liquid odorant 2-nonenone in a tank and subjected them to gas chromatographic analysis to obtain a calibration curve. Then, we aspirated a small amount of gas phase from a small hole on an agar plate and measured the odor concentration. By repeating this at different spatial and temporal points, we were able to detect a gradient of the odor concentration that increased over time. Furthermore, by applying these measured values to mathematical models of volatilization and diffusion, we were able to visualize an estimated dynamic change in odor concentration over an agar plate. Combining monitoring of odor concentration change in an agar plate with behavioral monitoring by machine vision will allow us to estimate how the brain computes information regarding odor concentration change in order to regulate behavior.

Keywords: Odorant, Gradient, Gas chromatograph, *C. elegans*, Diffusion, Evaporation

[Background] Odor is the most fundamental chemical stimulus that conveys the existence of food, reproductive partners, enemies, etc. in the surrounding environment. Small model animals, such as the nematode *Caenorhabditis elegans* and fruit fly *Drosophila melanogaster* are suitable for understanding brain responses to odor stimuli at the levels of behavior, neural activity, and molecules because: (1) behavioral responses to odor stimuli can be easily recorded with inexpensive high resolution cameras; (2) responses in multiple neurons/neuronal groups can be measured with calcium imaging and (3) genes responsible for behavioral and neural responses can be identified with various genetic methods (De Bono and Maricq, 2005; Venken et al., 2011).

However, it is difficult to measure the odor concentrations that are actually sensed by these small animals during their behavior in a small arena suited for observation. In general, the measurement of odor concentration requires constant air flow in a device supplying the odorant-containing air to the sensor. Thus, air should be constantly drawn from the air phase of the arena, destroying the odor

gradient. Measuring odor gradient in a small behavioral arena has been achieved either by strengthening the air flow for the odor gradient compared to the flow for sampling or by optically measuring the air phase odorant concentration. Gershoff *et al.* (2012) developed a relatively large apparatus (30 x 30 cm) for *Drosophila* larvae for slow but large (2 L/min) constant parallel flows with different concentrations, in order to create an odor concentration gradient perpendicular to the flow. Louis *et al.* (2008) used infrared beams to measure integrated concentrations of odor on one axis in a naturally evaporated and diffused gradient, and calculated the gradient shape mathematically based on Gaussian diffusion. The former method allows quantitative measurement of the odor gradient, although it is not based on natural evaporation and diffusion. It also requires specific, controlled apparatus. The latter method is suitable for natural gradients, although it does not allow accurate measurement of specific positions.

Here we report a method to measure a dynamic odor gradient in a widely-used plastic plate by gas chromatography (GC). Observing odor-taxis behaviors on plastic plates with an agar layer is easy and thus is conducted in many laboratories. In addition, we are able to video-record the behaviors using inexpensive USB cameras. Therefore, by measuring temporal changes in the odor gradient on an agar plate, we can obtain clues to estimate brain computations controlling how temporal changes in odor stimuli affect the animal's behavior.

For measurement, first, specific amounts of liquid odorant are individually volatilized in a vaporizing tank to make gas with known concentrations of odorant. Then, the gas is subjected to GC with different concentrations, in order to calculate a calibration curve for known gas concentrations and GC values. Next, a small amount of gas is sampled from a specific spatio-temporal point on an agar plate with evaporating and diffusing odorant, and subjected to GC analysis. Finally, the entire odor gradient is calculated by the measured concentrations at different spatio-temporal points. In our experiment, measurements suggested that *C. elegans* responds behaviorally to odor concentration changes as small as $\pm 0.01 \mu\text{M/sec}$ in $\sim 2 \mu\text{M}$ concentration on a natural odor gradient. This is consistent with results from an experiment with artificial and controlled odor concentration changes (Tanimoto *et al.*, 2017).

Materials and Reagents

1. ø 9 cm sterile Petri dish (IWAKI, catalog number: SH90-15) with nematode growth medium (NGM) agar

*Note: Pour 10 ml of autoclaved 1.5-2.5% agar solution per dish following the regular sterilized technique to make an agar plate for behavioral analysis. We used NGM agar for *C. elegans* behavioral analysis. This agar plate can be stored at 4 °C for a few weeks. The plates should be moved to a bench a few hours before the assay and kept without their lids for 15-30 min to dry. Dried plates with lids are placed upside-down on a bench. The plates are not sealed with either Parafilm or sticky tape.*

2. Microliter syringe, 50 µl, cemented needle (Hamilton, catalog number: 80565)

Note: This is a blunt needle point.

3. Micro-volume syringe, 5 μl , fixed needle (SGE, catalog number: 001000)
4. Plastic disposable syringe, 2.0 ml (Top, catalog number: 5079-01)
5. Replacement needle (Luer lock side hole), 23 G x 4 cm (GL Sciences, catalog number: 3008-46004)
6. Pasteur pipette (IWAKI, catalog number: 1K-PAS-5P)
7. Dropper bulb (AS ONE, catalog number: 1-6227-05)
8. 2-Nonanone (Wako Pure Chemical Industries, catalog number: 132-04173)
Note: Liquid at room temperature. Although we used only this odorant, this protocol could be used for other odorants as well.
9. EtOH (Wako Pure Chemical Industries, catalog number: 057-00456)
10. Sodium chloride (NaCl) (Wako Pure Chemical Industries, catalog number: 191-01665)
11. Bacto peptone (BD, BactoTM, catalog number: 211677)
12. Agar (Wako Pure Chemical Industries, catalog number: 010-08725)
13. Cholesterol (Wako Pure Chemical Industries, catalog number: 034-03002)
14. Calcium chloride dihydrate ($\text{CaCl}_2 \cdot 2\text{H}_2\text{O}$) (Wako Pure Chemical Industries, catalog number: 038-12775)
15. Magnesium sulfate heptahydrate ($\text{MgSO}_4 \cdot 7\text{H}_2\text{O}$) (Wako Pure Chemical Industries, catalog number: 131-00405)
16. Dipotassium hydrogenphosphate (K_2HPO_4) (Wako Pure Chemical Industries, catalog number: 164-04295)
17. Potassium dihydrogen phosphate (KH_2PO_4) (Wako Pure Chemical Industries, catalog number: 169-04245)

Equipment

1. Vaporizing tank (FIS, catalog number: DT-T1) (Figure 1)

Note: A custom-made acrylic tank of 50 L, equipped with a small metal block with a vaporizing groove, a heater with a temperature controller, and a fan. The odorant liquid is placed in the groove of the metal block through a liquid inlet on the lid, and the metal block is warmed with the heater to facilitate volatilization of the odorant. The fan stirs the air so that the volatilized odorant is distributed equally in the tank.

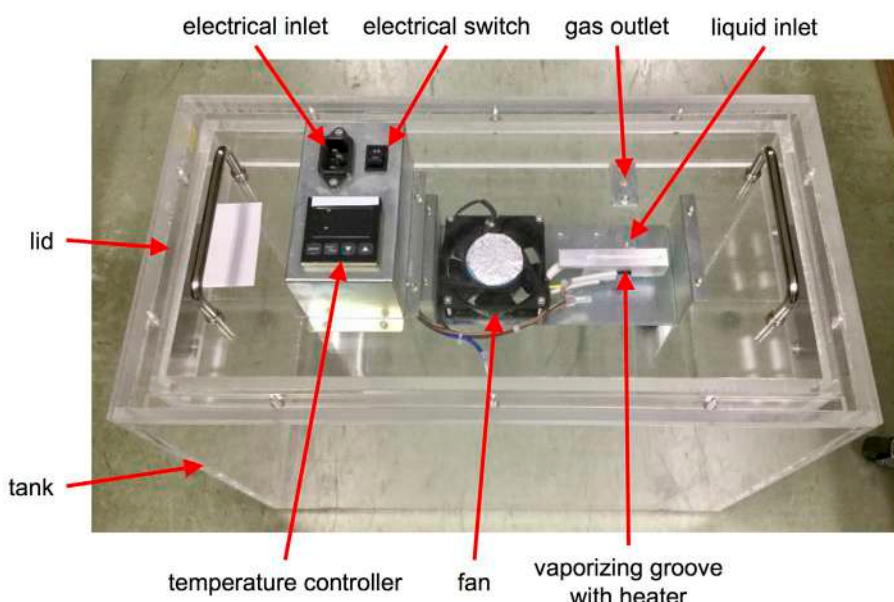


Figure 1. Vaporizing tank

2. Gas chromatograph (GC) (Nissha FIS, model: SGVA-N2) (Figure 2)

Note: A simple and inexpensive GC optimized for 2-nonenone with a semiconductor detector. Other GC can also be used.

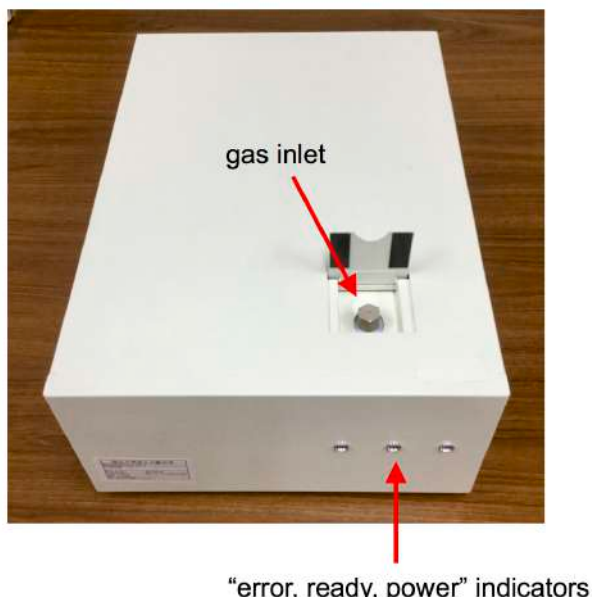


Figure 2. Gas chromatograph

3. Carrier gas cylinder (Air Liquide, model: Alphagaz 1)

Note: This was recommended by Nissha FIS Inc.

4. Vacuum cleaner (Toshiba, catalog number: VC-PC6A, L)

Note: A domestic vacuum cleaner.

5. Pin vise (Tamiya, Fine Pin Vise D [0.1-3.2 mm])
6. 1 mm drill (Tamiya, Basic Drill Bit set 5 pc)

Software

1. SGC.exe (Nissha FIS Inc., Hyogo, Japan)

Note: This is a specific software to control this type of GC provided by the manufacturer. Software should be installed on a Windows PC (XP, Vista, or 7) that is connected to the GC. Depending on the GC instrument being used, the manufacturer may have specific analysis software recommendations.

Procedure

Overview: We vaporized specific amounts of liquid 2-nonenone in the vaporizing tank to make 2-nonenone gas of known concentrations, and measured GC values to calculate a calibration curve. Next, a gas phase of 0.2 ml in an agar plate was sampled and measured with the GC. Although we did the following with 2-nonenone, our method should be applicable for other odorants that are vaporized from the liquid at room temperature and can be measured by gas chromatography. Important steps are summarized in Video 1.



Video 1. Important steps for measuring odor gradient. A video demonstrating the important apparatus and operations for the odor measurement.

A. Measuring known concentrations of 2-nonenone gas for a calibration curve

2-nonenone gas of known concentration can be obtained by vaporizing a specific amount of 2-nonenone liquid in the vaporizing tank (see below). A calibration curve can be obtained by measuring different concentrations of the gas with GC and correlating the measured values. However, the time to reach maximum odor concentration varied for each amount of liquid, likely

due to differences in vaporization, diffusion, and trace adhesion to the vaporizing tank wall. Therefore, we monitored temporal changes in odor concentration in the tank to find the optimal time for vaporization of each concentration.

1. Flow the carrier gas at 0.25–0.35 MPa from the air cylinder connected to the GC.

Note: Do this immediately before turning on the GC.

2. Turn on the GC immediately after Step A1.

Note: Flowing gas without turning on power will damage the column inside the GC.

3. Wait until the 'Ready' lamp is illuminated.

Notes:

a. *This may take about 90 min.*

b. *If the GC is used after a long interval (e.g., more than 2 weeks), the measured value tends to be higher. In that case, use the GC a few days before taking actual measurements. An interval of up to several days has no effect.*

c. *The high values recorded after long intervals are attributed to the following: During the interval, the sensor surface is coated with various small compounds in the air. Electrical conduction increases the temperature of the sensor to 300–400 °C, which clarifies the attached compounds and causes transient high sensitivity for several hours.*

d. *The directions above are specific to the GC instrument used in this study. Other instrumentation may require adapted methods and steps.*

4. Turn on the electrical switch of the vaporizing tank (Figure 1), and set the temperature at 50 °C: It will take about 10 min to reach 50 °C.
5. Take an appropriate amount of 2-nonenone liquid (Table 1) with a glass syringe of 5 µl or 50 µl, insert it in the liquid inlet on the lid of the tank, and place the liquid in the vaporizing groove installed on the back side of the lid.

Table 1. Volumes of 2-nonenone liquid for the vaporization

Liquid volume (µl)	Estimated conc. (µM)	gas ppm	Syringe used (µl)	Sampling time (min)	Time for the maximum (min)
0.36	0.04	1	5	1, 2, 3, 4	2
1.07	0.12	3	5	1, 2, 3, 4, 5	1
3.56	0.4	10	50	1, 2, 4, 8	4
35.6	4	100	50	6, 10, 14, 18, 22, 26	18
59.4	6.8	167	50	6, 18, 30, 42, 54, 66	42
97.2	11.1	273	50	6, 18, 30, 42, 54, 66	54
200	22.9	562	50	6, 18, 30, 42, 54, 66, 78, 102	66

6. The relationship between the liquid volume and the estimated gas concentration in Table 1 is as follows:

$$C = \frac{V_{liquid} \times d}{M V_{tank}}$$

where C is the required gas concentration (mol/L), V_{liquid} is the amount of liquid (ml) to be added, d is the density of liquid odorant (g/ml), M is the molecular weight (g), and V_{tank} is the volume of the vaporizing tank (L).

7. Start SGC.exe on a Windows PC connected to the GC and operate according to the manual.
8. Press the start button in SGC.exe.
9. After a certain period of time (see Table 1), carefully insert the replacement needle attached to the disposable syringe from the gas outlet. Extract 0.2 ml and quickly remove the needle from the tank. Carefully insert the needle in the gas inlet of the GC (Figure 2) until it hits the bottom, and immediately infuse the gas inside the syringe.
Note: This step should be completed in about 5-6 sec.
10. Measurement is started by gas injection. Drawing of the graph (Figure 3) starts and ends automatically. Data is automatically saved. In the default setting, a measurement takes 8 min. The file can be exported as a CSV file.

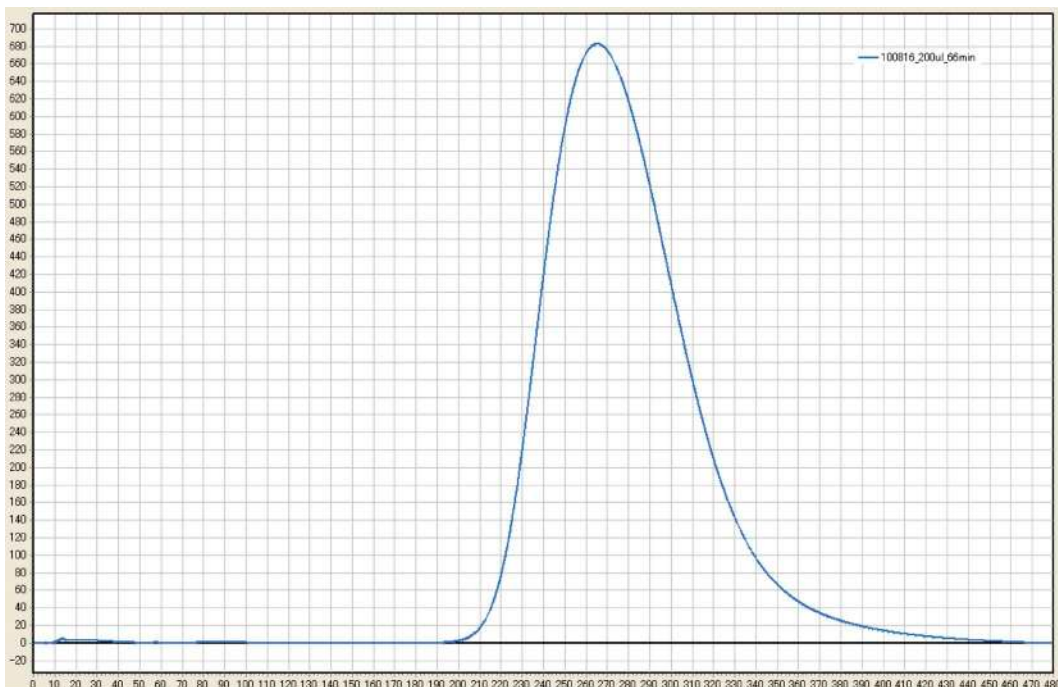


Figure 3. A representative result of one measurement for 22.9 μM (i.e., 200 μl) of 2-nonenone. The horizontal axis is time (sec), and the vertical axis is the signal (mV).

11. To measure temporal changes in the measured value for the specific amount of the odorant, odor gas sampling can be performed at different time points for one odorant injection (e.g., 6, 18, 30, and 42 min for 6.8 and 11.1 μM ; see Table 1). However, if there is no 8-min interval (e.g., 1, 2, 3, and 4 min for 0.04 and 0.12 μM), clean the tank (see the next section) and start from the gas vaporization.
12. If gas remains in the tank (likely by adhesion to the wall), vaporization of the residual amount affects the GC value, especially when a small concentration is being measured. In order to

avoid this, gas in the tank is removed with a vacuum cleaner, and the wall is wiped with a paper towel containing EtOH, followed by further suction with the vacuum cleaner. After this procedure, remaining gas was not detected in our experiment.

13. For all conditions, repeat the measurement 3-4 times (once daily and repeat over 3-4 days) and find the time at which the average value is at a maximum (Figure 4). In the case of 2-nonenone, the relationship between odor concentrations and measured values are nicely fitted to two regression lines for concentrations lower and higher than 4 μM ($R^2 = 0.9991$ and 0.9995, respectively; Figure 5) (Tanimoto *et al.*, 2017). In general, for semiconductor detectors, the correlation between the peak height of the signal and signal concentration in a log-log plot is well-fitted by two simple regression lines for lower and higher concentrations. Therefore, these results are adopted as calibration curves for low and high concentrations. Excel (Microsoft) is used for data analysis.

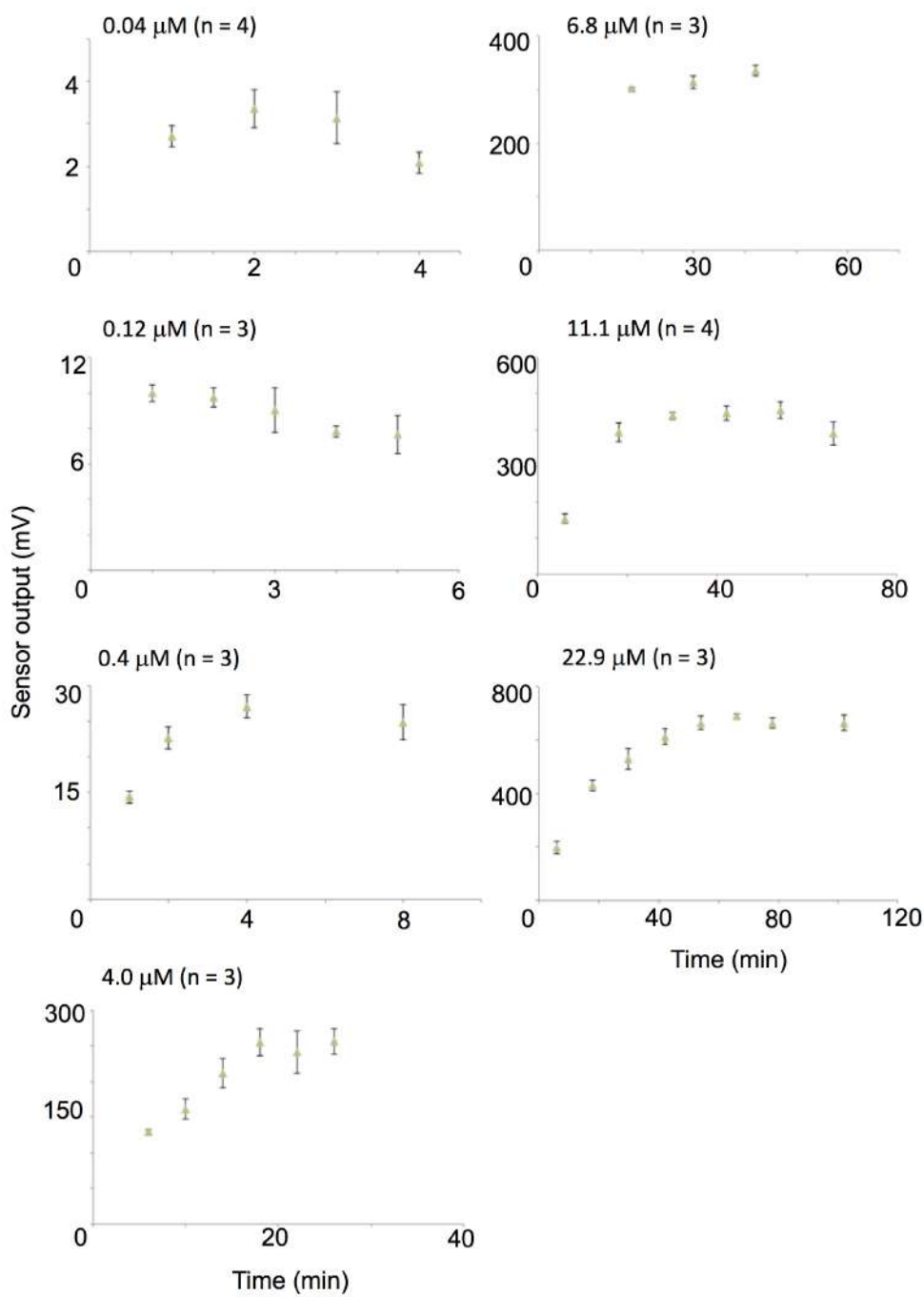


Figure 4. Changes over time of the measured value for different amounts of liquid odor.

On each graph, the expected 2-nonenone gas concentration at saturation is shown. The horizontal (vaporizing time) and vertical (sensor output) axes are different in each graph. For 2-nonenone gas with a low saturation concentration of 0.04-0.12 μM, the concentration became saturated immediately and then decreased slightly. This is likely because of adhesion of 2-nonenone to the wall. For each condition, results are shown as mean ± standard error of 3-4 repetitions.

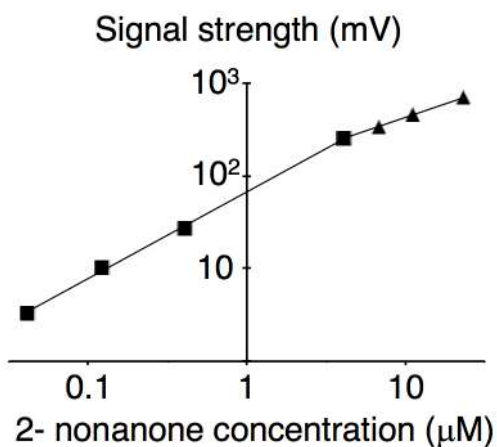


Figure 5. Calibration curve for 2-nonenone. Each dot represents average values of 3-4 experiments, and data on the log-log plot were fitted with two simple regression lines for lower (squares) and higher (triangles) concentrations. This figure was originally published in Tanimoto *et al.* (2017).

B. Measuring 2-nonenone gradient on an agar plate

1. On the back side of the agar plate, mark the positions of odor spot and gas sampling with a pen.

Note: We measured at six points (x, y, z) on the assay plate shown in Figure 6 at 1, 3, 6, 9, and 12 min. The motivations for adopting 6 points (x, y) for measurement are as follows:

- a. *Since we examined odor avoidance behavior of *C. elegans*, the four points on the x axis were chosen to measure the direction avoided by *C. elegans*, i.e., to measure the spatial gradient along the x direction. In the range of $x > 0$ in which *C. elegans* mainly existed, three points were chosen. Only one point was measured in the range $x < 0$ where *C. elegans* did not often exist.*
- b. *To measure the spatial gradient in the y direction, (22, 15) was selected. We chose only one point because the worms did not spread much along the y axis.*

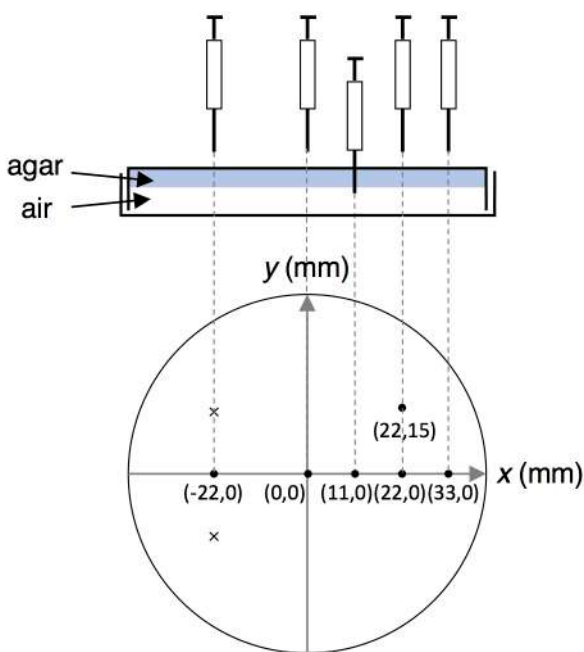


Figure 6. Gas sampling from the agar plate [originally published in Tanimoto *et al.* (2017).
[Creative Commons Attribution License](#)]

2. Remove the lid of the agar plate, and push the narrow end of a Pasteur pipette with a dropper bulb against the agar and extract the agar plug to make a hole of ϕ 1-2 mm in the agar layer. Then close the lid.
3. From the back of the plate (*i.e.*, the opposite side of the lid), make a hole with a pin vise with a 1 mm drill at the position of the agar hole. This will result in a hole in the same position on the plate and the agar.
4. If necessary, use cellophane tape to cover the hole from the back side. Turn back one side of the cellophane tape for ease of peeling. This is not necessary for odorants with large molecular weights such as 2-nonenone. We compared outcomes with and without taping, and found no difference.
5. Spot the liquid odorant at the odor source position (we used 2 μ l of 30% 2-nonenone diluted in EtOH), immediately cover the lid, place the plate upside-down (hole up) and leave it on the bench.

*Note: In the worm's odor avoidance assay, worms suspended in a small amount of buffer droplet are spotted at the center of the plate 1.5 min before the odor is spotted (Kimura *et al.*, 2010), and the time of odor spotting is counted as $t = 0$. In this odor measurement, however, the worms are not spotted for the sake of simplicity.*

6. When an appropriate amount of time (*i.e.*, 1, 3, 6, 9, or 12 min) has passed, remove the tape (if applied) without moving the plate. Carefully insert the replacement needle attached to the plastic 2.0 ml disposable syringe so that the needle hole is positioned in the gas phase 1 mm away from the agar surface (*i.e.*, just below the agar surface in the upside-down plate). Slowly

extract 0.2 ml of the gas so as not to disturb the gradient severely. Quickly remove the needle tip from the plate and insert it in the gas inlet of the GC, and inject the gas.

Note: Since sampling may destroy the gradient, only one sample was taken from each plate.

7. Several samples should be taken (we took 7-9) for each position and time, using the median to calculate the dynamic odor gradient.

C. Fitting the odor gradient

1. Model selection

At the beginning of curve fitting, a parametric function needs to be specified for the data. Physical phenomena caused in the assay plate are evaporation of the 2-nonenone-ethanol-mixed solution (30:70, v/v) and diffusion of their gaseous molecules in the three-dimensional closed cylindrical space. Although we previously calculated the evaporation and distribution of 2-nonenone numerically (Yamazoe-Umemoto *et al.*, 2015), in the recent study we employed a phenomenological curve fitting to the measured concentration by least squares method for better understanding of the odor gradient (Tanimoto *et al.*, 2017). After the odor sources are put at the two spots, the 2-nonenone concentration $C(t)$ in the plate increases from zero and asymptotically approaches a constant value over time. In this work, a saturation curve $C(t) = a(1-\exp(-bt))$ was used for fitting, where a and b denote an asymptotic concentration and an increasing rate, respectively. This function is a solution of the rate equation $dC(t)/dt = b(a - C(t))$ which implies that $C(t)$ changes with the rate proportional to the difference from the asymptotic concentration.

In the measurement, increasing of the 2-nonenone concentration was slow as the distance from the spots is far (Figure 7). A mass transfer by molecular diffusion accounts for this result. Therefore the increasing rate is a decreasing function of the distance r from the spot such as $b(r) = b_0 \exp(-b_1 r - b_2 r^2)$, where $b_0 (> 0)$, b_1 and b_2 are constant parameters. For good fitting in a relatively short time after putting the odor sources, furthermore, the asymptotic concentration is also a decreasing function of r such as $a(r) = a_0 \exp(-a_1 r - a_2 r^2)$, where $a_0 (> 0)$, a_1 and a_2 are constant parameters. Because there are two odor sources in the plate, the measured concentrations are fitted to the following function with two saturation curves.

$$C(x, y, t) = a(r_1)(1 - \exp(-b(r_1)t)) + a(r_2)(1 - \exp(-b(r_2)t)).$$

where r_1 and r_2 are the distances from the position (x, y) on the agar to the two spots $(X_1, Y_1) = (-22, 15)$ and $(X_2, Y_2) = (-22, -15)$, respectively.

$$r_i = \sqrt{(x - X_i)^2 + (y - Y_i)^2} \quad (i = 1, 2).$$

The radius of the plate is 44 mm (1 mm in the plate thickness).

Two constraint conditions are imposed on the fitting. The first constraint condition is that $a(r)$ and $b(r)$ should be decreasing functions of r at least in the range $0 \leq r \leq r_0$, where r_0 is the distance from the spot to the edge of the plate (44, 0). From $da(r)/dr = -a_0(a_1 + 2a_2 r) \exp(-a_1 r - a_2 r^2)$ and $db(r)/dr = -b_0(b_1 + 2b_2 r) \exp(-b_1 r - b_2 r^2)$, inequality conditions $da(r_0)/dr \leq 0$ and $db(r_0)/dr \leq 0$ (decreasing even at $r = r_0$) are expressed as:

$$a_1 + 2a_2 r_0 \geq 0,$$

$$b_1 + 2b_2 r_0 \geq 0,$$

under $a_0 > 0$ and $b_0 > 0$. The second constraint condition is that the asymptotic concentration on the odor sources should be lower than the saturation concentration 34.5 μM of the 2-nonenone (Yamazoe-Umemoto *et al.*, 2015). Letting $R = \sqrt{(X_1 - X_2)^2 + (Y_1 - Y_2)^2}$ be the distance between the two spots, this condition is expressed as:

$$C(X_1, Y_1, \infty) = C(X_2, Y_2, \infty) = a_0(1 + \exp(-a_1 R - a_2 R^2)) \leq 34.5.$$

2. Fitting algorithm

The fitting parameters in $C(x, y, t)$ are determined by the Levenberg-Marquardt method which is widely used to solve non-linear minimization problems (Press *et al.*, 1992). Letting θ^* be the parameter vector,

$$\theta^* = (\theta_1, \theta_2, \theta_3, \theta_4, \theta_5, \theta_6) = (a_0, a_1, a_2, b_0, b_1, b_2),$$

the sum of the squared errors is explicitly defined by:

$$E(\theta) = \frac{1}{2} \sum_{n=1}^N (C(\theta, x_n, y_n, t_n) - u_n)^2.$$

Where u_n is the n -th measured concentration at position (x_n, y_n) at time t_n ($n = 1, 2, \dots, N$). The inequality constraints are expressed as:

$$\begin{aligned}m_1(\theta) &= \theta_2 + 2\theta_3 r_0 \geq 0, \\m_2(\theta) &= \theta_5 + 2\theta_6 r_0 \geq 0, \\m_3(\theta) &= -\theta_1(1 + \exp(-\theta_2 R - \theta_3 R^2)) + 34.5 \geq 0.\end{aligned}$$

Introducing the following function with logarithmic barriers,

$$f(\theta, \mu) = E(\theta) - \mu \sum_{k=1}^3 \log(m_k(\theta))$$

the given constrained minimization problem is approximately replaced by an unconstrained minimization problem. Where μ is a penalty factor whose value is initially large positive and is reduced to zero as θ is converged. The iterative algorithm to determine θ which minimizes $f(\theta, \mu)$ is as follows.

Step 1: Initial values are set for θ , μ and λ . Where λ is a damping factor in the Levenberg-Marquardt method and is used in Step 2. θ is chosen to satisfy the inequality constraints. Initial μ and λ are large positive.

Step 2: The Jacobian matrices $J = (\{J_{ij}\})$, $G = (\{G_{ij}\})$, the diagonal matrix M and the residual vector d are calculated.

$$\begin{aligned}J_{ij} &= \frac{\partial C(\theta, x_i, y_i, t_i)}{\partial \theta_j}, \\G_{ij} &= \frac{\partial m_i(\theta)}{\partial \theta_j}, \\M &= \text{diag}(m_1(\theta), m_2(\theta), m_3(\theta)), \\d &= (C(\theta, x_1, y_1, t_1) - u_1, \dots, C(\theta, x_N, y_N, t_N) - u_N)^T\end{aligned}$$

Then, the following linear equation of δ is solved and $f(\theta + \delta, \mu)$ is calculated.

$$\begin{aligned}(H + \lambda \text{diag}(H))\delta &= -J^T d + \mu G^T M^{-1} e, \\H &= J^T J + \mu G^T M^{-2} G.\end{aligned}$$

Where $\vec{\delta} = (1,1,1)^T$.

Step 3: If $|f(\vec{\theta} + \vec{\delta}, \mu) - f(\vec{\theta}, \mu)| / f(\vec{\theta}, \mu) < \varepsilon$ for a small constant ε , then $\vec{\theta} + \vec{\delta}$ is determined as a solution, or else go to Step 2 with updating $\vec{\theta}$, μ and λ . If $f(\vec{\theta} + \vec{\delta}, \mu) < f(\vec{\theta}, \mu)$, $\vec{\theta}$ is updated by $\vec{\theta} + \vec{\delta}$ checking the inequality constraints. μ and λ are reduced by rates α and β ($0 < \alpha, \beta < 1$), respectively. If $f(\vec{\theta} + \vec{\delta}, \mu) \geq f(\vec{\theta}, \mu)$ or the inequality constraints are not satisfied, $\vec{\theta}$ and μ are not updated while λ is increased by a rate $1/\beta$.

3. Execution and result

In this work, the fitting algorithm is implemented in C language and is compiled by the GNU Compiler Collection. The convergence criterion is $\varepsilon = 1 \times 10^{-6}$. Setting of the decrement rates α and β depends on the choice of an initial $\vec{\theta}$. In particular, the slow reduction of μ requires the avoidance of invalid updating of $\vec{\theta}$, such that the reduction rate α for $\mu (\mu \rightarrow \alpha \mu)$ is $0.5 < \alpha < 1$. When $\alpha < 0.5$, the penalty factor μ rapidly converges to 0 and an incorrect solution $\vec{\theta}$ without inequality constraints is derived. Some combinations of initial parameters and decrement rates are tried for fitting. Furthermore, a converged value of $\vec{\theta}$ is used as an initial value in new iterations with different μ and λ . Good fitting parameters are $a_0 = 20.68 \text{ }\mu\text{M}$, $a_1 = 0.7355 \text{ cm}^{-1}$, $a_2 = -0.05408 \text{ cm}^2$, $b_0 = 0.8384 \text{ min}^{-1}$, $b_1 = 0.7835 \text{ cm}^{-1}$ and $b_2 = -0.05761 \text{ cm}^2$. Some software tools are useful for the non-linear curve fitting. Optimization Toolbox in MATLAB provides packages for non-linear least squares minimization. Solver Add-in in Microsoft Excel is also available for non-linear curve fitting.

Fitting result is shown in Figure 7. Temporal change of the 2-nonenone gradient is shown in Video 1 in Tanimoto *et al.* (2017). Although the odor sources spread in a round shape (~5 mm in diameter) in the experiment, their shape in the fitting is considered as a point which has no area. Therefore, the fitted 2-nonenone gradient around the spots became pointy.

When a simple exponential function $b(r) = b_0 \exp(-b_1 r)$ was used for fitting, the result was not good. A higher-order correction of more than r^2 term requires for good fitting. When $b(r) = b_0 \exp(-b_1 r - b_2 r^2 - b_3 r^3)$ was used for fitting, the result was almost the same as that without the r^3 term. Fitting using a polynomial function $b(r) = b_0 - b_1 r - b_2 r^2 - b_3 r^3$ or a fractional function $b(r) = 1/(b_0 + b_1 r + b_2 r^2)$ went bad. Fitting using other saturation curve $C(t) = c_0 t/(t + c_1)$ or $C(t) = c_0 t^2/(t^2 + c_1)$ also went bad.

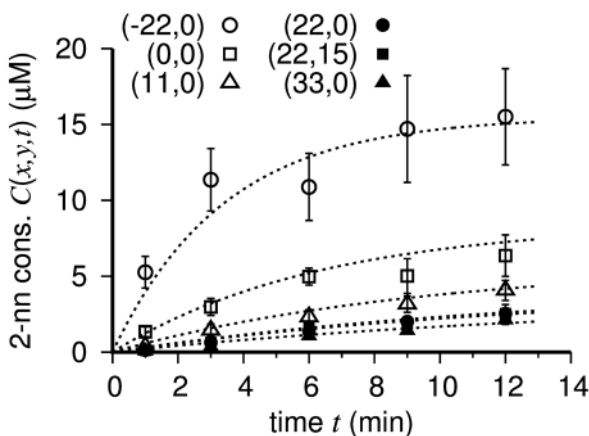


Figure 7. Temporal change of the measured 2-nonenone concentration at the position (x , y) on the agar. The odor sources were put at (-22, 15) and (-22, -15). The broken lines are the fitting curves.

Data analysis

All data related to this study are already published in Tanimoto *et al.* (2017).

Notes

1. We found that variations in odor concentration become considerably smaller with increasing distance from the odor source, *i.e.*, in the right half of the plate. Conversely, variations were greater near the odor source. We consider that this is because diffusion essentially equalizes variation, leading to less variation at greater distances from the source.
2. In the natural environment, odors are recognized to exist as plumes; they do not produce a smooth gradient. In this experiment, 0.2 ml was aspirated for one measurement, therefore we were not able to detect any spatial differences within this volume. However, based on the model of the smooth 2-nonenone gradient, *C. elegans* are estimated to respond to a concentration change of about 0.01 $\mu\text{M/sec}$, which is consistent with behavioral response in a constant odor concentration change in artificial flow (Tanimoto *et al.*, 2017). This suggests that the gradient is indeed smooth, at least in this case caused by volatilization and diffusion in the static space inside the plastic plate.
3. The shape of the gradient can differ substantially depending on the ratio of volatilization to diffusion. In the case of 2-nonenone, the ratio was appropriate for formation of a reasonable gradient.
4. The 2-nonenone concentration used in our paradigm is relatively high compared to concentrations of other odorants used in *C. elegans* odor-taxis analysis, which are in general 10^{-3} - 10^{-4} at odor source (Bargmann *et al.*, 1993). For these odorants, it would be better to use a

more sensitive GC. In addition, for these odorants, it may be important to use materials with less adhesion for the vaporizing tank and syringe, such as glass or metal, instead of plastic.

Recipes

1. NGM plate (for 1 L)
970 ml ddH₂O
3 g NaCl
2.5 g peptone
17 g agar
1 ml cholesterol (5 mg/ml EtOH)
Autoclave; wait until 50-60 °C
Add the following autoclaved buffers:
1 ml 1 M CaCl₂
1 ml 1 M MgSO₄
25 ml 1 M KPO₄ buffer (pH 6)
2. KPO₄ buffer (pH 6.0), 1 M
108.3 g KH₂PO₄
35.6 g K₂HPO₄
Add ddH₂O up to 1 L
Autoclave

Acknowledgments

We especially thank K. Tanaka (FIS Inc., Japan) for all the technical support of odor measurement. This work was supported by a Grant-in-Aid for JSPS fellows (A.Y.-U.), the Osaka University Life Science Young Independent Researcher Support Program, Precursory Research for Embryonic Science and Technology from MEXT, and research grants from Mitsubishi Foundation, Shimadzu Science Foundation, and Takeda Science Foundation (K.D.K.). The authors declare that no competing interests exist.

References

1. Bargmann, C. I., Hartwig, E. and Horvitz, H. R. (1993). [Odorant-selective genes and neurons mediate olfaction in *C. elegans*](#). *Cell* 74(3): 515–527.
2. De Bono, M. and Maricq, A. V. (2005). [Neuronal substrates of complex behaviors in *C. elegans*](#). *Annu Rev Neurosci* 28: 451-501.
3. Gershow, M., Berck, M., Mathew, D., Luo, L., Kane, E. A., Carlson, J. R. and Samuel, A. D. (2012). [Controlling airborne cues to study small animal navigation](#). *Nat Methods* 9(3): 290-296.

4. Kimura, K. D., Fujita, K., and Katsura, I. (2010). [Enhancement of odor avoidance regulated by dopamine signaling in *Caenorhabditis elegans*](#). *J Neurosci* 30(48): 16365-16375.
5. Louis, M., Huber, T., Benton, R., Sakmar, T. P. and Vosshall, L. B. (2008). [Bilateral olfactory sensory input enhances chemotaxis behavior](#). *Nat Neurosci* 11(2): 187-199.
6. Press, W. H., Teukolsky, S. A., Vetterling, W. T. and Flannery, B. P. (1992). [Numerical recipes in C](#). Cambridge University Press.
7. Tanimoto, Y., Yamazoe-Umemoto, A., Fujita, K., Kawazoe, Y., Miyanishi, Y., Yamazaki, S. J., Fei, X., Busch, K. E., Gengyo-Ando, K., Nakai, J., Iino, Y., Iwasaki, Y., Hashimoto, K. and Kimura, K. D. (2017). [Calcium dynamics regulating the timing of decision-making in *C. elegans*](#). *Elife* 6: e21629.
8. Venken, K. J., Simpson, J. H. and Bellen, H. J. (2011). [Genetic manipulation of genes and cells in the nervous system of the fruit fly](#). *Neuron* 72(2): 202-230.
9. Yamazoe-Umemoto, A., Fujita, K., Iino, Y., Iwasaki, Y. and Kimura, K. D. (2015). [Modulation of different behavioral components by neuropeptide and dopamine signalings in non-associative odor learning of *Caenorhabditis elegans*](#). *Neurosci Res* 99: 22-33.

Magnetic Resonance Imaging and Histopathological Visualization of Human Dural Lymphatic Vessels

Seung-Kwon Ha, Govind Nair, Martina Absinta, Nicholas J. Luciano and Daniel S. Reich*

Division of Neuroimmunology and Neurovirology, National Institute of Neurological Disorders and Stroke (NINDS), National Institutes of Health (NIH), Bethesda, MD, USA

*For correspondence: daniel.reich@nih.gov



[Abstract] In this protocol, we describe a method to visualize and map dural lymphatic vessels *in-vivo* using magnetic resonance imaging (MRI) and *ex-vivo* using histopathological techniques. While MRI protocols for routine imaging of meningeal lymphatics include contrast-enhanced T2-FLAIR and T1-weighted black-blood imaging, a more specific 3D mapping of the lymphatic system can be obtained by administering two distinct gadolinium-based MRI contrast agents on different days (gadofosveset and gadobutrol) and subsequently processing images acquired before and after administration of each type of contrast. In addition, we introduce methods for optimal immunostaining of lymphatic and blood vessel markers in human dura mater *ex-vivo*.

Keywords: Lymphatic vessels, Brain, Meninges, MRI, Histopathology, Immunohistochemistry

[Background] Among the causes of immune privilege in the brain is the absence of parenchymal lymphatic vessels. However, recent studies have uncovered an extensive lymphatic circulating system in the dura mater of rodents (Aspelund *et al.*, 2015; Louveau *et al.*, 2015), providing possible routes for the elimination of the brain's waste products and for immune cells to access the deep cervical lymph nodes. In this protocol, we describe a way to: (1) visualize the lymphatic vessels *in-vivo* in the dura mater using MRI of the head, and (2) assess the local presence of lymphatic vessels using optimized immunostaining methods (Absinta *et al.*, 2017). *In-vivo* imaging of lymphatics may enable more detailed studies of mechanisms of waste removal and immune function and their potential abnormalities in various diseases and aging.

Materials and Reagents

1. Superfrost Plus Microslides (Daigger Scientific, catalog number: EF15978Z)
2. Cover Glasses (Daigger Scientific, catalog number: EF15972L)
3. Paper towel (KCWW, Kimberly-Clack, catalog number: 05511)
4. Polypropylene Coplin jar (IHC World, catalog number: IW-2501)
5. Super HT PAP pen (Biotium, catalog number: 22006)
6. Gadavist, gadobutrol (0.1 mmol/kg body weight, i.v., Bayer Health Care, NDC 50419-325-12)
7. Ablavar, gadofosveset (0.03 mmol/kg body weight, i.v., Lantheus Medical Imaging, NDC 11994-012-02)

8. 10% Neutral Buffered Formalin Fixatives, methanol < 2% (Leica Biosystems, catalog number: 3800602)
9. Ethanol (Pharmaco-AAPER, catalog number: 111000200)
10. Target Retrieval Solution, pH 9 (Agilent Technologies, Dako, catalog number: S2367)
11. Target Retrieval Solution (Agilent Technologies, Dako, catalog number: S1699)
12. Tris buffered saline 10x, pH 7.4 (KD Medical, catalog number: RGF-3385)
13. Hydrogen Peroxide, 30% (Fisher Scientific, catalog number: H325-500)
14. Protein Block, Serum-Free (Agilent Technologies, Dako, catalog number: X0909)
15. LYVE1 antibody (Abcam, catalog number: ab36993)
16. Podoplanin (D2-40) antibody (Bio-Rad Laboratories, catalog number: MCA2543)
17. CD31 antibody (Abcam, catalog number: ab28364)
18. PROX1 antibody (AngioBio, catalog number: 11-002P)
19. COUP-TF II antibody (R&D Systems, catalog number: PP-H7147-00)
20. CCL21 antibody (Abcam, catalog number: ab9851)
21. CD68 (KP-1) antibody (Thermo Fisher Scientific, Invitrogen, catalog number: MA5-13324)
22. CD3 antibody (Agilent Technologies, Dako, catalog number: A0452)
23. Antibody Diluent (Agilent Technologies, Dako, catalog number: S0809)
24. PV Poly-HRP Anti-Mouse IgG (Leica Biosystems, catalog number: PV6114)
25. PV Poly-HRP Anti-Rabbit IgG (Leica Biosystems, catalog number: PV6119)
26. ImmPRESS™-AP Anti-Rabbit IgG (Vector Laboratories, catalog number: MP-5401)
27. ImmPRESS™-AP Anti-Mouse IgG (Vector Laboratories, catalog number: MP-5402)
28. Goat anti-Mouse IgG, Alexa Fluor 488 (Thermo Fisher Scientific, Invitrogen, catalog number: A-11029)
29. Goat anti-Rabbit IgG, Alexa Fluor 594 (Thermo Fisher Scientific, Invitrogen, catalog number: A-11012)
30. DAB substrate kit (Abcam, catalog number: ab94665)
31. Vector Blue Alkaline Phosphatase Substrate Kit (Vector Laboratories, catalog number: SK-5300)
32. Hematoxylin 560 MX (Leica Biosystems, catalog number: 3801575)
33. Blue buffer 8 (Leica Biosystems, catalog number: 3802916)
34. VectaMount Permanent Mounting Medium (Vector Laboratories, catalog number: H-5000)
35. Fluoro-Gel II Mounting Medium (Electron Microscopy Sciences, catalog number: 17985-50)
36. Tween 20 (Agilent Technologies, Dako, catalog number: S1966)
37. TBS-0.5% Tween 20 (TBST) (see Recipes)

Equipment

1. 18-22 gauge catheter (Smiths Medical)
2. Pressure infusion tubing (ICU Medical)

3. Automatic pressure injector (Bayer, model: Medrad® Spectris Solaris® EP MR Injection System)
4. 3-tesla MRI scanner unit (Siemens Skyra, Siemens Healthcare)
5. 32-channel head coil for MRI signal reception (Siemens Skyra, Siemens Healthcare)
6. Water bath (Leica Biosystem, model: Leica HI1210)
7. Humidified chamber (Simport, model: StainTray™ M920)
8. Manual Rotary Microtome (Leica Biosystem, model: Leica RM2235)
9. Leica RM CoolClamp™ (Leica Biosystem, model: Leica RM CoolClamp)
10. Steamer (IHC World, model: IHC-Tek™ Epitope Retrieval Steamer Set)
11. Digital rocker (VWR, catalog number: 12620-906)
12. Microscope (Carl Zeiss, model: AxioObserver Z.1)
13. Microscope camera (Carl Zeiss, model: Axiocam 503)
14. Magnetic stirrer

Software

1. MIPAV software (<https://mipav.cit.nih.gov/>)
2. OsiriX software (<http://www.osirix-viewer.com/>)
3. Zeiss Zen 2 Blue edition (<https://www.zeiss.com/microscopy/int/products/microscope-software/zen.html>)

Procedure

A. Ethical approval

All human research was carried out under an Institutional Review Board approved protocol, after obtaining informed consent. Formalin-fixed human dura was retrieved at autopsy after obtaining appropriate consent.

B. Human imaging

1. Place an intravenous line using an 18-22 gauge catheter and pressure infusion tubing linked to an MRI compatible automatic pressure injector. (Figure 1)



Figure 1. MRI preparation. Auto injector setup showing the injector (A), linked to the catheter through extension tubing (B, C), and the setup before the subject is moved into the MRI for scanning (D).

2. Set up the subject in the MRI scanner with a 32-channel head coil.
3. Perform cranial MRI as following sequences, a quoted method from Absinta *et al.* (2017).
 - a. Whole-brain T1-Magnetization Prepared Rapid Acquisition of Gradient Echoes (MPRAGE, sagittal 3D turbo-fast low angle shot sequence, acquisition matrix 256 x 256, isotropic resolution 1 mm, 176 slices, repetition time [TR]/echo time [TE]/inversion time [TI] = 3,000/3/900 msec, flip angle 9°, acquisition time 5 min 38 sec).
 - b. Limited T2-weighted Fluid Attenuation Inversion Recovery (FLAIR, coronal 2D acquisition over the superior sagittal sinus, field-of-view 256 mm², 22 slices, reconstructed in-plane resolution 0.25 mm², 42 contiguous 3 mm slices, TR/TE/TI = 6,500/93/2,100 msec, echo train length 17, bandwidth 80 Hz/pixel, acquisition time 5 min), optimized for detection of gadolinium-based contrast agent in the subarachnoid space.
 - c. Black-blood scan (coronal acquisition, Sampling Perfection with Application optimized Contrasts using different flip angle Evolution [SPACE] sequence, field-of-view 174 mm², matrix 320 x 320, reconstructed in-plane resolution 0.27 mm², 64 contiguous 0.5 mm sections, TR/TE = 938/22 msec, echo train length 35, bandwidth 434 Hz/pixel, acquisition time 7 min 50 sec). Acquire a series of 2 or three overlapping coronal acquisitions to cover most of the cerebral hemispheres.
 - d. Whole-brain T2-FLAIR scan (coronal 3D SPACE sequence, field-of-view 235 mm², matrix 512 x 512, reconstructed in-plane resolution 0.46 mm², 176 1 mm sections, TR/TE/TI = 4,800/354/1,800 msec, nonselective inversion pulse, echo-train length 298, bandwidth 780 Hz/pixel, acceleration factor 2, acquisition time 14 min).
 - e. Whole-brain T1-SPACE (axial 3D acquisition, acquisition matrix 256 x 256, isotropic resolution 0.9 mm, 112 sections, TR/TE = 600/20 msec, flip angle 120°, echo-train length 28, acquisition time 10 min).
4. Inject MRI contrast agent, either gadobutrol (0.1 mmol/kg body weight, i.v., Bayer HealthCare) or another standard agent, at a rate of 0.3 ml/min followed by 10 ml of saline flush.
5. Repeat MRI sequences A3a, A3c, and A3d after completion of the infusion.

6. Convert scanner-generated DICOM images into NIFTI files for processing using dcm2nii script (nitrc.org, open source).
7. Co-register pre- and post-contrast images, perform skull-stripping, and subtract pre-contrast images from post-contrast images using standard algorithms implemented in MIPAV software (select Algorithms/Registration/Optimized Automatic Registration and Utilities/Image Calculator/Subtract, respectively).
8. Import subtraction images into OsiriX software for maximum intensity projection (MIP) 3D rendering (select 2D/3D and then 3D Surface Rendering). (Figure 2)

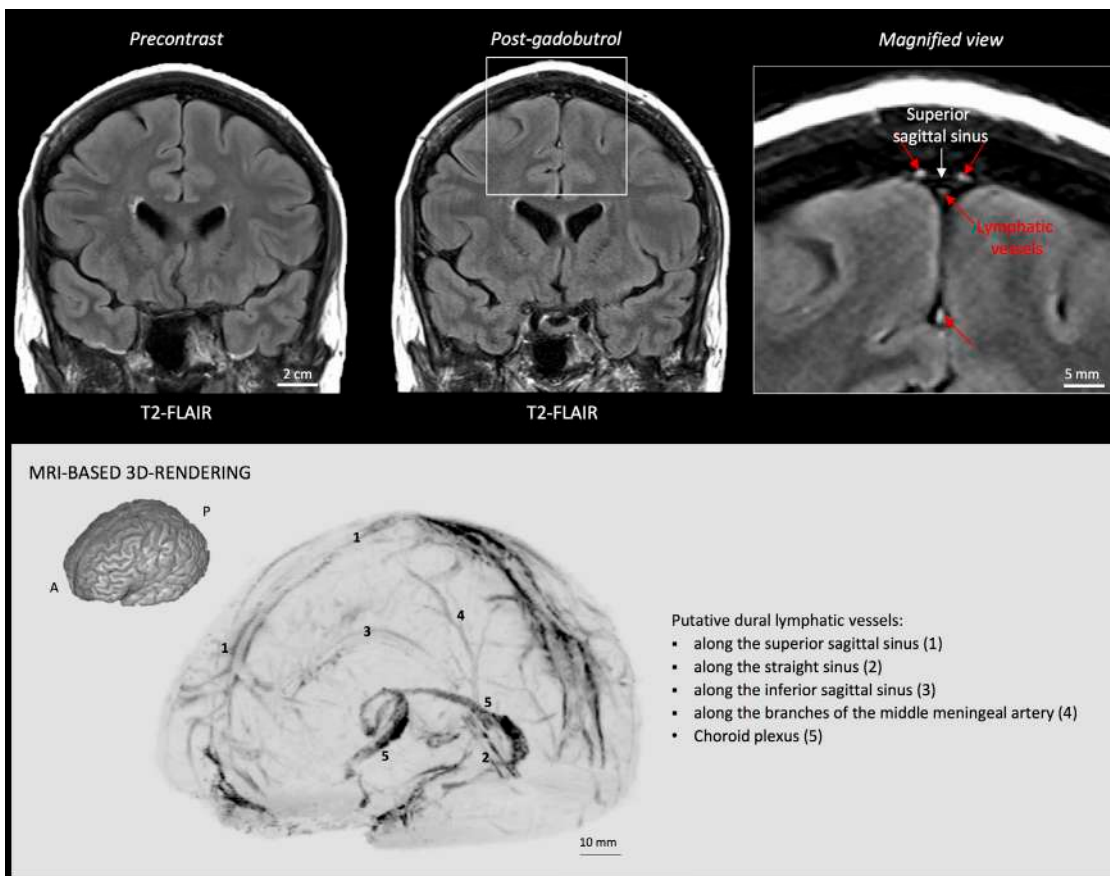


Figure 2. MRI visualization of dural lymphatic vessels in human. On post-gadobutrol coronal T2-FLAIR, the dura does not enhance, and lymphatic vessels (red arrows), running alongside the venous dural sinuses and within the falx cerebri, can be appreciated. 3D rendering, using OsiriX software, of putative dural lymphatics (black) in a 47-year old woman, derived from whole-brain T1-weighted SPACE MRI. (Modified from Figure 1 and Figure S1 in Absinta et al. [2017]. [Creative Commons Attribution License](#))

9. For more specific lymphatic imaging, perform Steps B1-B8 using gadofosveset (0.03 mmol/kg body weight, i.v., Lantheus Medical Imaging) rather than gadobutrol. Compare the subtraction

images obtained from gadofovest and gadobutrol experiments to identify the lymphatic vessels (Figure 3).

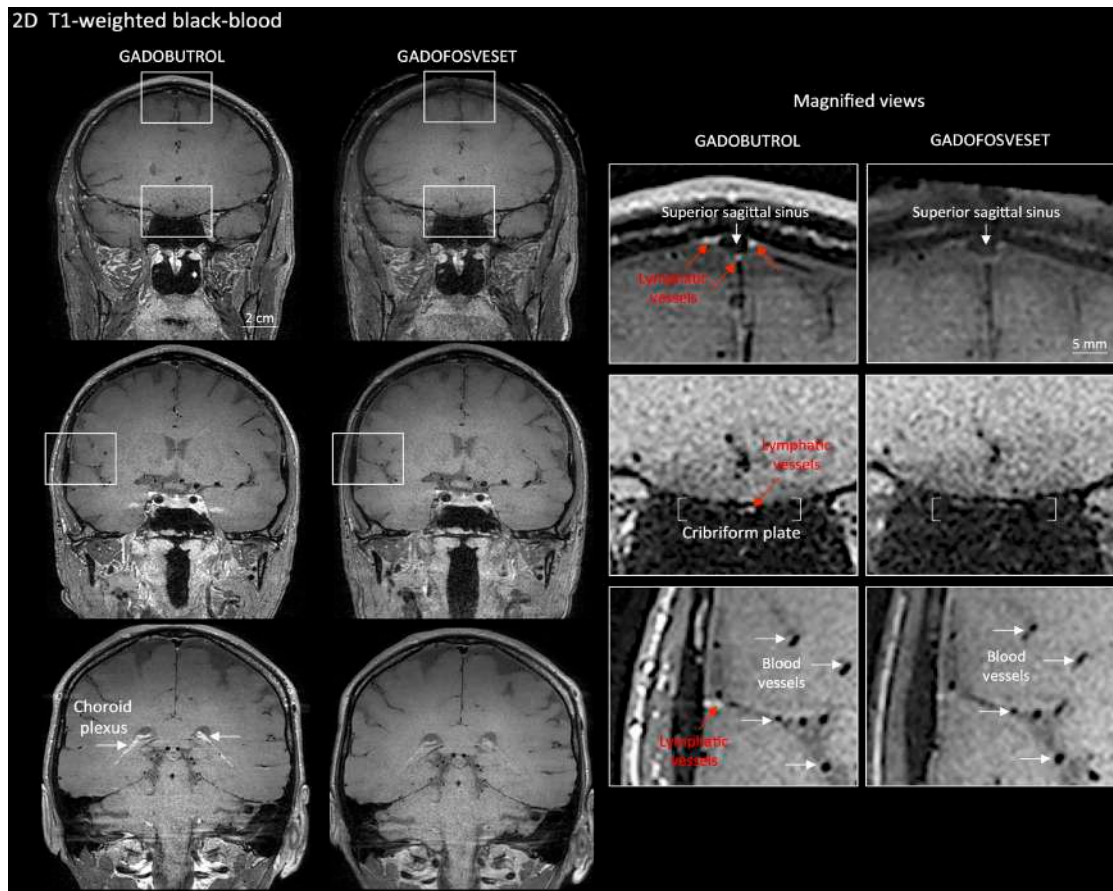


Figure 3. Gadobutrol vs. gadofoveset in MRI visualization of dural lymphatic vessels.

Coronal T1-weighted black-blood images were acquired after intravenous injection of two different gadolinium-based contrast agents during two MRI sessions separated by one week. Dural lymphatics (red arrows in magnified view boxes) were better discerned using gadobutrol (standard MRI contrast agent, which readily enters the dura) compared to gadofoveset (serum albumin-binding contrast agent, which remains largely intravascular) and were localized around dural sinuses, middle meningeal artery, and cribriform plate (white arrows). Notably, the choroid plexus (white arrows) enhanced less with gadofoveset than gadobutrol, whereas meningeal and parenchymal blood vessels (both veins and arteries) did not enhance with any contrast agent and appeared black. (Originally published in Absinta *et al.* [2017]. [Creative Commons Attribution License](#))

C. Immunohistochemistry, single staining

1. Fix freshly dissected human dura mater with 10% formalin for 24-48 h at room temperature. Commercial 10% neutral buffered formalin (NBF) contains a small percentage of methanol as a stabilizer, which is not a problem for the majority of procedures. Dura should be fixed as soon as possible using gentle agitation (swirling) of the specimen to aid penetration and fixation

reaction. Tissue should be fixed for 24-48 h in NBF, and then stored in 1x PBS with a few drops of 10% formalin at room temperature.

2. Trim the dura into coronal sections and embed the tissue in a paraffin block (see Figure 4). Our recommendation is to focus on the coronal sections near the superior sagittal sinus, which can be easily identified in the dura.

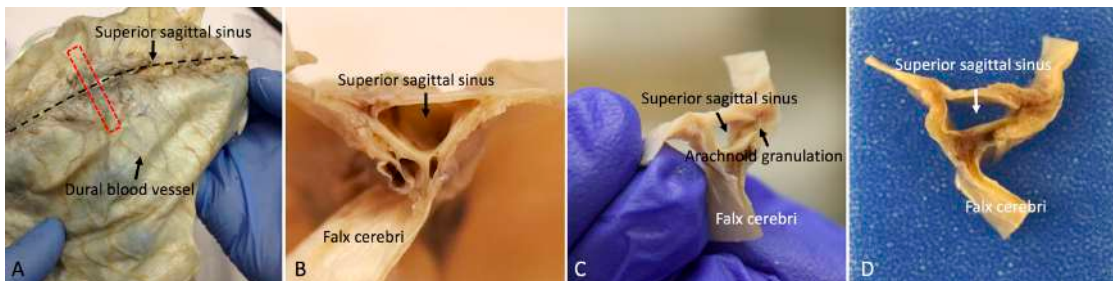
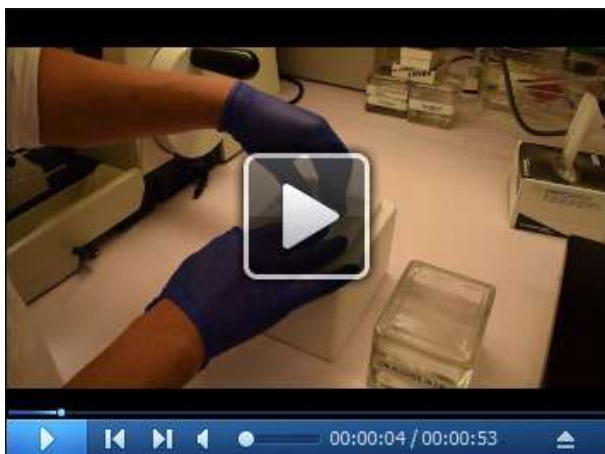


Figure 4. Whole-mount and coronal sections of the human dura mater for histological analysis. A. The red dotted line shows the sampling direction. B, C, and D. Show the coronal view of the dura mater sample before tissue processing.

3. Using rotary microtome, cut the paraffin-embedded tissue block into sections of 3-8 μm thickness. Float the sections in 20% ethanol at room temperature, then transfer them to a 44 °C water bath. (see Note 1 and Video 1)



Video 1. Demonstration of the sectioning of the human dura mater using a microtome. Before sectioning, place the paraffin tissue block surface on melting ice or cold wet paper towel. After sectioning, place the section in 20% ethanol and then into a warm floating bath.

4. Transfer the sections onto Superfrost Plus Microslides, as uncoated or uncharged slides may not retain the tissue. Before drying out the slides, remove residual water using a snap of the wrist (imagine wielding a whip), which is important to prevent sections from lifting from slides.

Allow the slides to dry vertically overnight, at room temperature, to allow trapped water to escape downward.

5. Deparaffinize slides using xylene (3 changes of xylene, each 3 min).
6. Rehydrate slides using 100% alcohol (3 changes, each 3 min), 80% alcohol (3 min) and 50% alcohols (3 min), respectively.
7. Rinse slides in deionized water for 1 min.
8. Perform heat-induced antigen retrieval to unmask the antigenic epitope using a steamer. Add tap water to the water base, to the “Max” line, and put the steaming plate onto the water reservoir. Fill a plastic Coplin jar with Target Retrieval Solution or Target Retrieval Solution, at pH 9, and dip deparaffinized/rehydrated slides in the jar. Place the plastic Coplin jar in the steamer and cover it. Turn on the steamer and set the timer for 20 min to incubate it at 95-100 °C. We recommend steamer for heat-induced antigen retrieval instead of microwave or pressure cooker, because it reduces the chance of the section falling off the slide.
9. Take out the Coplin jar and allow it to cool down for 10 min at room temperature.
10. Rinse slides gently in Tris-buffered saline (TBS) for 5 min. Use TBS or TBS-0.5% Tween 20 (TBST) during slide washing to prevent sections from falling off.
11. Immerse sections in 0.3% H₂O₂ solution in deionized water at room temperature for 10 min to block endogenous peroxidase activity.
12. Rinse slides gently in TBST for 1 min.
13. Draw the hydrophobic barrier around the tissues using PAP pen.
14. Rinse slides gently in TBST 20 for 1 min.
15. Drop 3-4 of Dako Protein Block on the tissue and incubate at room temperature for 20 min in a humidified chamber.
16. Gently drop off the excess Dako Protein Block from the slides. Do not rinse the slides in this step.
17. Apply primary antibody + Dako Antibody Diluent (see Table 1 for antibody dilution factor; 100-200 µl is required to cover the tissue) on the tissues, and incubate at room temperature for 2 h or at 4 °C overnight in a humidified chamber. Make sure that the antibody is spread well on the tissues.

Table 1. Condition of antigen retrieval, antibody dilution and time of incubation

1 st Antibody	Function	Antigen retrieval	Antibody dilution and time of incubation
LYVE1	Lymphatic endothelial cells	Target Retrieval Solution, pH 9 20 min by steamer	1:200, 4 °C overnight
Podoplanin (D2-40)	Lymphatic endothelial cells	Target Retrieval Solution, pH 9 20 min by steamer	1:50, 2 h RT
CD31	Blood endothelial cells	Target Retrieval Solution, pH 9 20 min by steamer	1:50, 2 h RT
PROX1	Lymphatic nuclear transcription factor	Target Retrieval Solution, 20 min by steamer	1:300, 4 °C overnight
COUP-TF II	Lymphatic nuclear transcription factor	Target Retrieval Solution, 20 min by steamer	1:200, 4 °C overnight
CCL21	Lymphatic endothelial cells	Target Retrieval Solution, pH 9 20 min by steamer	1:200, 1 h RT

18. Wash slides in TBST 3 times, 5 min each, using a rocker.
19. Apply secondary antibody (HRP anti-Mouse IgG or HRP anti-rabbit IgG) on the tissues and incubate for 30 min at room temperature in a humidified chamber.
20. Wash slides in TBST 3 times, 5 min each, using a rocker.
21. Drip 3-4 drops of freshly made DAB substrate solution on the slide and check the brown color of antibody signal by microscopy.
22. If the staining reveals adequate intensity, stop the DAB reaction by dipping slides in deionized water. Over-staining will lead to high background that will obscure the true signals.
23. Dip slides in Leica Hematoxylin 560 MX for 10 sec, for better morphology and contrast.
24. Rinse slides in tap water for 5 min.
25. Immerse slides in bluing solution (Leica Blue buffer or 0.2% ammonia solution or 0.1% lithium carbonate solution).
26. Dehydrate slides through air dry and coverslip using Permount mounting solution. The mounted slides can be kept at room temperature constantly.

- D. Immunohistochemistry, double staining of D2-40 and CD31 (simultaneous double staining of lymphatic and blood vessels, respectively)
 1. Follow Steps C5-C16 above.
 2. Apply cocktails of primary antibodies + Dako Antibody Diluent on the tissues and incubate at room temperature for 2 h in a humidified chamber.
 3. Wash slides in TBST 3 times, 5 min each, using a rocker.
 4. Apply secondary antibody (HRP anti-Mouse IgG for D2-40 and ImmPRESS™-AP anti-Rabbit IgG for CD31) on the tissues and incubate for 30 min at room temperature in a humidified chamber.

5. Wash slides in TBST 3 times, 5 min each, using a rocker.
6. Drip 3-4 drops of freshly made DAB substrate solution on the slide and check the brown color of D2-40 antibody signal by microscopy.
7. Wash slides in deionized water to stop the DAB reaction.
8. Drip 3-4 drops of fresh Vector Blue substrate solution on the same slide and check the blue color of CD-31 antibody signal by microscopy.
9. If the staining reveals enough intensity, stop the Vector Blue reaction by dipping slides in deionized water.
CAUTION: Do NOT perform hematoxylin counterstaining following use of the Vector Blue chromogen.
10. Dehydrate slides through air dry and coverslip using Permount mounting solution.

- E. Immunohistochemistry, double staining of PROX1 and CD31 (sequential double staining)
1. Follow Steps C5-C22 above. Finish PROX1 immunostaining without counterstaining.
 2. Drip 3-4 drops of Dako Protein Block on the tissue and incubate at room temperature for 20 min in a humidified chamber.
 3. Gently drop off the excess Dako Protein Block from the slides. Do not rinse the slides in this step.
 4. Apply CD31 antibodies + Dako Antibody Diluent on the tissues and incubate at room temperature for 2 h in a humidified chamber.
 5. Wash slides in TBST 3 times, 5 min each, using a rocker.
 6. Apply secondary antibody (ImmPRESS™-AP anti-Rabbit IgG for CD31) on the tissues and incubate for 30 min at room temperature in a humidified chamber.
 7. Wash slides in TBST 3 times, 5 min each, using a rocker.
 8. Drip 3-4 drops of fresh Vector Blue substrate solution on the same slides and check the blue color of CD-31 antibody signal by microscopy.
 9. Stop the Vector Blue reaction by dipping slides in deionized water if the staining reveals enough intensity.
CAUTION: Do NOT perform hematoxylin counterstaining following use of the Vector Blue chromogen.
 10. Dehydrate slides through air drying and coverslip using Permount mounting solution.

- F. Immunofluorescence, double staining of D2-40 + CD31 (simultaneous double staining)
1. Follow Steps D1-D3 above.
 2. Apply cocktails of secondary antibodies (Goat anti-Mouse IgG Alexa Fluor 488 and Goat anti-rabbit IgG Fluor 594, 1:200 diluted in Dako Antibody Diluent) on the tissues and incubate for 30 min at room temperature in a humidified chamber.
 3. Wash slides in TBST 3 times, 5 min each, using a rocker.
 4. Dehydrate slides through air dry and coverslip using Fluoro-Gel II Mounting Medium.

5. Observe the localization of D2-40 and CD31 with fluorescence microscopy.

Data analysis

Scan the entire slide and stitch it together by greater than 10x magnification using Zeiss Microscope, camera, and Zeiss Zen Blue software. On slides double-stained for lymphatic and vascular endothelial markers (D2-40/CD31 and PROX1/CD31), identify lymphatic structures and mark them on the screen under the microscope using the following criteria: (a) structures of endothelial cell-lined vessel; (b) vessel with thin endothelial cells, the nuclei of cell bulge into the lumen; (c) semi-collapsed thin vessel wall with poor basal lamina; and (d) no or only a few red blood cells in the lumen of the vessel (Killer *et al.*, 2008). Lymphatic vessels are counted, and their dimensions are measured. If samples vary in disease type or treatment status, simple comparative statistics may be computed on the count and diameter data (Figure 5).

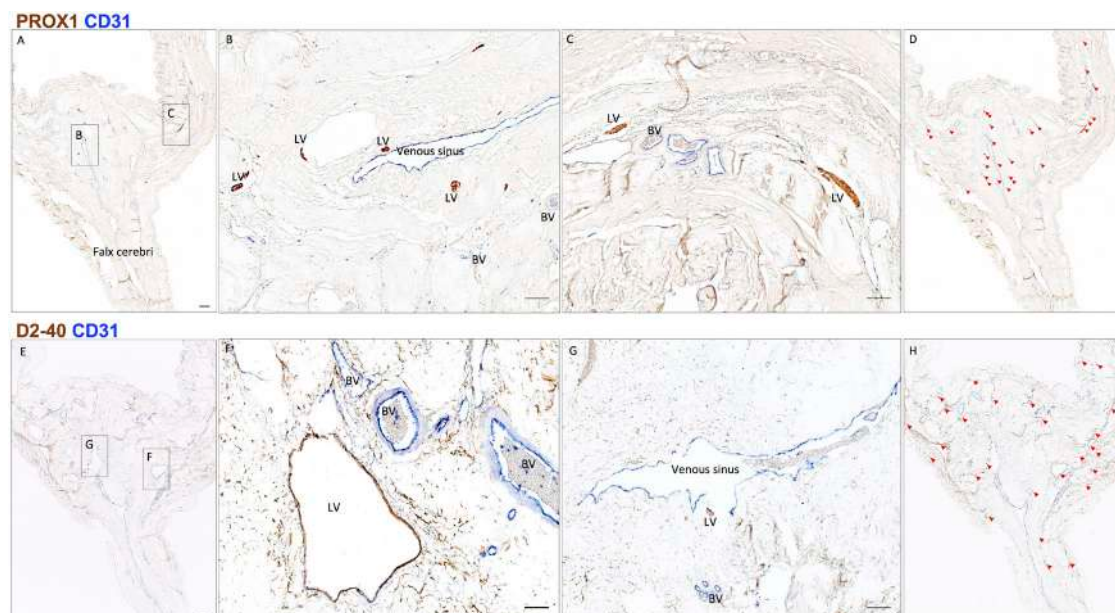


Figure 5. Neuropathology of human dural lymphatic vessels, coronal section. A, B and C. Within the dura mater, lymphatic and blood vessels can be differentiated using double staining for PROX1 (a transcription factor involved in lymphangiogenesis, nuclear staining) and CD31 (a vascular endothelial cell marker). E, F and G. Similarly, lymphatic and blood vessels can be differentiated using double staining for D2-40 (endothelial membrane staining) and CD31. Red blood cells are seen within blood vessels, but not within lymphatic vessels. D and H. Using Zeiss Zen Blue software, lymphatic structures are marked on the digitalized slide. Insets (B, C, F, G) were rotated relative to the original Figures in A and E. Scale bars: 1 mm (A, G), 100 µm (B, C, F, G). Abbreviations: LV—lymphatic vessels; BV—blood vessels. (Modified from Figure 3 in Absinta *et al.* [2017]. [Creative Commons Attribution License](#))

Notes

1. Human dura mater is a very tough tissue, and microtome sectioning is difficult. Chilling the paraffin blocks (e.g., Leica RM Cool Clamp™) makes sectioning of dura easier. Also, when tissue is exposed on the surface of a paraffin block by rough trimming, it has the capacity to absorb water, which can penetrate a small distance into the tissue, resulting in softening and swelling it. For the dura mater, this effect may allow a couple of sections to be cut easily. By placing the trimmed block surface on melting ice or in a tray of ice water at 4 °C for 1 min, followed by use of a cold wet paper towel for 30 sec to 1 min, the sectioning becomes easier. Generally, after this procedure, the best quality sections are achieved by cutting very slowly.
2. Paraffin sections of dura may wrinkle easily, which can generate artifacts and ultimately nonspecific staining. Non-standard flotation techniques may be useful if the sections obtained from a block are highly wrinkled. If sections are initially floated in 20% ethanol then transferred, on a slide, to a hot flotation bath, the wrinkling may be mitigated. 20% ethanol actively removes the wrinkles out because it has lower surface tension than water.
3. Formalin fixed-paraffin embedded (FFPE) human skin can be used as a positive control for lymphatic vessel marker and assessment. FFPE Hippocampus (CA3) of brain tissue can be used as good positive control for PROX1 staining.

Recipes

1. TBS-0.5% Tween 20 (TBST)
200 ml 10x TBS
1,800 ml deionized water
Add 1 ml of Tween 20, mixed well using a magnetic stirrer

Acknowledgments

The Intramural Research Program of NINDS supported this study. This protocol was adapted from procedures published in Absinta *et al.* (2017). Figures 2, 3, and 5 were modified and reproduced with permission from Absinta *et al.* (2017). The authors declare no conflicts of interest.

References

1. Absinta, M., Ha, S. K., Nair, G., Sati, P., Luciano, N. J., Palisoc, M., Louveau, A., Zaghloul, K. A., Pittaluga, S., Kipnis, J. and Reich, D. S. (2017). [Human and nonhuman primate meninges harbor lymphatic vessels that can be visualized noninvasively by MRI](#). *eLife*: e29738.

2. Aspelund, A., Antila, S., Proulx, S. T., Karlsen, T. V., Karaman, S., Detmar, M., Wiig, H. and Alitalo, K. (2015). [A dural lymphatic vascular system that drains brain interstitial fluid and macromolecules.](#) *J Exp Med* 212(7): 991-999.
3. Louveau, A., Smirnov, I., Keyes, T. J., Eccles, J. D., Rouhani, S. J., Peske, J. D., Derecki, N. C., Castle, D., Mandell, J. W., Lee, K. S., Harris, T. H. and Kipnis, J. (2015). [Structural and functional features of central nervous system lymphatic vessels.](#) *Nature* 523(7560): 337-341.
4. Killer, H. E., Jaggi, G. P., Miller, N. R., Flammer, J. and Meyer, P. (2008). [Does immunohistochemistry allow easy detection of lymphatics in the optic nerve sheath?](#) *J Histochem Cytochem* 56(12): 1087-92.

A blue-tinted photograph of a scientist's hands in gloves performing a precise task with small tools, likely a pipetting or microdissection. Overlaid on the top left is the Bio-Protocol logo: "bio-protocol" in white lowercase letters, with "Improve Research Reproducibility" in smaller white text below it. In the center, the text "Free access to ~4000 high-quality protocols" is displayed in white. Below this, a bulleted list of features is shown: "Contributed by 10,000+ scientists (including Nobel Laureates)", "Validated in a primary research paper", ">91% reproducibility (survey of 2165 Bio-protocol users)", and "~1000 videos of key procedural steps". At the bottom of the ad is a blue button with white text that reads "Sign up at: www.bio-protocol.org".

bio-protocol
Improve Research Reproducibility

Free access to ~4000 high-quality protocols

- Contributed by 10,000+ scientists (including Nobel Laureates)
- Validated in a primary research paper
- >91% reproducibility (survey of 2165 Bio-protocol users)
- ~1000 videos of key procedural steps

Sign up at: www.bio-protocol.org

Preparation of Cerebellum Granule Neurons from Mouse or Rat Pups and Evaluation of Clostridial Neurotoxin Activity and Their Inhibitors by Western Blot and Immunohistochemistry

Domenico Azarnia Tehran^{1, \$, *} and Marco Pirazzini^{1, *}

¹Department of Biomedical Sciences, University of Padova, Padova, Italy; ^{\$}Present address: Leibniz-Forschungsinstitut für Molekulare Pharmakologie (FMP), Robert-Rössle-Straße 10, Berlin, Germany

*For correspondence: doazte@gmail.com; marcopiraz@gmail.com



[Abstract] Cerebellar Granule Neurons (CGN) from post-natal rodents have been widely used as a model to study neuronal development, physiology and pathology. CGN cultured *in vitro* maintain the same features displayed *in vivo* by mature cerebellar granule cells, including the development of a dense neuritic network, neuronal activity, neurotransmitter release and the expression of neuronal protein markers. Moreover, CGN represent a convenient model for the study of Clostridial Neurotoxins (CNT), most notably known as Tetanus and Botulinum neurotoxins, as they abundantly express both CNT receptors and intraneuronal substrates, *i.e.*, Soluble N-ethylmaleimide-sensitive factor activating protein receptors (SNARE proteins). Here, we describe a protocol for obtaining a highly pure culture of CGN from postnatal rats/mice and an easy procedure for their intoxication with CNT. We also illustrate handy methods to evaluate CNT activity and their inhibition.

Keywords: Cerebellar granule neurons, Clostridial neurotoxins, Tetanus, Botulinum, SNARE proteins, Inhibitors, Cell-based assay

[Background] The large family of Clostridial Neurotoxins (CNT) is formed by Tetanus Neurotoxin (TeNT) and the many variants of Botulinum Neurotoxins (BoNT) which are the neuroparalytic toxins responsible for tetanus and botulism, respectively (Schiavo *et al.*, 2000; Johnson and Montecucco, 2008; Rossetto *et al.*, 2014). TeNT, the seven BoNT serotypes (BoNT/A to /G) and their many subtypes are metalloproteases that cause neuroparalysis by blocking neurotransmitter release via the cleavage of SNARE proteins (Soluble N-ethylmaleimide-sensitive factor activating protein receptors), the three essential proteins governing the fusion of synaptic vesicle with the presynaptic plasma membrane (Rossetto *et al.*, 2014; Montecucco and Rasotto, 2015; Pirazzini *et al.*, 2017). In addition, some putative novel serotypes (BoNT/X and BoNT/En aka eBoNT/J) (Zhang *et al.*, 2017; Brunt *et al.*, 2018; Zhang *et al.*, 2018) and a BoNT-like toxin (BoNT/Wo) (Zornetta *et al.*, 2016) displaying metalloprotease activity against SNARE proteins have been recently identified (Azarnia Tehran and Pirazzini, 2018). Yet, whether they are naturally produced and can be considered true BoNT still requires validation. Each toxin has a selective action against one specific protein that is cleaved at a distinct peptide bond (Binz, 2013; Pantano and Montecucco, 2014; Zornetta *et al.*, 2016; Zhang *et al.*, 2017; Zhang *et al.*, 2018): BoNT/B, /D, /F /G, /Wo and /X hydrolyze VAMP-1/2 (vesicle-associated membrane protein) while BoNT/A and BoNT/E cleave the membrane protein SNAP-25 (synaptosomal-associated protein of 25

kDa). BoNT/C and BoNT/En are unique as they cleave more than one SNARE type: BoNT/C cleaves SNAP-25 and many isoforms of syntaxin (Pirazzini *et al.*, 2017; Zanetti *et al.*, 2017); instead BoNT/En cleaves different members of VAMP family and SNAP-25/23 (Zhang *et al.*, 2018). To reach their intraneuronal substrates, CNT carry out a very sophisticated mechanism of intoxication aimed at delivering the catalytic part of the toxin within the cytosol of nerve terminals (reviewed in [Montal, 2010; Rossetto *et al.*, 2014; Pirazzini *et al.*, 2017]).

This process relies on cardinal functions of neuron physiology which are exploited by BoNT to enter the neuron: the expression of appropriate glycolipid and protein receptors for binding (Binz and Rummel, 2009; Rummel, 2017), the recycling of synaptic vesicles for internalization (Matteoli *et al.*, 1996; Harper *et al.*, 2011; Colasante *et al.*, 2013), the generation of an electrochemical gradient across synaptic vesicle membrane to translocate the catalytic domain in the cytosol (Montal, 2010; Pirazzini *et al.*, 2016) and the presence of a redox-chaperone system to enable SNARE proteins' cleavage (Pirazzini *et al.*, 2018). These features are fully preserved by cultured Cerebellar Granule Neurons (CGN), a primary culture of cerebellar granule cells from post-natal rodent cerebellum. The cerebellar cortex is composed of a few neuronal types like Purkinje cells, inhibitory interneurons and granule cells that form a highly organized tissue with well-characterized neuronal circuitries (Bilimoria and Bonni, 2008). Cerebellar granule cells constitute the most numerous and homogeneous neuronal population and can be easily isolated (Messer, 1977). Cultured CGN recapitulate many characteristics of development and maturation observed *in vivo* and have been extensively used as a useful model to study basic molecular and biological processes of neuron physiology like apoptosis, migration and differentiation (Contestabile, 2002).

Many neuronal models, including spinal cord neurons, hiPSC derived neurons, mES derived neurons, hippocampal neurons, cortical neurons and several methods have been developed to study BoNT activity *in vitro* (Pellett, 2013). In our laboratory, we choose CGN as their preparation is relatively simple, rapid and very reliable and it provides a highly pure (more than 95%) and homogeneous (mostly granule cells) neuronal culture model to conveniently evaluate CNT activity by monitoring the cleavage of SNARE proteins via Western blotting or immunocytochemistry (Pirazzini *et al.*, 2011; Eleopra *et al.*, 2013; Pirazzini *et al.*, 2013b and 2013c). Moreover, CGN can be adapted to the investigation of putative inhibitors and can be used as a solid platform for screening anti-BoNT antitoxins (Pirazzini *et al.*, 2013a and 2014; Azarnia Tehran, *et al.*, 2015; Zanetti *et al.*, 2015; Pirazzini and Rossetto, 2017). Here, we describe a simple protocol for fast isolation of CGN, an easy procedure for their intoxication with CNT, and two methods (Western blot and immunocytochemistry) to evaluate their toxicity and inhibition.

Materials and Reagents

1. 0.22 µm filters (33 mm – Merck, Millex, catalog number: SLGP033RS)
 2. Culture plates
- 6 wells (Corning, Falcon®, catalog number: 353046)

- 24 wells (Corning, Falcon®, catalog number: 353047)
- 96 wells (Corning, Falcon®, catalog number: 353072)
- 3. 35 mm Petri dishes (Corning, Falcon®, catalog number: 353001)
- 4. 50 ml sterile conical plastic tubes (Corning, Falcon®, catalog number: 352070)
- 5. Coverslips 13 mm #1 (Thermo Fisher Scientific, catalog number: 1014355113NR1)
- 6. Micropipette tips
 - 1,000 µl tips (SARSTEDT, catalog number: 70.762.211)
 - 200 µl tips (SARSTEDT, catalog number: 70.760.211)
 - 10 µl tips (SARSTEDT, catalog number: 70.1130.210)
- 7. Nitrocellulose membranes (Sartorius, Stedim Biotech, catalog number: 11306-41BL)
- 8. Plastic Pasteur pipettes (LP ITALIANA, catalog number: 133030)
- 9. Serological plastic pipettes:
 - 5 ml plastic pipettes (Corning, Falcon®, catalog number: 357543)
 - 10 ml plastic pipettes (Corning, Falcon®, catalog number: 357551)
 - 25 ml plastic pipettes (Corning, Falcon®, catalog number: 357525)
- 10. Single-use steri-cups 0.22 µm filters Express™ Plus (Merck, catalog number: SCGPU0SRE)
- 11. Sterile scalpel (CHEMIL, catalog number: 11230028)
- 12. Mice or rats (any gender) postnatal day 4-6
- 13. Distilled H₂O
- 14. Ethanol (Sigma-Aldrich, catalog number: 46139)
- 15. Poly-L-lysine hydrobromide solution (Sigma-Aldrich, catalog number: P8920)
- 16. Phenol red (Sigma-Aldrich, catalog number: P3532)
- 17. Potassium chloride (KCl) (Sigma-Aldrich, catalog number: P5405)
- 18. Sodium chloride (NaCl) (Sigma-Aldrich, catalog number: S3014)
- 19. D-(+)-Glucose (Sigma-Aldrich, catalog number: G7528)
- 20. Sodium phosphate monobasic monohydrate (NaH₂PO₄) (Sigma-Aldrich, catalog number: S3522)
- 21. KH₂PO₄ (Sigma-Aldrich, catalog number: P5655)
- 22. HEPES (Sigma-Aldrich, catalog number: H3375)
- 23. Calcium chloride dihydrate (CaCl₂·2H₂O) (Sigma-Aldrich, catalog number: C3306)
- 24. Magnesium sulfate heptahydrate (MgSO₄·7H₂O) (Sigma-Aldrich, catalog number: 63138)
- 25. Fatty acid free bovine serum albumin (Sigma-Aldrich, catalog number: A7030)
- 26. Trypsin from porcine pancreas (Sigma-Aldrich, catalog number: T4799)
- 27. Trypsin inhibitor from soybean (Sigma-Aldrich, catalog number: T9003)
- 28. Complete™ Mini, EDTA-free Protease Inhibitor Cocktail (Sigma-Aldrich, Roche Diagnostics, catalog number: 04693159001)
- 29. Trypan blue solution, 0.4% (Thermo Fisher Scientific, catalog number: 15250061)
- 30. Deoxyribonuclease I from bovine pancreas (Sigma-Aldrich, catalog number: D5025)
- 31. Basal Medium Eagle (BME) (Thermo Fisher Scientific, Gibco™, catalog number: 21010046)

32. Glutamax™ Supplement (Thermo Fischer Scientific, Gibco™, catalog number: 35050061)
33. Gentamicin solution (Sigma-Aldrich, catalog number: G1272)
34. Cytosine β-D-arabinofuranoside (AraC) (Sigma-Aldrich, catalog number: C1768)
35. Fetal Bovine Serum (FBS) (EUROCLONE, catalog number: EUS 028877)
Note: Comparative testing for culture optimization is needed when changing serum lot or supplier.
36. Trizma® base (Sigma-Aldrich, catalog number: T1503)
37. Trizma® hydrochloride (Sigma-Aldrich, catalog number: T3253)
38. Glycine (Sigma-Aldrich, catalog number: G8898)
39. Sodium dodecyl sulfate (SDS, Sigma-Aldrich, catalog number: L3771)
40. Bromophenol Blue (Sigma-Aldrich, catalog number: B0126)
41. Glycerol (Sigma-Aldrich, catalog number: G9012)
42. 2-mercaptoethanol (Sigma-Aldrich, catalog number: M6250)
43. NuPAGE™ 12% Bis-Tris Gels (Thermo Fisher Scientific, catalog number: NP0341BOX)
44. NuPAGE™ 4-12% Bis-Tris Gels (Thermo Fisher Scientific, catalog number: NP0321BOX)
45. NuPAGE™ MES SDS Running Buffer (20x) (Thermo Fisher Scientific, catalog number: NP0002)
46. NuPAGE™ MOPS SDS Running Buffer (20x) (Thermo Fisher Scientific, catalog number: NP0001)
47. Methanol (Sigma-Aldrich, catalog number: 322415)
48. Ponceau S (Sigma-Aldrich, catalog number: P3504)
49. Acetic acid (Sigma-Aldrich, catalog number: 45726)
50. Tween 20® (Sigma-Aldrich, catalog number: P9416)
51. Anti Syntaxin-1A/1B antibody (homemade)
52. Anti-BoNT/A-cleaved SNAP-25 antibody (homemade)
53. Anti-BoNT/B-TeNT-cleaved VAMP2 antibody (homemade)
54. Anti-BoNT/E-cleaved SNAP-25 antibody (homemade)
55. Anti-SNAP-25 antibody (SMI81, Abcam, catalog number: ab24737)
56. Anti-Syntaxin1 antibody (Synaptic System, catalog number: 110 011)
57. Anti-VAMP-2 antibody (Synaptic System, catalog number: 104 211)
58. Paraformaldehyde (Sigma-Aldrich, catalog number: P6148)
59. Ammonium chloride (Sigma-Aldrich, catalog number: A9434)
60. Fluorescence mounting medium (Agilent Technologies, Dako, catalog number: S3023)
61. HRP-conjugated or fluorescent-conjugated secondary antibodies (any supplier)
62. Sodium dodecyl sulfate (Sigma-Aldrich, catalog number: 74255)
63. Tetanus neurotoxin and botulinum neurotoxins. The neurotoxins used in our laboratory are purified as previously described (Schiavo and Montecucco, 1995; Shone and Tranter, 1995) or produced recombinantly (Bade *et al.*, 2004; Zanetti *et al.*, 2017)
64. Krebs solution (10x) (see Recipes)

65. 155 mM MgSO₄ stock solution (see Recipes)
66. 12.2 mM CaCl₂ stock solution (see Recipes)
67. Solution A (see Recipes)
68. Solution B (see Recipes)
69. Solution C (see Recipes)
70. Solution D (see Recipes)
71. Solution E (see Recipes)
72. Poly-L-lysine solution (see Recipes)
73. BME complete medium, CGN culture medium (see Recipes)
74. Cytosine β-D-arabinofuranoside (AraC) stock solution (see Recipes)
75. PBS (see Recipes)
76. PBST (see Recipes)
77. SDS-PAGE Sample loading buffer (4x) (see Recipes)
78. Transfer buffer (see Recipes)
79. Ponceau S solution (see Recipes)
80. Blocking buffer (see Recipes)
81. 4% Paraformaldehyde solution (see Recipes)
82. Quenching solution (see Recipes)
83. Permeabilization solution (see Recipes)
84. Blocking solution (see Recipes)

Equipment

1. Micropipettes (any supplier)
2. Pipette controller (any supplier)
3. Centrifuge for conical tubes (Eppendorf, model: 5804 R)
4. Dissecting hood (any supplier)
5. Dissecting stereomicroscope (OPTIKA Microscopes, model: SZM-LED2)
6. Sterile laminar flow hood (any supplier)
7. Hemacytometer (any supplier)
8. Humidified incubator (5% CO₂ at 37 °C) (any supplier)
9. Ice bucket and ice
10. Scissors #1 (Rudolf Medical GmbH, catalog number: RU 2675-18)
11. Forceps #2 (Rudolf Medical GmbH, catalog number: RU 7584-16)
12. Scissors #3 (Rudolf Medical GmbH, catalog number: RU 2246-09)
13. Tweezers #4 (Rudolf Medical GmbH, catalog number: RU 4240-05)
14. Mini gel tank (Thermo Fisher Scientific catalog number: A25977)
15. Mini Trans-Blot® Cell (Bio-Rad Laboratories, catalog number: 1703930)
16. Thermoblock (any supplier)

17. Thermosettable water-bath (37 °C) (any supplier)
18. Vortex mixer (any supplier)
19. Epifluorescence or confocal microscope: Leica CTR6000 equipped with X5 N PL AN (Leica Microsystems, model: Leica CTR6000)
20. 0.12, x20 N PL AN 0.40 objectives or Leica SP5 equipped with 100x HCX PL APO NA 1.4 objective, respectively (Leica Microsystems, Wetzlar, Germany)

Procedure

A. Culturing Cerebellar Granule neurons (CGN)

1. Prepare poly-L-lysine coated 24 well-plates at least 1 h before preparation.

Notes:

- a. According to the experimental design, different cell cultures plates (6, 12, 24, 96 wells) or dishes can be used.
- b. Cover with 1,000, 500, 250, 50 µl of poly-L-lysine solution each well of 6, 12, 24, 96 wells cell cultures plates respectively. Incubate at room temperature for at least 2 h.
- c. Poly-L-lysine solution has to be aspirated, and dry the plate/dish/coverslip before cell plating (see Step A8, Note b).

2. Wipe down with 70% ethanol the dissecting area of the hood and the stereomicroscope to be used for dissection. Under a dissection hood, add 2.5 ml of cold Solution A into two 35 mm plastic Petri dish and keep them on ice in an ice bucket. The surgical tools to be used hereafter must be sterile.

3. Wipe the head of the pup with 70% ethanol and euthanize it by decapitation with scissors #1. Use forceps #2 to grab the head of the pup (Figure 1A) and with scissors #3 remove the skin covering the skull and the muscles at the base of the head (Figure 1B).

Note: Skin incision should be performed starting from the forehead (roughly between eyes, black star in Figure 1A) and should continue straight toward the neck (green dotted traces of Figure 1A and of Figure 1B top left). The result of this step is shown in Figure 1B (top right). Then, starting from the sagittal incision (few millimeters above the original incision site), cut the skin perpendicularly toward the jaw (red dotted trace of Figure 1A and of Figure 1B bottom left). Repeat the step for the other side and pull away the skin. If necessary cut the muscles at the base of the skull (white star in Figure 1B, bottom right panel). Muscles can be chopped roughly but avoiding damage of the skull because the cerebellum is underneath this area. The final result of these steps is shown in Figure 1C.

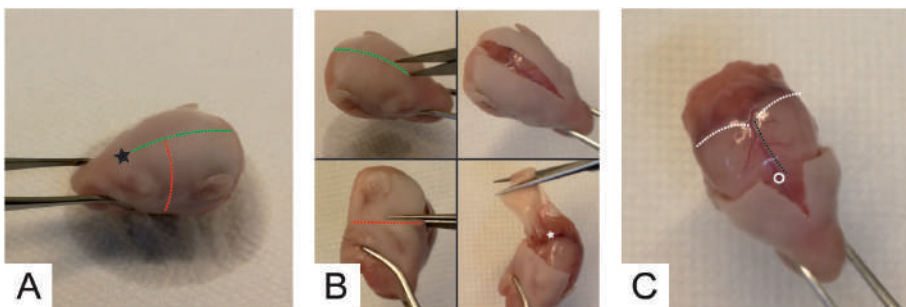


Figure 1. Skinning of pups' head to expose the skull for cerebellum dissection

- With a second pair of scissors #3 (clean, i.e. not used for skinning to avoid contamination), incise the skull over the hemispheres area (white circle in Figure 1C) and cut the cranial bone along the sagittal suture (black dotted lines in Figures 1C and 2A) until the interception with the interaural line (white dotted traces of Figure 1C and Figure 2A). Once there, cut perpendicularly in both directions following the interaural lines until the acoustic *meati* (white arrow in Figure 2A bottom panel) to generate a coronal craniotomy of the parietal bone. Lift up the bone to spot the mid brain, the cerebellum and part of the brain stem (cyan dotted lines in top left Figure 2B). Cut sagittal (black dotted line in Figure 2B top right) until the foramen magnum without damaging the cerebellum. Pull out the two “bone-lids” with a pair of tweezers #4 (left bottom panel of Figure 2B). As a result, mid brain, cerebellum and brainstem are fully exposed (right bottom panel of Figure 2B).

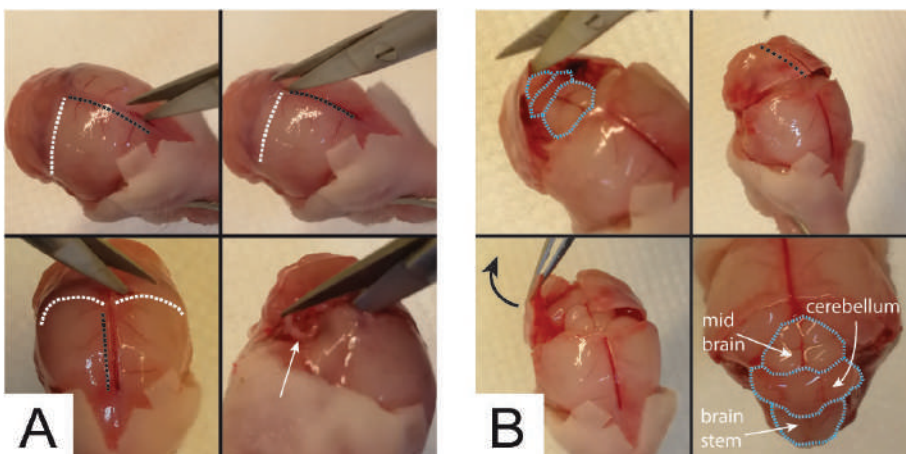


Figure 2. Craniotomy to expose the cerebellar area

- Using a second pair of forceps #2 (clean, i.e., different from that used to grab the pup face), gently detach the mid brain from the hemispheres (Figure 3A). This step is achieved by introducing forceps #2 in between the midbrain and the hemispheres (Figure 3A) and cutting the connections between them by tightening forceps endings. Then, using the same forceps as a spoon, gently grab the midbrain, cerebellum and brainstem (Figure 3B) and transfer them into a 35 mm plastic Petri dish filled with 2.5 ml of ice cold Solution A (Figure 3C).

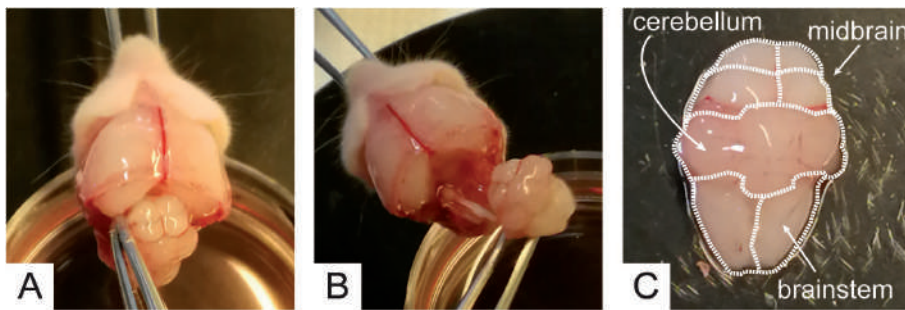


Figure 3. Isolation of midbrain, cerebellum and brainstem. Dotted lines spot the cerebellum, the mid brain and the brainstem.

6. Under the dissection microscope, use one pair of tweezers #4 to hold the brainstem and a second pair of tweezers #4 to remove the meninges from the cerebellum until it takes on a matted white appearance. With tweezers #4, gently separate the cerebellum from the brainstem and move it into a fresh 35 mm plastic Petri dish filled with 2.5 ml of ice cold fresh Solution A to be kept on ice (Figure 4A). Repeat this procedure for 5 cerebella maximum.

Notes:

- a. *Decapitation must be performed at the base of the neck to avoid cerebellum damage.*
 - b. *Dissect one pup per time and try to reduce the dissection time to avoid neuronal death.*
 - c. *Blood vessels of the meningeal branches are very useful to spot meninges as they are red-colored and run along the entire wrapping, forming a visible network. Larger vessels can be grasped with the tweezers and pulled to remove the meninges. Once skilled, a user can take advantage of this trick to rapidly peel off very large portions of the meningeal wrapping to speed up this step.*
 - d. *Use fresh Solution A for each cerebellum.*
7. Remove Solution A, gather (Figure 4A) and mince cerebella using a sterile scalpel (Figure 4B).
Note: Mincing is carried out by repetitive up-and-down movements of the scalpel. Scalpel blade must be sharp to produce clear incisions to the tissue, thus limiting neuron damage. A "mortar-pestle" mincing (non-sharp scalpel) must be avoided as it may cause neuronal death.
 8. Using a small volume of pre-warmed Solution B (~1 ml) and a sterile plastic Pasteur pipette, collect minced cerebella and transfer them into a 50 ml plastic tube with the remaining Solution B and incubate for 15-30 min at 37 °C, gently swirling every 2-3 min (Figure 4C).

Notes:

- a. *For 3 cerebella, 15 min at 37 °C is sufficient; with more cerebella (4-5) 25-30 min is recommended.*
- b. *During this incubation period, remove poly-L-lysine by aspiration under a sterile laminar flow hood and let the plates to dry.*

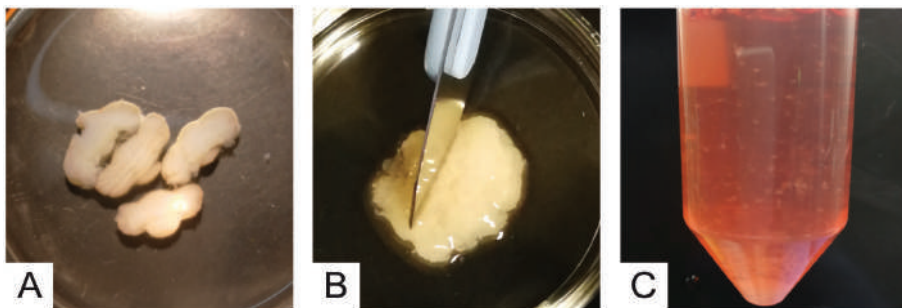


Figure 4. Cerebella mincing and trypsinization

9. Add 10 ml of Solution D and centrifuge at $300 \times g$ for 2 min at RT.
10. In a sterile laminar flow hood, carefully discard the supernatant without losing cerebellar tissue.
11. Add 3 ml of Solution C to the pelleted cerebella and use a sterile P1000 (1,000 μl) micropipette to mechanically dissociate the tissue with 20-30 pipette-strokes.

Notes:

- a. *Before pipetting, the solution is transparent with big tissue aggregates floating around (Figure 5A). After pipetting, the solution gets cloudy due to dissociated cells going in suspension (Figure 5B).*
- b. *Some undigested tissue fragments may be present. Leave them to settle down before proceeding.*
12. With a P1000 (1,000 μl) micropipette, collect the cell suspension (900 μl per time) avoiding undissociated tissue fragments (Figure 5C) and transfer it into a new sterile 50 ml conical tube, adding an equal volume of Solution E.

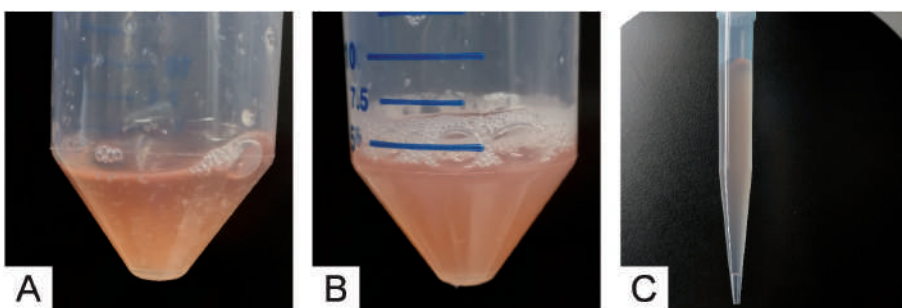


Figure 5. Mechanical disruption and recovery of neurons

13. Repeat Steps A11-A12 a second time.
14. Centrifuge the cell suspension at $300 \times g$ for 8 min at RT.
15. Discard the supernatant and resuspend the cell pellet in 10 ml of pre-warmed (37°C) culture medium.
16. Count dissociated neurons with a hemocytometer and plate at the desired density.

Notes:

- a. A typical yield is about 20-25 million (rat) and 10-15 million (mouse) neurons per cerebellum.
 - b. Lower yields may be due to i) inefficient trypsinization: prolong incubation time of Step A6; ii) neuronal death due to excessive trypsinization and/or too harsh mechanical tissue disruption: shorten incubation time of Step A8 and/or reduce trypsin concentration, and/or be gentler during mechanical dissociation in Step A11.
 - c. Trypan blue (permeable to dead cells, not taken up by healthy cells) can be used for a more accurate cell counting.
 - d. Plate neurons with a minimal density of 1.5×10^5 cells/cm² (i.e., 3.0×10^5 cells in a 24-well culture plate). This density is suitable for imaging experiments. For biochemistry (Western blotting), a recommended density is of 2×10^5 cells/cm² (i.e., 4.0×10^5 cells in a 24-well culture plate), yet optimal densities should be set according to planned experiments.
 - e. At lower density, maturation of neuronal networks is slower, viability is lower and cells tend to group forming clumps.
17. Incubate at 37 °C and 5% CO₂. Eighteen to twenty-four hours after plating, add Cytosine β-D-arabinofuranoside (araC) to a final concentration of 10 µM to block the growth of non-neuronal cells.

Notes:

- a. araC allows the culture of CGNs as an almost pure neuronal culture by blocking the proliferation of non-neuronal cells.
 - b. The concentration of araC suggested blocks proliferation of non-neuronal cells without causing detectable stress/death of CGNs.
 - c. araC-free medium can be used but CGN tend to be overrun by non-neuronal cells at longer DIVs, even if cultured in a serum-free medium (Wong et al., 2001).
18. Incubate at 37 °C and 5% CO₂. Depending on cell density, neuron maturation takes 5 to 6 days *in vitro* (DIV). Starting from DIV 5-6, neuronal culture is suitable for testing clostridial neurotoxins. Figure 6 shows mature neurons at DIV 6.

Notes:

- a. The culture has to be considered mature when neurons have formed a thick network of neuronal processes. Typically, the culture is suitable for use at DIV 5-6.
- b. The culture should not be used when neurons get grouped forming clasps. In our experience, this is a sign of cellular stress.
- c. Variability in the serum lot for culture medium strongly influences culture maturation and neuron viability. Comparative trials of multiple serum lots are recommended for culture optimization.

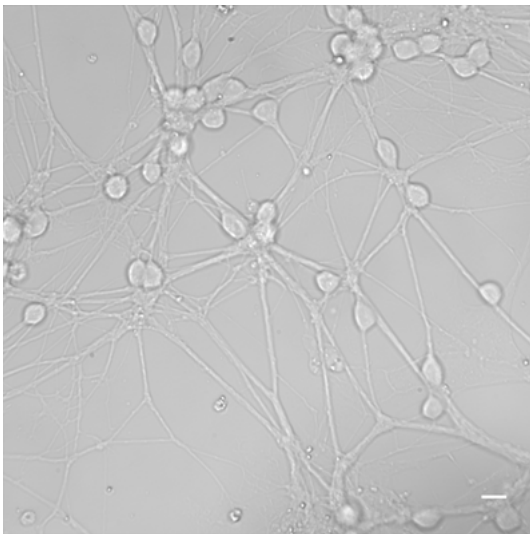


Figure 6. Mature CGN at DIV 6. Scale bar = 10 μ m.

B. Investigation of CNT activity by Western blotting

1. Prepare the clostridial neurotoxin at the intended concentration(s) in culture medium. Typical concentrations range from low pM to nM, depending on experimental design. Intoxicate cultured CGNs by replacing the culture medium with fresh pre-warmed medium supplemented with the toxin.

Notes:

- a. *CNT concentration, time and incubation protocol hardly impacts on the number of toxin molecules entering the neurons, thus on the overall cleavage of SNARE. In general, a pulse incubation allows the entry of less molecules than leaving the toxins for the entire duration of the experiment. As a consequence, the cleavage of SNARE proteins with pulse incubation is slower.*
- b. *Pulse experiments can be done by incubating neurons in ice-cold toxin medium to allow CNT binding to neurons not followed by internalization. Addition of fresh, 37 °C pre-warmed, medium will trigger toxin internalization in a synchronized fashion.*
- c. *Media replacements (removal followed by addition of fresh medium) is critical and must be performed carefully to avoid neuron damage or detachment.*
- d. *If using different media for intoxication, note that CNT entry into neurons is strongly influenced by neuronal activity that strictly depends on calcium (at least 1-2 mM). Depolarizing conditions, like high K⁺, significantly increase toxin entry (and toxicity). The culture medium of CGN contains ~1.6 mM calcium and is slightly depolarizing (25 mM K⁺), allowing CNT internalization by itself. For short pulse-intoxication (5-10 min at 37 °C), K⁺ concentration can be risen up to 90 mM. Intoxication with basal potassium in CGN can be performed but for short time incubations as these neurons deprived of high potassium in culture undergo apoptosis (D'Mello et al., 1993).*

- e. Although not essential for toxin activity *in vitro*, extracellular fluids *in vivo* contain serum. Thus, intoxication using media supplemented with serum can be considered more similar to the environment where CNT naturally act.
2. Prolong the incubation time according to the experimental design.
Note: CNT are metalloproteases (enzymes) thus the longer the incubation time the more efficient will be the cleavage of SNARE substrates.
3. Aspirate culture medium, rinse the neurons with a saline solution (PBS is fine) and directly lyse the cells into the wells using LSB (Laemmli Sample Buffer 1x).
Note: LSB volume must be set according to neuron density and plate surface. We typically use 25 µl/4.0 x 10⁵ cells (24-well culture plate).
4. Collect cell lysates into 1.5 ml tubes and heat-denature proteins for at least 15 min at 100 °C.
5. Separate proteins by SDS-PAGE.

Notes:

- a. We routinely use SDS-PAGE buffers and reagents from Thermo Fischer Scientific following manufacturer's instructions. For BoNT/A and BoNT/C, we use NuPAGE™ 12% Bis-Tris gels and 1x MOPS running buffer (70 V until the running front exits the gel). For BoNT serotypes and TeNT cleaving VAMP, NuPAGE™ 4-12% Bis-Tris gels and 1x MES running buffer (200 V, ~1 h) are recommended. These parameters may vary and may need optimization depending on the SDS-PAGE gel used, in particular to separate BoNT/A- and BoNT/C-truncated SNAP-25 from intact SNAP-25 whose molecular weights differ for less than 2 kDa.
- b. A pre-stained protein standard can be loaded to estimate the progression of band separation.
6. Transfer proteins onto a matrix suitable for Western blotting.
Note: We use nitrocellulose and a transfer buffer containing 20% methanol.
7. Check protein transfer by Ponceau S staining (optional).
8. De-stain Ponceau S with extensive washes with PBST.
9. Block the membrane for 1 h at room temperature using blocking buffer.
10. Incubate the membrane overnight with indicated dilutions of primary antibodies in blocking buffer.
Note: We routinely use the following primary antibodies for SNARE proteins: anti VAMP-2 (1:2,000, Synaptic System, 104 211), anti SNAP-25 (1:5,000, SMI81, Abcam, ab24737), anti syntaxin-1A (1:2,000, Synaptic System, 110 011), anti BoNT/B-TeNT-cleaved VAMP-2 (1:200, homemade), anti BoNT/A-cleaved SNAP-25 (1:5,000, homemade), anti BoNT/E-cleaved SNAP-25 (1:5,000, homemade) and anti syntaxin-1A/1B (1:2,000, homemade). Characterization of homemade antibodies have been previously reported (Antonucci et al., 2008; Antonucci et al., 2009; Pirazzini et al., 2014; Azarnia Tehran et al., 2015).
11. Wash the membrane three times with PBST 5 min each. Incubate the membrane with appropriate secondary antibodies in PBST for 1 h.

Note: We routinely use HRP-conjugated secondary antibodies. However, comparable results have been obtained using different developing system (and appropriate secondary antibodies) like the Odyssey imaging system from LI-COR Biosciences.

12. Wash the membrane three times using PBST and twice with PBS, 5 min each. Develop the membrane with the appropriate developing system (according to secondary antibodies used).

C. Investigation of CNT activity by imaging

Alternatively to Western blot analysis, CNT activity can be evaluated using CGN seeded on glass coverslips via immunofluorescence analysis. Although this method is sensitive, this analysis has to be considered more qualitative than quantitative.

1. Following intoxication (Steps B1-B2 previous paragraph), aspirate culture medium, rinse the neurons with PBS and fix neurons for 15 min at RT using 4% paraformaldehyde solution.
2. Wash neurons two times with PBS and quench paraformaldehyde for 20 min using quenching solution.
3. Remove quenching solution and permeabilize neurons with permeabilization solution for 20 min at -20 °C.
4. Remove permeabilization solution and saturate cells with blocking solution for 30 min at RT.
5. Add primary antibodies in blocking solution and incubate using a humid chamber at 37 °C for at least 2 h or at 4 °C overnight.

Notes:

- a. Primary antibodies used for Western blotting can also be used for imaging.
 - b. Non-treated (with a CNT) samples must always be included in the experimental design.
 - c. A control using only secondary antibodies is recommended to evaluate unspecific binding of secondary antibodies.
6. Wash neurons at least three times with PBS.
 7. Detect primary antibodies using fluorescently labeled secondary antibodies in blocking solution. Perform the incubation using a humid chamber at 37 °C for 45 min.
 8. Wash neurons three times with PBS.
 9. Mount coverslips using Fluorescence Mounting Medium.
Collect images with a fluorescence microscope with appropriate optical filters. Confocal microscopy is more suitable, yet satisfactory results can also be obtained with epifluorescence microscopy.

D. Use CGNs as a platform for screening inhibitors of CNT

1. Use CGNs at 5-6 DIV seeded in 24-well plates with a density of at least 4.0×10^5 neurons.
2. Prepare a stock solution of the compound to be tested and then make serial dilutions in culture medium.

Notes:

- a. We usually prepare 500 μ l of compound solution per well and test each concentration in triplicate.
 - b. Different media can be used to prepare compound dilution. We prefer to use culture medium to keep the neurons in the same culture conditions where they grew avoiding extra stress. In addition, culture medium contains serum which helps in solubilizing poorly water soluble compounds avoiding the need of excessive amounts of organic solvents.
3. Replace the culture medium with the inhibitor solution.

Notes:

- a. The control condition is carried out with fresh culture medium supplemented with an equal amount of the vehicle used to prepare the inhibitor stock solution (e.g., ethanol, dimethyl sulfoxide, etc.).
 - b. Preincubation (addition of the inhibitor before intoxication) is recommended to figure out if the tested compound is actually effective as an inhibitor. This preliminary assay should be followed by further experiments aimed at understanding which stage of the intoxication process is inhibited. This can be carried out by adding the putative inhibitor at distinct stages of intoxication: i) preincubation with the compound before intoxication; ii) addition of the compound to the cells together with the toxin; iii) addition of the compound after intoxication; iv) addition of the compound at different stages after intoxication.
 - c. Preincubation time may vary depending on different parameters of the inhibitors: physico-chemical properties, neuronal membrane permeability, molecular target(s) of the compound, etc.
 - d. The range of effective concentrations and possible intrinsic toxicity on neurons must be taken into account.
 - e. A control condition evaluating whether the diluent (e.g., ethanol, dimethyl sulfoxide, etc.) of putative inhibitor blocks CNT by itself must be included.
 - f. Chemical compounds can alter neuron physiology and block toxin activity/uptake due to an indirect effect. This should be tested by an appropriate experiment which depends on the nature of the putative inhibitor.
4. Add the toxin at the desired concentration(s) and prolong the incubation time according to the experimental design.

Notes:

- a. Several concentrations of inhibitors should be tested to achieve a dose-response curve.
- b. The toxin can be added as a pulse or left for the entire duration of the experiment (see Steps B1 and B2).
- c. Multiple CNT (targeting different SNARE substrates) can be added simultaneously to investigate the possibility that the mechanism of inhibition is shared.

5. If the toxin is given as a pulse, after toxin washed out restore the culture medium with the desired concentration of inhibitor and prolong the incubation according to the experimental design.

Notes:

- In this case, prepare (in Step D2) a double amount of culture medium containing the desired concentration of inhibitor or vehicle.
 - Incubation time significantly impact on SNARE proteins cleavage and on inhibitor efficacy as well.
6. Continue from Step B1 (WB protocol) or from Step C1 (imaging protocol) of previous paragraphs.

Data analysis

CNT cleave SNARE proteins with very high selectivity. Not only does each toxin hydrolyze one specific SNARE, but it also cleaves a very specific peptide bond (Pirazzini *et al.*, 2017) (Figure 7A). This is due to multiple and selective interactions taking place between CNT protease and the SNARE protein involving the active site and many exosites (Binz, 2013; Rossetto *et al.*, 2014; Pirazzini *et al.*, 2017). Cleavage sites within SNARE proteins are remarkably conserved in vertebrates, including humans (Carle *et al.*, 2017). At the same time, even a single mutation in the peptide bond or in exosites mediating toxin-substrate recognition, make the SNARE protein non-cleavable and the vertebrate carrying this alteration non-sensitive to that particular toxin (Patarnello *et al.*, 1993; Eleopra *et al.*, 2013; Peng *et al.*, 2014).

This specificity makes easy to interpret the results of intoxicated CGN both via Western blotting and via imaging using specific antibodies. Figure 7B shows a schematization of a Western blot membrane in which the use of the most popular antibodies is simulated. Depending on the CNT, toxin activity can be clearly evaluated by following the staining of SNARE proteins' bands.

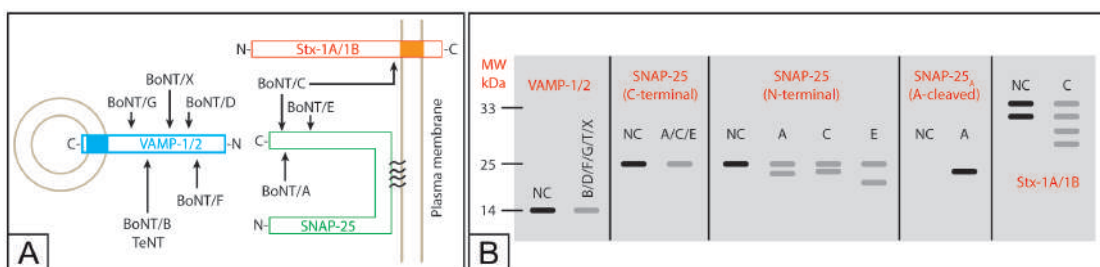


Figure 7. Schematization of CNT activity on SNARE proteins (A) and simulation of Western blotting results with indicated antibodies (B). Note that these results would be achieved by ideally cleaving 50% of the considered SNARE protein(s). NC is “negative control” and corresponds to the normal electrophoretic mobility and band intensity of indicated SNARE proteins in samples not treated with CNT. Bands in grey represent a decreased intensity (~50%) of the band. Syntaxins-1A/1B are simultaneously expressed by CGNs and are shown as a

doublet because syntaxin-1A and syntaxin-1B, in spite of very similar molecular weights (~33 kDa), run slightly different when separated by SDS-PAGE. Since BoNT/C cleaves both stx-1A and stx-1B, it generates the 4-bands pattern shown in the last panel on the right.

Figure 8 shows typical Western blotting results. Although Western blotting is a semiquantitative assay, with modern developing techniques and instruments, CNT activity (or inhibition) can be accurately determined by band densitometry.

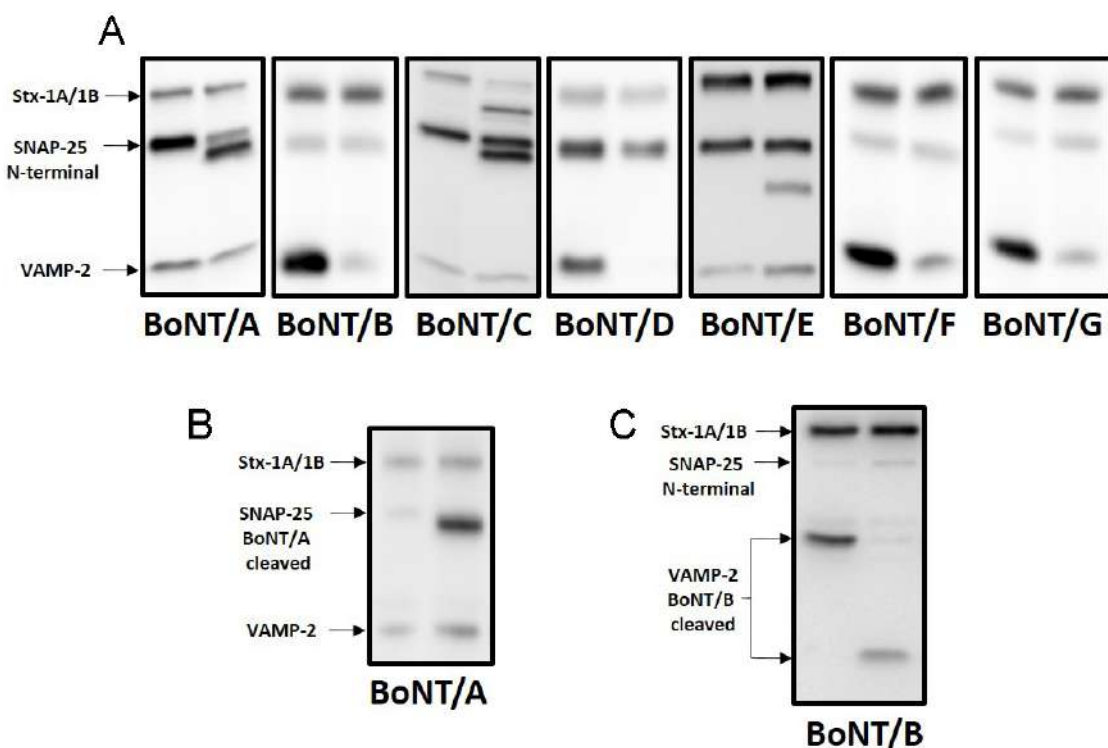


Figure 8. Investigation of CNT activity by Western blotting. The image shown are representative experiments in which CGN were treated with different serotypes of BoNT. A. In each panel are shown two samples: a not-treated with the toxin (toxin free, untreated cells, left) and another treated with the indicated serotype of BoNT (right). The antibodies used were: anti-syntaxin1A, anti-SNAP-25 and anti-VAMP-2. BoNT/B, /D, /F and /G cleave VAMP-2 leading to the disappearance of VAMP-2 signal. BoNT/A and BoNT/E cleave SNAP-25 leading to the appearance of the SNAP-25 C-terminal fragment. Instead, BoNT/C hydrolyze both Syntaxin 1A/1B and SNAP-25 leading to appearance of both generated fragments. B. SNAP-25-BoNT/A-cleaved antibody recognize the generated C-terminal fragment after BoNT/A cleavage. This antibody is raised against the C-terminus newly generated after BoNT/A cleavage and does not cross-react with intact SNAP-25. C. VAMP-2 BoNT/B cleaved antibody recognize the generated N-terminal fragment after BoNT/B cleavage. Quantitative interpretation critically depends on the developing techniques, the linear dynamic ranges of the type of secondary antibodies and of the detection systems used.

VAMP-2 BoNT/B cleaved antibody and SNAP-25-BoNT/A-cleaved antibody can also be used to stain neurons for imaging CNT activity in fixed neurons. Figure 9 shows some examples.

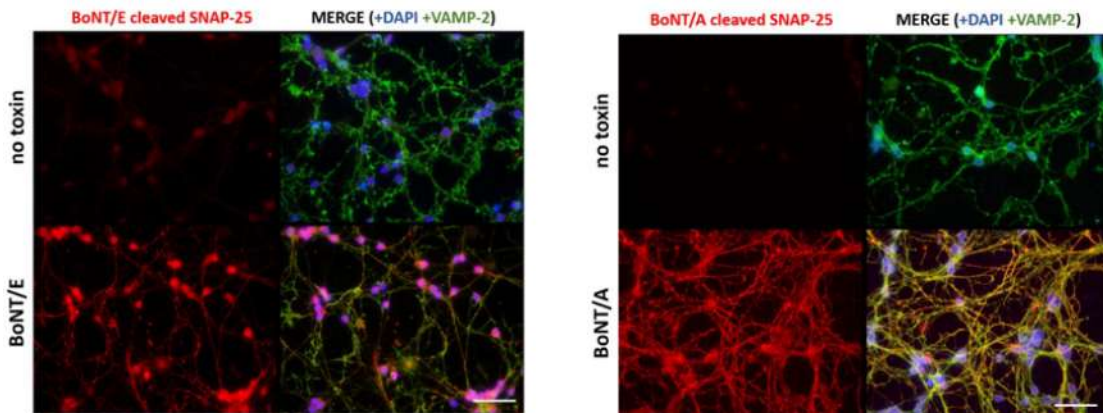


Figure 9. Investigation of CNT activity by imaging. CGNs were treated with vehicle (no toxin) or with the indicated serotype of BoNT for 2 h. Neurons were fixed and stained with an antibody against BoNT/E-cleaved SNAP-25 (left panel) or BoNT/A-cleaved SNAP-25 (right panel) and VAMP2 as housekeeping staining. Both BoNT/A and BoNT/E cleaved-SNAP25 are detected with an Alexa555 conjugated secondary antibody while VAMP2 with an Alexa488 secondary antibody. DAPI is used to stain nuclei. Scale bars = 10 μ m.

Recipes

1. Krebs solution (10x)

Material	Final Concentration	For 250 ml (g)
NaCl	1.24 M	18.12
KCl	53.65 mM	1.00
Glucose	144.31 mM	6.5
NaH ₂ PO ₄ ·H ₂ O	11.67 mM	0.35
HEPES	249.26 mM	14.85
Phenol red	0.001%	0.025

Adjust to pH 7.4 and filter using a 0.20 μ m filter. This solution can be aliquoted (50 ml each) and stored at -20 °C until further usage (stable for at least three months)

2. 155 mM MgSO₄ stock solution

To make 155 mM MgSO₄ solution:

- Dissolve 1.91 g of MgSO₄·7H₂O in 50 ml of distilled H₂O
- Filter the solution in the laminar flow hood using a 0.20 μ m filter and keep at 4 °C (stable for at least two months)

3. 12.2 mM CaCl₂ stock solution

To make 12.2 mM CaCl₂ solution:

- a. Dissolve 0.09 g of $\text{CaCl}_2 \cdot 2\text{H}_2\text{O}$ in 50 ml of distilled H_2O
- b. Filter the solution in the laminar flow hood using a 0.20 μm filter and keep at 4 °C (stable for at least two months)
4. Solution A

Material	Final Concentration	For 500 ml
Bovine Serum Albumin (Fatty acid free)	0.3%	1.5 g
Krebs buffer	1x	50 ml using Krebs buffer 10x
MgSO_4	0.46 mM	1.5 ml using 155 mM stock solution

Filter the solution in the laminar flow hood using single-use steri-cups. This solution can be aliquoted (50 ml each) and stored at -20 °C until further usage (stable for at least three months)

5. Solution B
 - a. Add 0.01 g of Trypsin in 12.5 ml of Solution A
 - b. Filter the solution in the laminar flow hood using a 0.20 μm filter

Note: Always prepare fresh.
6. Solution C
 - a. Add 120 μl of DNase (10 mg/ml, stock solution), 7.8 mg of trypsin inhibitor and 150 μl of 155 mM MgSO_4 stock solution in 15 ml of Solution A
 - b. Filter the solution in the laminar flow hood using a 0.20 μm filter

Note: Always prepare fresh.
7. Solution D

Mix 2.4 ml of Solution C with 12.6 ml Solution A

Note: Always prepare fresh.
8. Solution E
 - a. Add 120 μl of 12.2 mM CaCl_2 stock solution and 120 μl of 155 mM MgSO_4 stock solution in 15 ml of Solution A
 - b. Filter the solution in the laminar flow hood sing a 0.20 μm filter

Note: Always prepare fresh.
9. Poly-L-lysine solution

Prepare a stock solution of Poly-L-lysine in the range of 5-10 mg/ml

Working concentration is 50 $\mu\text{g}/\text{ml}$

10. BME complete medium, CGN culture medium

Material	Final Concentration	For 500 ml
Basal Medium Eagle (BME)		445 ml
Fetal Bovine Serum (FBS)	10%	50 ml
GlutaMAX	1x	5 ml using GlutaMAX 10x
Gentamicin	50 µg/ml	500 µl using Gentamycin 50 mg/ml solution
KCl	25 mM	0.73 g

Filter the medium in the laminar flow hood using single-use stericups. The medium can be stored at 4 °C (stable for at least one month)

11. Cytosine β-D-arabinofuranoside (AraC) stock solution

- Add 4.9 mg of Cytosine β-D-arabinofuranoside in 5 ml of distilled H₂O (1 mg/ml, 4 mM)
- Incubate at 37 °C for a few minutes and vortex until the solution appears clear and colorless
- Filter in the laminar flow hood using a 0.20 µm filter

Note: This solution can be aliquoted and stored at -20 °C (stable for at least one year).

12. PBS

NaCl 137 mM

KCl 2.7 mM

Na₂HPO₄ 10 mM

KH₂PO₄ 1.8 mM

13. PBST

PBS supplemented with 0.1% (v/v) Tween 20

14. Laemmli Sample Buffer. Recipe for 10 ml (4x)

2.5 ml of 1 M Tris-HCl (pH 6.8):

1 g of SDS

0.8 ml of 0.1% Bromophenol Blue

4 ml of 100% glycerol

2 ml of 14.3 M β-mercaptoethanol

4 tablets of protease inhibitors

Adjust the final volume to 10 ml with distilled H₂O

15. Transfer buffer

To make a 10x transfer buffer:

- Dissolve 288 g of glycine and 60.4 g of Tris base and add distilled H₂O to a final volume of 2 L
- To make 1x transfer buffer mix 700 ml distilled H₂O, 200 ml methanol and 100 ml 10x transfer buffer

16. Ponceau S solution

0.5% (w/v) Ponceau S, 1% acetic acid in distilled H₂O

17. Blocking buffer

5% nonfat dry milk in PBST

18. 4% Paraformaldehyde solution

- a. Place 450 ml of distilled H₂O in a glass beaker and heat at 60 °C using a hot plate with stirring
- b. Add 20 g of paraformaldehyde
- c. Then, add 5 drops of 2 N NaOH and wait until the solution becomes clear (few minutes)
- d. Remove from the heat and add 50 ml of 10x PBS and adjust pH to 7.4
- e. Filter using a 0.2 µm filter and aliquots

Note: 4% paraformaldehyde solution can be frozen at -20 °C.

19. Quenching solution

50 mM ammonium chloride in PBS

20. Permeabilization solution

5% acetic acid in pure ethanol

Store at -20°C

21. Blocking solution

2.5% BSA in PBS

Acknowledgments

This work was supported by the University of Padova with the grant DOR to MP. DAT is currently supported by an Alexander von Humboldt (AvH) Research Fellowship for Postdoctoral Researcher. All the procedures have been optimized in the laboratory of 'Neurotoxins, Neuroparalysis and Regeneration' headed by Prof. Cesare Montecucco at the Department of Biomedical Sciences (University of Padova). The method for the preparation of CGN was adapted from the previous work of Anne Messer and Parizad M. Bilimoria *et al.* The authors declare no competing interests. MP and DAT wrote the paper with equal contribution.

References

1. Antonucci, F., Bozzi, Y. and Caleo, M. (2009). [Intrahippocampal infusion of botulinum neurotoxin E \(BoNT/E\) reduces spontaneous recurrent seizures in a mouse model of mesial temporal lobe epilepsy](#). *Epilepsia* 50(4): 963-966.
2. Antonucci, F., Rossi, C., Gianfranceschi, L., Rossetto, O. and Caleo, M. (2008). [Long-distance retrograde effects of botulinum neurotoxin A](#). *J Neurosci* 28(14): 3689-3696.
3. Azarnia Tehran, D., Zanetti, G., Leka, O., Lista, F., Fillo, S., Binz, T., Shone, C. C., Rossetto, O., Montecucco, C., Paradisi, C., Mattarei, A. and Pirazzini, M. (2015). [A novel inhibitor prevents the peripheral neuroparalysis of botulinum neurotoxins](#). *Sci Rep* 5: 17513.

4. Bade, S., Rummel, A., Reisinger, C., Karnath, T., Ahnert-Hilger, G., Bigalke, H. and Binz, T. (2004). [Botulinum neurotoxin type D enables cytosolic delivery of enzymatically active cargo proteins to neurones via unfolded translocation intermediates.](#) *J Neurochem* 91(6): 1461-1472.
5. Bilimoria, P. M. and Bonni, A. (2008). [Cultures of cerebellar granule neurons.](#) *CSH Protoc* 2008: pdb prot5107.
6. Binz, T. (2013). [Clostridial neurotoxin light chains: devices for SNARE cleavage mediated blockade of neurotransmission.](#) *Curr Top Microbiol Immunol* 364: 139-157.
7. Binz, T. and Rummel, A. (2009). [Cell entry strategy of clostridial neurotoxins.](#) *J Neurochem* 109(6): 1584-1595.
8. Brunt, J., Carter, A. T., Stringer, S. C. and Peck, M. W. (2018). [Identification of a novel botulinum neurotoxin gene cluster in *Enterococcus*.](#) *FEBS Lett* 592(3): 310-317.
9. Carle, S., Pirazzini, M., Rossetto, O., Barth, H. and Montecucco, C. (2017). [High conservation of tetanus and botulinum neurotoxins cleavage sites on human SNARE proteins suggests that these pathogens exerted little or no evolutionary pressure on humans.](#) *Toxins (Basel)* 9(12).
10. Colasante, C., Rossetto, O., Morbiato, L., Pirazzini, M., Molgo, J. and Montecucco, C. (2013). [Botulinum neurotoxin type A is internalized and translocated from small synaptic vesicles at the neuromuscular junction.](#) *Mol Neurobiol* 48(1): 120-127.
11. Contestabile, A. (2002). [Cerebellar granule cells as a model to study mechanisms of neuronal apoptosis or survival *in vivo* and *in vitro*.](#) *Cerebellum* 1(1): 41-55.
12. D'Mello, S. R., Galli, C., Ciotti, T. and Calissano, P. (1993). [Induction of apoptosis in cerebellar granule neurons by low potassium: inhibition of death by insulin-like growth factor I and cAMP.](#) *Proc Natl Acad Sci U S A* 90(23): 10989-10993.
13. Eleopra, R., Montecucco, C., Devigili, G., Lettieri, C., Rinaldo, S., Verriello, L., Pirazzini, M., Caccin, P. and Rossetto, O. (2013). [Botulinum neurotoxin serotype D is poorly effective in humans: an *in vivo* electrophysiological study.](#) *Clin Neurophysiol* 124(5): 999-1004.
14. Harper, C. B., Martin, S., Nguyen, T. H., Daniels, S. J., Lavidis, N. A., Popoff, M. R., Hadzic, G., Mariana, A., Chau, N., McCluskey, A., Robinson, P. J. and Meunier, F. A. (2011). [Dynamin inhibition blocks botulinum neurotoxin type A endocytosis in neurons and delays botulism.](#) *J Biol Chem* 286(41): 35966-35976.
15. Johnson, E. A. and Montecucco, C. (2008). [Botulism.](#) *Handb Clin Neurol* 91: 333-368.
16. Matteoli, M., Verderio, C., Rossetto, O., Iezzi, N., Coco, S., Schiavo, G. and Montecucco, C. (1996). [Synaptic vesicle endocytosis mediates the entry of tetanus neurotoxin into hippocampal neurons.](#) *Proc Natl Acad Sci U S A* 93(23): 13310-13315.
17. Messer, A. (1977). [The maintenance and identification of mouse cerebellar granule cells in monolayer culture.](#) *Brain Res* 130(1): 1-12.
18. Montal, M. (2010). [Botulinum neurotoxin: a marvel of protein design.](#) *Annu Rev Biochem* 79: 591-617.
19. Montecucco, C. and Rasotto, M. B. (2015). [On botulinum neurotoxin variability.](#) *MBio* 6(1).

20. Pantano, S. and Montecucco, C. (2014). [The blockade of the neurotransmitter release apparatus by botulinum neurotoxins](#). *Cell Mol Life Sci* 71(5): 793-811.
21. Patarnello, T., Bargelloni, L., Rossetto, O., Schiavo, G. and Montecucco, C. (1993). [Neurotransmission and secretion](#). *Nature* 364(6438): 581-582.
22. Pellett, S. (2013). [Progress in cell based assays for botulinum neurotoxin detection](#). *Curr Top Microbiol Immunol* 364: 257-285.
23. Peng, L., Adler, M., Demogines, A., Borrell, A., Liu, H., Tao, L., Tepp, W. H., Zhang, S. C., Johnson, E. A., Sawyer, S. L. and Dong, M. (2014). [Widespread sequence variations in VAMP1 across vertebrates suggest a potential selective pressure from botulinum neurotoxins](#). *PLoS Pathog* 10(7): e1004177.
24. Pirazzini, M., Azarnia Tehran, D., Leka, O., Zanetti, G., Rossetto, O. and Montecucco, C. (2016). [On the translocation of botulinum and tetanus neurotoxins across the membrane of acidic intracellular compartments](#). *Biochim Biophys Acta* 1858(3): 467-474.
25. Pirazzini, M., Azarnia Tehran, D., Zanetti, G., Megighian, A., Scorzeto, M., Fillo, S., Shone, C. C., Binz, T., Rossetto, O., Lista, F. and Montecucco, C. (2014). [Thioredoxin and its reductase are present on synaptic vesicles, and their inhibition prevents the paralysis induced by botulinum neurotoxins](#). *Cell Rep* 8(6): 1870-1878.
26. Pirazzini, M., Azarnia Tehran, D., Zanetti, G., Rossetto, O. and Montecucco, C. (2018). [Hsp90 and Thioredoxin-Thioredoxin Reductase enable the catalytic activity of Clostridial neurotoxins inside nerve terminals](#). *Toxicon* 147: 32-37.
27. Pirazzini, M., Bordin, F., Rossetto, O., Shone, C. C., Binz, T. and Montecucco, C. (2013a). [The thioredoxin reductase-thioredoxin system is involved in the entry of tetanus and botulinum neurotoxins in the cytosol of nerve terminals](#). *FEBS Lett* 587(2): 150-155.
28. Pirazzini, M., Henke, T., Rossetto, O., Mahrhold, S., Krez, N., Rummel, A., Montecucco, C. and Binz, T. (2013b). [Neutralisation of specific surface carboxylates speeds up translocation of botulinum neurotoxin type B enzymatic domain](#). *FEBS Lett* 587(23): 3831-3836.
29. Pirazzini, M. and Rossetto, O. (2017). [Challenges in searching for therapeutics against botulinum neurotoxins](#). *Expert Opin Drug Discov* 12(5): 497-510.
30. Pirazzini, M., Rossetto, O., Bertasio, C., Bordin, F., Shone, C. C., Binz, T. and Montecucco, C. (2013c). [Time course and temperature dependence of the membrane translocation of tetanus and botulinum neurotoxins C and D in neurons](#). *Biochem Biophys Res Commun* 430(1): 38-42.
31. Pirazzini, M., Rossetto, O., Bolognese, P., Shone, C. C. and Montecucco, C. (2011). [Double anchorage to the membrane and intact inter-chain disulfide bond are required for the low pH induced entry of tetanus and botulinum neurotoxins into neurons](#). *Cell Microbiol* 13(11): 1731-1743.
32. Pirazzini, M., Rossetto, O., Eleopra, R. and Montecucco, C. (2017). [Botulinum neurotoxins: Biology, pharmacology, and toxicology](#). *Pharmacol Rev* 69(2): 200-235.
33. Rossetto, O., Pirazzini, M. and Montecucco, C. (2014). [Botulinum neurotoxins: genetic, structural and mechanistic insights](#). *Nat Rev Microbiol* 12(8): 535-549.

34. Rummel, A. (2017). [Two feet on the membrane: Uptake of clostridial neurotoxins.](#) *Curr Top Microbiol Immunol* 406: 1-37.
35. Schiavo, G., Matteoli, M. and Montecucco, C. (2000). [Neurotoxins affecting neuroexocytosis.](#) *Physiol Rev* 80(2): 717-766.
36. Schiavo, G. and Montecucco, C. (1995). [Tetanus and botulism neurotoxins: isolation and assay.](#) *Methods Enzymol* 248: 643-652.
37. Shone, C. C. and Tranter, H. S. (1995). [Growth of clostridia and preparation of their neurotoxins.](#) *Curr Top Microbiol Immunol* 195: 143-160.
38. Tehran, D. A. and Pirazzini, M. (2018). [Novel botulinum neurotoxins: Exploring underneath the iceberg tip.](#) *Toxins (Basel)* 10(5).
39. Wong, J. K., Kennedy, P. R. and Belcher, S. M. (2001). [Simplified serum- and steroid-free culture conditions for high-throughput viability analysis of primary cultures of cerebellar granule neurons.](#) *J Neurosci Methods* 110(1-2): 45-55.
40. Zanetti, G., Azarnia Tehran, D., Pirazzini, M., Binz, T., Shone, C. C., Fillo, S., Lista, F., Rossetto, O. and Montecucco, C. (2015). [Inhibition of botulinum neurotoxins interchain disulfide bond reduction prevents the peripheral neuroparalysis of botulism.](#) *Biochem Pharmacol* 98(3): 522-530.
41. Zanetti, G., Sikorra, S., Rummel, A., Krez, N., Duregotti, E., Negro, S., Henke, T., Rossetto, O., Binz, T. and Pirazzini, M. (2017). [Botulinum neurotoxin C mutants reveal different effects of syntaxin or SNAP-25 proteolysis on neuromuscular transmission.](#) *PLoS Pathog* 13(8): e1006567.
42. Zhang, S., Lebreton, F., Mansfield, M. J., Miyashita, S. I., Zhang, J., Schwartzman, J. A., Tao, L., Masuyer, G., Martinez-Carranza, M., Stenmark, P., Gilmore, M. S., Doxey, A. C. and Dong, M. (2018). [Identification of a botulinum neurotoxin-like toxin in a commensal strain of *Enterococcus faecium*.](#) *Cell Host Microbe* 23(2): 169-176 e166.
43. Zhang, S., Masuyer, G., Zhang, J., Shen, Y., Lundin, D., Henriksson, L., Miyashita, S. I., Martinez-Carranza, M., Dong, M. and Stenmark, P. (2017). [Identification and characterization of a novel botulinum neurotoxin.](#) *Nat Commun* 8: 14130.
44. Zornetta, I., Azarnia Tehran, D., Arrigoni, G., Anniballi, F., Bano, L., Leka, O., Zanotti, G., Binz, T. and Montecucco, C. (2016). [The first non Clostridial botulinum-like toxin cleaves VAMP within the juxtamembrane domain.](#) *Sci Rep* 6: 30257.

Measurement of Dopamine Using Fast Scan Cyclic Voltammetry in Rodent Brain Slices

Madelyn I. Mauterer[#], Paige M. Estave[#], Katherine M. Holleran and Sara R. Jones*

Wake Forest School of Medicine, Department of Physiology and Pharmacology, Winston Salem North Carolina, United States of America

*For correspondence: srjones@wakehealth.edu

[#]Contributed equally to this work



[Abstract] Fast scan cyclic voltammetry (FSCV) is an electrochemical technique that allows sub-second detection of oxidizable chemical species, including monoamine neurotransmitters such as dopamine, norepinephrine, and serotonin. This technique has been used to record the physiological dynamics of these neurotransmitters in brain tissue, including their rates of release and reuptake as well as the activity of neuromodulators that regulate such processes. This protocol will focus on the use of *ex vivo* FSCV for the detection of dopamine within the nucleus accumbens in slices obtained from rodents. We have included all necessary materials, reagents, recipes, procedures, and analyses in order to successfully perform this technique in the laboratory setting. Additionally, we have also included cautionary points that we believe will be helpful for those who are novices in the field.

Keywords: Electrochemistry, Voltammetry, FSCV, Dopamine, Rodent, Slice physiology

[Background] Since the ability to examine the electrical properties of physiological systems was first appropriated for use in preclinical scientific research, many techniques used to study synaptic physiology have been developed. From the early days of electrophysiological recordings in squid axons to present day fast scan cyclic voltammetry (FSCV) performed in human Parkinson's patients (Kishida *et al.*, 2016; Lohrenz *et al.*, 2016), the field has made significant advances in a relatively short amount of time. This protocol's focus, FSCV, is the technical result of over 40 years of innovation and collaboration between physicists, analytical chemists, and neuroscientists. While electrochemistry was born with Michael Faraday and Alessandro Volta as early as the 19th century (Bard and Zoski, 2000), modern voltammetry did not come to fruition until the 1920s with Jaroslav Heyrovsky in his quest to measure the surface tension of mercury (Heyrovsky, 1922). Through his pursuit, Heyrovsky developed a dropping mercury electrode to perform polarography. This technique would be introduced as "voltammetry" in the United States in the 1940s and utilized platinum, gold, or carbon electrodes, in addition to the dropping mercury electrode, to study metal ions in solution. With the advent of computing technology, voltammetry methodology advanced dramatically from the late 1960s to today (for review see Bard and Zoski, 2000). Of note, in the 1970s, Ralph Adams pioneered the use of voltammetry, using a fast scanning method, in translational neuroscience specifically to study oxidizable neurotransmitters (Adams, 1976), a technique further applied to awake, freely-moving animals by Mark Wightman (Bucher and Wightman, 2015).

FSCV is a powerful electrochemical technique and is currently the only method available to directly measure extracellular levels of neurotransmitters on a sub-second timescale in discrete brain regions. One of the few comparable techniques is *in vivo* microdialysis—a method used to examine extracellular levels of multiple different neurotransmitters. However, even with the most recent advancements, microdialysis can only resolve neurotransmitter levels on a timescale of minutes, whereas FSCV has a temporal resolution of milliseconds. Other electrophysiological techniques utilize indirect measurements of neurotransmitter activity such as downstream postsynaptic ion channel-induced alterations in electrical signaling as a proxy. FSCV offers the unique ability to directly measure neurotransmitters in the extracellular space. This is due to the oxidizable nature of various chemical species, such as the monoamines dopamine, serotonin, and norepinephrine.

Since there are numerous publications regarding the fundamental theory of FSCV (for detailed review see: Yorgason *et al.*, 2011; Rodeberg *et al.*, 2017), we will not concentrate heavily on this topic here. Briefly, FSCV functions by passing an electrical current through an electrode implanted with a conductive substance such as carbon (referred to as the recording electrode), which receives electrochemical signals from a second stimulating electrode. More specifically, upon brief tissue stimulation by a bipolar stimulating electrode, dopamine is released into the extracellular space, which comes into contact with the recording electrode. A triangular waveform is passed within the carbon fiber of the electrode, ramping up to 1.2 m/sec and back down to -0.4 m/sec to detect dopamine, for example. In this way, when dopamine interacts with the carbon fiber at this specific command voltage, it rapidly oxidizes into dopamine-o-quinone, and reduces back into dopamine, which results in a signal that is communicated to the computing software. This results in the generation of a dopamine “trace” that can be modeled by the experimenter using Michaelis-Menten kinetics.

While the FSCV technique spans both *in vivo* and *ex vivo* applications, this protocol will specifically focus on FSCV execution in rodent brain slices. We will concentrate on *ex vivo* methods, as an analysis of current literature indicates there are few *ex vivo* FSCV protocols in rodent brain tissue—particularly using the new, freely available Demon Voltammetry Software (Maina *et al.*, 2012; Fortin *et al.*, 2015). While there are many reviews available regarding the history and theory of both *in vivo* and *ex vivo* FSCV, training in the execution of this technique in translational neuroscience is traditionally passed from mentor to mentee through direct hands-on training, with equipment often unique to each laboratory, rather than by formal instruction universal to all. Furthermore, until recently, commercial kits for FSCV were unavailable, and knowledge of these kits is still not widespread. Thus, it is imperative that trainees in the technique of FSCV be well versed in equipment usage and maintenance as well as technical performance. To this end, this protocol seeks to address technical execution of FSCV while directing the user to the tools and equipment the authors personally use to conduct experiments.

This protocol’s goal is to focus on rodent brain slice preparation, isolating a monoamine response (with a focus on dopamine in the nucleus accumbens), and data analysis. We also include a section with what we believe are helpful notes on the technique obtained from personal execution.

Brief Summary of Fast Scan Cyclic Voltammetry Procedure:

1. Production of carbon fiber electrodes.

2. Preparation Krebs stock solution and ACSF solution.
3. Brain extraction and brain slicing using a vibratome.
4. Isolation of an oxidizable neurotransmitter via stimulation of terminal fields using the fast scan cyclic voltammetry setup and Demon Voltammetry software.
5. Application of pharmacological agents or variation of stimulation parameters to study desired neurotransmitter dynamics.
6. Calibration of carbon fiber electrodes to identify electrode sensitivity to studied neurotransmitter
7. Model neurotransmitter signals via Michaelis-Menten fitting to obtain various kinetic parameters, using Demon Voltammetry Analysis software.
8. Data exportation from Demon Voltammetry Analysis software to Microsoft Excel Spreadsheet
9. Statistical analysis using program of choice (*i.e.*, GraphPad Prism).

Materials and Reagents

1. Transfer Pipette, wide bore (Globe Scientific, catalog number: 135040)
2. Stir bar (SP Scienceware - Bel-Art Products - H-B Instrument, catalog number: F37122-0060)
3. Insulin Syringe, 28 Gauge (Fisher Scientific, catalog number: 14-826-79)
Manufacturer: BD, catalog number: 329461.
4. Borosilicate Capillary Glass with Microfilament, 1.2 mm x 0.68 mm, 4" (A-M Systems, catalog number: 602000)
5. Carbon Fiber (GoodFellow, catalog number: C 005722)
6. Stainless steel conductive wire (L 3,000 x 1,000 s x 1,000 s UL 1423, UL1423 30/1 BLU) with insulated segment (Kauffman Engineering, custom made)
7. Platinum wire, 0.5 mm dia, annealed (Alfa Aesar, catalog number: 43288)
8. 1 mm dia x 4 mm Ag/AgCl reference electrode (pellet form) (World Precision Instruments, catalog number: EP1)
9. Bipolar Stimulating Electrode (Plastics One, catalog number: 8IMS3033SPCE)
10. Loctite® 404™ Instant Adhesive (VWR, catalog number: 300001-033)
Manufacturer: Henkel, Loctite® Professional Super Glue, catalog number: 442-46548.
11. Ultrapure Water
12. Deionized Water
13. Isoflurane (Patterson Veterinary Supply, catalog number: 140430704)
14. Sodium bicarbonate (NaHCO₃) (Sigma-Aldrich, catalog number: S6014)
15. Sodium phosphate monobasic monohydrate (H₂NaO₄P·H₂O) (Fisher Scientific, catalog number: S369-500)
16. Sodium chloride (NaCl) (Sigma-Aldrich, catalog number: S7653)
17. Potassium chloride (KCl) (Sigma-Aldrich, catalog number: P5405)
18. Magnesium chloride Hexahydrate (MgCl₂·6H₂O) (VWR, catalog number: BDH9244)
19. D-(+)-Glucose (C₆H₁₂O₆) (Sigma-Aldrich, catalog number: G8270)

20. Calcium chloride dihydrate ($\text{CaCl}_2 \cdot 2\text{H}_2\text{O}$) (Sigma-Aldrich, catalog number: C5080)
21. L-ascorbic acid ($\text{C}_6\text{H}_8\text{O}_6$) (Sigma-Aldrich, catalog number: A0278)
22. Dopamine hydrochloride (Sigma-Aldrich, catalog number: H8502)
23. Perchloric Acid (HClO_4), ACS reagent, 60% (Sigma-Aldrich, catalog number: 311413)
24. 70% Ethanol solution (Fisher Scientific, catalog number: BP8201500)
25. Artificial cerebrospinal fluid (ACSF) (see Recipes)
26. 10x Krebs stock solution (see Recipes)
27. 1 mM dopamine stock solution (see Recipes)

Equipment

1. 100 ml plastic beaker (Cole-Parmer, catalog number: EW-06020-03)
2. 1 L plastic bottle (Cole-Parmer, catalog number: EW-06058-85)
3. -20 °C freezer
4. Light source (Fisher Scientific, catalog number: 12-562-21)
5. Acrylic Coronal Brain Matrix (Harvard Apparatus, catalog number: 62-0047 [for rat], 62-0050 [for mouse])
6. Personna Double Edge Stainless Razor Blade (Electron Microscopy Sciences, Personna, catalog number: 72000)
7. Silver Print II (GC Electronics, catalog number: 22-023)
8. Scissors (Harvard Apparatus, catalog number: 72-8422)
9. Bone Rongeurs (Harvard Apparatus, catalog number: 72-8906)
10. Spoonula™ Lab Spoon (Fisher Scientific, catalog number: 14-375-10)
11. Forceps (Fisher Scientific, catalog number: 10-300)
12. Scalpel (Harvard Apparatus, catalog number: 72-8350)
13. No. 13 Scalpel blade (Harvard Apparatus, catalog number: 72-8366)
14. Induction Chamber (Harvard Apparatus, catalog number: 60-5246)
15. Guillotine (Harvard Apparatus, catalog number: 73-1918)
16. Alligator clips (Mueller, catalog number: BU-34)
17. Gas Dispersion Tube (Corning, catalog number: 39533-12C)
18. Medical Gas Tank, carbogen (Linde)
19. Gas Regulator (VWR, catalog number: 55850-444)
20. Stirrer (Thermo Fisher Scientific, catalog number: HP88857100)
21. Vertical Microelectrode Puller (NARISHIGE, catalog number: PE-22)
22. House Vacuum Line
23. Semiautomatic Vibrating Blade Microtome (Leica Microsystems, model: VT1200 S)
24. Chem-Clamp potentiostat (Dagan, catalog number: CHEM-5-MEG)
25. Headstage (5 Megohms) (Dagan, catalog number: 8024)

26. Breakout Box, custom made (visit [pineresearch- WaveNeuro Fast-Scan CV Potentiostat](#) for FSCV bundles offered by PINE research. Many of their bundle options include the breakout box)
27. High-speed Analog Output Card (National Instruments, catalog number: PCI-6711)
28. Data acquisition card (National Instruments, catalog number: PCIe-6351)
29. Current Stimulus Isolator (Digitimer, model: NL800A)
30. Temperature Controller TC-344C (Harvard Apparatus, catalog number: 64-2401)
31. Peristaltic Pump P-70 (Harvard Apparatus, catalog number: 70-7000)
32. Upright Light Microscope with Reticle (example of suitable, Olympus, model: BX53M and Microscope World, model: KR887)
33. 3-Axis Manual Micromanipulator (NARISHIGE, model: MM-3)
34. Calibration System, custom made (see Figure 5A)
 - a. Tygon® Tubing (Sigma-Aldrich, catalog number: Z685666)
Manufacturer: Saint-Gobain, catalog number: AJK00022.
 - b. Syringe, 5 ml (Sigma-Aldrich, catalog number: Z116866)
 - c. Syringe, 30 ml (Sigma-Aldrich, catalog number: Z683671)
 - d. T connector with stopcock (Cole-Parmer, catalog number: UX-30600-02)
35. Single Syringe Infusion Pump (Fisher Scientific, catalog number: 14-831-200)
36. Fume hood (optional)
37. Superfusion chamber (Custom Scientific, custom order)
38. Clearlink System extension set with Control-A-Flo Regulator (Baxter, catalog number: 2C8891)

Software

1. Demon Voltammetry and Analysis Software Suite, available free-of-charge at the following site:
<https://www.wakeforestinnovations.com/technologies/demon-voltammetry-and-analysis-software/>

Note: A request for a license has to be submitted in order to download.

Procedure

Prior to Day of Experimentation

- A. Carbon fiber electrode preparation (Figure 1)
 1. Using a house vacuum line, suction a single carbon fiber (approximately 12 cm long) into a capillary tube (Figures 1A-1D). Hold one end of the carbon fiber down with a finger to prevent it from being suctioned into the vacuum line (Figure 1C).
Note: Separating carbon fibers over a piece of white paper can assist in visualizing individual fibers, as it is important to aspirate only a single carbon fiber into the capillary tube.

2. Load the carbon fiber-filled capillary tube into a vertical microelectrode puller, with the midpoint positioned in the center of the heating element (Figure 1E). Once the two electrodes have been pulled from the single capillary tube, use scissors to cut the carbon fiber connecting the two halves (Figure 1F).

Notes:

- a. *It may be helpful to mark the glass capillary tube at its midpoint with a permanent marker prior to pulling. The marked midpoint is placed in the center of the heating element, thus creating two carbon fiber electrodes of equivalent length.*
 - b. *Settings for the microelectrode puller vary from lab to lab. Our laboratory uses the following settings: 89.1 main-magnet; 20.9 sub-magnet; 54.2 heater. Ideal settings allow the pulled glass to fuse tightly with the carbon fiber at the tip while being sturdy enough to resist cracking near the glass-carbon fiber interface (typically settings that yield a taper length of approximately 0.75 cm are optimal). Trial and error testing may be necessary to determine the best settings for individual pullers.*
3. Under a light microscope with a reticle at 10x magnification (Figures 1G-1K), use a scalpel to trim the carbon fiber at the tip of the carbon fiber electrode to a desired length.
Note: Our laboratory uses a carbon fiber tip length of approximately 30-100 µm. Optimal length may vary between labs depending on the sensitivity of individual setups.
 4. Apply a layer of Silver Print II to a stainless steel conductive wire and thread it into the carbon fiber electrode (Figures 1L-1N). Allow the paint to dry in an open, ventilated area (such as a fume hood) for at least 12 h before use (Figure 1O).

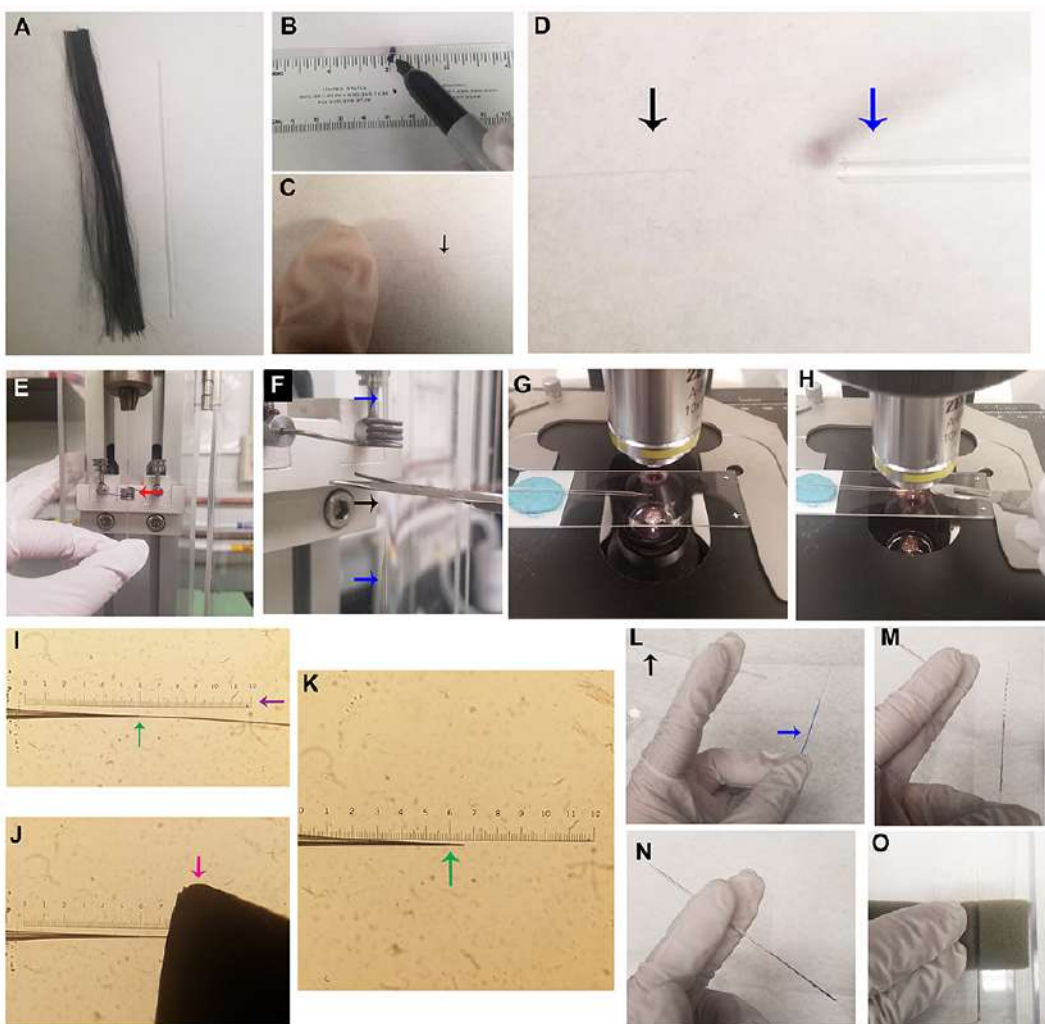


Figure 1. Production of carbon fiber electrodes (CFEs). A. Cut a bundle of carbon fiber to a slightly longer length than a capillary tube. B. Marking the center point of a capillary tube is helpful for placement into the gravity electrode puller (see Figure 1E). C. While wearing gloves, isolate a single carbon fiber, and gently restrain one end of the fiber with a finger. D. Affix a capillary tube in the house vacuum line (blue arrow), and, while holding one end of the carbon fiber, suction the other end of the carbon fiber (black arrow) into the capillary tube. E. Load the capillary tube containing a single carbon fiber into the gravity electrode puller, and position the center point of the capillary tube in the heating element (red arrow). F. Upon completion of electrode pulling, cut the carbon fiber (black arrow) connecting the two electrodes (blue arrows) with scissors, to create two CFEs. G. Using a light microscope with a reticle and a 10x objective, position the CFE on a slide with the tip touching the glass slide (a small piece of putty may be used to prop the CFE in the correct position). H. Use a scalpel blade to cut the carbon fiber to the appropriate length. I. The uncut CFE is shown under the 10x objective. The interface between the glass and the carbon fiber is shown at the green arrow. J. Use a scalpel blade to cut the CFE to appropriate length (30-100 μm). It is very helpful to make sure the tip of the razor blade is against the slide glass and visible in the microscope for more accurate

cutting (pink arrow indicates blade tip). K. CFE shown after cutting the carbon fiber, shown with glass interface indicated by the green arrow. L-N. Insertion of a stainless steel conductive wire coated with Silver Print II into CFE. L. Stainless steel wire (blue arrow) and cut CFE (black arrow). M. Coat one end of the wire and blue insulation in Silver Print II. N. Insert wire into CFE. O. Completed CFEs should be left in a fume hood to dry for at least 12 h prior to use; store in a plastic box with foam to hold the CFE, as shown.

B. Other preparations

1. Preparation of ACSF and Krebs solutions

- a. Prepare 10x Krebs solution (see Recipes) and stir on a stir plate (with a stir bar) until all the solutes are dissolved (at least 1 h).

Note: Our laboratory makes a 1 L stock solution of Krebs, which is kept at 4 °C for a maximum of 1 month.

- b. Prior to the day of experimentation, prepare 500 ml of ACSF. Pour 75 ml of ACSF into a 150 ml plastic beaker, and 250 ml of ASCF into a 500 ml plastic bottle. Place the plastic beaker and bottle into a -20 °C freezer. This frozen portion of ACSF will maintain ACSF used on the day of experiment at an ice-cold temperature (slicing at a cold temperature improves the health of tissue).

Note: On the day of slicing, fresh ACSF will be prepared and added to the plastic bottle containing frozen ACSF to be oxygenated and used for slicing (described below). After slicing, return the bottle and beaker half filled with to the freezer for subsequent experiments.

Day of Experimentation

A. Setting up

1. Prepare fresh ACSF solution and aliquot to the approximate volumes noted below:

- a. 200 ml into the bottle containing frozen ACSF (described above), to be used for slice preparation (referred to as bottle 1a).
- b. 500 ml into a cylinder for each FSCV rig, to be used during experiment (additional ACSF may be needed for longer experiments) (referred to as cylinder 1b).
- c. 200 ml into a storage beaker with netted wells to retain extra slices, to be oxygenated and maintained at room temperature (referred to as storage beaker).

2. Oxygenate prepared ACSF (a-c listed above) by turning on the gas regulator of the carbogen tank, and place a gas dispersion tube into each container. Oxygen should flow continuously, and a steady stream of bubbles should be observed.

Note: Take care not to over-oxygenate, which has the appearance of vigorous or rolling bubbles.

3. Place the vibratome stage and brain matrix (Figure 1A) in the freezer at -20 °C, and add a fresh blade to the vibratome; set the thickness and slicing speed (mouse—speed 0.46 mm/sec and thickness 300 µm; rat—speed 0.60 mm/sec and thickness 400 µm).

4. Prepare the FSCV rigs by adding deionized water to fill the bottom portion of the recording dish.

Note: Ensure that water is covering the heater coil to prevent melting of tubing.

5. Flow oxygenated ACSF from cylinder 1b into the slice well at 1 ml/min by using a peristaltic pump or gravity flow with a Control-A-Flo Regulator.

6. Turn on the following equipment: (1) temperature controller TC-344C, set to 32 °C in the recording dish; (2) Current Stimulus Isolator, output set to 1 mA; (3) Chem-Clamp; (4) light source, and (5) microscope (visualized in Figures 3A-3B).

7. Draw fluid from the recording dish's outflow tubing using a syringe, which will allow fluid to start flowing out of the dish and into the waste bottle.

Note: Throughout experimentation, outflow needs to be maintained. This can be particularly troublesome with new tubing, which may require the outflow to be reestablished several times throughout the day.

8. Before brain extraction, add ~50 ml of the cold, oxygenated ACSF from bottle 1a to cylinder 1b containing frozen ACSF. This will be used for transporting the brain to the vibratome.

B. Brain extraction (refer to Papouin and Haydon [2018] for further details)

1. Add isoflurane to an induction chamber, and allow the gas to disburse throughout the chamber (2-3 min for mice; 5-10 min for rats.).

2. Deeply anesthetize the rodent in the induction chamber, followed by immediate decapitation.

Note: It is important to make sure the animal is still breathing (at a depressed rate) prior to decapitation. In our laboratory, rat and mouse decapitation occurs via guillotine.

3. Expose the skull by making a midline incision (caudal to rostral) with scissors; pull the skin laterally to visualize the suture lines of the skull.

4. Use rongeurs (for rats) or small scissors (for mice) to carefully remove the skull to expose the dorsal surface of the brain.

5. Peel away surface blood vessels and meninges.

6. Carefully run a spatula under the brain to free it from any cranial nerves.

7. Once free, completely submerge the brain in cylinder 1b containing frozen and fresh ACSF.

C. Brain slicing

1. Use forceps to transfer the brain from cylinder 1b to the brain matrix, arranging the brain ventral side up. Use a plastic pipette to transfer chilled, oxygenated ACSF (approximately 2 ml) to the brain matrix.

Note: The brain does not have to be fully submerged at this step. Addition of ACSF onto the brain while it is in the matrix will help straighten the brain and prevent it from sticking to the surface of the matrix.

2. While still covered in paper, snap a Personna double-edged blade into two single edge blades.
3. Place a single edge blade at the desired location(s) in the matrix to remove excess brain tissue (referred to below as blocking) (Figure 2A).

Note: When our group isolates slices containing the nucleus accumbens, we block caudally at the level of the hindbrain to remove the cerebellum, and block rostrally to remove the olfactory bulb and early prefrontal cortex. Take care not to block off too much tissue, preserving the desired area of interest.

4. Place a small amount (approximately one drop) of Loctite® 404™ glue onto the stage, and use forceps to transfer the brain from the matrix to the stage. Quickly position the caudal side of the brain onto the glue (Figure 2B).

Note: Be careful not to use too much glue. Overuse of glue can cause the brain to detach from the stage when ACSF is added, which will result in poor slicing conditions.

5. Carefully push a single edge blade down the midline (dorsal to ventral) to hemisect the brain.
6. Place the stage onto the vibratome, and fill the stage with ice-cold, oxygenated ACSF (from bottle 1a) to submerge the brain.

Note: Avoid pouring ACSF directly onto the brain, as this could cause the brain to detach from the stage.

7. Lower the blade into the ACSF solution, and set the slicing window to at least 1 mm beyond the dorsal and ventral ends of the brain; slice the brain at the suggested settings listed above.
8. Using a transfer pipette or a spatula, transfer slices to slice wells of the recording dish (Figure 2C).

Note: Extra slices can be stored in the storage beaker (Figure 2F), for up to 6 h. This storage beaker should be filled with ACSF, with continuous oxygen flow via gas dispersion tube. If needing to transfer a slice from the storage beaker to a slice well (in a recording dish), use Step C8 as noted above. Please refer to Papouin and Haydon (2018) to create the storage beaker (nest beaker).

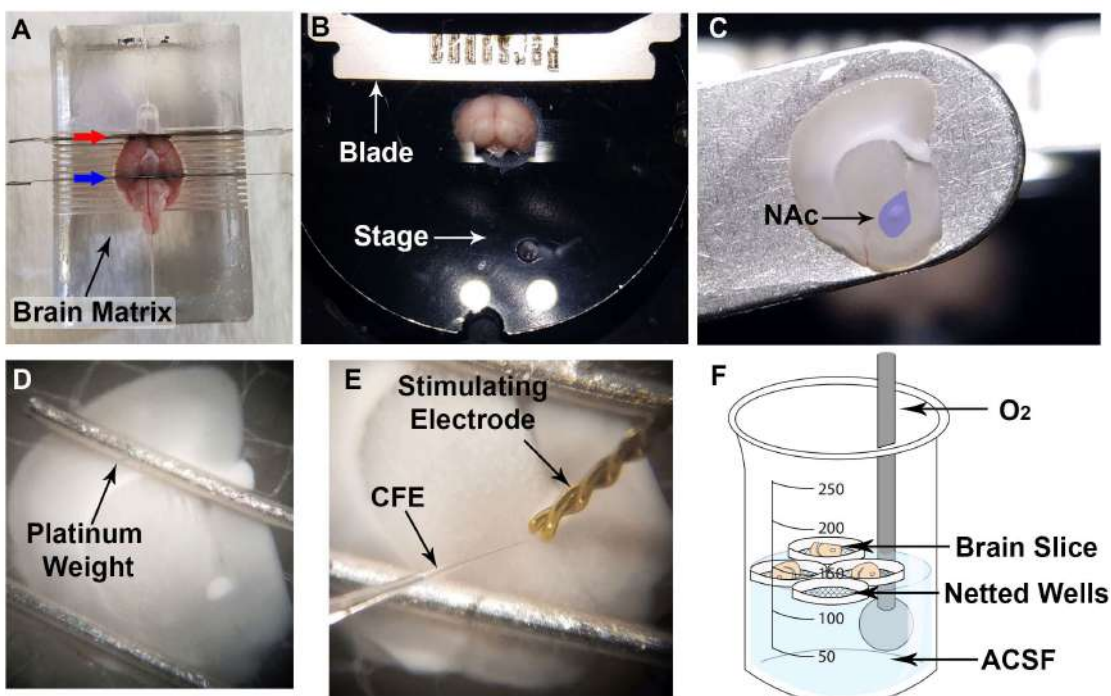


Figure 2. Brain slicing (mouse shown). A. Using a brain matrix, block the brain at the appropriate rostral (red arrow) and caudal (blue arrow) locations using single edge blades. B. Adhere the brain rostral side up onto the stage, hemisect, and submerge the brain in cold, oxygenated ACSF. C. Using spatula or transfer pipette (not shown), carefully transfer brain slice to recording dish (nucleus accumbens (NAc) shown in purple). D. Secure the brain slice using platinum weights, placed distally from region of interest. E. Place bipolar stimulating electrode and carbon fiber electrode in the region of interest (NAc shown). F. Diagram of storage beaker containing oxygenated ACSF with netted wells to retain slices (O_2 refers to carbogen that is flowed into the beaker via a gas dispersion tube).

D. Setup of FSCV equipment

1. To weigh down the brain slice, place platinum wires at the edges of the slice distant from the recording location (Figure 2D).

Note: Typical equipment setup for FSCV is shown in Figure 3.

2. Place the cover onto the recording dish, and fully submerge the Ag/AgCl reference electrode pellet into ACSF solution. Use alligator clips to connect the reference electrode and the carbon fiber electrode to the headstage (Figure 3D).
3. Prior to beginning experimentation, use an insulin syringe 28 Gauge to carefully remove any bubbles that have formed under the netting of the slice well.

Note: It may be necessary to remove bubbles during experimentation if they affect the signal (see Note 6).

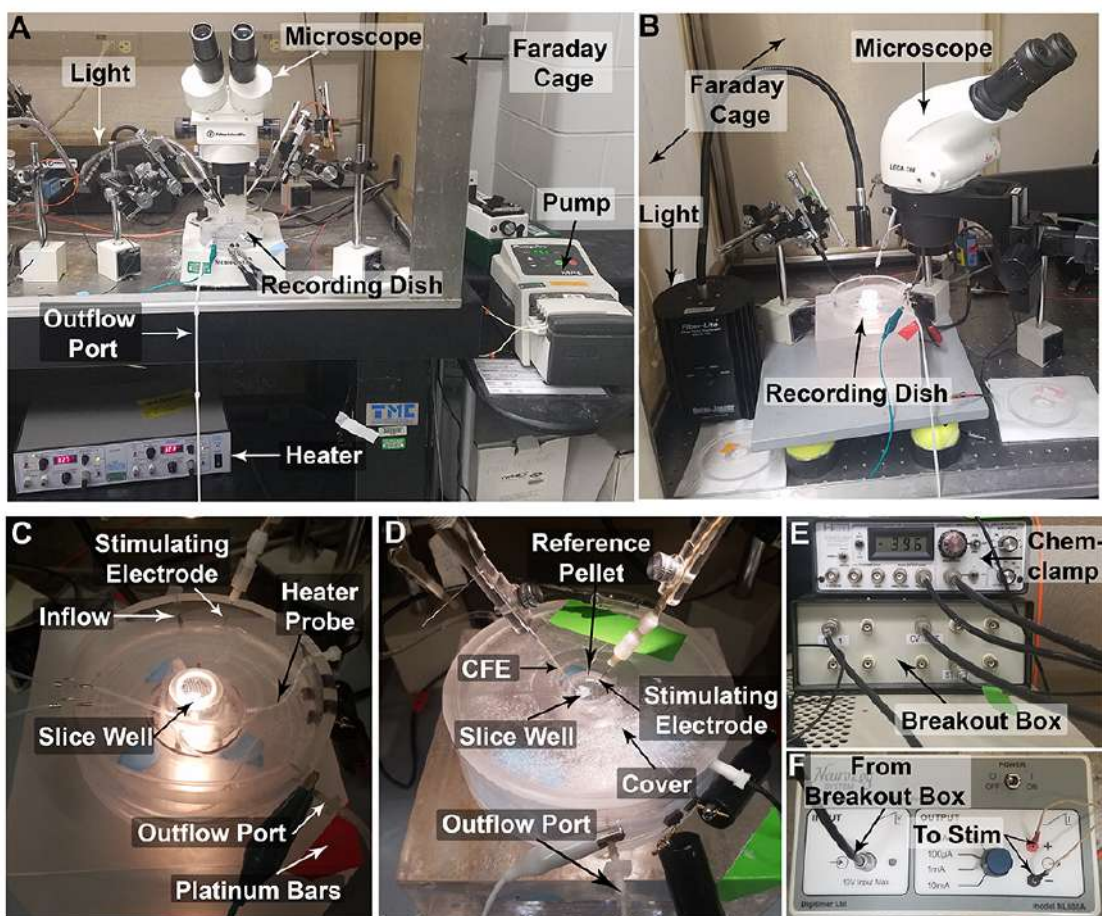


Figure 3. Setup of Fast Scan Cyclic Voltammetry Equipment. A. A typical FSCV setup (referred to as FSCV rig). B. Alternate typical FSCV setup. C. Closer view of the recording dish, without the cover. D. Recording dish with cover, brain slice in slice well, and stimulating electrode and carbon fiber electrode in place. E. Amplifier (Chem-clamp) and digitizer (Breakout Box) setup. F. Stimulus generator (Neurolog) showing input from Breakout box and output to bipolar stimulating electrode.

- E. Setup of software (Demon Voltammetry and Analysis) for Measuring Dopamine
1. Click **Edit CV and Stim**, which will allow the command voltage and stimulation settings to be set.
 2. Click **Apply** once parameters are set. Standard settings are shown in (Figure 4).

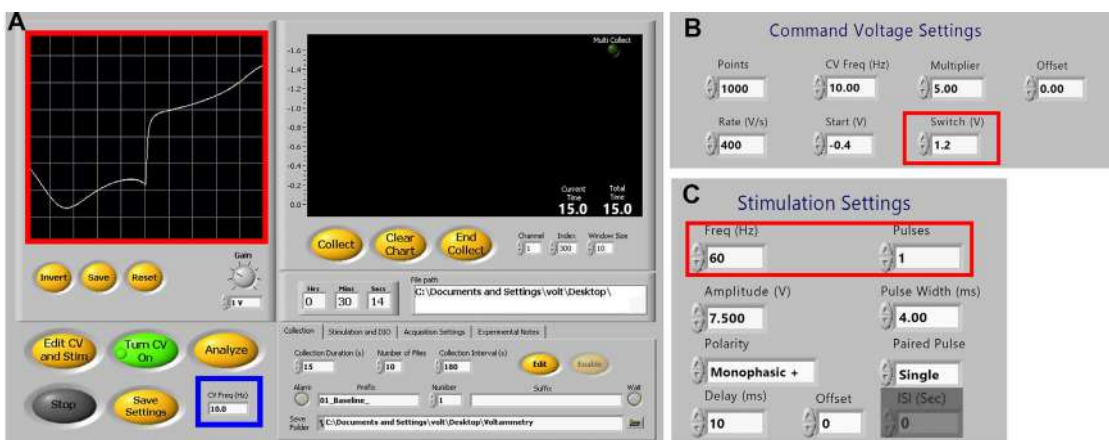


Figure 4. Demon Voltammetry setup for dopamine detection. A. User Interface showing typical experimental settings with ideal current-voltage plot from an electrode (red box). For carbon fiber electrode conditioning, the **CV freq** (blue box) may be increased from 10 Hz to 60 Hz. B. Command Voltage settings. Switching potential can be adjusted as needed (red box; see Note 4). C. Stimulation settings for single pulse experiments (frequency is not used for single pulses). Frequency and pulse number (red box) can be adjusted as needed for multipulse experiments (see Note 5).

F. Electrode conditioning (for new electrodes only)

1. Using a micromanipulator, lower the carbon fiber electrode to submerge the carbon fiber tip into ACSF (do not lower the carbon fiber electrode into the brain).
2. Turn on the **CV**, and repeatedly scan at a frequency of 60 Hz for at least 20 min.
3. After the above conditioning step, turn off the **CV** and change the frequency to 10 Hz (the working cyclic voltammetry frequency for FSCV).

Note: Electrodes can be used 2-4 times, and this conditioning step is only required for the first use. If the electrode is not new, start at the working cyclic voltammetry frequency of 10 Hz and skip to collecting dopamine signals. The conditioning step allows stabilization of new electrodes to occur quicker.

G. Collecting dopamine signals

1. Using a micromanipulator, lower the carbon fiber electrode approximately 75 μ m (visual estimation) into the brain region of interest.
2. Lower the bipolar stimulating electrode (using a micromanipulator) onto the surface of the slice, 100-200 μ m from the carbon fiber electrode (Figure 1E).

Note: A common early mistake is puncturing the surface of the slice when lowering the stimulating electrode. It is helpful to slowly lower the stimulating electrode until the surface of the slice dimples. When the dimpling effect occurs, slightly elevate the stimulating electrode to ensure it rests on top of the slice surface.

3. Name the collection files and set the save folder.

4. Set the number of collection files to 1, and uncheck the “Wait” button. The file name can be set to “default” for this step, or renamed.
 - a. A few electrode placements may be needed in order to achieve an optimal signal (depicted in Figure 4).
 - b. When trying to achieve an optimal signal, it is better for slice health to move the carbon fiber electrode rather than the stimulating electrode (which, due to size, can damage the tissue).
5. Once a reasonable dopamine signal is obtained (optimally greater than 3 nA for rat slices and greater than 7 nA for mouse slices; Figure 5), set the desired number of collection files. Set the collection interval to either 180 sec (for single pulse experiments) or 300 sec (for multi-pulse experiments).
6. Click the **Collect** button to begin collecting dopamine signals.

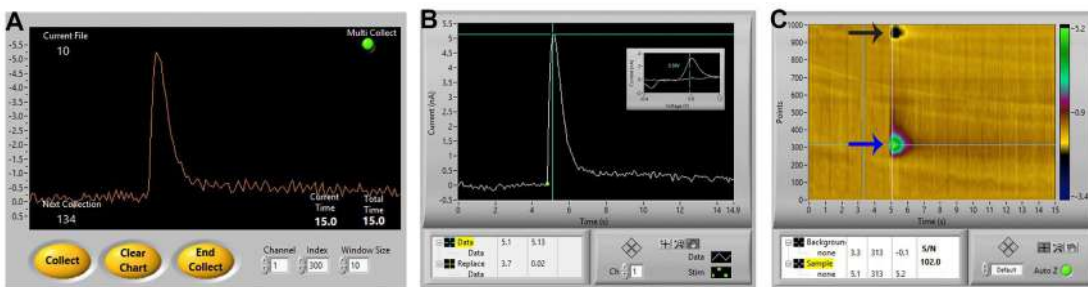


Figure 5. Ideal dopamine signal. A. An ideal signal of stimulated dopamine as observed in the Demon collection window. B and C. The same signal in the Demon Analysis window, showing (B) the dopamine signal (cyclic voltammogram inset showing oxidation and reduction peaks), and (C) associated color plot, showing the oxidation peak (blue arrow) and reduction peak (black arrow) of dopamine.

7. Stop the collection after 30-40 min of collecting baseline signals (at least 10 collections with a 180 sec interstimulus interval or at least 8 collections with a 300 sec interstimulus interval).
8. Click the **Analyze** button, and check the last three signals to see if collections have stabilized (amplitude varying less than 10% between collections, and not all increasing or decreasing. For example, if the last three collections have amplitudes of 9.8 nA, 10.2 nA, and 10.5 nA, the dopamine signal is not stable. If the collections were 9.8 nA, 10.2 nA, and 9.7 nA, the signal is stable, and the experimenter can move on to Step G7).

Note: Do not let the slice sit without regular stimulation at the selected interstimulus interval, or else the signal will need to be restabilized.

9. After stability, a pharmacological agent of interest can be added to the ACSF cylinder. Change the collection name, and collect for a minimal of 30 min to allow the pharmacological agent to reach maximal effect.

Note: A pharmacological agent can be added at cumulative doses to create a

concentration-response curve. Once the curve is complete at the desired concentrations, the experiment has ended, and the slice is no longer usable for other experimentation.

10. Upon completion of experimentation, turn off the **CV** button.
11. Disconnect the carbon fiber electrode and the stimulating electrode from the headstage.
12. Move the carbon fiber electrode to the calibration system to determine the electrode's sensitivity to dopamine.

Note: It is best practice to perform calibration at the end of each experiment, or prior to using the electrode for another experiment. Even if the same electrode is used for two experiments, sensitivity to dopamine can change due to fouling of the electrode.

H. Calibration of carbon fiber electrode (Figure 6)

1. Dilute dopamine in ACSF to a known concentration of dopamine (our laboratory uses 3 μ M), and fill a 5 ml syringe with the diluted dopamine solution.
2. Fill a 30 ml syringe with ACSF solution, and place it on a single syringe infusion pump.
3. Open the Demon Voltammetry software and use the same settings as listed above, except change the collection interval to 0 sec and number of files to 5.
4. Reconnect the carbon fiber electrode and reference electrode to the same headstage as the performed experiment.
5. Run ACSF through the calibration system using the single syringe infusion pump, and lower the carbon fiber electrode into the ACSF solution (Figure 6A).
6. Turn on the **CV** button (electrode signal shape should appear the same as during experimentation), and start the collection.
7. Allow ACSF to flow for 5 sec, and then apply a consistent flow of the diluted dopamine solution for the next 5 sec, followed by ACSF solution. Continue for each additional collection.

Note: Dopamine signal should have an approximately square-shaped peak (Figure 6B).

8. Analyze calibration collections to ensure the dopamine signals are stable (not trending in one direction). If the dopamine current continued to increase or decrease, repeat Step H6 to collect additional calibration data.
9. Once the dopamine signals are stable, average all of the dopamine currents (nA) collected. Divide the average current by the concentration of the dopamine solution used for calibration (3 μ M) in order to determine the calibration factor (nA/ μ M).

Note: If any collection amplitudes vary drastically from other collections, exclude it and average accordingly.

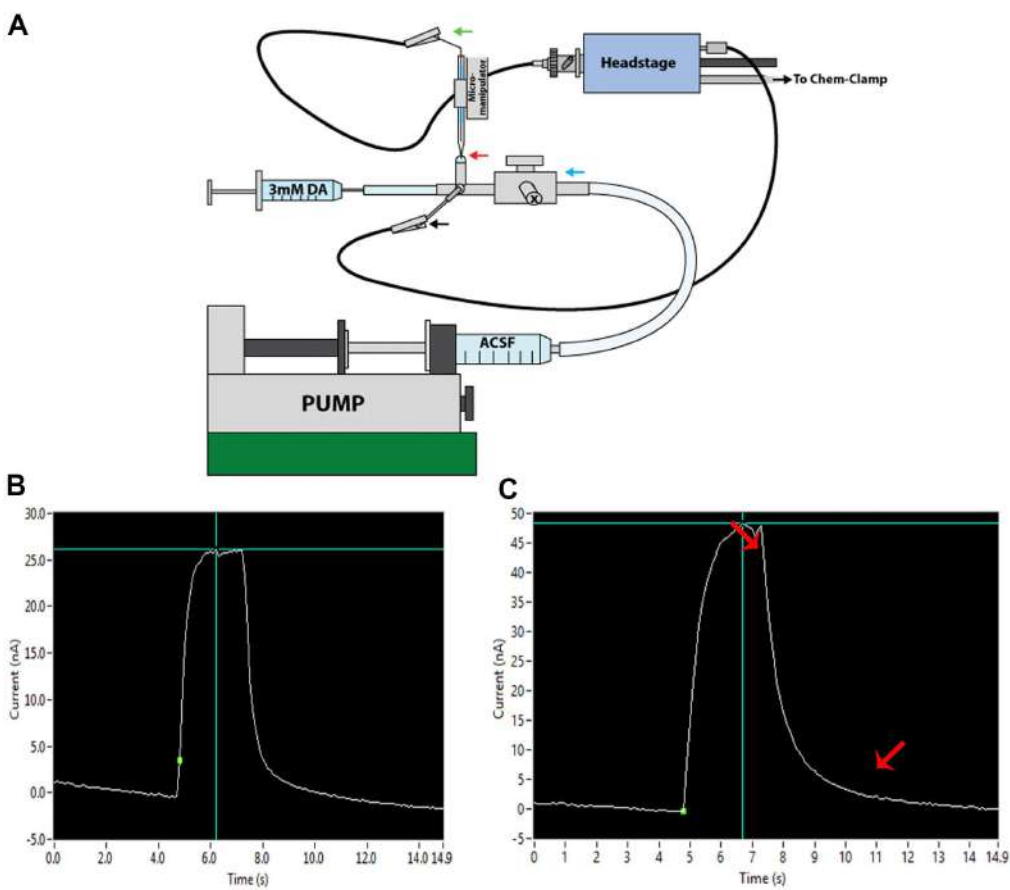


Figure 6. Electrode Calibration. A. Electrode calibration system. A pump is used to drive ACSF through a T connector with stopcock (blue arrow). Electrodes are lowered into the ACSF droplet (red arrow), and electrodes and reference wire (black arrow) are connected to the headstage. B. Ideal calibration curve showing a square shape with fast kinetics. C. Non-ideal calibration curve obtained from a “slow” electrode that has been overused. Lipids and proteins can adhere to and foul the surface of the carbon fiber following repeated usages. This slows the kinetics of dopamine detection, resulting in sloping—rather than square—calibration curves (red arrows indicate regions of slowed kinetics).

I. Clean up

1. Flow a 70% Ethanol solution through each recording dish for 10 min at an increased flow rate (e.g., 2 ml/min). Repeat with 3% hydrogen peroxide, then distilled water.
2. If using a peristaltic pump, allow air to flow through the line until all liquid has been displaced from the tubing. If using a gravity flow system, set the Control-A-Flo Regulator to the “prime” function, and use a syringe to push air through the tubing to clear out any residual liquid.
3. Empty used ACSF into an appropriate waste container.

Data analysis

- A. Demon voltammetry analysis with Michaelis-Menten modeling (see Yorgason et al., 2011)

Note: This procedure describes the Michaelis-Menten curve fitting analysis technique. However, a number of kinetic parameters can be analyzed by Demon Voltammetry and Analysis program. Please see Yorgason et al. (2011) for thorough review.

1. Open the program and click **Analyze**.
2. Click the **Open File** button to allow the user to choose the file of interest.
3. Click **Kinetics**, and input the calculated calibration factor ($nA/\mu M$) for the experiment
4. Go to the **Baseline Correction Tab**, and move the start (green) line and end (red) line to the beginning of the collected signal. Click **Reset**, then **Pre Stim Shift**. The Baseline offset should now appear as 0.00.
5. Go to the **Peak and Decay** tab. Position the Pre (green) line at the start of the dopamine signal, the peak (purple) line at the peak of the signal, and the post (red) line at the end of the dopamine signal. Click **Analyze**, and ensure that the modeled (yellow) line appropriately fits the curve. Click **Export** to save the file (Figure 7A). When prompted, name the file accordingly, and select save. When saving subsequent analyses from the same experiment, you may select this file which will then retain all peak-decay data in one text file that can be tab-delimited in Excel later (see below).
6. Go to the **Michaelis-Menten Analysis** tab. Enter the K_m constant of 160 nM. Alter the $[DAp]$ so that the curve matches the peak of the trace, the V_{max} to fit the first one-third of the descending portion of the curve. Increase the thickness until one point exactly overlays the trace on the ascending portion of the curve. Check Pearson Coefficient closeness of modeling fit, aiming for 0.95 (note that curves analyzed from experiments using drugs that decrease dopamine release will likely show poorer fit due to decreased ratio of signal:noise). Click **Export** to save the file (Figure 7B).
7. When prompted, name the file accordingly (being sure to assign a name discrete from the peak-decay file), and select save. When saving subsequent analyses from the same experiment, you may select this file which will then retain all modeled data in one text file that can be tab-delimited in Excel later (see below).

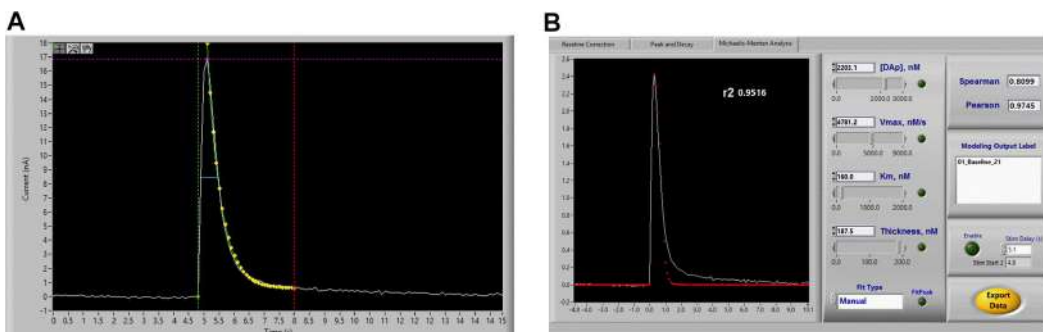


Figure 7. Voltammetry analysis using Demon Software. A. Peak-Decay analysis. Demon

software will automatically attempt to fit these parameters, but may need to be corrected slightly. The green, purple, and red lines should be placed at the stimulation time point, the peak of the signal, and a time point after the signal that has returned to baseline, respectively. The yellow dots are indicative of the program's automated peak-decay fit. B. Michaelis-Menten model fitting, showing Demon user interface for adjusting kinetic parameters to properly fit the signal.

B. Exporting data to Excel

1. Open Excel, and the **CYE** file containing peak/decay or modeled data to export.

Be sure to select **All Files** from the dropdown list in order to see the **CYE** file format.

2. When the prompt appears, ensure that the **Delimited** option is chosen, and click **Next**.
3. When the next prompt appears, ensure that the **Tab** option is chosen, and click **Finish**.

A table containing all files from the analyzed experiment will result. It can be helpful to create a master spreadsheet containing all experimental files from a study. Values of interest can then be analyzed using statistics software, such as Prism.

Notes

1. **Electrode placement:** When placing electrodes, it is important to maintain consistency in location between experiments. Dopamine signals change not only between locations in the region of interest (for example, the core and shell of the nucleus accumbens), but also along the dorsal-ventral and rostral-caudal axes.
2. **Timing of experiments:** Maintaining a consistent time in the animal's light-dark cycle is important to ensure that temporal fluctuations in dopamine levels do not confound any potential findings (Ferris *et al.*, 2013). It is also important to extract brains at the same time points post-drug in order to consistently observe the same temporally defined drug effects.
3. **Competitive inhibitors of the dopamine transporter:** The kinetic constant " K_m " measures the affinity of dopamine for the dopamine transporter, and has been estimated as 160 nM based on competition binding assays (previously determined; Wightman *et al.*, 1988). However, FSCV can be used to measure the effect of a competitive inhibitor of the dopamine transporter (such as cocaine) on the reuptake of dopamine. In this instance, "apparent" K_m is used, which models dopamine uptake inhibition. In order to analyze experiments in which the dopamine transporter is known to be affected, set K_m to 160 nM for analysis of the baseline curve, and fit the descending portion of the curve by adjusting V_{max} . For curves in the presence of inhibitor, maintain V_{max} at the value determined in the baseline traces, and adjust K_m . Values obtained are denoted "apparent K_m " to indicate that the constant itself is not changing, but the apparent affinity of dopamine for the dopamine transporter changes with transporter inhibition. Please note that this technique of adjusting K_m only applies in the case of dopamine transporter targeted drugs, and for all other experiments K_m should be maintained at 160 nM throughout

curve fitting analysis.

4. **Determining the appropriate switching potential:** In the Demon Collection Software, the switching potential can be adjusted as needed. For measurement of dopamine, the switching potential can vary between 1.1 V and 1.3 V. In most FSCV labs (including our own), a switching potential of 1.2 V is utilized to provide sufficient sensitivity while also preserving the integrity of the carbon fiber electrodes for 3-4 usages. Increasing the switching potential to 1.3 V increases electrode sensitivity; however, a switching potential of 1.3 V may result in electrode “drift” or continuously changing sensitivity, and thus making it necessary to replace carbon fiber electrodes more often. The switching potential can also be reduced to 1.0 or 1.1 V to decrease sensitivity. Generally, the switching potential is only reduced when an electrode begins to “limit” during the baselining portion of the experiment (Figure 5C), and new electrodes are unavailable. Upon altering the switching potential, a new baseline needs to be collected as the peak heights (in nA) of the evoked release will be altered by the changed sensitivity of the electrode. Switching potentials are specific to the species being analyzed. Here we describe guidelines for dopamine FSCV.
5. **Determining frequency and number of pulses:** The frequency (Hz) and number of pulses can be altered as needed, typically when examining drug or treatment effects on “phasic-like” stimulation kinetics. While the frequency setting has no effect on single pulse experiments, typical multi-pulse experiments consist of a set number of pulses (typically 5 or 10) applied for each of a number of increasing frequencies (*i.e.*, 5, 10, 20, 40, 60, 100 Hz) with a 300 sec inter-stimulus interval (see Ferris *et al.* [2013] for review).
6. **Troubleshooting**
 - a. Electrode (Table 1)

Table 1. Common electrode complications and solutions

Complication	Solution
Noise (Figure 8A)	<ol style="list-style-type: none">1. Seal between glass and carbon fiber is not intact.2. Connection from reference electrode to the headstage may be loose.3. Headstage malfunction.
Not Sensitive (Figure 8B)	Carbon fiber is too short.
Too Sensitive (Figure 8C)	<ol style="list-style-type: none">1. Carbon fiber is too long (Figure 5C).2. Lack of seal between glass and carbon fiber.
Stimulator Artifact (Figures 8D-8F)	<ol style="list-style-type: none">1. Carbon fiber electrode is placed too close to stimulating electrode.2. Stimulating electrode is not level on tissue surface.
Wide (Figure 8G)	<ol style="list-style-type: none">1. Electrode is old (slow).2. Recording from shell instead of core.3. Heater is not on.
Lack of Waveform	<ol style="list-style-type: none">1. Broken electrode

	2. Malfunctioning breakout box
	3. Malfunctioning headstage
	4. Malfunctioning National Instruments card

b. Carbon fiber electrode (Figure 8)

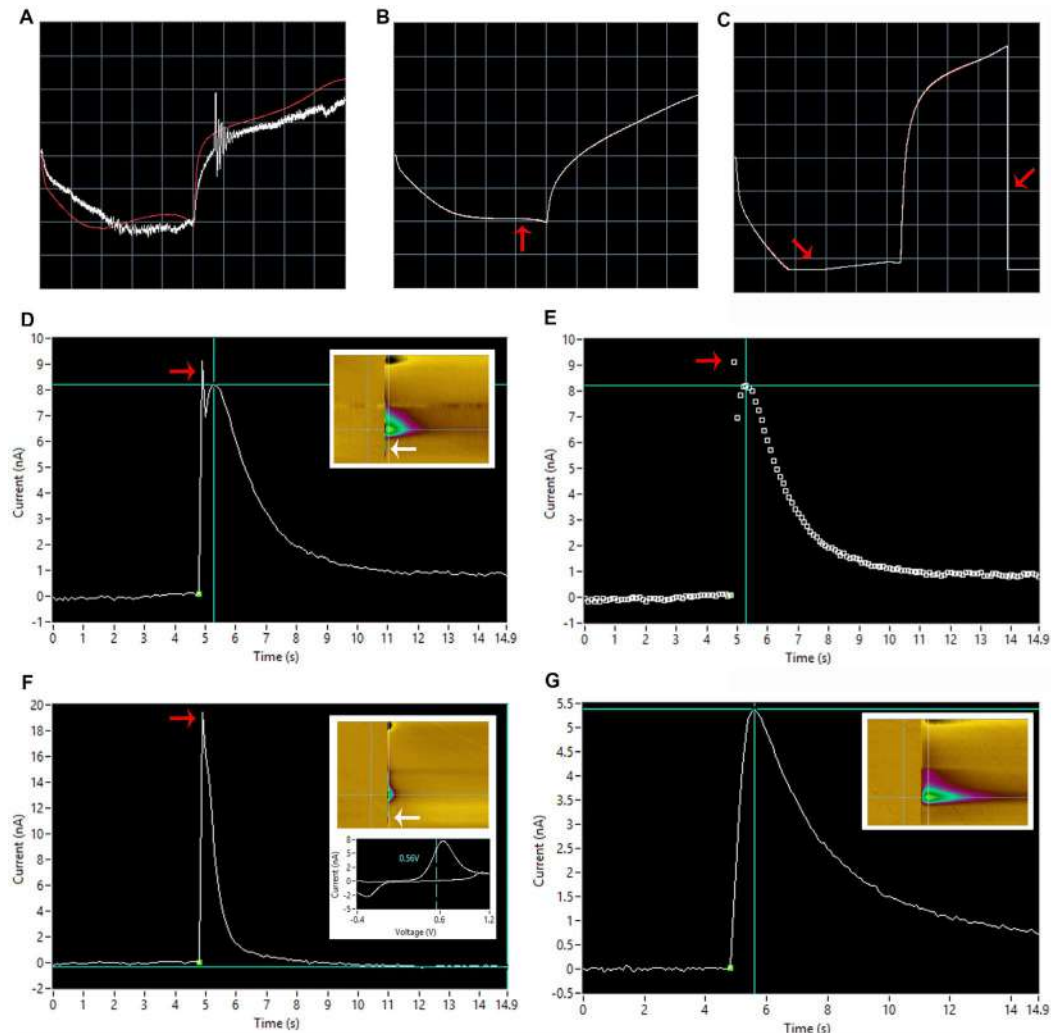


Figure 8. Common carbon fiber electrode problems. See Table 1 for troubleshooting tips. A. Improperly grounded carbon fiber electrode (properly grounded trace shown in red). B. Carbon fiber electrode with less-than optimal sensitivity. Note the relatively flat shape indicated by the red arrow. C. Limiting (too sensitive) carbon fiber electrode. The electrode current is exceeding the maximum limit of the computer interface, resulting in loss of data. Note that the full current range has been cut off at the red arrows. D and E. Stimulator artifact separated from signal (note that decay kinetics appear slow due to the presence of 3 μ M cocaine bathing the slice). D) Trace with colorplot inset depicting voltage on y-axis, time on x-axis and current in heatmap form on z-axis; see Yorgason *et al.* (2011) (red and white arrows indicate visual indication of spike presence on I/T plot and colorplot, respectively). E) Dot plot representation of the trace

with red arrow indicating a noise spike present. F. Stimulator artifact not separated from signal with colorplot and cyclic voltammogram inset (red and white arrows indicate visual indication of spike presence on I/T plot and colorplot, respectively). Note that the peak of dopamine in the cyclic voltammogram (~7 nA) does not correspond to an apparent peak in the trace (~19 nA), another indication of potential interfering stimulator artifact. G. Wide baseline signal with colorplot inset.

c. **Noise:** Increased signal noise is often caused by one of the following issues: noise in the electrodes (see above), static electricity from the experimenter, bubbles in the dish, or interference from outside electrical noise (so called 60 Hz noise). As discussed previously, a “noisy” electrode can be replaced. In order to prevent static electricity from the experimenter, it is good practice to touch the grounded Faraday cage prior to touching the micromanipulators or other rig components. This will eliminate any potential static electrical build-up that may occur due to clothing or general electricity in the area. Bubbles in the dish can also contribute to noise. In this case, the bubble itself can be removed as previously described. Bubble traps can also be installed to decrease the frequency of air bubbles in the tubing reaching the dish. Interference from outside electrical noise is the most common cause of spontaneous noise in signals. The origin of electrical noise can be difficult to ascertain and often arises without warning; however, precautions can be taken to ameliorate spontaneous noise. For example, dry air can increase static and thus noise, but the use of humidifiers on dry days can provide relief. Other troubleshooting options include completely enclosing the faraday cage, ensuring that the surface of the rig is free from all tools used during setup such as forceps and syringes, and turning off the lights in the rig. In general, electronic devices such as peristaltic pumps and voltammetry equipment must be kept outside of the Faraday cage to reduce noise from these devices as much as possible.

d. Common electrode placement errors (Figure 9)

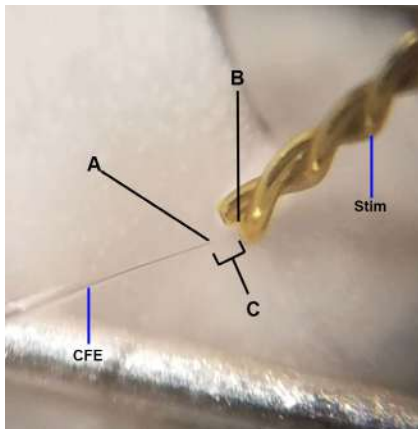


Figure 9. Ideal electrode placement. This image is adapted from Figure 1D. Above represents ideal positioning of carbon fiber electrode and bipolar stimulating electrodes (Stim)

for FSCV. A. The carbon fiber electrode should be placed approximately 75 μm into the brain slice; placement too deep or too shallow will yield less-than-optimal dopamine responses. The carbon fiber electrode should also be triangulated centrally between the two stimulating wires. B. The stimulating electrode should just touch the surface of the brain; placement too deep into the tissue will result in poor FSCV signals and tissue damage. The two wires of the stimulating electrode should lie flat on the tissue; crooked stimulating electrodes can result in increased stimulation artifact observance (see Figure 5D). C. The stimulating electrode and carbon fiber electrode should be placed approximately 100-200 μm apart; placement too close together increases artifact occurrence, while placement too far apart may result in diminished dopamine signal.

Recipes

1. Artificial cerebrospinal fluid (ACSF)

Material	Final Concentration (in mM)
NaCl	126
KCl	2.5
NaH ₂ PO ₄ ·H ₂ O	1.2
CaCl ₂ ·2H ₂ O	2.4
MgCl ₂ ·6H ₂ O	1.2
NaHCO ₃	25.0
Ascorbic Acid	0.4
D-Glucose	11.0
Store at 4 °C for up to 1 day	
Use deionized water to prepare the solution	

2. 10x Krebs stock solution

Material	Final Concentration (in mM)
NaCl	1259.4
KCl	24.95
NaH ₂ PO ₄ ·H ₂ O	12.03
CaCl ₂ ·2H ₂ O	8.16
MgCl ₂ ·6 H ₂ O	12.0
Store at 4 °C for up to 1 month	
Use ultrapure water to prepare the solution	

Notes:

- a. 10x Krebs Stock Solution is used for preparing Artificial Cerebrospinal Fluid (ACSF).

- b. A 10x Krebs stock solution, containing the majority of solutes above (with the exception of those, NaHCO_3 , ascorbic acid, and D-glucose) is prepared in advance.
3. 1 mM dopamine stock solution

Material	Amount
DA hydrochloride	9.4 mg
HClO_4	500 μl
Ultrapure water	50 ml
Store at 4 °C for up to 6 months	

On each day of experimentation, make a 3 μM solution of dopamine that will be used for calibration. For example, add 150 μl of the dopamine stock solution to 50 ml of ACSF.

Acknowledgments

This research was supported by the National Institute of Health grants P50 DA006634, R01 DA014030, T32 DA041329, U01 AA014091, P50 AA12298125, and R01 AA023999. Demon Voltammetry and Analysis software suite was written by Jordan Yorgason and Rodrigo España in the Jones laboratory.

Competing interests

The authors declare no competing financial interests.

Ethics

Experimental protocols adhered to National Institutes of Health Animal Care guidelines and were approved by the Wake Forest University Institutional Animal Care and Use Committee.

References

1. Adams, R. N. (1976). [Probing brain chemistry with electroanalytical techniques](#). *Anal Chem* 48(14): 1126A-1138A.
2. Bard, A. J. and Zoski, C. G. (2000). [Voltammetry retrospective](#). *Anal Chem* 72(9): 346A-352A.
3. Bucher, E. S. and Wightman, R. M. (2015). [Electrochemical analysis of neurotransmitters](#). *Annu Rev Anal Chem (Palo Alto Calif)* 8: 239-261.
4. Ferris, M. J., Calipari, E. S., Yorgason, J. T. and Jones, S. R. (2013). [Examining the complex regulation and drug-induced plasticity of dopamine release and uptake using voltammetry in brain slices](#). *ACS Chem Neurosci* 4(5): 693-703.

5. Fortin, S. M., Cone, J. J., Ng-Evans, S., McCutcheon, J. E. and Roitman, M. F. (2015). [Sampling phasic dopamine signaling with fast-scan cyclic voltammetry in awake, behaving rats.](#) *Curr Protoc Neurosci* 70: 7. 25. 21-20.
6. Heyrovsky, J. (2012). [\[Reproduction of: J. Heyrovsky, Chemicke Listy 1922, 16, 256-264\].](#) *Chem Rec* 12(1): 17-25.
7. Kishida, K. T., Saez, I., Lohrenz, T., Witcher, M. R., Laxton, A. W., Tatter, S. B., White, J. P., Ellis, T. L., Phillips, P. E. and Montague, P. R. (2016). [Subsecond dopamine fluctuations in human striatum encode superposed error signals about actual and counterfactual reward.](#) *Proc Natl Acad Sci U S A* 113(1): 200-205.
8. Lohrenz, T., Kishida, K. T. and Montague, P. R. (2016). [BOLD and its connection to dopamine release in human striatum: a cross-cohort comparison.](#) *Philos Trans R Soc Lond B Biol Sci* 371(1705): 20150352.
9. Maina, F. K., Khalid, M., Apawu, A. K. and Mathews, T. A. (2012). [Presynaptic dopamine dynamics in striatal brain slices with fast-scan cyclic voltammetry.](#) *J Vis Exp*(59): 3464.
10. Papouin, T. and Haydon, P. G. (2018). [Obtaining acute brain slices.](#) *Bio-protocol* 8(2): e2699.
11. Rodeberg, N. T., Sandberg, S. G., Johnson, J. A., Phillips, P. E. and Wightman, R. M. (2017). [Hitchhiker's guide to voltammetry: Acute and chronic electrodes for *in vivo* fast-scan cyclic voltammetry.](#) *ACS Chem Neurosci* 8(2): 221-234.
12. Wightman, R. M., Amatore, C., Engstrom, R. C., Hale, P. D., Kristensen, E. W., Kuhr, W. G. and May, L. J. (1988). [Real-time characterization of dopamine overflow and uptake in the rat striatum.](#) *Neuroscience* 25(2): 513-523.
13. Yorgason, J. T., Espana, R. A. and Jones, S. R. (2011). [Demon voltammetry and analysis software: analysis of cocaine-induced alterations in dopamine signaling using multiple kinetic measures.](#) *J Neurosci Methods* 202(2): 158-164.

Optical Clearing and Index Matching of Tissue Samples for High-resolution Fluorescence Imaging Using SeeDB2

Meng-Tsen Ke¹ and Takeshi Imai^{1, 2, *}

¹Laboratory for Sensory Circuit Formation, RIKEN Center for Developmental Biology, Kobe, Japan;

²Graduate School of Medical Sciences, Kyushu University, Fukuoka, Japan

*For correspondence: t-imai@med.kyushu-u.ac.jp



[Abstract] Tissue clearing techniques are useful for large-scale three-dimensional fluorescence imaging of thick tissues. However, high-resolution imaging deep inside tissues has been challenging, as it is extremely sensitive to light scattering and spherical aberrations. Here, we present a water-based optical clearing and mounting media, SeeDB2, which is designed for high numerical aperture (NA) objective lenses with oil or glycerol immersion. Using quick and simple soaking procedures, the refractive indices of samples can be matched either to that of immersion oil (1.52) or glycerol (1.46), thus minimizing light scattering and spherical aberrations. Fine morphology and various fluorescent proteins are highly preserved during the clearing and imaging process. Our method is useful for the three-dimensional fluorescence imaging of neuronal circuitry at synaptic resolution using confocal and super-resolution microscopy. SeeDB2 is also useful as a mounting media for the super-resolution imaging of fluorescent proteins.

Keywords: Tissue clearing, Fluorescence imaging, Confocal imaging, Super-resolution imaging, Connectome, SeeDB2

[Background] Biological tissues are organized in 3D. In addition, many of important cellular machineries, e.g., synapses in neurons, are at sub-micron scale. Therefore, there have been increasing demands for a method for sub-micron-scale 3D imaging. Serial electron microscopy techniques (e.g., FIB-SEM or SBF-SEM) are promising, but they cannot make the best use of the genetic fluorescent labeling tools available in modern life science. To facilitate 3D imaging with fluorescence microscopy, a number of tissue clearing techniques have been developed in recent years (Richardson and Lichtman, 2015 and 2017). They are designed for large-scale 3D imaging, and some of them allow for whole-brain, and even whole-body-scale fluorescence imaging of fixed samples combined with confocal, two-photon, or light-sheet microscopy. However, many of them have not been fully optimized for high-resolution imaging.

In fluorescence microscopy, lateral resolution (d) is given as:

$$d = 0.61\lambda/\text{NA}$$

where λ is the wavelength of the light and NA represents the numerical aperture. The resolution improves as d decreases. Therefore, we need to use high NA objective lenses for high-resolution imaging.

NA is defined as:

$$\text{NA} = n \sin\alpha$$

where n is the refractive index (RI) of the immersion media, and α is the half angular aperture. Therefore, many of the high NA objective lenses are designed for oil (RI = 1.52) or glycerol (RI = 1.46) immersion for the best resolution. Previously, high NA objective lenses are intended to image thin sections or just the surface of samples. However, if we try to image deeper in the samples with these objective lenses, image quality will be easily impaired due to “spherical aberrations”. As RI of tissue samples are lower than that of immersion oil (RI = 1.52) and a glass coverslip (RI ~1.52), the excitation light will refract at the interface between the coverslip and samples, and it will no longer converge onto a small focal spot. This is known as spherical aberrations, reducing resolution and brightness in microscopy.

To minimize spherical aberrations, index matching of samples is crucial. However, many of the existing mounting media and clearing solutions have low RI, ranging from 1.33 (water) to 1.46 (glycerol-based mounting media). Even our previous clearing agent, SeeDB (RI = 1.49), did not reach RI 1.52 (Ke *et al.*, 2013, 2014). 2,2'-thiodiethanol (TDE, RI = 1.52) has been previously proposed for index matching for oil-immersion objective lenses and has been widely used for synthetic fluorescent dyes (Staudt *et al.*, 2007). However, a major drawback of TDE is that most of fluorescent proteins are totally quenched in TDE. To overcome this limitation, we developed a new tissue clearing agent, SeeDB2S, that has a high refractive index (RI = 1.52), but also highly preserves fluorescent proteins (Ke *et al.*, 2016). We also formulated SeeDB2G (RI = 1.46) for glycerol-immersion objective lenses. As fluorescent proteins are better preserved than in commercialized mounting media, SeeDB2G/S are also useful as mounting media for high-resolution imaging. SeeDB2G/S is particularly powerful for high-resolution confocal microscopy and super-resolution microscopy of fluorescent proteins in tissues, sections, and cells.

Materials and Reagents

1. 1.5 ml Eppendorf tube (Eppendorf, for 1 ml solution)
2. 5 ml Eppendorf tube (Eppendorf, catalog number: 0030119401; optional for 3 ml solution, for thick brain slices or whole-mount samples)
3. Paint brush (for thin brain slices, No. 1-2, see Figure 1)
4. Silicone rubber sheet (translucent, 0.2 mm thick; e.g., AS ONE, catalog number: 6-9085-13; see Figure 1)

Note: Various thickness of silicone rubber sheets are available from Togawa Rubber (AS ONE), Professional Plastics, CS Hyde, etc., ranging from 0.1 mm to 8.0 mm. The thickness should match that of brain slices.

5. Glass slide (76 mm x 26 mm; MATSUNAMI Glass; Figure 1)
6. Coverslips (18 x 18 mm, No 1.5H; e.g., Paul Marienfeld, catalog number: 0107032 or ZEISS, catalog number: 474030-9000-000; Figure 1)

Note: No 1.5H (170 ± 5 µm thick) is highly recommended for super-resolution imaging.

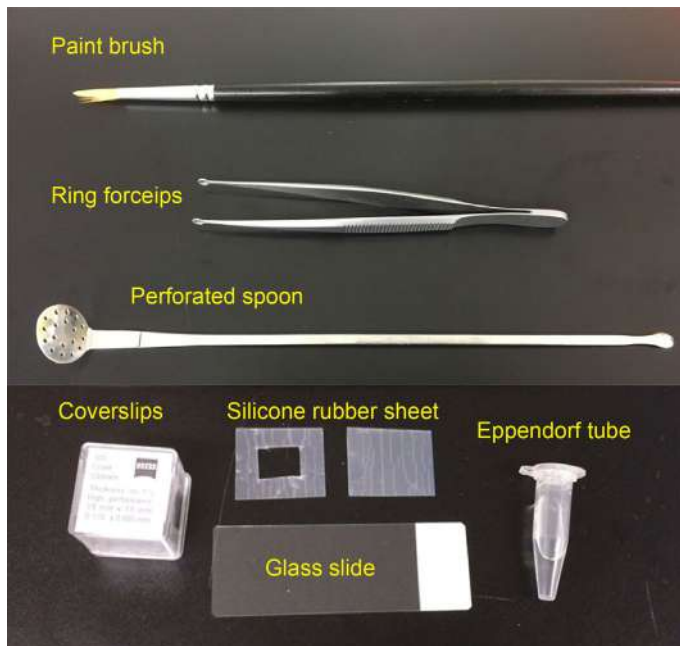


Figure 1. Materials required for preparing imaging chamber and slice mounting

7. Sodium chloride (NaCl)
8. Sodium hydrogen phosphate dodecahydrate ($\text{Na}_2\text{HPO}_4 \cdot 12\text{H}_2\text{O}$)
9. Potassium chloride (KCl)
10. Potassium dihydrogen phosphate (KH_2PO_4)
11. 4% paraformaldehyde (PFA; e.g., NACALAI TESQUE, catalog number: 26126-25) in PBS
12. 20% Saponin (NACALAI TESQUE, catalog number: 30502-42) in ddH₂O with filter sterilization

Note: Different vendors prepare saponin from different species of plants. We strongly recommend NACALAI TESQUE. Brownish lots (often found in Sigma-Aldrich) should be avoided.
13. Low-melting point agarose (e.g., Thermo Fisher Scientific, catalog number: 16520100)
14. Omnipaque 350 (e.g., DAIICHI SANKYO, Omnipaque 350 Injection, 50 ml in 1 bottle; also available from GE healthcare)
15. Histodenz (e.g., Sigma-Aldrich, catalog number: D2158)
16. Sodium azide (e.g., Sigma-Aldrich, catalog number: 13412)
17. 1 M stock of Tris-HCl, pH 7.6 (e.g., NACALAI TESQUE, catalog number: 35436-01), used to prepare Tris-EDTA buffer
18. 0.5 M stock of EDTA, pH 8.0 (e.g., Dojindo, catalog number: 347-07481), used to prepare Tris-EDTA buffer
19. Immersion media:
Glycerol (e.g., Type G Immersion Liquid, Leica Microsystems, catalog number: 11513910;
Glycerine solution, Leica Microsystems, catalog number: 11513872) for SeeDB2G
Oil (Type F, Olympus, MOIL-30; also available from Leica, Zeiss, etc.) for SeeDB2S
20. (Optional) SeeDB2 Trial Kit (Wako Pure Chemical Industries, catalog number: 294-80701)

21. Phosphate-buffered saline (PBS) (see Recipes)
22. Tris-EDTA buffer, pH 7.6 (see Recipes)
23. Permeabilization solution (see Recipes)
24. Solution 1 (see Recipes)
25. Solution 2 (see Recipes)
26. SeeDB2 solutions (see Recipes)
 - a. SeeDB2G with saponin (clearing)
 - b. SeeDB2G (mounting)
 - c. SeeDB2S with saponin (clearing)
 - d. SeeDB2S (mounting)

Equipment

1. Perforated spoon (optional for handling thick brain slices, custom-ordered, flat head, head diameter = 15 mm, see Figure 1 and Video 1)
2. Ring forceps (optional for whole-mount samples, e.g., Natsume Seisakusho, NAPOX, catalog number: A-26, see Figure 1)
3. Vibratome (e.g., LinearSlicer, DOSAKA, model: PRO7N)
4. Seesaw shaker (e.g., Bio Craft, model: BC-700)
5. Rotator (e.g., TAITEC, model: RT-30mini, catalog number: 0057154-000)
6. Fluorescence microscope
 - a. Confocal microscope (e.g., Olympus, model: FV3000; Leica Microsystems, model: Leica TCS SP8; Nikon, model: A1+)
 - b. Super-resolution microscope (e.g., Zeiss, model: LSM 880 with Airyscan; Leica Microsystems, model: Leica TCS SP8 with Hyvolution 2; Leica Microsystems, model: Leica TCS SP8 STED)
7. Objective lenses

Examples: 63x oil-immersion (NA = 1.4, WD = 0.14 mm) (Leica Microsystems, model: HC PL APO 63x/1.4 Oil CS2, catalog number: 15506350); 100x oil-immersion (NA = 1.4, WD = 0.13 mm) (Leica Microsystems, model: HC PL APO 100x/1.4 Oil CS2, catalog number: 15506325); 63x glycerol-immersion (NA = 1.3, WD = 0.28 mm) (Leica, model: HCX PL APO 63x/1.30 GLYC CORR, catalog number: 11506193); 63x oil-immersion (NA = 1.4, WD = 0.19 mm) (Carl Zeiss, model: Plan-APOCHROMAT 63x/1.40 Oil DIC, catalog number: 440762-9904-000)

Procedure

- A. Choice of optical clearing protocol
 1. SeeDB2G (RI = 1.46): SeeDB2G is optimized for glycerol-immersion lenses to achieve the highest resolution, but water- and multi-immersion objective lenses are also useful with

reasonable resolution. SeeDB2G is useful for larger tissues due to lower viscosity.

2. SeeDB2S ($RI = 1.52$): SeeDB2S is optimized for high-NA oil-immersion objective lenses. Since SeeDB2S is viscous and oil-immersion lenses typically have a short W.D. (0.1-0.2 mm), we recommend using relatively thin samples (< 300 μm thick slices) for SeeDB2S.

In this protocol, we describe the protocol for high-resolution/super-resolution imaging of mouse brain slices. However, SeeDB2 is also useful for high-resolution imaging of other organisms (e.g., *Drosophila*), other organs and sample types (mouse oocytes), cultured cells, and frozen sections. See the original paper (Ke *et al.*, 2016) and [SeeDB Resources](#) for details.

Note: SeeDB Resources (<https://sites.google.com/site/seedbresources/>) provide updated information from the authors, see Ke *et al.*, 2014.

B. Choice of objective lenses and slice thickness

Because of the working distance limitations in high-NA lenses, only one-fourth to half of the depth accessible by 20x lens can be reached by 63x or 100x lenses. Be sure to select neurons located close to the surface. See Table 1 showing examples of objective lenses used for confocal imaging.

Table 1. Examples of objective lenses

Objective lens	10x air	20x multi	40x oil	63x glycerol	63x oil	100x oil
N.A.	0.4	0.75	1.3-1.4	1.3	1.4	1.4-1.46
W.D. (mm)	2.2-3.1	0.68	0.21-0.24	0.3	0.14-0.19	0.11-0.13
Immersion	-	Water/glycerol/oil	Oil	Glycerol	Oil	Oil
Lateral resolution	2 μm	0.5 μm	0.3 μm	0.25 μm	0.21 μm	0.2 μm
Confocal	+	+	+	+	+	+
Super-resolution	-	-	\pm	\pm	+	+
SeeDB2G	\pm	+	\pm	+	\pm	\pm
SeeDB2S	\pm	\pm	+	\pm	+	+
Suitable sample thickness	< 2 mm	< 1 mm	< 500 μm	< 500 μm	< 300 μm	< 200 μm

+, optimal; \pm , non-optimal; -, not suitable. Data based on Leica and Zeiss objective lenses.

C. SeeDB2G (Figure 2)

1. Dissect the mouse brain after an intracardiac perfusion of 4% PFA in PBS. Post-fix the brain sample in 4% PFA at 4 °C with gentle shaking overnight.
2. Wash the sample in PBS three times with gentle shaking (10 min each).
3. Embed the sample in 4% low-melting point agarose/PBS with desired orientation and then cut the brain with a vibratome.
4. Transfer the sample into the permeabilization solution and incubate with shaking overnight (> 16 h) at 4 °C. Antibody staining and counterstaining should be performed prior to the clearing process.

Optional: Perform antibody staining in 3 ml using 5 ml Eppendorf tubes on a rotator. After blocking with blocking buffer (0.5% skim milk, 0.25% fish gelatin, 2% saponin in PBS) for 24 h at 4 °C, incubate samples with primary antibodies in washing buffer (2% saponin in PBS) for 24 h. After three washes with washing buffer, incubate samples with secondary antibodies and DAPI for 12-16 h. Wash samples three times (2 h each) in washing buffer.

Note: We recommend 2% saponin for thick mouse brain samples; however, for the thinner slices, lower concentrations of Triton X-100 are also workable. Antibodies are able to penetrate up to 200-300 µm in depth.

5. Transfer the sample into a new tube filled with solution 1 and place it on a rotator. Incubate for 6-10 h for whole-mount samples, 2-4 h for slice samples (200-500 µm).
6. Transfer the sample into a new tube filled with solution 2 and place it on a rotator. Incubate for 6-10 h for whole-mount samples, 2-4 h for slice samples (200-500 µm).
7. Transfer the sample into a new tube filled with SeeDB2G with saponin and place it on a rotator. Incubate for 6-10 h for whole-mount samples, 2-4 h for slice samples (200-500 µm). An example of transmission images is shown in Figure 4.

Notes:

- a. *Do not store samples in solutions containing saponin. For thin slice or neonate samples, prolonged incubation (> 24 h) in solutions containing saponin may cause damage to the sample.*
- b. *Store the sample in SeeDB2G (without saponin) till mounting and imaging.*
SeeDB2-cleared samples can be stored in Eppendorf at 4 °C for up to 6 months. Sodium azide (0.05%) should be added for the long-term storage.

D. SeeDB2S (Figure 2)

1. Dissect the mouse brain after intracardiac perfusion of 4% PFA in PBS. Post-fix the brain sample in 4% PFA at 4 °C with gentle shaking overnight.
2. Wash the sample in PBS three times with gentle shaking (10 min each).
3. Embed the sample in 4% low-melting point agarose/PBS with desired orientation and then cut the brain with a vibratome.
4. Transfer the sample into permeabilization solution and incubate with shaking overnight (> 16 h) at 4 °C. Antibody staining and counterstaining should be performed prior to the clearing process.

Note: We recommend 2% saponin for thick mouse brain samples; however, for the thinner slices, lower concentrations of Triton X-100 are also workable. Antibodies penetrate up to 200-300 µm depth.

5. Transfer the sample into a new tube filled with solution 1 and place it on a rotator. Incubate for 2-4 h for slice samples (200-500 µm).
6. Transfer the sample into a new tube filled with solution 2 and place it on a rotator. Incubate for 2-4 h for slice samples (200-500 µm).

7. Transfer the sample into a new tube filled with SeeDB2G with saponin and place it on a rotator. Incubate for 2-4 h for slice samples (200-500 μm).
8. Transfer the sample into a new tube filled with SeeDB2S with saponin and place it on a rotator. Incubate for 2-4 h for slice samples (200-500 μm).
9. Transfer the sample into a new tube filled with SeeDB2S (without saponin, 0.01% sodium azide can be added for long-term storage) for mounting. An example of transmission images are shown in Figure 4.

Note: Do not store samples in solutions containing saponin. For thin slice or neonate samples, prolonged incubation (> 24 h) in solutions containing saponin may cause damages to the sample.

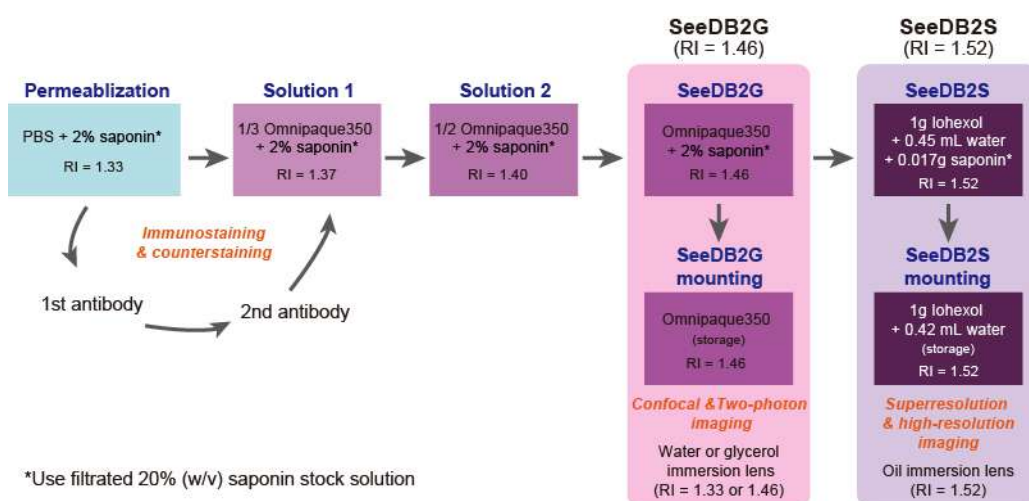


Figure 2. Graphic protocol for SeeDB2

- E. Imaging chamber preparation and sample mounting (Video 1 and Figure 3)
1. (Optional) Stand the sample in SeeDB2G/S for 2-4 h to remove the air bubbles.
Note: If air bubbles are heavily accumulated in the tube, transfer the sample to a new tube filled with SeeDB2G/S and incubate it for 2-4 h.
 2. Cut the silicone rubber sheet into appropriate size using scissors or a utility knife.
 3. Remove the protection sheets (stuck to both sides, only found in 0.2 mm silicone sheet) and press the sheet onto the glass slide. Push the rubber sheet to remove air bubbles between the glass slide and the rubber sheet.
 4. Leave a drop of SeeDB2G/S (from the storage tube, not a fresh one) into the chamber, and pick up the brain slice with a perforated spoon and a paint brush to mount the sample.
Note: Do not place the brain slices onto a dry surface. Do not expose SeeDB2S solution or SeeDB2S-cleared samples to the air for long time (> 5 min).
 5. (Optional) Remove the air bubbles in the imaging chamber with a paint brush.
 6. Gently press the cover glass onto the imaging chamber and use the spillover of SeeDB2G/S to seal the cover glass. See Figure 3 for mounted samples on a glass slide.

Note: Do not use nail polish to seal the sample. The excess amount of SeeDB2G/S will form a tight film after air drying.

7. Use an appropriate immersion media for high-resolution fluorescence imaging. Use glycerol (Refractive index = 1.46) for SeeDB2G, and oil (Refractive index = 1.52; Type F) for SeeDB2S. SeeDB2G/S cannot be used as an immersion media. Figure 5 shows an example of confocal images. Figure 6 shows super-resolution images (Airyscan and STED).



Video 1. Imaging chamber preparation and sample mounting. Cut a silicone rubber sheet (1 mm-thick and 0.2 mm-thick are shown in this video) into an appropriate size with scissors or a utility knife. A silicone rubber sheet will adhere to a glass slide, by removing air between the rubber sheet and the glass slide. Mount cleared samples (cleared samples are often difficult to find) using a perforated spoon and a paint brush. Use No. 1.5H coverslips to seal the samples.

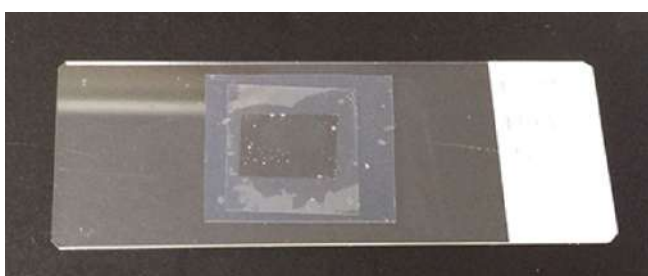


Figure 3. Slice sample ready for imaging. A 220 μm brain slice was mounted within the imaging chamber. A silicone rubber sheet (0.2 mm thick) was used for the spacer, and a coverslip is placed to seal the sample. The silicone rubber sheet will adhere to the glass slide and coverslip without adhesive. The spill-over of the SeeDB2G/S will form a tight film after air drying.

F. Anticipated Results (Figure 4)

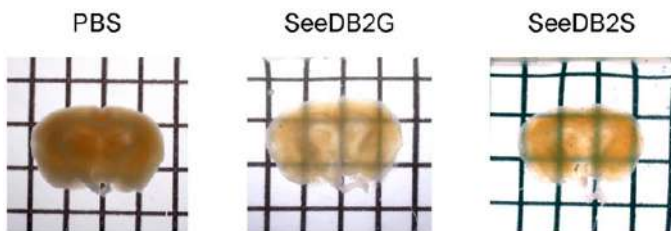


Figure 4. Transmission images of 500 μm adult mouse brain slices after optical clearing with SeeDB2G and SeeDB2S (Ke *et al.*, 2016). Grids are 2.6 x 3.2 mm.

Data analysis

Data analysis procedures have been described in the original publication (Ke *et al.*, 2016). No statistical analysis was performed in this protocol paper. We used Neurolucida (MBF Bioscience) for the 3D rendering in Figure 5.

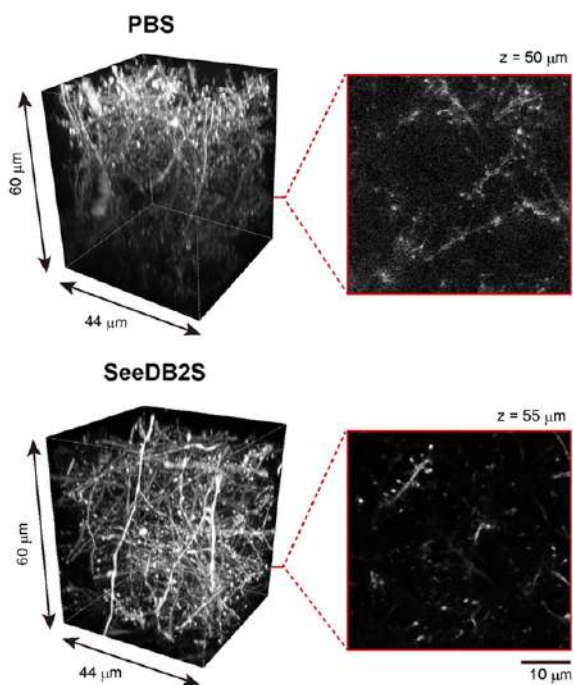


Figure 5. Confocal imaging of adult brain slices (*Thy1-YFP-H* mouse). Adult brain slices (220 μm thick) were imaged with 63x oil-immersion lens under confocal microscopy (Leica TCS SP8). In the PBS sample (uncleared), due to light scattering and spherical aberrations, the resolution and fluorescence signals intensity were damped. The highest resolution was maintained throughout all depths when cleared with SeeDB2S.

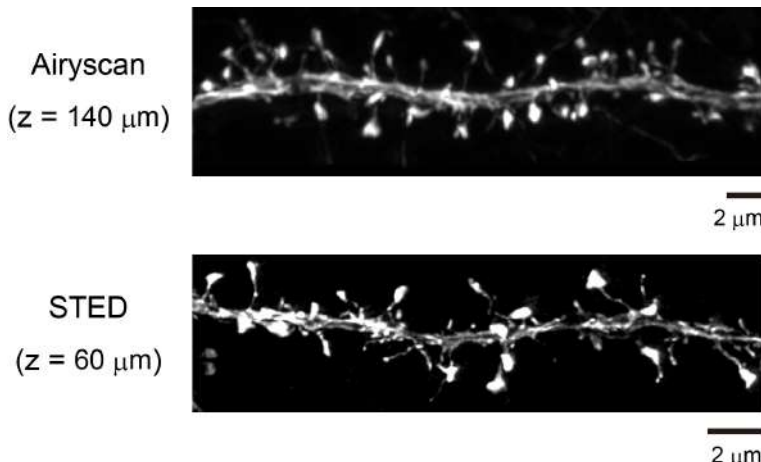


Figure 6. Super-resolution imaging of adult brain slices (*Thy1-YFP-H* mouse). Due to the minimized spherical aberrations, SeeDB2S is also useful for various kinds of super-resolution microscopy, such as STED (Leica), Airyscan (Zeiss), Hyvolution2 (Leica), and SpinSR (Olympus). For large-scale super-resolution imaging, we first imaged with a 20x objective lens. Then, we focused on a particular neuron and obtained super-resolution images along the target neuron to save imaging time and data volume. We used Neurolucida (MBF Bioscience) for the quantification and reconstruction of neuronal morphology. Images adapted from Ke *et al.* (2016).

Notes

1. The saponin solution is brownish

We strongly recommend saponin from NACALAI TESQUE. Different vendors prepare saponin from different species of plants. Brownish lots should be avoided. Alternatively, a low concentration of Triton X-100 can be used.

2. Histodenz does not dissolve completely

Prepare ~10 ml SeeDB2S solution in a 50 ml conical tube to prevent insufficient mixing of iohexol power and Tris buffer. Use rotator for gentle mixing.

3. White or yellow aggregations in SeeDB2 solutions

To avoid bacterial contamination, filter and sterilize the 20% saponin stock solution. Add 0.01%-0.1% of sodium azide to each clearing solution and store the solutions containing saponin at 4 °C.

4. Water evaporation

The surface of SeeDB2 forms a film as the water evaporates from the surface. SeeDB2 should be sealed in the imaging chamber during imaging.

5. Sealing samples in the imaging chambers/glass slides

Nail polish should not be used to seal the samples. For thick samples, we routinely use a silicone rubber. To seal samples on glass slides, we use an excess amount of SeeDB2, which then forms a tight film after water evaporation.

6. Samples are floating within SeeDB2

To avoid movement artifacts during imaging, we prepared brain slices that are slightly thicker than the thickness of the spacer (translucent silicone rubber sheet). For example, we prepared 220 μm brain slices when we used 200 μm -thick rubber sheets. For small samples, it is also useful to prepare SeeDB2 with 0.1% low-melting agarose to immobilize the sample; we used low-melting agarose to image mouse oocyte samples. Embedding small samples in agarose may also be useful to avoid the loss of samples during clearing, as it is often difficult to find invisible samples from clearing solution.

7. Movement artifacts

Because SeeDB2 allows for imaging up to the limit of the working distance (W.D.) of the objective lens, glass slides are often pushed up by the objective lenses as you get closer to the upper limit, which leads to movement artifacts. We recommend using a clamp or placing a weight on the glass slide in order to avoid the movement of samples during imaging.

8. Detecting sample surface

Because the refractive index of SeeDB2 is the same as that of coverslips, it is difficult to determine the surface of the sample when you perform the fluorescence imaging. Make sure to attach the sample to the coverslip (see Note 6).

9. Photo-bleaching

Various fluorescent proteins (e.g., TagBFP2, ECFP, mTurquoise2, EGFP, EYFP, CyOFP, tdTomato, tdKatushka2) are very stable and resistant to photo-bleaching in SeeDB2 solution. Indeed, SeeDB2 performs much better than commercialized mounting media for fluorescent proteins. However, some Alexa dyes and DAPI are easily photo-bleached in SeeDB2. In these situations, we suggest 2,2'-Thiodiethanol (TDE, refractive index up to 1.52) as an alternative for chemical dyes (Staudt *et al.*, 2007), however, fluorescent proteins are quenched in TDE.

Recipes

1. 10x Phosphate-buffered saline (10x PBS)

80 g NaCl

29 g Na₂HPO₄·12H₂O

2 g KCl

2 g KH₂PO₄

Add ddH₂O to prepare 1 L 10x PBS

Dilute 10 times with ddH₂O to prepare 1x PBS

2. Tris-EDTA buffer, pH 7.6

10 mM Tris-HCl

0.25 mM EDTA

3. Permeabilization solution

100 μl 20% saponin solution + 900 μl PBS

4. Solution 1

100 µl 20% saponin solution + 333 µl Omnipaque350 + 567 µl ddH₂O

5. Solution 2

100 µl 20% saponin solution + 500 µl Omnipaque350 + 400 µl ddH₂O

6. SeeDB2 solutions

Notes:

- a. *Tris-EDTA buffer pH 7.6 (Recipe 2) is used to prepare SeeDB2S from Histodenz powder. Do not use PBS. Phosphate buffer will generate white precipitates after long-term storage and impair imaging quality.*
- b. *The solution of 0.01% sodium azide can be included in the buffer for long-term preservation. Do not store clearing solution for long time.*
- c. *Pre-made SeeDB2 solutions are also commercialized from FUJIFILM Wako Pure Chemical.*

Solutions	Composition
SeeDB2G with saponin (clearing)	2% saponin in Omnipaque350
SeeDB2G (mounting)	Use Omnipaque350 directly Or 7,500 µl Tris-EDTA (pH 7.6) + 10 g Histodenz
SeeDB2S with saponin (clearing)	3,780 µl Tris-EDTA (pH 7.6) + 420 µl 20% saponin solution + 10 g Histodenz
SeeDB2S (mounting)	4,200 µl Tris-EDTA (pH 7.6) + 10 g Histodenz Add 4,200 µl Tris-EDTA to a 50 ml conical tube, and then add 10 g Histodenz. Use a rotator to fully dissolve the Histodenz in the conical tube

Acknowledgments

This protocol was adapted from our original publication of the protocol (Ke *et al.*, 2016). We thank J.R. Sanes for providing the Thy1-YFP-H mouse line, R. Sakaguchi for help with video, and M. Leiwe for proofreading. This work was supported by grants from the PRESTO program of the Japan Science and Technology Agency (JST), the Brain/MINDS project of the Japan Agency for Medical Research and Development (AMED), the Mitsubishi Foundation, the Strategic Programs for R&D (President's Discretionary Fund) of RIKEN, the JSPS KAKENHI (grant numbers 23680038, 15K14336, 16K14568, 16H06456, 17H06261), and RIKEN CDB intramural grant. M.-T.K. was supported by RIKEN Foreign Postdoctoral Researcher program. The imaging experiments were supported by the RIKEN Kobe Light Microscopy Facility. Animal experiments were supported by Laboratory for Animal Resources and Genetic Engineering (LARGE) at the RIKEN Center for Life Science Technologies.

Competing interests

M.-T.K. and T.I. have filed a patent application on SeeDB2, assigned to RIKEN.

References

1. Ke, M. T., Fujimoto, S. and Imai T. (2013). [SeeDB: a simple and morphology-preserving optical clearing agent for neuronal circuit reconstruction](#). *Nat Neurosci* 16(8): 1154-1161.
2. Ke, M. T., Fujimoto, S. and Imai T. (2014). [Optical clearing using SeeDB](#). *Bio-protocol* 4(3): e1042.
3. Ke, M. T., Nakai, Y., Fujimoto, S., Takayama, R., Yoshida, S., Kitajima, T. S., Sato, M. and Imai, T. (2016). [Super-resolution mapping of neuronal circuitry with an index-optimized clearing agent](#). *Cell Rep* 14(11): 2718-2732.
4. Richardson, D. S. and Lichtman, J. W. (2015). [Clarifying tissue clearing](#). *Cell* 162(2):246-257.
5. Richardson, D. S. and Lichtman, J. W. (2017). [SnapShot: tissue clearing](#). *Cell* 171(2): 496-496.e1.
6. Staudt, T., Lang, M. C., Medda, R., Engelhardt, J., Hell, S. W. (2007). [2,2'-thiodiethanol: a new water soluble mounting medium for high resolution optical microscopy](#). *Microsc Res Tech*. 70(1):1-9.



The banner features the Bio-protocol logo at the top left, followed by the tagline "Improve Research Reproducibility". Below this, a large heading reads "Free access to ~4000 high-quality protocols". A bulleted list highlights the following features:

- Contributed by 10,000+ scientists (including Nobel Laureates)
- Validated in a primary research paper
- >91% reproducibility (survey of 2165 Bio-protocol users)
- ~1000 videos of key procedural steps

A blue button at the bottom encourages users to "Sign up at: www.bio-protocol.org".

Estimation of the Readily Releasable Synaptic Vesicle Pool at the *Drosophila* Larval Neuromuscular Junction

Pragya Goel[#], Xiling Li[#] and Dion Dickman*

Department of Neurobiology, University of Southern California, Los Angeles, USA

*For correspondence: dickman@usc.edu

[#]Contributed equally to this work



[Abstract] Presynaptic boutons at nerve terminals are densely packed with synaptic vesicles, specialized organelles for rapid and regulated neurotransmitter secretion. Upon depolarization of the nerve terminal, synaptic vesicles fuse at specializations called active zones that are localized at discrete compartments in the plasma membrane to initiate synaptic transmission. A small proportion of synaptic vesicles are docked and primed for immediate fusion upon synaptic stimulation, which together comprise the readily releasable pool. The size of the readily releasable pool is an important property of synapses, which influences release probability and can dynamically change during various forms of plasticity. Here we describe a detailed protocol for estimating the readily releasable pool at a model glutamatergic synapse, the *Drosophila* neuromuscular junction. This synapse is experimentally robust and amenable to sophisticated genetic, imaging, electrophysiological, and pharmacological approaches. We detail the experimental design, electrophysiological recording procedure, and quantitative analysis necessary to determine the readily releasable pool size. This technique requires the use of a two-electrode voltage-clamp recording configuration in elevated external Ca^{2+} with high frequency stimulation. We have used this assay to measure the readily releasable pool size and reveal that a form of homeostatic plasticity modulates this pool with synapse-specific and compartmentalized precision. This powerful approach can be utilized to illuminate the dynamics of synaptic vesicle trafficking and plasticity and determine how synaptic function adapts and deteriorates during states of altered development, stress and neuromuscular disease.

Keywords: Readily releasable pool, Neuromuscular junction, Synaptic vesicle pool, Two-electrode voltage clamp, *Drosophila*

[Background] The small fraction of synaptic vesicles (SVs) docked at the plasma membrane and primed for immediate fusion upon synaptic stimulation are referred to as the readily releasable vesicle pool (RRP), a key biophysical parameter that is a major determinant of synaptic strength. A reliable estimate of RRP is crucial for understanding the unique release properties within and across distinct types of synapses (Stevens, 2003; Abbott and Regehr, 2004) and for distinguishing between different modes of short-term plasticity (Regehr, 2012). Estimation of the RRP has provided important insights into the dynamics of synaptic transmission and various forms of plasticity such as short-term depression (Hallermann *et al.*, 2010; Regehr, 2012). At the *Drosophila* neuromuscular junction (NMJ), a powerful model of homeostatic plasticity has been established at this model glutamatergic synapse (Frank, 2013;

Davis and Muller, 2015). An adaptive enhancement in presynaptic vesicle release is observed in response to reduced postsynaptic glutamate receptor functionality, a process referred to as Presynaptic Homeostatic Potentiation (PHP, Figure 1; Petersen *et al.*, 1997; Frank *et al.*, 2006; Davis and Muller, 2015). This increase in the size of the RRP is an important expression mechanism underlying PHP, and demonstrates that modulation of the RRP is a target of plasticity at synapses (Weyhersmuller *et al.*, 2011; Muller *et al.*, 2012; Chen *et al.*, 2017; Goel *et al.*, 2017; Kiragasi *et al.*, 2017; Goel and Dickman, 2018; Li *et al.*, 2018a and 2018b). In contrast, an inverse mode of homeostatic plasticity, referred to as Presynaptic Homeostatic Depression (Daniels *et al.*, 2004), reduces presynaptic neurotransmitter release without any modulation to the size of the RRP (Gavino *et al.*, 2015; Li *et al.*, 2018b). A decrease in the RRP is observed in mutants that diminish presynaptic calcium influx (Muller *et al.*, 2012; Muller *et al.*, 2015; Wang *et al.*, 2016). Alterations in other synaptic vesicle pools and recycling dynamics have been reported in mutations of synaptic genes in *Drosophila*, including *shibire* (*dynamin*), *endophilin*, *synaptjanin*, and *synaptotagmin* (Li and Schwarz, 1999; Delgado *et al.*, 2000; Verstreken *et al.*, 2002; Dickman *et al.*, 2005; Bacaj *et al.*, 2015). Thus, the RRP is an important parameter that establishes synaptic strength and can be selectively and dynamically modulated during plasticity.

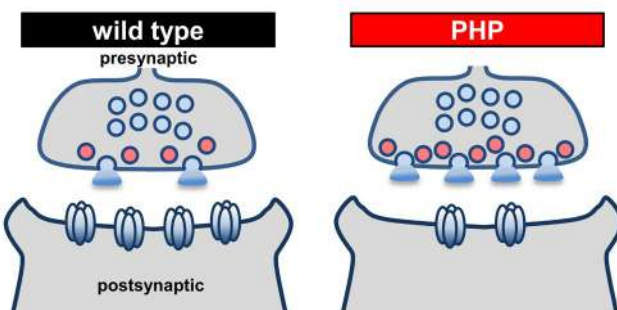


Figure 1. The RRP is enhanced during presynaptic homeostatic plasticity at the *Drosophila* NMJ. Schematic of the fly NMJ at baseline (wild type) and following the expression of presynaptic homeostatic potentiation (PHP). Note that in response to loss of postsynaptic glutamate receptors, presynaptic neurotransmitter release is enhanced through increased RRP size (red vesicles). RRP size is quantified by the method detailed in this protocol.

A variety of anatomical and physiological methods for determining the size of various synaptic vesicle pool have been utilized, all loosely described as the RRP (Neher, 2015; Kaeser and Regehr, 2017). Each of these approaches have certain strengths and weaknesses. Anatomical measurements of the number of docked vesicles, defined as synaptic vesicles in close proximity to the active zone, have been assessed using electron microscopy and suggested to participate in the RRP (Schikorski and Stevens, 2001; Rizzoli and Betz, 2004). Though straightforward to measure, the main weakness of this method is that not all docked vesicles are primed and may not even be releasable. Therefore, not all docked vesicles contribute to the RRP physiologically, while the RRP might be capable of recruiting undocked vesicles (Kaeser and Regehr, 2017). A second approach for determining RRP size utilizes

electrophysiology, where a hypertonic sucrose solution is applied near presynaptic terminals, inducing synaptic vesicle fusion. In this approach, osmotic shock is assumed to drive membrane fusion of vesicles that are located close to plasma membranes, but this measure assumes that osmotic shock and action potential-dependent calcium influx target the same vesicle pool. A third quantitative methodological approach is to induce a large and sustained elevation of presynaptic calcium by either chemical uncaging or through depolarization of the presynaptic terminal (Schneggenburger *et al.*, 2002; Rizzoli and Betz, 2005). Finally, a fourth commonly used approach to estimate RRP size is to use a high-frequency train of action potentials to stimulate the synapse, which results in immediate fusion of readily releasable vesicles followed by rapid replenishment by endocytosis. It is assumed that the depression of the excitatory postsynaptic current (EPSC) amplitude is primarily caused by the depletion of the readily releasable quanta, after which a steady-state is established in which exocytosis is balanced by endocytosis. Thus, the RRP size can be estimated by calculating the cumulative EPSC amplitude (Figure 5; Schneggenburger *et al.*, 1999). At the *Drosophila* NMJ, RRP size has been assayed either by using a stimulus train or by EPSC amplitude fluctuation analysis during single stimuli (Weyhersmuller *et al.*, 2011; Muller *et al.*, 2012; Penney *et al.*, 2016; Wentzel *et al.*, 2018). In this analysis, it is assumed that no contributions from the synaptic vesicle reserve pool (RP) contribute to the release dynamics during the initial rapid stimulation, and that the RP therefore is mobilized only after RRP depletion following strong stimulation intensity (Schneggenburger *et al.*, 1999; Delgado *et al.*, 2000; Denker and Rizzoli, 2010; Kaeser and Regehr, 2017). Indeed, the definition and make up of the RRP, RP and other vesicle pools (“exo-endo recycling”, “docked and primed”, *etc.*) vary depending on the synapse type, experimental approach, and experimental conditions used, leading to difficulty in making direct comparisons between the various vesicle pools (Rizzoli and Betz, 2005; Alabi and Tsein, 2012; Kaeser and Regehr, 2017). It is therefore important to be aware of the strengths and limitations in analyzing and interpreting differences between the various vesicle pools measured.

Here, we describe a detailed protocol to estimate the physiologically relevant RRP at the *Drosophila* NMJ. This method is based on TEVC recordings of a nerve-evoked train of EPSCs from muscle fibers of third-instar larvae. In particular, NMJs are stimulated at 60 Hz frequencies in 3 mM external Ca^{2+} saline, followed by back-extrapolation of the cumulative EPSC to obtain an estimate of the RRP size. We have recently used this method to demonstrate that PHP signaling is compartmentalized, where RRP size can be specifically increased at only a subset of synapses within a single motor neuron (Li *et al.*, 2018a). In addition, we successfully applied this technique to confirm that although RRP size is increased during PHP, RRP is unchanged in an inverse form of plasticity, PHD (Gavino *et al.*, 2015; Li *et al.*, 2018b). Thus, this method is a powerful approach that can be easily adapted to investigate SV dynamics in baseline synaptic transmission and plasticity, and to study how these properties may be altered in neuromuscular and motor neuron disease states using the powerful *Drosophila* NMJ as a model.

Materials and Reagents

1. Suction (World Precision Instruments, catalog number: TW120-4) and recording (World Precision Instruments, catalog number: TW120F-4) micropipettes
2. 60 mm Petri dish
3. Glue gun (Tacklife, catalog number: GGO20AC)
4. Silver wire (Molecular Devices, Axon Accessories, catalog number: 1-HLA-005)
5. 10 ml syringe (Thermo Fisher Scientific, Thermo Scientific™, catalog number: S7510-10) to fill micro-electrodes and apply negative pressure for suction electrode
6. MicroFil (World Precision Instruments, catalog number: MF28G67-5) to fill micro-electrodes
7. *Drosophila* third-instar larvae
8. KCl (Millipore Sigma, catalog number: P9333)
9. NaCl (Millipore Sigma, catalog number: S7653)
10. MgCl₂·6H₂O (Millipore Sigma, catalog number: M2670)
11. NaHCO₃ (Millipore Sigma, catalog number: M2670)
12. Sucrose (Fisher Scientific, catalog number: S233-500)
13. D-(+)- Trehalose dihydrate (Millipore Sigma, catalog number: T9531)
14. HEPES (Millipore Sigma, catalog number: H3375)
15. CaCl₂·2H₂O (Millipore Sigma, catalog number: C5080)
16. Regular liquid bleach (such as CloRox)
17. Modified hemolymph-like solution (HL-3) (see Recipes)
18. Recording electrode solution (see Recipes)

Equipment

1. PC Computer with a minimum requirement of 1.2 GB RAM, 2 GHz processor, Windows 7, 2 USB ports, 50 G disk space
2. Upright microscope (such as Olympus, model: BX51W1) with 4x air and 40x water dipping objectives, air table (TMC)
3. Micro-electrode puller (Sutter Instrument, model: P-97) with box platinum filament
Puller settings for Recording Electrode: Heat = ramp + 10; Pull = 110; VEL. = 80; Time = 250; Pressure = 500
Setting for Suction Electrode: Heat = Ramp - 15; Pull = 10; VEL. = 10; Time = 200; Pressure = 500
4. ISO-Flex stimulator isolator unit (A.M.P.I.)
5. Micromanipulators
We use Siskiyou, including one manual manipulator for the suction electrode (Siskiyou, model: MX160L) and two motorized micromanipulators for TEVC (current injection and voltage;

- Siskiyou, models: MX7600 and MC1000C controller)
6. Electrode headstages: Axon CNS; 0.1x and 10x (HS-9Ax0.1, HS-13Sx10)
 7. Amplifier: Axoclamp 900A (Axon CNS, model: Axoclamp™ 900A)
 8. Digidata board: Digidata 1440A (Axon CNS)
 9. Dissection tools and equipment:
 - a. 7x-45x Stereo microscope for dissection (AmScope, models: SM 1-B), LED light source (SciOptic, 3W*2PCs)
 - b. *Drosophila* larval dissection and recording chamber: 3" x 4" glass cover slip, magnetic tape, magnetic pins (Sullivan *et al.*, 2000)
 - c. Scissors (Fine Science Tools, catalog number: 15000-08) and Forceps (Fine Science Tools, catalog number: 11295-20)
 - d. Razor (Darice, catalog number: B002C12EHM)
 10. Microforge (Narishige, model: MF-830) for polishing suction electrode tip
 11. Ice and ice bucket for maintaining ice cold modified HL-3 saline

Software

1. Acquisition
 - a. Clampex 10.7 software (Molecular Devices, Sunnyvale, CA, USA, licenses needed)
 - b. Axoclamp (Axon CNS, licenses needed)
2. Analysis
 - a. Clampfit (Molecular Devices, Sunnyvale, CA, USA: <http://moleculardevices.app.box.com>)
 - b. MiniAnalysis (Synaptosoft: www.synaptosoft.com/MiniAnalysis/)
 - c. SigmaPlot (licenses needed)
 - d. Microsoft Excel (licenses needed)
 - e. GraphPad Prism (licenses needed)

Note: MATLAB (MathWorks, USA) and other software can be used instead of 2c, 2d and 2e.

Procedure

A. *Drosophila* larval dissection and preparation

1. The *Drosophila* third-instar larval dissection has been described and video recorded (Brent, 2009), and the basic background for TEVC electrophysiological preparation, configuration, and recording has also been outlined (Kyriacou, 2010). Suction pipettes should be pulled with an opening of ~5 µm, while the recording electrodes should be pulled with resistances of ~15 MΩ (Figure 2). Polish the tip of the suction pipette using the microforge listed in the equipment, and fill both recording micropipettes with 3 mM KCl and the suction pipette with 3 mM Ca²⁺ modified HL-3 saline with microfill and syringe (Stewart *et al.*, 1994; Dickman *et al.*, 2005). Additional details of electrode preparation have been previously detailed in Zhang and Stewart (2010b).

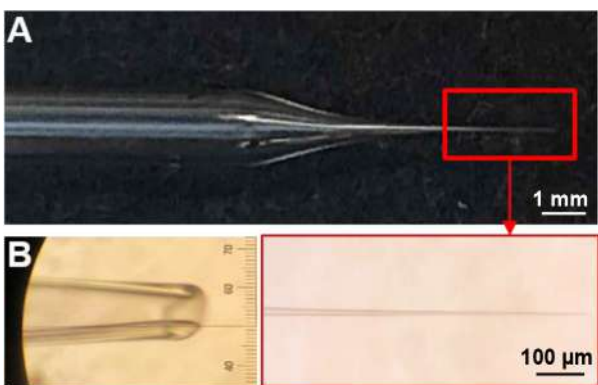


Figure 2. Examples of recording and suction electrodes. A. Representative recording electrode tip pulled by using the puller program described in Equipment. B. Representative suction electrode tip pulled by the program detailed in Equipment and polished to a diameter of $\sim 5 \mu\text{m}$.

2. A magnetic recording chamber (shown in Figures 3A and 3B; detailed in Ramachandran and Budnik, 2010) is used. The magnetic tape is necessary to attract the pins to the chamber and to hold down the filleted larvae while performing electrophysiology. While any glass can be used to form the foundation, a 3"x 4" chamber is a standard size that can be purchased cheaply and thus is what most experimentalist will prefer to use. A simple razor is used to manually cut out the diamond shape area of the magnetic tape in the middle of the chamber, and a simple glue gun is used to seal the edges between the glass and the magnetic tape around the diamond cut out. This glue seal is used to hold the saline around the dissected larvae while performing electrophysiology. Alternatively, a 60 mm dish lined with Sylgard and sharp pins can be used to impale the filleted larvae for electrophysiological preparation (Singh and Wu, 1999; Budnik and Ruiz-Canada, 2006; Imlach and McCabe, 2009; Zhang and Stewart, 2010a and 2010c; Itoh *et al.*, 2016; Bykhovskaia and Vasin, 2017). However, we recommend and prefer the magnetic chamber because of the gentler dissection, the lower saline volume necessary and the superior microelectrode accessibility.
3. Dissect third-instar larvae in ice-cold Ca^{2+} free modified HL-3 saline (to prevent muscle movement during dissection). The recipe of the Ca^{2+} free modified HL-3 saline is the same as the modified HL-3 without CaCl_2 . Loosely pin the larvae (Figures 3A and 3B), remove the guts, trachea and ventral nerve cord from the larval body walls. Cut all motor nerves that originated from the ventral nerve cord (Figure 3C) and perfuse the preparation several times with fresh HL-3 saline via pipetting. Ensure that the motor nerves are not cut too short, as this may result in difficulty with suctioning and stimulating the nerve. Finally, fill the chamber with 3 mM Ca^{2+} modified HL-3 saline.
4. Orient the NMJ preparation on the microscope stage for optimal electrode positioning (Figures 3C and 4A).

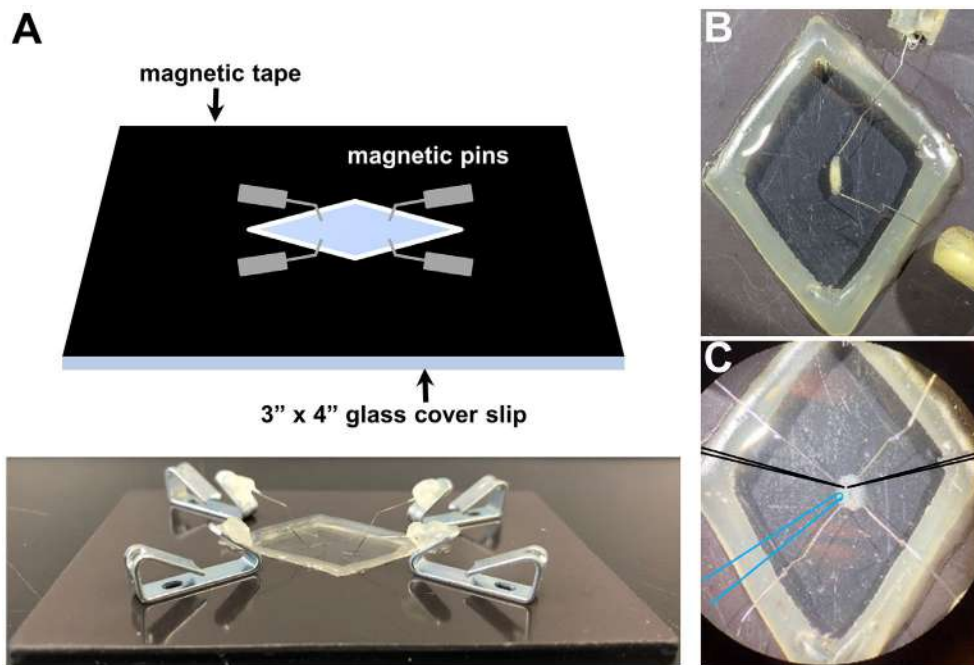


Figure 3. *Drosophila* larvae before and after dissection in the recording chamber. A. Representative schematic (top) and picture (bottom) of the recording chamber used for larval dissection and electrophysiology with magnetic pins. Representative images of a third-instar larva before (B) and after dissection (C) using this system. Note that optimal positioning of recording electrodes (schematized in black) and the stimulation pipette (schematized in blue).

B. Electrophysiological recordings

1. Place the larval preparation and the tips of the three electrodes in the middle field of view using the 4x objective, and lower the electrodes closer to the plane of the preparation. We typically record from muscle 6 at abdominal segments A2 or A3. Switch to the 40x objective, move the target muscle close to the electrodes, and lower the suction electrode near the nerve bundle. Provide a small negative pressure through the syringe to withdraw the nerve into the pipette. Use suction to establish a seal between the suction electrode and the motor nerve that innervates the muscle segment (Figure 4B).

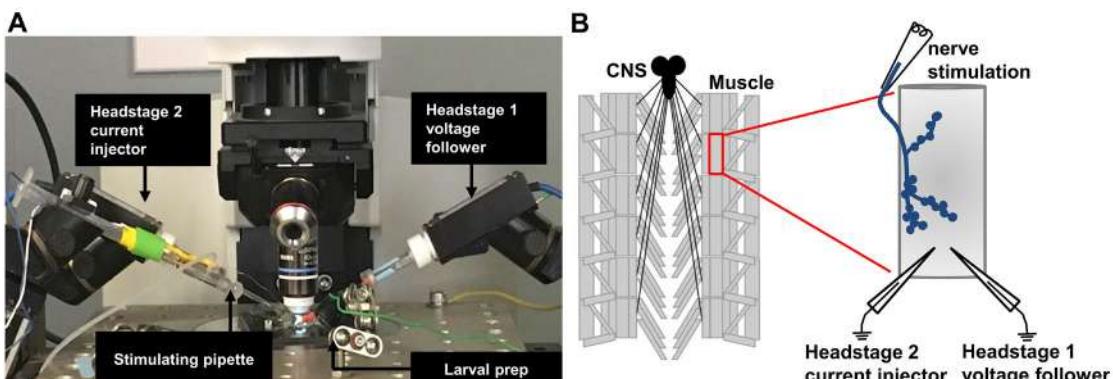


Figure 4. Schematic illustrating the TEVC recording configuration of the third-instar larval NMJ. A. Picture of the electrophysiology setup, with electrodes placed to stimulate and record from the larval preparation. B. Schematic of a dissected third-instar larva with a detailed view of the muscle 6 NMJ after all electrodes are properly positioned. A stimulating electrode is used to suck the severed motor nerve innervating the muscle segment to be recorded from (top) and the recording electrodes are used for current injection or voltage following (bottom). The presynaptic nerve terminal (blue) is shown in a classical “beads on a string” bouton structure.

2. Move the recording electrodes right above muscle 6, which is innervated by the motor nerve isolated in the stimulation electrode (Figures 3C and 4B). Set electrode baseline potentials to 0 by resetting the bridge balance and pipette offset. Chloride the silver wire in the recording pipette if the pipette offset value is higher than 100 mV.
3. Digitize electrophysiological sweeps at 10 kHz by setting the sampling rate in the Clampex software, and filter the lowpass signal at 1 kHz.
4. Impale the muscle 6 fiber with the voltage follower electrode (HS-9Ax0.1) and record the resting potential (V_{rest}). Inject a 500 msec pulse of -1 nA current to measure the muscle input resistance (R_{in}) by Ohm's law: $R_{in} = \frac{V_{rest}}{-1 \text{ nA}}$. Reject recordings with V_{rest} more depolarized than -60 mV or more hyperpolarized than -85 mV, or if the R_{in} is less than 5 MΩ.
5. Impale the same muscle fiber with the current injection electrode (HS-13Sx10) and wait for 15-20 s until the voltage potential readings from both electrodes become stable (both more hyperpolarized than -55 mV). Switch to TEVC mode, clamp the muscle membrane potential at -70 mV, and monitor the leak current. Reject recordings with leak current values higher than 10 nA. Miniature excitatory postsynaptic currents (mEPSCs) are recorded in the absence of any stimulation for one minute with a typical gain value of 80. Stimulate motor axons to elicit excitatory postsynaptic currents (EPSCs) using an ISO-Flex stimulus isolator (A.M.P.I.) to modulate the amplitude of stimulatory currents. Adjust intensity for each recording to consistently elicit responses from both neurons innervating the muscle segment, but avoid overstimulation, in which case responses with multiple peaks can be initiated.
6. Switch to the protocol necessary to measure the RRP using the same optimal stimulation

intensity established in the previous step. The RRP protocol stimulates evoked responses and records EPSCs using a 60 Hz train of 30 stimuli in 3 mM extracellular Ca^{2+} HL-3 (Figure 5). The train sweeps were repeated for five times in each recording. The train of stimulus at a high Ca^{2+} concentration leads to a progressive depression of EPSC amplitude during the stimulation paradigm due to a depletion of readily releasable vesicles (Figure 5B).

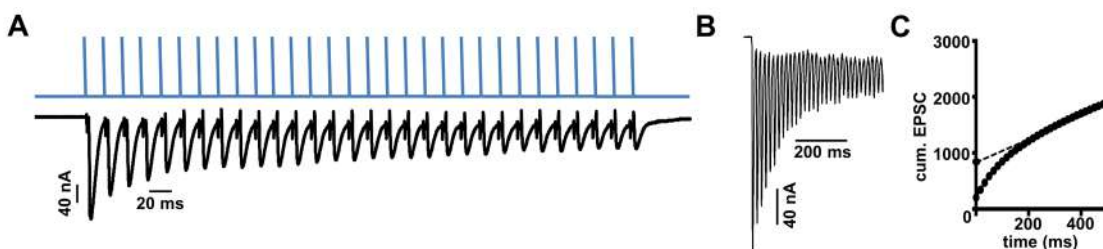


Figure 5. Stimulation and analysis paradigm for estimating the RRP. A. Representative stimulation paradigm (above) and electrophysiological responses (below) of the 60 Hz/30 stimuli protocol necessary to determine the RRP. B. Representative EPSC recording during a 60 Hz stimulus train at a typical NMJ. C. Average cumulative EPSC amplitude plotted as a function of time. A line fit to the 18-30th stimuli was back extrapolated to time 0; this y-intercept value is divided by the mEPSC value to determine the size of the RRP.

Data analysis

1. Amplify and digitize the recorded signal using an Axoclamp 900A amplifier in combination with the Digidata 1440A acquisition system and pClamp 10.5 software. Appropriate software and hardware from other vendors can also be used.
2. Analyze the amplitude of mEPSC events using Mini Analysis (Synaptosoft, Figure 6; additional details of using this program can be found here: http://www.synaptosoft.com/MiniAnalysis/Tutorial/index_files/frame.htm). Briefly, open the “.abf” file in Mini Analysis and increase Gain to 200 (Figure 6) to clearly visualize miniature EPSC events. Use the “Analysis” setting shown in Figure 6 to accurately capture and quantify mini events. Export the results of ~100 events to Microsoft Excel and average the mEPSC amplitude of at least 100 events from each recording to get the average mEPSC amplitude for that particular muscle cell.
3. Use SigmaPlot and Clampfit to analyze the amplitude of each EPSC in the stimulus train.
 - a. Transfer the sweeps of train stimulation from each cell to data points in Clampfit.
 - b. Calculate EPSC amplitudes by taking the difference between peak and baseline before stimulus onset of a given EPSC manually (using Mini-Analysis) or using an optimized program (user defined code) in SigmaPlot or MATLAB. Such a custom-written script can be provided upon request.
 - c. Obtain the average amplitude of the 30 EPSCs from five sweeps using SigmaPlot. Then

tabulate 19th-30th twelve averaged EPSC amplitudes paired with the corresponding time point onto a new result sheet in Clampfit.

4. We are estimating the RRP size by using the cumulative EPSC amplitude method as first described by Schneggenburger *et al.*, 1999. This method was performed at the Calyx of Held in the mammalian central nervous system. Briefly, a train of high frequency stimulation in saline containing elevated calcium concentration introduces a fast depression in synaptic responses, indicative of RRP depletion. A relatively steady state phase follows this initial rapid depression, where endocytosis and exocytosis rates are assumed to be balanced due to vesicle recycling and the contribution of vesicles mobilized from other pools. This has been adapted and applied to the *Drosophila* NMJ (Hallermann *et al.*, 2010; Weyhersmuller *et al.*, 2011; Muller *et al.*, 2012; Davis and Muller, 2015; Muller *et al.*, 2015; Chen *et al.*, 2017; Kiragasi *et al.*, 2017; Li *et al.*, 2018a and 2018b).
 - a. Calculate the cumulative EPSC from a line fit to the linear phase (stimuli #18-30) of the EPSC data back-extrapolated to time 0 (Figure 5).
 - b. Estimate RRP size by normalizing the ratio of the cumulative EPSC value at time 0 and the average mEPSC amplitude in Microsoft Excel. Finally, copy the mEPSC, cumulative EPSC and RRP size values to GraphPad Prism and perform appropriate statistical analyses to assess significance (Li *et al.*, 2018a and 2018b; Materials and Methods). Generally, compare multiple data sets with a one-way ANOVA followed by a Tukey's multiple comparison test. A good illustration of this analysis can be found in Figures 5B and 5C of Li *et al.* (2018a). Optimal recordings of 6-10 NMJs from at least three different larvae of the same genotype are typically used for final analysis.

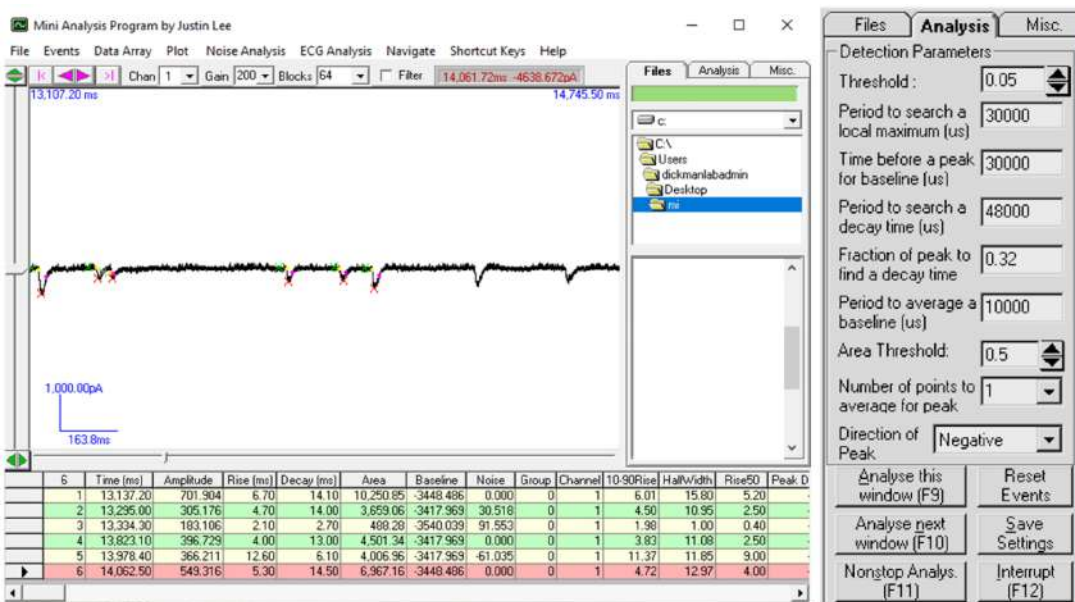


Figure 6. Data analysis to determine mEPSC amplitude necessary to estimate RRP size.
Screenshot of the Mini-Analysis Program showing a representative analysis of mEPSC

amplitude from acquired electrophysiological traces. Shown at right are the Mini Analysis settings used.

Notes

A cautionary point is in order regarding the acquisition of mEPSCs and EPSCs. It can be difficult to accurately record mEPSCs and EPSCs from the same muscle cell. This is due to the necessity for low noise to resolve small mEPSC events in the TEVC configuration, which requires two 0.1x headstages. While this is optimal for resolving small mEPSC events, these low gain headstages are unable to voltage clamp excitability of the muscle during the large currents driven by evoked stimulation at elevated extracellular Ca^{2+} recording conditions (3 mM). In these conditions, we use a 0.1x headstage for voltage follower and a 10x headstage for current injection to provide sufficient current to clamp the muscle. The installment noise with the 10x current injection headstage is suboptimal for resolving mEPSC signals, particularly the small miniature events induced by genetic or pharmacological perturbations to the postsynaptic glutamate receptors. Hence, the average mEPSC amplitudes are typically obtained from the same genotype but averaged between different larvae and NMJs.

Recipes

1. Modified hemolymph-like solution (HL-3); pH 7.2

Chemical	Final concentration (mM)
NaCl	70
KCl	5
MgCl ₂	10
NaHCO ₃	10
Sucrose	115
Trehalose	5
HEPES	5
CaCl ₂	3

Note: Prepared solution without calcium can be stored at -20 °C and thawed before use. CaCl₂ is added to the saline right before beginning the experiments. The dissolved HL-3 containing the desired Ca^{2+} concentration can be stored at 4 °C and reused for up to 3-4 days.

2. Recording electrode solution

Chemical	Final concentration
KCl	3 M

Acknowledgments

Work in the Dickman lab is funded by a grant from the National Institutes of Health (NS091546). We thank Martin Müller (University of Zürich) for insightful discussions and technical insights into TEVC recording and RRP analysis.

Competing interests

The authors declare no conflicts or other competing interests.

References

1. Abott, L. F. and Regehr, W. G. (2004). [Synaptic computation](#). *Nature* 431(7010): 796-803.
2. Alabi, A. A. and Tsein, R. W. (2012). [Synaptic vesicle pools and dynamics](#). *Cold Spring Harb Perspect Biol* 4: a013680.
3. Bacaj, T., Wu, D., Burre, J., Malenka, R. C., Liu, X. and Sudhof, T. C. P. B. (2015). [Synaptotagmin-1 and -7 are redundantly essential for maintaining the capacity of the readily-releasable pool of synaptic vesicles](#). *PLoS Biol* 13: e1002267.
4. Brent, J. R., Werner, K. M. and McCabe, B. D. (2009). [Drosophila larval NMJ dissection](#). *J Vis Exp* 24(e1107).
5. Budnik, V. and Ruiz-Canada, C. (2006). [The fly neuromuscular junction: structure and function](#). 75.
6. Bykhoverkaia, M. and Vasin, A. (2017). [Electrophysiological analysis of synaptic transmission in Drosophila](#). *Wiley Interdiscip Rev Dev Biol* 6(5).
7. Chen, X., Ma, W., Zhang, S., Paluch, J., Guo, W. and Dickman, D. K. (2017). [The BLOC-1 subunit pallidin facilitates activity-dependent synaptic vesicle recycling](#). *eNeuro* 4(1): 1-18.
8. Daniels, R. W., Collins, C. A., Gelfand, M. V., Dant, J., Brooks, E. S., Krantz, D. E. and DiAntonio, A. (2004). [Increased expression of the Drosophila vesicular glutamate transporter leads to excess glutamate release and a compensatory decrease in quantal content](#). *J Neurosci* 24(46): 10466-10474.
9. Davis, G. W. and Muller, M. (2015). [Homeostatic control of presynaptic neurotransmitter release](#). *Ann Rev Physiol* 77: 251-270.
10. Delgado, R., Maureira, C., Oliva, C., Kidokoro, Y. and Labarca, P. (2000). [Size of vesicle pools, rates of mobilization, and recycling at neuromuscular synapses of a Drosophila mutant, shibire](#). *Neuron* 28(3): 941-953.
11. Denker, A. and Rizzoli, S. O. (2010). [Synaptic vesicle pools: an update](#). *Front Synaptic Neurosci* 2: 135.

12. Dickman, D. K., Horne, J. A., Meinertzhagen, I. A. and Schwarz, T. L. (2005). [A slowed classical pathway rather than kiss-and-run mediates endocytosis at synapses lacking synaptojanin and endophilin.](#) *Cell* 123(3): 521-533.
13. Frank, C. A. (2013). [Homeostatic plasticity at the *Drosophila* neuromuscular junction.](#) *Neuropharmacology* 78: 63-74.
14. Frank, C. A., Kennedy, M. J., Goold, C. P., Marek, K. W. and Davis, G. W. (2006). [Mechanisms underlying the rapid induction and sustained expression of synaptic homeostasis.](#) *Neuron* 52(4): 663-677.
15. Gavino, M. A., Ford, K. J., Archila, S. and Davis, G. W. (2015). [Homeostatic synaptic depression is achieved through a regulated decrease in presynaptic calcium channel abundance.](#) *eLife* 4: e05473.
16. Goel, P. and Dickman, D. (2018). [Distinct homeostatic modulations stabilize reduced postsynaptic receptivity in response to presynaptic DLK signaling.](#) *Nat Commun* 9(1): 1856.
17. Goel, P., Li, X. and Dickman, D. (2017). [Disparate postsynaptic induction mechanisms ultimately converge to drive the retrograde enhancement of presynaptic efficacy.](#) *Cell Rep* 21(9): 2339-2347.
18. Hallermann, S., Heckmann, M. and Kittel, R. J. (2010). [Mechanisms of short-term plasticity at neuromuscular active zones of *Drosophila*.](#) *HFSP Journal* 4: 72-84.
19. Imlach, W. and McCabe, B. D. (2009). [Electrophysiological methods for recording synaptic potentials from the NMJ of *Drosophila* larvae.](#) *J Vis Exp* 24: e1109.
20. Itoh, K., Komatsu, A. and Nishihara, S. (2016). [Electrophysiological recording in the *Drosophila* larval muscle.](#)
21. Kaeser, P. S. and Regehr, W. G. (2017). [The readily releasable pool of synaptic vesicles.](#) *Curr Opin Neurobiol* 43: 63-70.
22. Kiragasi, B., Wondolowski, J., Li, Y. and Dickman, D. K. (2017). [A presynaptic glutamate receptor subunit confers robustness to neurotransmission and homeostatic potentiation.](#) *Cell Rep* 19(13): 2694-2706.
23. Kyriacou, C. (2010). [Drosophila neurobiology: a laboratory manual.](#) Cold Spring Harbor Laboratory Press.
24. Li, J. and Schwarz, T. L. (1999). [Genetic evidence for an equilibrium between docked and undocked vesicles.](#) *Philos Trans R Soc Lond B Biol Sci* 354(1381): 299-306.
25. Li, X., Goel, P., Chen, C., Angajala, V., Chen, X. and Dickman, D. (2018a). [Synapse-specific and compartmentalized expression of presynaptic homeostatic potentiation.](#) *eLife* 7: e34338.
26. Li, X., Goel, P., Wondolowski, J., Paluch, J. and Dickman, D. (2018b). [A glutamate homeostat controls the presynaptic inhibition of neurotransmitter release.](#) *Cell Rep* 23(6): 1716-1727.
27. Muller, M., Genc, O. and Davis, G. W. (2015). [RIM-binding protein links synaptic homeostasis to the stabilization and replenishment of high release probability vesicles.](#) *Neuron* 85(5): 1056-1069.

28. Muller, M., Liu, K. S., Sigrist, S. J. and Davis, G. W. (2012). [RIM controls homeostatic plasticity through modulation of the readily-releasable vesicle pool.](#) *J Neurosci* 32(47): 16574-16585.
29. Neher, E. (2015). [Merits and limitations of vesicle pool models in view of heterogeneous populations of synaptic vesicles.](#) *Neuron* 87: 1131-1142.
30. Penney, J., Tsurudome, K., Liao, E. H., Kauwe, G., Gray, L., Yanagiya, A., M, R. C., Sonenberg, N. and Haghghi, A. P. (2016). [LRRK2 regulates retrograde synaptic compensation at the Drosophila neuromuscular junction.](#) *Nat Commun* 7: 12188.
31. Petersen, S. A., Fetter, R. D., Noordermeer, J. N., Goodman, C. S. and DiAntonio, A. (1997). [Genetic analysis of glutamate receptors in Drosophila reveals a retrograde signal regulating presynaptic transmitter release.](#) *Neuron* 19(6): 1237-1248.
32. Ramachandran, P. and Budnik, V. (2010). [Dissection of Drosophila larval body-wall muscles.](#) *Cold Spring Harb Protoc* 2010(8): pdb.prot5469.
33. Regehr, W. G. (2012). [Short-term presynaptic plasticity.](#) *Cold Spring Harb Perspect Biol* 4(7): a005702.
34. Rizzoli, S. O. and Betz, W. J. (2004). [The structural organization of the readily releasable pool of synaptic vesicles.](#) *Science* 303: 2037-2039.
35. Rizzoli, S. O. and Betz, W. J. (2005). [Synaptic vesicle pools.](#) *Nat Rev Neurosci* 6(1): 57-69.
36. Schikorski, T. and Stevens, C. F. (2001). [Morphological correlates of functionally defined synaptic vesicle populations.](#) *Nat Neurosci* 4: 391-395.
37. Schneggenburger, R., Meyer, A. C. and Neher, E. (1999). [Released fraction and total size of a pool of immediately available transmitter quanta at a calyx synapse.](#) *Neuron* 23: 399-409.
38. Schneggenburger, R., Sakaba, T. and Neher, E. (2002). [Vesicle pools and short-term synaptic depression: lessons from a large synapse.](#) *Trends Neurosci* 25: 206-212.
39. Singh, S. and Wu, C.-F. (1999). [Ionic currents in the larval muscles of Drosophila.](#) *Neuromuscular Junctions in Drosophila. Int Rev Neurobiol* 43: 191-220.
40. Stevens, C. F. (2003). [Neurotransmitter release at central synapses.](#) *Neuron* 40: 381-388.
41. Stewart, B. A., Atwood, H. L., Renger, J. J., Wang, J. and Wu, C. F. (1994). [Improved stability of Drosophila larval neuromuscular preparations in haemolymph-like physiological solutions.](#) *J Comp Physiol A* 175(2): 179-191.
42. Sullivan, W., Ashburner, M. and Hawley, R. S. E. (2000). [Drosophila protocols.](#) *Cold Spring Harbor Laboratory Press.*
43. Verstreken, P., Kjaerulff, O., Lloyd, T. E., Atkinson, R., Zhou, Y., Meinertzhagen, I. A. and Bellen, H. J. (2002). [Endophilin mutations block clathrin-mediated endocytosis but not neurotransmitter release.](#) *Cell* 109(1): 101-112.
44. Wang, T., Jones, R. T., Whippen, J. M. and Davis, G. W. (2016). [α2δ-3 is required for rapid transsynaptic homeostatic signaling.](#) *Cell Rep* 16(11): 2875-2888.
45. Wentzel, C., Delvendahl, I., Sydlik, S., Georgiev, O. and Muller, M. (2018). [Dysbindin links presynaptic proteasome function to homeostatic recruitment of low release probability vesicles.](#) *Nat Commun* 9(1): 267.

46. Weyhersmuller, A., Hallermann, S., Wagner, N. and Eilers, J. (2011). [Rapid active zone remodeling during synaptic plasticity](#). *J Neurosci* 31(16): 6041-6052.
47. Zhang, B. and Stewart, B. (2010a). [Electrophysiological recording from Drosophila larval body-wall muscles](#). *Cold Spring Harb Protoc* (9).
48. Zhang, B. and Stewart, B. (2010b). [Fabrication of microelectrodes, suction electrodes, and focal electrodes](#). *Cold Spring Harb Protoc* (9).
49. Zhang, B. and Stewart, B. (2010c). [Synaptic physiology at the Drosophila neuromuscular junction \(chapter 12\)](#). *Drosophila Neurobiology: A Laboratory Manual*.

Analysis of the Mitochondrial Membrane Potential Using the Cationic JC-1 Dye as a Sensitive Fluorescent Probe

Farzane Sivandzade¹, Aditya Bhalerao¹ and Luca Cucullo^{1, 2, *}

¹Department of Pharmaceutical Sciences, Texas Tech University Health Sciences Center, Amarillo, TX 79106, USA; ²Center for Blood-Brain Barrier Research, Texas Tech University Health Sciences Center, Amarillo, TX 79106, USA

*For correspondence: luca.cucullo@ttuhsc.edu



[Abstract] In recent years, fluorescent dyes have been frequently used for monitoring mitochondrial membrane potential to evaluate mitochondrial viability and function. However, the reproducibility of the results across laboratories strongly depends upon following well validated and reliable protocols along with the appropriate controls. Herein, we provide a practical user guide for monitoring mitochondrial membrane potential in whole cells using a fluorescent cationic probe. The data analysis of mitochondrial membrane potential we provide is one associated with the impact of xenobiotics such as tobacco smoking on blood-brain barrier endothelial cells including both mouse primary (mBMEC) and a mouse-based endothelial cell line (bEnd3) in a side by side comparison.

Keywords: Mitochondrial membrane potential, JC-1 dye, Fluorescent probe, Cationic, Flow cytometry

[Background] Apoptosis is a cellular process which involves genetical events causing the death of a cell. Several major events occur in mitochondria, of which, the most significant is the loss of mitochondrial transmembrane potential ($\Delta\Psi_M$) (Green and Reed, 1998). Throughout the life of a cell, the mitochondria uses oxidizable substrates to produce an electrochemical proton gradient across the mitochondrial membrane which is used to produce ATP. The direction of the mitochondrial membrane potential (with the interior of the organelle being electronegative) is such to produce inward transport of cations and outward transport of anions, thus promoting accumulation of cations in the mitochondria (Zorova *et al.*, 2018). This electrochemical gradient drives the synthesis of ATP. However, during apoptosis, $\Delta\Psi_M$ decreases as the process is associated with the opening of the mitochondrial permeability pores and loss of the electrochemical gradient. Thus, $\Delta\Psi_M$ is an essential parameter of the mitochondrial function that can be used as an indicator of cell health since mitochondria are inherently involved in the apoptotic process of cells.

In recent years, $\Delta\Psi_M$ has been studied using several fluorescent cationic dyes including rhodamine-123 and DiOC₆ as common monitoring tools (Cossarizza and Salvioli, 1998). The technique involving using 5,5,6,6'-tetrachloro-1,1',3,3' tetraethylbenzimi-dazoylcarbocyanine iodide (JC-1) dye has been developed to detect $\Delta\Psi_M$ in healthy and apoptotic cells across multiple cell types, such as neurons, myocytes, endothelial cells *etc.* JC-1 can be used to assess the $\Delta\Psi_M$ both in intact isolated mitochondria and tissues. In fact, the JC-1 dye is a lipophilic, cationic dye (naturally exhibiting green fluorescence) which is able to enter into the mitochondria where it accumulates and (in a

concentration-dependent manner) starts forming reversible complexes called J aggregates. Differently, from JC-1 molecules, these J aggregates exhibit excitation and emission in the red spectrum (maximum at ~590 nm) instead of green. Thus, in healthy cells with a normal $\Delta\Psi_M$, the JC-1 dye enters and accumulates in the energized and negatively charged mitochondria and spontaneously forms red fluorescent J-aggregates. By contrast, in unhealthy or apoptotic cells the JC-1 dye also enters the mitochondria but to a lesser degree since the inside of the mitochondria is less negative because of increased membrane permeability and consequent loss of electrochemical potential. Under this condition, JC-1 does not reach a sufficient concentration to trigger the formation of J aggregates thus retaining its original green fluorescence.

Based on these premises, the red/green fluorescence ratio of the dye in the mitochondria can be considered as a direct assessment of the state of the mitochondria polarization whereas the higher is the $\Delta\Psi_M$, the more elevated is the red shift of the dye (more J aggregates are formed). Vice-versa; the lower is the $\Delta\Psi_M$ of the mitochondria and the lower is the red to green ratio of the fluorescent marker (few J aggregates are formed). Therefore, mitochondrial depolarization is indicated by a reduction in the red to green fluorescence intensity ratio.

The aggregate green monomeric form has absorption/emission of 510/527 nm, and the aggregate red form has absorption/emission 585/590 nm (Smiley *et al.*, 1991). The red to green fluorescence intensity ratio is only dependent on the membrane potential and no other factors such as shape, mitochondrial size, and density, which may influence single-component fluorescence signals. It is noteworthy JC-1 dye can be used both as qualitative (considering the shift from green to red fluorescence emission) and quantitative (considering only the pure fluorescence intensity) measure of mitochondrial membrane potential (Cossarizza and Salvioli, 1998).

Fluorescent dye accumulation in mitochondria can be optically detected by flow cytometry, fluorescent microscopy, confocal microscopy, and through the use of a fluorescence plate reader (Perry *et al.*, 2011). Indeed, the use of fluorescence ratio detection provides researchers with a means to compare measurements of membrane potential while also assessing the percentage of mitochondrial depolarization occurring in a pathological condition (e.g., cellular stress, apoptosis, etc.).

Thus, the main objective of this paper is to provide a practical step by step user protocol to assess and monitor mitochondrial membrane potential in whole cells using the JC-1 fluorescent cationic probe. As a positive control, carbonyl cyanide *m*-chlorophenyl hydrazone (CCCP) which is a chemical inhibitor of oxidative phosphorylation, affecting the protein synthesis reactions in seedling mitochondria and causing the gradual destruction of living cells and death of the organism is used. In order to illustrate an example for the use of the JC-1 dye, we also provide data analysis related to the mitochondrial membrane potential of two types of mouse-derived brain microvascular endothelial cells subjected to oxidative stress insults by exposure to tobacco.

Materials and Reagents

1. Pipette tips (Eppendorf, catalog number: 022491083)
2. Sterile centrifuge tube
3. Glass coverslips (typically 22 x 22 mm or 22 x 50 mm in Square and Rectangular Sizes respectively)
4. Petri dish (typically 100 x 21 mm or 35 x 10 mm based on the experiment design, Thermo Fisher Scientific, USA)
5. 96-well plate or chamber slides
6. Foil
7. BD™ CS&T beads
8. JC-1 dye (lyophilized) (MitoProbe JC-1 Assay Kit, Thermo Fisher Scientific, USA, catalog number: M34152)
9. Carbonyl cyanide 3-chlorophenylhydrazone (CCCP) (MitoProbe JC-1 Assay Kit, Thermo Fisher Scientific, USA, catalog number: M34152)
10. Phosphate-buffered saline (PBS) (Sigma-Aldrich, catalog number: D8537)
11. Dimethyl sulfoxide (DMSO) (MitoProbe JC-1 Assay Kit, Thermo Fisher Scientific, USA, catalog number: M34152; or Sigma-Aldrich, catalog number: D5879)
12. 50 mM CCCP (solvent: DMSO)
13. BD FC Bead 4c Plus Research Kit
14. FC Bead 4c Research Kits
15. FC Bead Violet Research Kits

Equipment

1. Pipettes (Eppendorf)
2. Incubator
3. Microcentrifuge (e.g., Sorvall™ Legend™ Micro 21R Microcentrifuge) or a comparable instrument is suggested (Thermo Fisher Scientific, model: Sorvall™ Legend™ Micro 21R), including 24 x 1.5/2.0 ml Rotor with Click Seal (Biocontainment, catalog number: 75002447)
4. Flow cytometer, equipped with a 488 nm argon excitation laser, and bandpass filters designed to detect rhodamine or Texas Red dye (BD FACSCalibur System or comparable platform) (BD, model: FACSCalibur™)
5. Valid alternatives include either a fluorescence microscope (EVOS™ FL color Imaging System, catalog number: AMEFC4300) with a dual-bandpass filter designed to simultaneously detect fluorescein and rhodamine or fluorescein and Texas Red dyes or a fluorescence plate reader (Synergy™ Mx Monochromator-Based Multi-Mode Microplate Reader-BioTek, catalog number: 236219) equipped with laser/fluorescent filters and black 96-well plates.

Software

1. FACSsuite software

Procedure

A. Preparation and setup

Note: As a first step, allow the JC-1 powder and DMSO solutions to come to 25 °C before use.

1. Prepare a fresh 200 µM JC-1 dye stock solution immediately prior to use by reconstituting the lyophilized JC-1 dye with DMSO to obtain a 100x stock solution.
2. Mix the preparation until the solution is clear of aggregates and the dye powder is completely dissolved.

B. Staining protocol for cells in suspension

The following protocol describes the preparation steps for the use of the JC-1 dye on cultured cells in Suspension followed by analysis of the cells preparation by flow cytometry, fluorescence microscopy or fluorescence plate reader.

1. Based on the experiment design, the cells are seeded on gelatin-coated cell culture flasks or glass chamber slides, cultured in the warm culture medium and maintained at 37 °C with 5% CO₂ exposure. The culture medium is changed every other day until the cells reach confluence.
2. Split the adhered cells from the flasks or glass chamber slides.
 - a. Briefly, remove the medium from culture vessel by aspiration and then dispense enough trypsin or trypsin/EDTA solution into culture vessel(s) to cover the monolayer of cells completely and then place in 37 °C incubator for ~6 min.
 - b. Remove the trypsin or trypsin/EDTA solution and add it to sterile centrifuge tube (15 ml) containing the equal amount of warm cell culture medium (~37 °C) and centrifuge for 7 min at 25 °C at 125 x g.
 - c. Then remove the medium from the tube by aspiration.
3. In order to suspend cells in the tube, for each sample, add 1 ml warm cell culture medium (~37 °C), PBS, or another buffer not to exceed 1 x 10⁶ cells/ml
4. Wash cells by adding 2 ml of warm PBS (~37 °C) or another buffer to each tube containing cells and centrifuge for 5 min at 25 °C at 400 x g.
5. Remove the supernatant.
6. Suspend the cell pellet again in 1 ml of fresh cell culture medium or PBS (~37 °C).
7. Add 10 µl of 200 µM JC-1 dye (2 µM in final concentration) and incubate the cells at 37 °C, 5% CO₂ for 15-30 min. Then follow the procedure of Steps B8 and B9 to prepare the positive control.
8. Induce cell apoptosis in one of the sample preparations which will be used as a positive control for the remaining samples.

9. To provide the positive control, add 1 μ l of 50 mM of CCCP (50 μ M in final concentration) just to one sterile centrifuge tube (1.5 ml) containing 1 ml warm cell culture medium (\sim 37 °C), PBS, or another buffer not to exceed 1 \times 10⁶ cells/ml and incubate at 37 °C for 5 min.
10. Wash all samples by adding 2 ml of warm PBS (\sim 37 °C or another buffer to each tube and centrifuge for 5 min at 25 °C at 400 \times g.
11. Remove the supernatant.
12. Re-suspend the cell pellet again in 300 μ l fresh cell culture medium or PBS (\sim 37 °C).
13. Begin observation and measuring immediately after completing the last step using one of the following methods including flow cytometry, fluorescence microscopy or fluorescence plate reader analysis as described below. Typically, for each sample, the number of replicates should be n = 3 and the number of observation and measurement should be more than 5 for each sample.

C. Staining protocol of monolayer cells

The following protocol describes the process of JC-1 staining in cultured cell monolayers and following analysis using either fluorescence microscopy or fluorescence plate reader.

1. Cells can be cultured on pre-coated glass coverslips (in a Petri dish), 96 wells plate supports or chamber slides. Make sure not to exceed a max cell density of \sim 1 \times 10⁶ cells/cm².
2. Precoating (agent and density) depends upon the cells used. Refer to your specific cell culture protocol.
3. Remove the cell culture medium and then replace it with a warm medium (\sim 37 °C), PBS, or another buffer.
4. Wash cells once by adding warm PBS (\sim 37 °C) or another buffer and add again fresh cell culture medium or PBS (\sim 37 °C).
5. Add 2 μ M (final concentration) of JC-1 dye and incubate the cells at 37 °C, 5% CO₂ for 15-30 min.
6. For the positive control, add 50 μ M final concentration of CCCP and incubate the cells at 37 °C for 5 min.
7. Remove the culture medium of all samples and wash the cells once by adding warm PBS or another buffer (\sim 37 °C).
8. Add PBS to samples (about 100 μ l into each of the 96 wells plate or corresponding amount in a petri dish or chamber slides depending on the culture platform and detection methods that was selected). Cover with a sheet of foil to keep the culture platform and its content out of light.
9. Analyze the fluorescence of the test cultures (including controls) immediately. For the quantification methods, please refer to Note A.

Data analysis

The main role of $\Delta\Psi_M$ is to drive ATP synthesis using oxidative phosphorylation. The magnitude of $\Delta\Psi_M$ keeping the electron traveling across the electron transport chain to maintain an optimum electrochemical gradient is determined by the balance between the production of ATP and its consumption. Increased ATP generation or mitochondrial dysfunction can lead to a decrease in mitochondrial membrane potential (Suski *et al.*, 2012; Logan *et al.*, 2016). JC-1 as a fluorescent cationic carbocyanine dye exhibits potential-dependent accumulation in mitochondria, which form J aggregates and it diffuses across mitochondria to form monomeric state upon depolarization (Figure 1).

As a study example, we show data relative a previously published study by us related to tobacco smoke (TS) and electronic cigarette (e-Cig) toxicity at the brain microvascular endothelium (Kaisar *et al.*, 2017; Prasad *et al.*, 2017). It is well proven that tobacco smoking causes vascular endothelial dysfunction in a causative and dose-dependent manner primarily relevant to the content of reactive oxygen species (ROS) (Kaisar *et al.*, 2018). In this study example, it was assumed that the detrimental cellular effect of TS exposure on the BBB endothelium was partially promoted by induction of mitochondrial depolarization. We also assumed that exposure to e-Cig could lead to a similar outcome. As previously suggested, we first established a positive control (to be used as the term of comparison) treating the cultured cells with CCCP (a potent mitochondrial membrane disruptor). We then analyzed the impact of TS and e-Cig on mitochondrial $\Delta\Psi_M$ using the fluorescent cationic JC-1 dye. The results showed that acute exposure to TS and e-Cig promotes mitochondrial depolarization in primary brain membrane endothelial cells (mBMEC) however, the impact of e-Cig on mitochondrial depolarization was significantly less severe when compared with TS (see example Figure 2). Accordingly, the data showed a decreased red (~590 nm) to green (~529 nm) fluorescence intensity ratio in response to both TS and e-Cig exposure in relation to mitochondria depolarization which is clearly observable in the fluorescence images. The results also showed that the impact of e-Cig was less severe than TS. These data are provided as a convenient example of both qualitative and quantitative measurements of changes in mitochondrial $\Delta\Psi_M$ that can be assessed with the use of JC-1 dye.

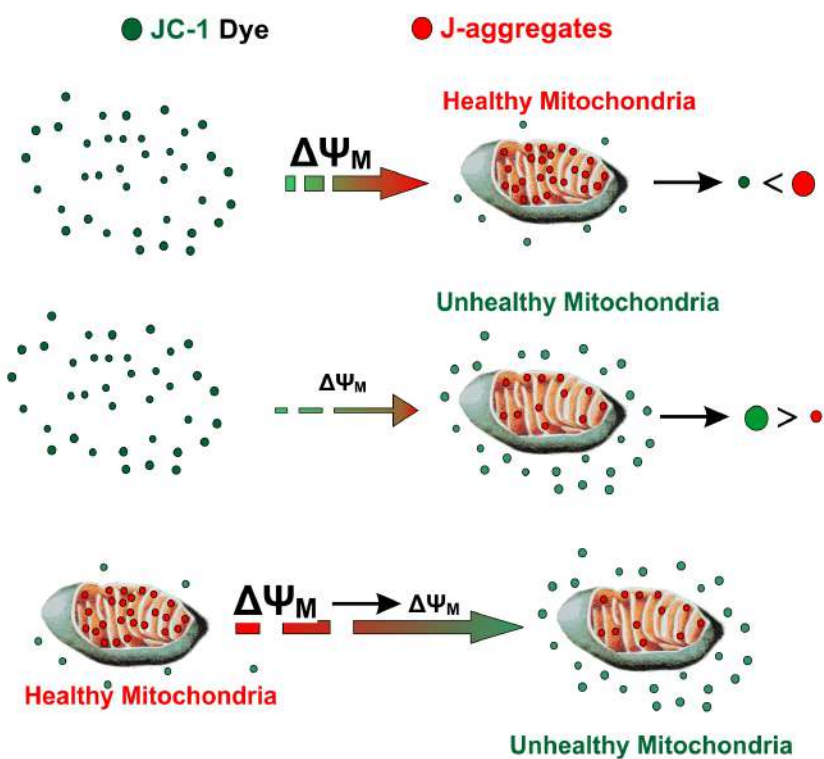


Figure 1. Schematic illustration depicting JC-1 entry into the mitochondria and the generation of J aggregates. JC-1, a cationic carbocyanine dye (green) exhibits potential-dependent accumulation in mitochondria where it starts forming J aggregates (red); upon depolarization, it remains as monomer showing green fluorescence.

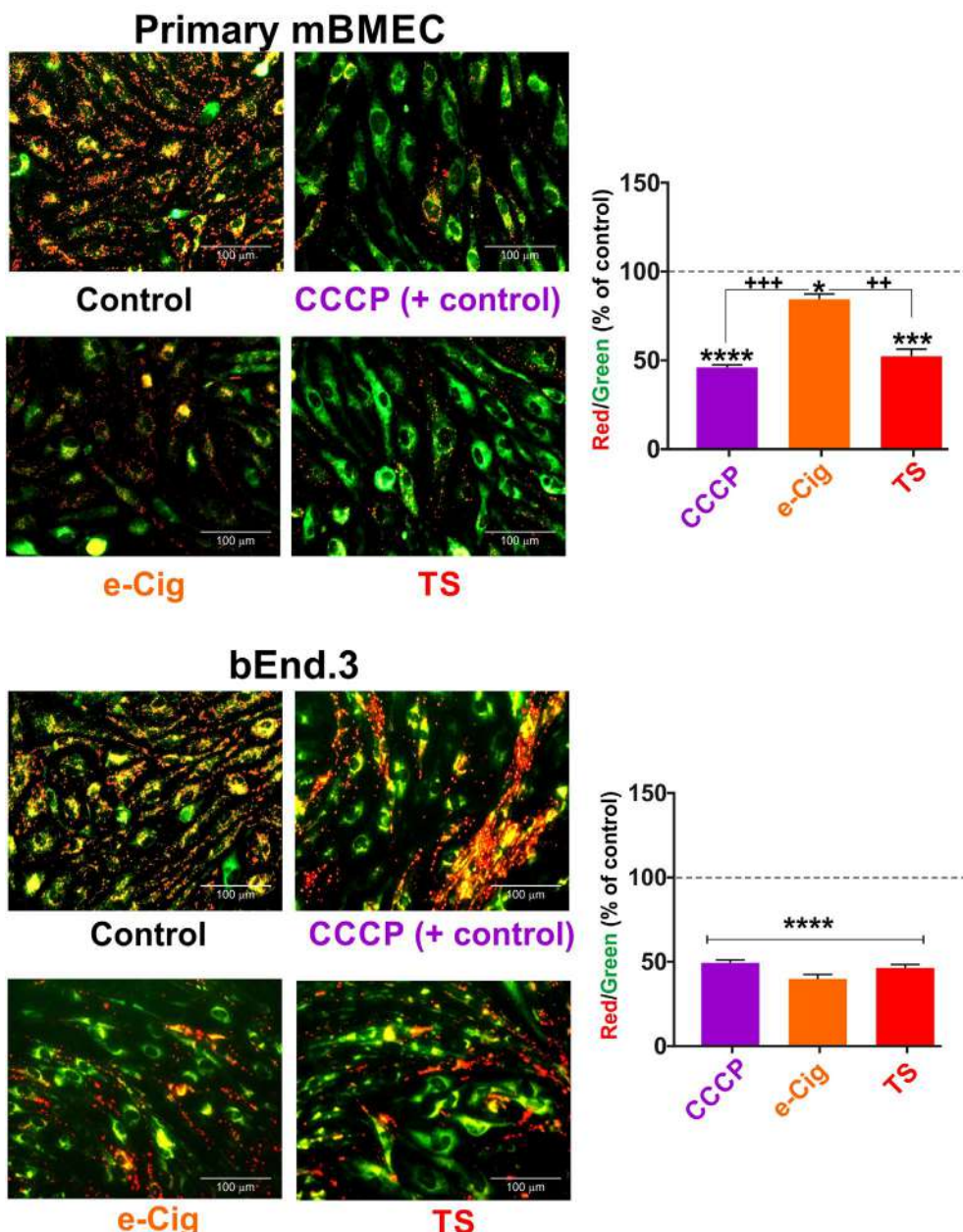


Figure 2. Assessment of mitochondrial depolarization using JC-1 die: a practical example. A decrease in the red (~590 nm)/green (~529 nm) fluorescence intensity ratio by acute exposure to TS is indicative of depolarization/disruption of the mitochondrial membrane in primary mBMEC and bEnd.3. Note also how JC-1 staining allows comparing side by side the impact of different experimental treatments (TS vs. e-Cig) on mitochondrial $\Delta\psi_m$ of different cell types. Note in fact how primary mBMEC and bEnd.3 respond differently to the same treatment. CCCP = Carbonyl cyanide 3-chlorophenylhydrazone, mitochondrial membrane potential disruptor. * $P < 0.05$; ** $P < 0.01$; *** $P < 0.01$, **** $P < 0.001$ compared to control. N = 3 biological replicates.

Notes

A. Notes for flow cytometry, fluorescence microscopy or fluorescence plate reader analysis

Concerning the Photomultiplier tube (PMT) voltage setting, different Cytometers work differently. In our specific case we used BD FACSVerse, which operates by FACSsuite software and calibrated by running BD™ CS&T beads.

Running CS&T beads before every experiment is necessary to provide a standardized method to perform quality control of the instrument's optics, electronics, and fluidics, and for adjusting fluorescence compensation and detector voltages. The FACSVerse has an automatic compensation function for nine kinds of fluorochrome. The auto-compensation function is updating every month by running BD FC Bead 4c Plus Research Kit, FC Bead 4c Research Kits, FC Bead Violet Research Kits.

The value of the PMT Voltage is decided by placing the control cells on the center of the dot plot, see below FSC/SSC plot (Figure 3A).

To find the value of FL1-FITC/FL2-PE or APC PMT voltage unstained cells are placed on the LL, and around 0 on the histogram (see Figures 3B, 3C and 3D). Although the FACSVerse will do the compensation automatically, it is still necessary to make sure that the compensation is correct.

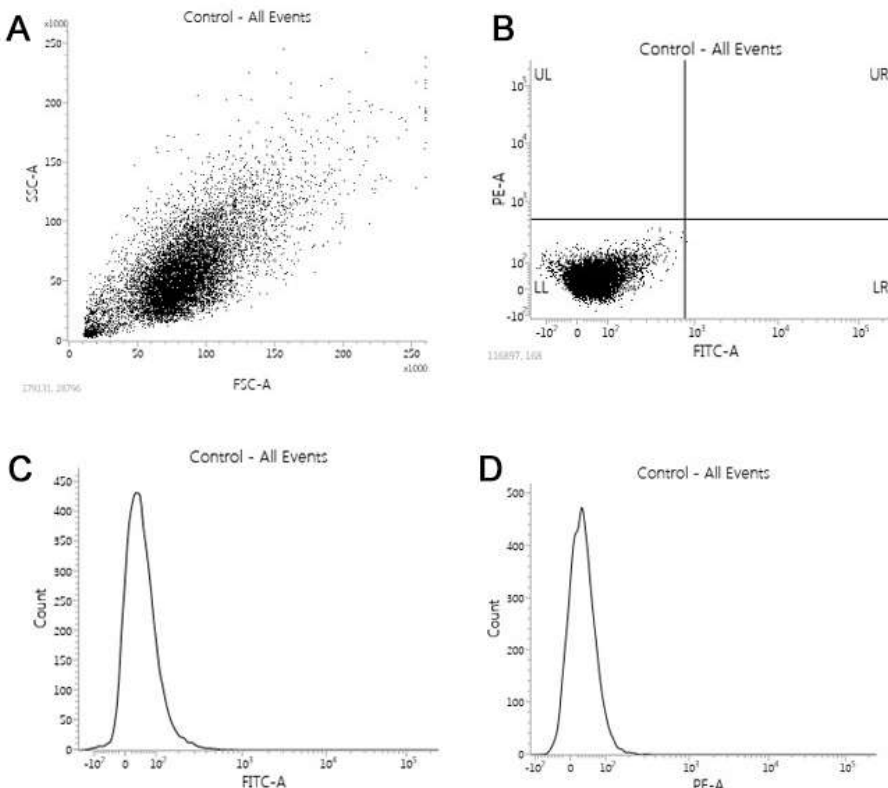


Figure 3. Flow cytometry assay. A and B. Discrimination of the cells based on two scatter parameters by flow cytometric gating strategy (dot plot). C and D. Cell counting based on the specified marker (log histogram).

Quantification by flow cytometry

On a small sample volume containing few cells and heterogeneous cell populations, flow cytometry allows analyzing with high sensitivity the cell size, its contents, frequency and the intensity of these stained cells. It is recommended that analysis by flow cytometry is initiated right after completion of the above-mentioned Step B10. The flow cytometer must be equipped with a 488 nm argon excitation laser and the value of photomultiplier (PMT) detecting the signal must be set at 390 V in FL1, and 320 V in FL2 with a FL2-FL1 compensation around 10.6% while FL1-FL2 compensation should be approximately 4.0% (Cossarizza and Salvioli, 1998). Mitochondria containing green JC-1 monomers in apoptotic cells will be detectable in the FL1 channel (FITC, GFP), while the red fluorescent JC-1 aggregates in healthy cells will be detected in the FL2 channel (PE, R-PE, RD1).

The JC-1 dye is excited using an argon laser at a wavelength of 488 nm. Both JC-1 aggregates and JC-1 monomers exhibit green fluorescence (peak emission at 527 nm) which is measured in the FL1 channel (530 nm) however, the JC-1 aggregates show also a red fluorescence (peak emission at 590 nm) which is detected and measured in the FL2 channel (585 nm). Thus, healthy non-apoptotic cells will be detected in both FL1, and FL2 channels and apoptotic cells will remain bright in the FL1 channel, however, will show decreased FL2 intensity.

Finally, determine the ratio of red fluorescence divided that of green fluorescence. For flow cytometry 10,000 cells will be analyzed and separated according to the fluorescence intensity.

Evaluation by fluorescence microscopy

Fluorescence intensity detection is the measurement of the light emitted by a fluorophore upon excitation by light at a higher energy and smaller wavelength. A sample is excited by the light produced by a light source and filtered at a specific wavelength by either a filter or a monochromator.

A good quantitative fluorescence microscopy experiment is performed with the goal of defining an event or object of interest with numbers, which most often represent fluorescence intensity associated with spatial or temporal measurements. The procedure requires a fluorescence microscope and the use of a “dual-bandpass” filter. In apoptotic and dead cells, the dye will appear green with an emission at 530 nm, remaining in its monomeric form, while in live non-apoptotic cells, the mitochondria will appear red following aggregation of the JC-1 dye at 590 nm. Finally, evaluate the images taken by the microscopy to find the proportion of red fluorescence to green fluorescence. For fluorescence microscopy qualitative and no quantitative measurement has been done by microscopy. It is usual to take ten photos of each sample.

Quantification by fluorescence plate reader

The working principle of fluorescence plate reader is so close to fluorescence microscopy, although the plate reader will only record total fluorescence and also the resolution and sensitivity of fluorescence microscopy are superior compared to plate reader-based assays. Transfer 300 μ l cell suspension into three wells of a black 96-well plate (100 μ l to each well). Then, measure the red

fluorescence in excitation (550 nm)/emission (600 nm) and green fluorescence excitation/emission (485 nm/535 nm) using a fluorescence plate reader. Then, determine the ratio of red fluorescence divided that of green fluorescence. For fluorescence plate reader each sample could be run for three times.

B. Notes of procedural recommendation and troubleshooting

1. Since JC-1 dye is very sensitive to alterations of temperature and pH, all reagents must be kept at 25 °C and carefully checked for pH (7.4) during the experiment.
2. Due to the light sensitivity of JC-1 Staining procedure must be carried under no direct intense light and incubation in the dark.
3. Since detached apoptotic cells may be in the media, be careful how to dispose of the media after replacing that with fresh media according to biowaste disposal methods.
4. Always wear gloves when handling JC-1 dye.
5. Based on the available equipment and also the kind of the cells each of the methods of quantification can be selected. For example, some cells naturally live in suspension in body fluids and do not attach to surfaces, such as cells of hematopoietic origin found in the bloodstream. Moreover, culturing suspension cells is somewhat easier than adherent cell cultures because suspension cells do not require trypsinization as they are already free floating.
6. It is strongly suggested to analyze the samples immediately with a flow cytometer, fluorescence microscope or fluorescence plate reader. Otherwise, keep samples refrigerated (not frozen) and in the dark for a later (no more than 24 h).
7. The protocol of staining with JC-1 dye does not require a long time (~30 min). The duration depends on the number of samples to be analyzed.
8. If cells are not well stained using JC-1 then it is possible that the staining solution may have been centrifuged, or stained cells have been exposed to intense light. Do not centrifuge JC-1 staining solution. Analyze the stained cells immediately after washing and increase the amount of JC-1 dye if needed.
9. Cells can be fixed with paraformaldehyde or other fixatives and stored in fridge until JC-1 staining. But do not include any fixative during the JC-1 staining.
10. If cells are over stained, decrease the amount of JC-1 dye, and keep the cells a little longer in contact with the free-PBS JC-1 dye. This will help to reach the appropriate distribution's equilibrium.
11. If control cells without treatment show a low ratio of red to green signal, then the viability of the control cells may be compromised.
12. Culture cells at densities higher than 10^6 /ml may promote natural apoptosis.
13. Initial steps may require modifications and tweaking due to differences in cell types and culture conditions.
14. The concentration of JC-1 dye for optimal staining may vary depending upon the application. It

is suggested to start testing concentration range around 2 μ M JC-1 dye.

15. CCCP controls should be used to confirming the sensitivity of JC-1 dye to changes in membrane potential.

Acknowledgments

Funding: This work was supported by the National Institutes of Health/National Institute on Drug Abuse 2R01-DA029121-01A1 and ARDF to Dr. Luca Cucullo.

Competing interests

The authors declare no competing interests.

References

1. Cossarizza, A. and Salvioli, S. (1998). *Purdue Cytometry CD-ROM Series* vol. 4.
2. Green, D. R. and Reed, J. C. (1998). [Mitochondria and apoptosis](#). *Science* 281(5381): 1309-1312.
3. Kaisar, M. A., Sivandzade, F., Bhalerao, A. and Cucullo, L. (2018). [Conventional and electronic cigarettes dysregulate the expression of iron transporters and detoxifying enzymes at the brain vascular endothelium: In vivo evidence of a gender-specific cellular response to chronic cigarette smoke exposure](#). *Neurosci Lett* 682: 1-9.
4. Kaisar, M. A., Villalba, H., Prasad, S., Liles, T., Sifat, A. E., Sajja, R. K., Abbruscato, T. J. and Cucullo, L. (2017). [Offsetting the impact of smoking and e-cigarette vaping on the cerebrovascular system and stroke injury: Is Metformin a viable countermeasure?](#) *Redox Biol* 13: 353-362.
5. Logan, A., Pell, V. R., Shaffer, K. J., Evans, C., Stanley, N. J., Robb, E. L., Prime, T. A., Chouchani, E. T., Cocheme, H. M., Fearnley, I. M., Vidoni, S., James, A. M., Porteous, C. M., Partridge, L., Krieg, T., Smith, R. A. and Murphy, M. P. (2016). [Assessing the mitochondrial membrane potential in cells and in vivo using targeted click chemistry and mass spectrometry](#). *Cell Metab* 23(2): 379-385.
6. Perry, S. W., Norman, J. P., Barbieri, J., Brown, E. B. and Gelbard, H. A. (2011). [Mitochondrial membrane potential probes and the proton gradient: a practical usage guide](#). *Biotechniques* 50(2): 98-115.
7. Prasad, S., Sajja, R. K., Kaisar, M. A., Park, J. H., Villalba, H., Liles, T., Abbruscato, T. and Cucullo, L. (2017). [Role of Nrf2 and protective effects of Metformin against tobacco smoke-induced cerebrovascular toxicity](#). *Redox Biol* 12: 58-69.
8. Smiley, S. T., Reers, M., Mottola-Hartshorn, C., Lin, M., Chen, A., Smith, T. W., Steele, G. D.,

- Jr. and Chen, L. B. (1991). [Intracellular heterogeneity in mitochondrial membrane potentials revealed by a J-aggregate-forming lipophilic cation JC-1.](#) *Proc Natl Acad Sci U S A* 88(9): 3671-3675.
9. Suski, J. M., Lebiedzinska, M., Bonora, M., Pinton, P., Duszynski, J. and Wieckowski, M. R. (2012). [Relation between mitochondrial membrane potential and ROS formation.](#) *Methods Mol Biol* 810: 183-205.
10. Zorova, L. D., Popkov, V. A., Plotnikov, E. Y., Silachev, D. N., Pevzner, I. B., Jankauskas, S. S., Babenko, V. A., Zorov, S. D., Balakireva, A. V., Juhaszova, M., Sollott, S. J. and Zorov, D. B. (2018). [Mitochondrial membrane potential.](#) *Anal Biochem* 552: 50-59.

A Mouse Model of Postoperative Pain

Ashley M. Cowie and Cheryl L. Stucky*

Department of Cell Biology, Neurobiology and Anatomy, Medical College of Wisconsin, Milwaukee, WI 53226, USA

*For correspondence: cstucky@mcw.edu



[Abstract] Postoperative pain is highly debilitating and hinders recovery. Opioids are the main pain medication used for acute postoperative pain. Given the devastating opioid addiction and overdose epidemic across the US, non-opioid pain therapeutics are desperately needed. In order to develop novel, non-opioid therapies for the treatment of postoperative pain and identify the mechanisms underlying this pain, rodent models of incisional pain have been established. The protocol herein describes in detail how to create a mouse model of postoperative pain that was adapted from established protocols. This model of postoperative pain is frequently-used, highly reproducible, and results in peripheral and central nervous system alterations.

Keywords: Postoperative pain, Inflammatory pain, Hypersensitivity, Plantar incision, Mouse, Skin and muscle incision

[Background] Postoperative pain is a significant, worldwide problem. Approximately 234.2 million people undergo major surgeries each year (Weiser *et al.*, 2008) and about 80% of patients experience acute postoperative pain (Gan, 2017). Of these, between 10% and 50% of patients, develop chronic pain that continues to severely impact their quality of life (Chapman and Vierck, 2017). One of the factors that are associated with the development chronic postoperative pain, but unlikely the cause, is the severity of acute pain experienced during the first postoperative week (Fletcher *et al.*, 2015; Chapman and Vierck, 2017). Opioids are the main pain medication used for acute postoperative pain (Sen and Bathini, 2015; Tan *et al.*, 2018). Given the opioid epidemic, non-opioid pain therapeutics are needed. Therefore, identifying the mechanisms that underlie acute postoperative pain is necessary for the development of optimal therapies for postoperative pain that may ultimately decrease the severity and/or incidence of chronic postoperative pain. Both rat (Brennan *et al.*, 1996) and mouse (Pogatzki and Raja, 2003) models of acute incisional pain have been developed as preclinical models to identify the molecular, cellular and physiological mechanisms that underlie postoperative pain. However, a detailed description of the mouse model of postoperative pain is lacking. Here we describe in detail a mouse model of postoperative pain that requires incision of both the skin and muscle. Incision of both skin and muscle best mimics invasive surgery that causes intense acute pain and leads to chronic pain (Brennan, 2011; Chapman and Vierck, 2017). Furthermore, incision of skin and muscle (~6 days) creates hypersensitivity that lasts substantially longer than the skin-only (~3 days) incision model (Xu and Brennan, 2010). In this protocol, we provide detailed, step-by-step methods adapted from previous protocols (Brennan *et al.*, 1996; Pogatzki and Raja, 2003) for development of a mouse model of

postoperative pain.

Materials and Reagents

1. Stainless steel sterile No. 11 surgical blade (World Precision Instruments, Feather Safety Razor Co. Ltd., catalog number: 504170)
2. Sterile 5-0 nylon surgical sutures (AD Surgical, Unify, catalog number: S-N518R13)
3. Surgical tape (3M, Transpore, catalog number: 1527-0)
4. Cotton swab (VWR, Critical Swab, catalog number: 89031-270)
5. Glad Press'n Seal (SAI Infusion Technologies, Glad, catalog number: PSS-70)
6. Sterile nitrile gloves (Kimberly-Clark Professional, Kimtech Pure, catalog number: HC61170)
7. Petri dishes [VWR, 14.5 and 9 663161, Greiner Bio-One, catalog numbers: 82050-912 (small) and 82050-600 (large)]
8. Sterile gauze (Allied Medical, Ardes, catalog number: GA441221)
9. Sharpie extra fine point permanent marker (Staples, Sharpie, catalog number: 37001)
10. 8-16 week old C57BL/6J mice (JAX, catalog number: 000664)
11. Bacitracin zinc ointment (Fougera Pharmaceuticals Inc, catalog number: 0168-0011-04)
12. Isoflurane (Clipper distributing company LLC., Phoenix, catalog number: 0010250)
13. 75% ethanol (Fisher Scientific, Decon Laboratories, Inc., catalog number: 22-281-562)
14. Surgical scrub 7.5% povidone-iodine (Betadine, Veterinary, catalog number: 67618-154-01)
15. Eye lube (Patterson Veterinary, Optixcare Ophthalmic, catalog number: 07-893-2779)

Equipment

1. 1,000 ml beaker (VWR, PYREX, catalog number: 13912-284)
2. #55 Dumostar Forceps (Fine Science Tools, Dumont, catalog number: 11295-51)
3. Scalpel handle (Fine Science Tools, catalog number: 10003-12)
4. Iris Forceps, 10 cm, Curved, Serrated (World Precision Instruments, catalog number: 15915)
5. Halsted Mosquito Hemostatic Forceps, 12.5 cm, Straight (World Precision Instruments, catalog number: 15920-G)
6. Vannas Scissors, 8 cm, Curved (World Precision Instruments, catalog number: 14122)
7. Small animal surgery board (Braintree Scientific, Inc., CD+, catalog number: ACD 014)
8. Isoflurane dispenser (Highland Medical Equipment, Drager, catalog number: 16-7001)
9. Sliding top isoflurane induction chamber (Kent Scientific Corporation, catalog number: VetFlo-0530LG)
10. Heat Therapy Pump with Pad (Adroit Medical Systems, catalog number: HTP-1500)
11. Isothermal pad (Braintree Scientific, Inc., Deltaphase, catalog number: DPPIP)
12. Digital calipers (VWR, catalog number: 62379-531)
13. Steri 250 Bead Sterilizer Bead Bath (Lab Unlimited, Simon Keller Ltd., catalog number:

4AJ-6286283)

14. Microwave (Emerson, 1,000 W, catalog number: B007Q45CIS)
15. Home cage containing Aspen Sani Chips® (P.J. Murphy Forest and Products, Sani Chips®)

Software

1. GraphPad Prism 7

Procedure

1. Sterilize surgical area with ethanol and sterilize tools in bead bath of at least 325 °C for 30 s. Rest sterile tools, sutures, and blade on sterile gauze.
2. Warm Heat Therapy Pump pad to 41 °C and warm the Isothermal pad in microwave for 1 min. Place a new, clean home cage on the Heat Therapy Pump pad. Place a laboratory paper towel over the warm Isothermal pad and cover with sterile Press'n Seal and surgery board.
3. To induce anesthesia, put the mouse in the beaker chamber with paper towel on lid containing 1 ml of isoflurane (Figure 1) and wait for approximately 30 s or until the mouse can no longer right itself. Alternatively, an isoflurane induction chamber that is included with the isoflurane dispenser can be used to induce anesthesia.



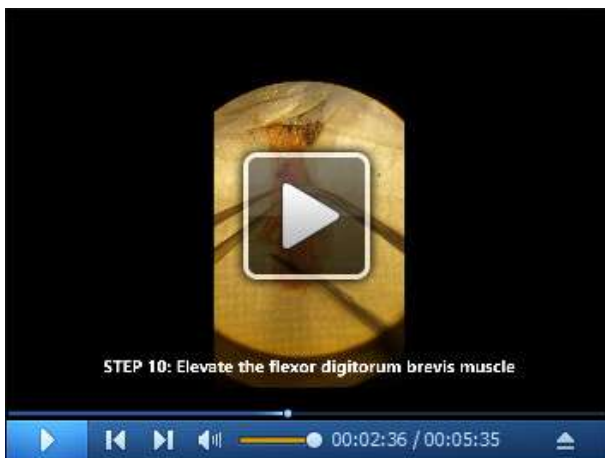
Figure 1. Brief inhalational anesthesia. The mouse was briefly anesthetized by inhalation in chamber with 1 ml isoflurane.

4. Quickly remove the mouse from the isoflurane chamber and apply eye lube using a cotton swab to each eye. Further anesthetize the mouse with 1.5%-2% inhaled isoflurane by placing the head of the mouse into the nose cone attached to the isoflurane dispenser and cover the mouse (except the hindpaw designated for operation) with sterile Press'n Seal (Figure 2).



Figure 2. Continuous inhalational anesthesia. The mouse was continuously anesthetized through a nose cone with 1.5%-2% isoflurane.

For Steps 5-13 also see Video 1.



Video 1. Plantar incision surgery. This video shows how the model of postoperative pain is made by making an incision through the plantar skin and flexor digitorum brevis muscle (This video was made at the Medical College of Wisconsin and was performed according to guidelines on Animal Care and approved by the Animal Research Ethics Board of the Medical College of Wisconsin under protocol #0383).

5. Adhere the hindpaw to the surface by taping the toes down with surgical tape (Figure 3).



Figure 3. Securing the hindpaw to surgical surface. The hindpaw was secured to the surface using surgical tape.

6. Once the hindpaw is secured, apply a cotton swab of 75% ethanol followed by a new cotton swab of betadine. Repeat for a total of 3 applications each.
7. Measure 2 mm from the proximal edge of heel using a digital caliper and place a dot with a permanent marker at this location in the middle of the hindpaw. From the first dot, measure 5 mm towards the toes down the center of the hindpaw and place a second dot (Figure 4).

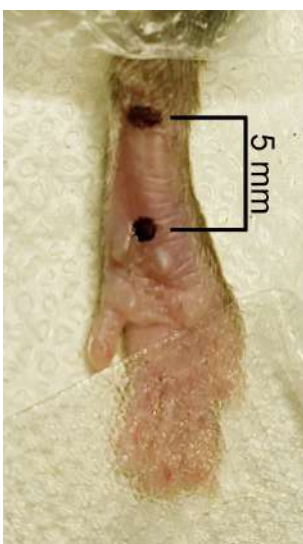


Figure 4. Measurement of incision. Two dots were placed in the middle of the hindpaw, one 2 mm from the heel and the second 5 mm from the first dot.

8. Check that the mouse is fully anesthetized by lightly pinching the most medial toe (most likely this toe could not be secured by the surgical tape) with the forceps. If the mouse flinches, wait until the mouse no longer reacts to the toe pinch before proceeding to Step 9.

9. Stabilize the hindpaw by placing the forceps on each side of the heel and make a longitudinal incision through the skin and fascia from the first dot to the second dot (Figure 5).



Figure 5. Cutaneous incision. A 5 mm longitudinal incision was made with a No. 11 scalpel.

10. Spread the skin away from the flexor digitorum brevis muscle with the forceps. Elevate the flexor digitorum brevis muscle by inserting one end of the curved forceps underneath the lateral edge of the flexor digitorum brevis muscle and pushing the forceps through to the medial side of the muscle (Figure 6).



Figure 6. Elevation of flexor digitorum brevis muscle. Curved forceps were inserted under the flexor digitorum brevis muscle to elevate the muscle.

11. Make a longitudinal incision with the scalpel through the entire belly of the muscle from the origin and insertion taking care not to sever the muscle completely from the origin and insertion, making sure to cut the belly of the muscle into two halves (Figure 7).



Figure 7. Muscle incision. A longitudinal incision was made through the muscle belly of the elevated flexor digitorum brevis muscle from proximal to distal ends of the cutaneous incision.

12. To suture the wound, remove the curved forceps from underneath the muscle and elevate the edges of the skin surrounding the wound with forceps. Close the wound by putting two sutures in the skin (but not muscle) approximately 2 mm apart using 5-0 nylon sutures and a hemostat (Figure 8).



Figure 8. Cutaneous suturing. The skin was closed with two 5-0 nylon sutures.

13. Apply a generous amount of bacitracin ointment to the wound using a cotton swab and place the mouse in the new cage located on the Heat Therapy Pump pad from Step 2.

Data analysis

Statistical significance was determined with GraphPad Prism 7 Software and graphs are shown as mean \pm SEM. A two-way ANOVA with a Sidak post-hoc was used to determine statistical significance for mechanical and heat thresholds. A complete description of statistics used for analyzing mechanical and heat threshold behavioral data is provided in Cowie *et al.* (2018).

Notes

1. It is important to perform the operation as quickly as possible to reduce the need for repeated anesthesia and any side effects from anesthesia. In our laboratory, it takes a trained surgeon approximately 5 min to perform this procedure.
2. For a control, a sham surgery is performed by anesthetizing the mouse, sterilizing the hindpaw as in Step 5, and applying bacitracin ointment to the plantar hindpaw.
3. If bleeding occurs during the procedure, apply pressure to the incision site with a cotton swab until the bleeding stops.
4. Mice are housed together.
5. No care is required after surgery except for monitoring of sutures.
6. If using mice past postoperative day 3, remove sutures on postoperative day 4. Mice that pulled out sutures before postoperative day 2 must be removed from the study due to poor wound closure.
7. For consistent behavioral results, apply mechanical and heat stimuli to the medial-posterior aspect of the plantar hindpaw (Figure 9). This area is the least sensitive at baseline because the heel is weight bearing whereas other areas near the pads are more sensitive and variable in withdrawal threshold. Therefore, using the heel area that provides a consistently high baseline withdrawal threshold allows for the best detection of change due to incision (Brennan *et al.*, 1996). Mice were acclimated for 1 h in Plexiglass chambers placed on either a mesh platform (mechanical threshold) or glass platform (heat threshold). Calibrated von Frey monofilaments (0.09 to 19.6 mN) were applied to the plantar hindpaw and the withdrawal threshold for each animal was calculated using the up-down method (Dixon, 1980; Chaplan *et al.*, 1994). The Hargreaves assay was used to measure heat sensitivity as previously established (Hargreaves *et al.*, 1988; Jackson *et al.*, 1995; Barabas and Stucky, 2013; Cowie *et al.*, 2018). Withdrawal latencies to a focused radiant heat source (IITC, Life Sciences Instruments) underneath the glass platform were measured 3 times and averaged for each mouse. A cutoff of 20 s was used to avoid injury. Examples of mechanical and heat hypersensitivity following incision are shown in Figure 10.



Figure 9. Application of von Frey monofilament. An orange von Frey monofilament was applied to most sensitive location following incision.

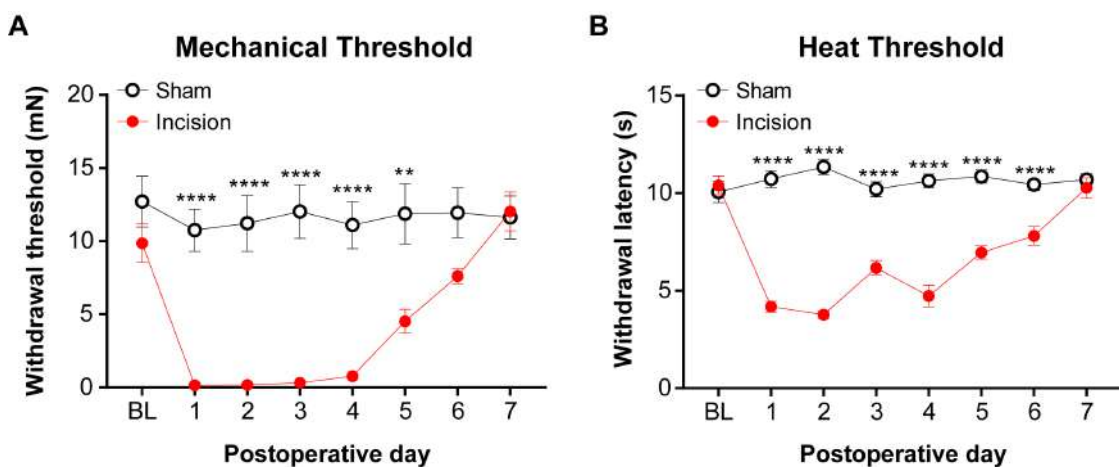


Figure 10. Mechanical and heat thresholds following incision. A. von Frey monofilaments was applied to most sensitive location following incision and the Dixon up-down method (Dixon, 1980) was used to determine mechanical threshold. B. The Hargreaves assay (Hargreaves *et al.*, 1988) was used to measure the withdrawal threshold in response to a radiant heat source that was applied to the most sensitive location following incision. These data were modified from Cowie *et al.* (2018). Data shown as mean \pm SEM, repeated-measures two-way ANOVA and Sidak post-hoc analysis, ** P < 0.01 and **** P < 0.0001 sham versus incision. For (A) and (B), n = 8 male mice per group.

Acknowledgments

This protocol was adapted from established published procedures (Brennan *et al.*, 1996; Pogatzki and Raja, 2003). This work was supported by the National Institute of Neurological Disorders and Stroke grants NS040538 and NS070711 to C.L.S and F31GM123778 to A.M.C. The Research and Education Component of the Advancing a Healthier Wisconsin Endowment at the Medical College of Wisconsin provided partial support. The authors thank Timothy J Brennan, Ph.D., MD for his review of the manuscript.

Competing interests

The authors declare no competing financial or non-financial interests.

Ethics

All animal procedures were carried out in accordance with the National Institute of Health guidelines and approved by the Institutional Animal Care and Use Committee of the Medical College of Wisconsin (AUA #0383).

References

1. Barabas, M. E. and Stucky, C. L. (2013). [TRPV1, but not TRPA1, in primary sensory neurons contributes to cutaneous incision-mediated hypersensitivity.](#) *Mol Pain* 9: 9.
2. Brennan, T. J. (2011). [Pathophysiology of postoperative pain.](#) *Pain* 152(3 Suppl): S33-40.
3. Brennan, T. J., Vandermeulen, E. P. and Gebhart, G. F. (1996). [Characterization of a rat model of incisional pain.](#) *Pain* 64(3): 493-501.
4. Chaplan, S. R., Bach, F. W., Pogrel, J. W., Chung, J. M. and Yaksh, T. L. (1994). [Quantitative assessment of tactile allodynia in the rat paw.](#) *J Neurosci Methods* 53(1): 55-63.
5. Chapman, C. R. and Vierck, C. J. (2017). [The transition of acute postoperative pain to chronic pain: An integrative overview of research on mechanisms.](#) *J Pain* 18(4): 359 e1-359 e38.
6. Cowie, A. M., Moehring, F., O'Hara, C. and Stucky, C. L. (2018). [Optogenetic inhibition of CGRP \$\alpha\$ sensory neurons reveals their distinct roles in neuropathic and incisional pain.](#) *J Neurosci* 38(25): 5807-5825.
7. Dixon, W. J. (1980). [Efficient analysis of experimental observations.](#) *Annu Rev Pharmacol Toxicol* 20: 441-462.
8. Fletcher, D., Stamer, U. M., Pogatzki-Zahn, E., Zaslansky, R., Tanase, N. V., Perruchoud, C., Kranke, P., Komann, M., Lehman, T. and Meissner, W. (2015). [Chronic postsurgical pain in Europe: An observational study.](#) *Eur J Anaesthesiol* 32(10): 725-734.

9. Gan, T. J. (2017). [Poorly controlled postoperative pain: prevalence, consequences, and prevention.](#) *J Pain Res* 10: 2287-2298.
10. Hargreaves, K., Dubner, R., Brown, F., Flores, C. and Joris, J. (1988). [A new and sensitive method for measuring thermal nociception in cutaneous hyperalgesia.](#) *Pain* 32(1): 77-88.
11. Jackson, D. L., Graff, C. B., Richardson, J. D. and Hargreaves, K. M. (1995). [Glutamate participates in the peripheral modulation of thermal hyperalgesia in rats.](#) *Eur J Pharmacol* 284(3): 321-325.
12. Pogatzki, E. M. and Raja, S. N. (2003). [A mouse model of incisional pain.](#) *Anesthesiology* 99(4): 1023-1027.
13. Sen, S. and Bathini, P. (2015). [Auditing analgesic use in post-operative setting in a teaching hospital.](#) *J Clin Diagn Res* 9(4): FC01-04.
14. Tan, W. H., Yu, J., Feaman, S., McAllister, J. M., Kahan, L. G., Quasebarth, M. A., Blatnik, J. A., Eagon, J. C., Awad, M. M. and Brunt, L. M. (2018). [Opioid medication use in the surgical patient: An assessment of prescribing patterns and use.](#) *J Am Coll Surg* 227(2): 203-211.
15. Weiser, T. G., Regenbogen, S. E., Thompson, K. D., Haynes, A. B., Lipsitz, S. R., Berry, W. R. and Gawande, A. A. (2008). [An estimation of the global volume of surgery: a modelling strategy based on available data.](#) *Lancet* 372(9633): 139-144.
16. Xu, J. and Brennan, T. J. (2010). [Guarding pain and spontaneous activity of nociceptors after skin versus skin plus deep tissue incision.](#) *Anesthesiology* 112(1): 153-164.

A blue-tinted promotional banner for Bio-Protocol. It features the Bio-Protocol logo at the top left, followed by the tagline "Improve Research Reproducibility". Below this, a large heading reads "Free access to ~4000 high-quality protocols". A bulleted list highlights the following features:

- Contributed by 10,000+ scientists (including Nobel Laureates)
- Validated in a primary research paper
- >91% reproducibility (survey of 2165 Bio-protocol users)
- ~1000 videos of key procedural steps

At the bottom of the banner is a blue button containing the text "Sign up at: www.bio-protocol.org".

bio-protocol
Improve Research Reproducibility

Free access to ~4000 high-quality protocols

- Contributed by 10,000+ scientists (including Nobel Laureates)
- Validated in a primary research paper
- >91% reproducibility (survey of 2165 Bio-protocol users)
- ~1000 videos of key procedural steps

Sign up at: www.bio-protocol.org

Protocol to Quantitatively Assess the Structural Integrity of Perineuronal Nets *ex vivo*

Bhanu P. Tewari¹ and Harald Sontheimer^{1, 2, *}

¹Glia Biology in Health, Disease, and Cancer Center, Fralin Biomedical Research Institute at VTC, 2 Riverside Cir., Roanoke, VA 24016, USA; ²School of Neuroscience, College of Science, Virginia Tech, 300 Turner Street NW, Blacksburg, VA 24061, USA

*For correspondence: sontheim@vt.edu



[Abstract] Perineuronal nets (PNNs) are extracellular matrix assemblies of highly negatively charged proteoglycans that wrap around fast-spiking parvalbumin (PV) expressing interneurons in the cerebral cortex. PNNs play important roles in neuronal plasticity and modulate biophysical properties of the enclosed interneurons. Various central nervous system diseases including schizophrenia, Alzheimer disease and epilepsy present with qualitative alteration in PNNs, however prior studies failed to quantitatively assess such changes at single PNN level and correlate them with functional changes in disease. We describe a method to quantify the structural integrity of PNNs using high magnification image analysis of *Wisteria Floribunda Agglutinin* (WFA)-labeled PNNs in combination with cell-type-specific marker such as PV and NeuN. A polyline intensity profile of WFA along the entire perimeter of cell shows alternate segments with and without WFA labeling, indicating the intact chondroitin sulfate proteoglycan (CSPG) and holes of PNN respectively. This line intensity profile defines CSPG peaks, where intact PNN is present, and CSPG valleys (holes) where the PNN is missing. The average number of peaks reflect the integrity of the lattice assembly of PNN. The average size of PNN holes can be readily computed using image analysis software. Furthermore, degradation of PNNs using a bacterial-derived enzyme, Chondroitinase ABC (ChABC), allows to experimentally manipulate PNNs *in situ* brain slices during which biophysical properties can be assessed by patch-clamp recordings. We describe optimized experimental parameters to degrade PNNs in brain slices before as well as during recordings to study the possible change in function in real time. Our protocols provide effective and appropriate methods to modulate and quantify the PNN's experimental manipulations.

Keywords: Perineuronal nets, Brain slices, Chondroitinase ABC, *Wisteria floribunda agglutinin*, PV, Extracellular matrix

[Background] The extracellular spaces of the central nervous system are filled by an amorphous interstitial matrix that is composed of dense network of proteoglycans, hyaluronic acid (HA), tenascins and link proteins, and is contiguous with well-organized lattice-like structures called PNNs that enclose the somata, axons and dendrites of PV expressing interneurons in the cerebral cortex (Härtig *et al.*, 1999). The lattice of PNNs is composed of chondroitin sulfate proteoglycans (CSPGs), HA, tenascins, various link proteins (Deepa *et al.*, 2006), etc. Owing to the high density of sulfated proteoglycans, PNNs are highly negatively charged (Morawski *et al.*, 2015). The development of PNN coincides with

the closure of ocular dominance critical period and studies have shown reinstatement of ocular dominance plasticity upon removal of the PNNs thereby suggesting inhibitory role of PNNs on neuronal plasticity (Pizzorusso *et al.*, 2002). PNNs are also suggested to modulate the biophysical properties PV interneurons (Balmer, 2016, Favuzzi *et al.*, 2017, Tewari *et al.*, 2018), and are prone to degradation by ECM remodeling enzymes. Most notably, under pathological conditions including epilepsy (McRae *et al.*, 2012, Rankin-Gee *et al.*, 2015, Dubey *et al.*, 2017, Tewari *et al.*, 2018, Patel *et al.*, 2019), schizophrenia and Alzheimer disease (Testa *et al.*, 2018) ECM remodeling is common.

One of the major challenges in reporting on the status of PNNs is the quantification of the structural integrity of their lattice-like assembly. Essentially all published studies use the CSPG binding lectin, WFA, as non-specific PNN marker to visualize PNNs, and use WFA intensity to quantify the overall CSPG levels without detailed analysis of individual PNN's architecture (Slaker *et al.*, 2015 and 2016, Lensjø *et al.*, 2017, Ueno *et al.*, 2018). We developed a method to quantify the structural integrity of individual PNNs using high-magnification fluorescence imaging. This method also minimizes the errors due to procedure-related variations in the WFA intensity. After acquiring multichannel high magnification images (40x objective lens with 5 digital zoom) of individual PNNs, a polyline is drawn around the periphery of the cell. The fluorescence intensity of WFA along this line shows a discrete pattern of peaks separated by low-intensity valleys. Each peak represents the continuous CSPG and the gap between the two consecutive peaks represent a hole in the PNN (Tewari *et al.*, 2018). The average number of peaks and average width of holes can be derived from the WFA intensity data points and are reflective of the PNN's structural integrity. The peaks in the line profile can be counted manually or by using clampfit program (Molecular Devices).

A vast majority of studies, which explore the function of PNNs and their influence on the neuronal physiology, use ChABC, which is a bacterial enzyme that cleaves the chondroitin sulfate side chains thereby dismantling the PNN assembly (Dityatev *et al.*, 2007, Balmer, 2016, Testa *et al.*, 2018). The most common approach in such studies involves degradation of PNN *in-vivo/in-situ* brain slices/primary cultures and studying the function afterward by comparing two different populations of samples. However, it would be advantageous to record from PNN bearing neurons during the real-time degradation of PNNs to evaluate the physiological role of PNN on neuronal function. Such studies are largely absent in the literature. Here, we report two variants of experimental PNN degradation in the brain slices, which reliably degrade PNNs to allow studying their function. The first variant includes degradation of PNNs by incubating brain slices with ChABC in an incubation chamber followed by performing experiments to compare their properties with non-treated controls. The other variant is to study the baseline physiology in the presence of intact PNNs followed by superfusing ChABC solution and recording the functional activity during and after PNN depletion in the experimental set-up. Both the variants involve controlled degradation of PNNs and identifiable traces of degraded PNNs around the cells can be observed to confirm the presence/absence of PNNs on the experimental cell/tissue after post-experimental WFA staining of the samples. These methods provide unparalleled advantages to study the physiological functions associate with the PNNs.

Materials and Reagents

Materials

- A. PNN degradation in brain slices outside experimental setup
 - 1. Carbogen inlet and outlet needles (BD PrecisionGlide needle, catalog number: 305198)
 - 2. Perfusion Tubes (Becton Dickinson, PE-160, catalog number: 427431)
 - 3. Carbogen bubbling tubes (Fisher Scientific, Tygon, catalog number: S3 E-3603)
 - 4. Multichannel splitter (Luner valve assortment, catalog number: WPI-14055)
 - 5. Transfer pipettes (Fisher brand, catalog number: 13-711-7M)
 - 6. Glass Petri dish (Cole-Parmer Instrument, catalog number: EW-34551-06)
 - 7. Polystyrene foam (from any commercial source)
- B. PNN degradation in brain slices in experimental setup
 - 1. 15 ml tube (Falcon, catalog number: 352097)
 - 2. Thin perfusion lines (PVC pump tubes-1.52 mm ID, catalog number: 116-0549-19)
 - 3. Bubbling tubes (Fisher Scientific, Tygon, catalog number: S3 E-3603)
 - 4. Perfusion Tubes (Becton Dickinson, PE-160, catalog number: 427431)
- C. PNN's structural integrity analysis
 - 1. High magnification (40 x 5 or higher) images of WFA with PV or NeuN
- D. WFA staining of brain slices
 - 1. 24-well plate (Falcon, catalog number: 35-3226)
 - 2. Paint Brush (Any fine tipped clean brush)
 - 3. Coverslips (Fisher Finest, catalog number: 12-548-5M)
 - 4. Glass slide (Micro slides, VWR, catalog number: 48311-703)
 - 5. Mounting medium (Thermo Fisher, Invitrogen, catalog number: S36936)
 - 6. Marker (Lab marker, VWR, catalog number: 52877-310)
 - 7. Transfer pipettes (Fisher brand, catalog number: 13711-7M)

Reagents

- 1. ChABC (Sigma-Aldrich, catalog number: C3667-10U)
- 2. Bovine serum albumin (BSA) (Sigma-Aldrich, catalog number: A8806-1G)
- 3. 4% Paraformaldehyde (PFA) (Electron Microscopy Science, catalog number: 15714-S)
- 4. PBS (Fisher Bioreagent, catalog number: BP661-10)
- 5. Biotinylated Wisteria Floribunda Agglutinin/Lectin (WFA/WFL) (Vector Laboratories, catalog number: B-1355)
- 6. Streptavidin, Alexa Fluor™ 555 Conjugate (Thermo Fisher, Invitrogen, catalog number:

S32355)

7. 4',6-Diamidino-2-Phenylindole, Dihydrochloride (DAPI) (Thermo Fisher, Life Tech, catalog number: D1306)
8. Mounting medium (Thermo Fisher, Invitrogen, catalog number: S36936)
9. Dimethyl sulfoxide (DMSO) (Sigma-Aldrich, catalog number: D8418)
10. ChABC (see Recipes)
11. PBS (see Recipes)
12. 4% PFA (see Recipes)
13. ACSF (standard ringer's ACSF for acute brain slices) (Papouin and Haydon, 2018, Tewari *et al.*, 2018) (see Recipes)
14. DAPI stock (see Recipes)

Equipment

1. Measurement pipettes (Gilson, catalog number: F123602)
2. Timer (from any commercial source)
3. Sterile empty glass vials, 30 ml (such as Hospire, catalog number: 5816-31)
4. Slice incubation assembly: assemble as shown in Figures 2B-2D
5. Bath heater (Fisher Scientific, model: Isotemp 205)
6. Peristaltic Perfusion pump (Gilson, model: mini-plus 3)
7. In-line heater (Warner instrument, catalog number: TC324B)
8. High resolution imaging microscope, such as Confocal microscope (Nikon Elements)
9. 95% O₂/5% CO₂ tank (such as AirGas)
10. -20 °C freezer (such as Norlake)

Software

1. Nikon NIS-Elements
2. Nikon NIS-Elements AR analysis
3. (Optional) Clampfit (Molecular Devices)
4. (Optional) Microsoft Excel/Origin (OriginLab)

Procedure

A. Structural integrity of PNNs in high-magnification images

1. Acquire high-magnification (40x objective lens with 5 digital zoom) multichannel (with PV or NeuN) single plane fluorescence images of individual PNNs in different experimental groups. The images should be taken from the optical plane that covers the largest perimeter of the cell.

2. Draw a manual/automated (depending on the used software) polyline along the periphery of the cell (stained with NeuN/PV) with PNN (Figures 1A and 1B, large images).
 - a. If using Nikon elements program, then use the auto ROI function to determine the perimeter of the cell followed by drawing a polyline along with this perimeter.
 - b. If using Fiji/ImageJ, use the freehand line tool to draw a line along the cell perimeter followed by clicking on “Analyze” then “Plot profile” buttons.
 - c. WFA peaks can be counted from the peak profile graph itself or numerical data for the plot profile can be exported to plot a graph in different software and count the peaks.
3. After establishing the line profile, the software generates a line profile graph that shows the fluoresce intensity of WFA along the line (Figures 1A and 1B, bottom panels). The line profile graph and its numerical data can be exported in a Microsoft Excel file that has length (in μm) and fluorescence intensity as x and y-axis respectively. Peaks can be counted either from this graph generated by the acquisition program (as shown in Figures 1A and 1B, lower panels) or data can be plotted in Excel/analysis software such as Sigma plot or Origin for peak counting and representation.
4. Mark and count the number of peaks in the line profile by setting a threshold of half the maximum intensity (Figures 1A-1B, lower panels). To determine the size of the biggest hole in the PNN, measure the distance between two consecutive peaks that appear to be farthest from each other (white double-headed arrows in lower panels in Figures 1A-1B). (Alternately, plot the data in Clampfit result window and save it as an .atf file. Open this file later and use the peak detection function to count the number of peaks. The parameters of peak detection function may detect few false peaks, which can be removed from the analysis. In addition, placing two cursors covering the gap and remarking the distance between them can be used to determine the size of the largest hole.)

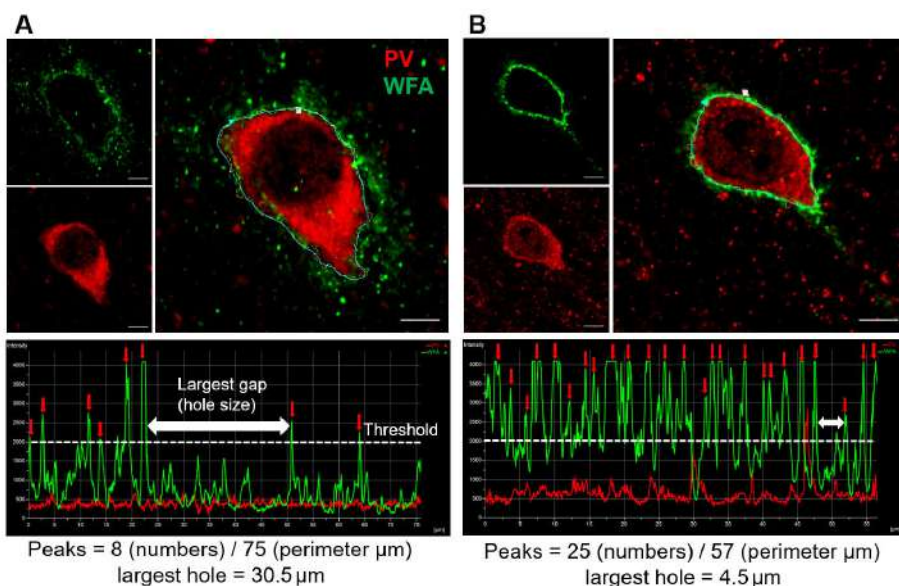


Figure 1. Analysis of WFA intensity peaks of PNN in two experimental conditions. A and

B. High magnification (40x objective lens with 5 digital zoom) immunohistochemical staining images of WFA (green), PV (red) and overlay (large images on the right) showing single PNN in the cerebral cortex of a mouse model of glioma-associated epilepsy (A), and corresponding sham control (B). The polyline (right) along the perimeter of the PV, encompasses WFA staining and shows discrete WFA intensity peaks (marked by red arrows) separated by low WFA intensity baseline. White dotted line indicates the threshold (Maximum WFA intensity/2) to determine the WFA intensity peak. The two-headed white arrows show the highest apparent distance between two consecutive WFA peaks and indicate the size of the largest holes in the PNN. The total number of peaks are divided by the perimeter to account for the different size of cells and their PNNs. Scale bars: 5 μ m.

B. Pre-experimental degradation of PNNs in brain slices

1. Prepare brain slices according to the standard brain slicing protocols and after completion of the recovery use for the experiments (Papouin and Haydon, 2018, Tewari *et al.*, 2018).
2. Prepare the slice incubation assembly using two glass vials; make two small holes on each cap to insert the inlet and outlet needles of carbogen gas supply. Insert an appropriate length piece of tube on the tip of needles to extend the gas supply close to the surface of the buffer. Do not dip these gas tubes into the solution (it can damage the slices).
3. Make one needle inlet by connecting it to the carbogen supplying tube and leave the other needle open to function as outlet (Figure 2B).
4. Next, fill 3 ml well-oxygenated ACSF in each vial and add ChABC stock to make a final concentration of 0.5 U/ml of ACSF in one of the vials labeled as treated.
5. Transfer 2-3 brain slices in each vial using a modified transfer pipette (cut the tip of transfer pipette to broaden the tip for the ease of slice transfer as shown in Figure 2C).
6. Set timer for 45 min from the time of ChABC addition and ensure that the carbogen gas supply through the inlet is working fine.
7. Place both the vials into a custom-made floating polystyrene foam (Figure 2D) that allows vials to stay straight while floating in the water bath during incubation.
8. Transfer both vials into the water bath, preset at 32 °C (Figure 2E).
9. On completion of 45 min incubation, carefully take out vials, rinse slices with ACSF, and transfer slices from both the vials back to the recovery chamber (Figure 2G). The slices can be used for experimentation now.
10. After completion of the experiment, carefully take out slices from the experimental setup and fix overnight with 4% PFA. Stain the fixed slices with WFA (and DAPI, if needed) to confirm the PNN degradation effect of ChABC as described in Procedure D.

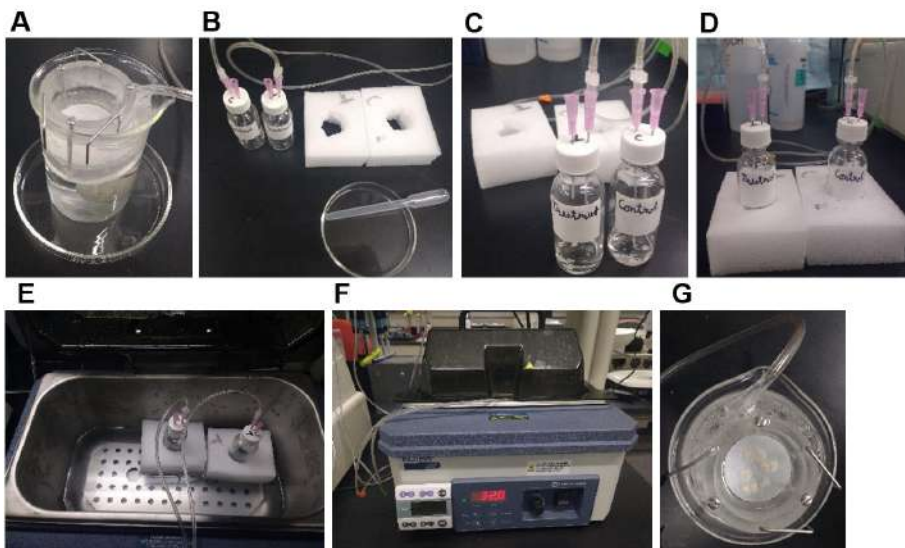


Figure 2. Degradation of PNNs in the acute brain slices using pre-experiment incubation method. A. Brain slice recovery chamber with cortical slices in the ACSF with continuous carbogen (95% O₂, 5% CO₂) bubbling. B. Fill the incubation vials (for control and ChABC-treated slices) with 3 ml ACSF (with/without ChABC) and assemble the carbogen gas supply tubes with an inlet and one outlet. C. Add 2-3 brain slices from (A) to each vial by modified transfer pipette (B on Petri dish) and subsequently insert the vials in the polystyrene foam to hold them straight in the water bath (E) while incubating at 32 °C for 45 min (F). G. On completion of incubation, transfer slices back into the recovery chamber at room temperature for experimental purposes.

C. PNN degradation during real time experimentation in brain slices

1. Record the baseline activity of cells/slices for 5-10 min (depending on the specific experiment) in the recording setup.
2. Superfuse 1 U/ml ChABC solution for 50 min while strictly maintaining the bath temperature at 32-33 °C (Figure 3A).
3. After 50 min of recording, perfuse ACSF again and record the activity in the presence of ACSF for 5-10 min (Figure 3B).
4. Stop the experiment and transfer slices to a 24-well plate and add 500 µl, 4% PFA to fix the slice and keep at room temperature for overnight.
5. Perform WFA staining next day as described in Procedure D.

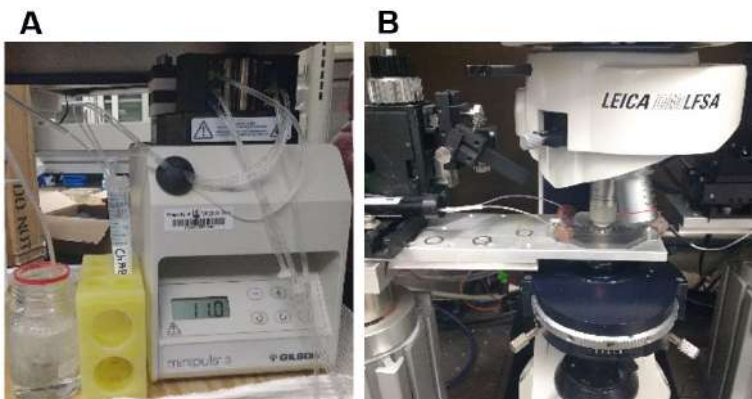


Figure 3. Degradation of PNNs in acute brain slices during real time data acquisition. A. ACSF containing ChABC with continuous carbogen bubbling is superfused and re-circulated at a speed of 2-3 ml/min to the experimental set-up using a peristaltic pump. B. Recording setup with an inline heater to keep the bath temperature constant at 32 °C.

D. WFA and DAPI staining in fixed acute brain slices

1. Rinse slices 4 times with PBS with 5 min interval between each wash.
2. Add 0.5 ml PBS that contains Biotinylated-WFA solution (1:300 in PBS), in each slice and incubate for 1 h at room temperature followed by 4 rinses with PBS at every 5 min interval.
3. Add 0.5 ml PBS that contains Streptavidin-conjugated Alexa fluor-555 solution (1:300 in PBS), in each slice and incubate for 1 h at room temperature followed by 4 rinses with PBS at every 5 min interval.
4. Incubate slices with PBS that contains DAPI (1:1,000 from 10 mg/ml stock in DMSO) for 4 min and rinse 3 times with PBS at every 5 min.
5. Mount slices in between 2 coverslips that allows user to access both the surfaces of the slice for imaging. Use mounting medium and do not press hard the coverslips to prevent tissue distortion.
6. Keep mounted tissue on a glass slide and take images of recorded cells/or regions of brain to confirm the degradation of PNNs.

Data analysis

1. PNN's structural integrity

Average the number of peaks/unit perimeter length of the cell. Use > 5 PNNs per mouse and pool data from all mice of the same experimental group. Compare the number of peaks in different experimental groups, apply appropriate statistical tests and plot the graph. Average the lengths of biggest gaps in the individual PNNs and pool data from all mice of the same experimental group. Compare the average size of holes (gap length) in different experimental groups, apply appropriate statistical tests, and plot the graph.

2. Confirmation of experimental PNN degradation

Take images from both sides of the slices using a fluorescence microscope. In case of pre-experimental degradation (Procedure B), both the surfaces of slice do not show any intact PNNs. However, magnified images show faint outlines of WFA around the PNN expressing cells (Inset image in Figure 4B). Only ACSF treated slices show intact PNNs (Figure 4A). In case of PNN degradation in experimental setup (Procedure C), only the top or exposed surface of slice shows the degradation effect of ChABC (Figure 4D). The high magnification images (20x) show faint outline of PNNs around the PNN expressing neurons (Inset image in Figure 4D). In case of whole cell patch clamp experiments, a traces dye can also be added to the pipette buffer to label the recorded cell, and presence of faint WFA outline around the recorded cells suggests that cells expressed PNN before the ChABC-treatment (Tewari *et al.*, 2018).

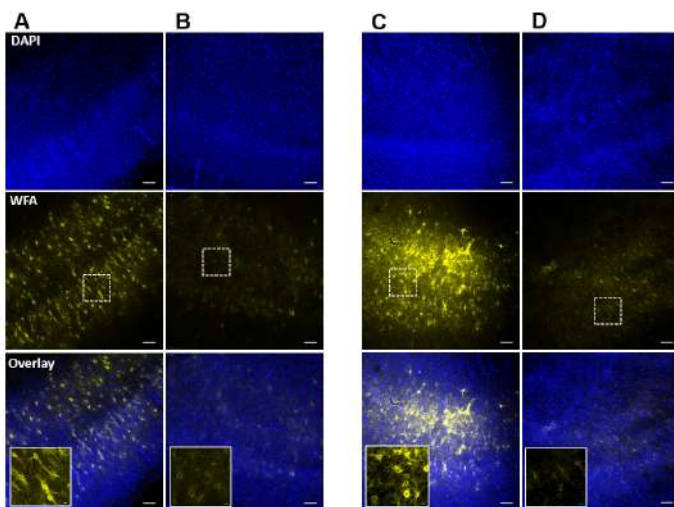


Figure 4. Confirmation of PNN degradation after ChABC-treatment of acute slices in incubation chamber and in recording setup. A and B. Confocal images of DAPI (top) and WFA (middle) fluorescence of acute cortical slices after post-experimental fixation from control (A), and ChABC-treated (B) groups. Inset images in overlay show the traces of controlled degradation of PNNs. C and D. Confocal images of DAPI (top) and WFA (middle) fluorescence from the ChABC-unexposed bottom surface (C), and ChABC-exposed top surface (D) of an acute brain slice in which PNNs were degraded in the experimental setup simultaneously with the experimental recording. The unexposed surface (C) shows relatively intact PNNs compared to the exposed surface (D), which shows degraded PNNs due to direct exposure of ChABC. Inset images in overlay are from the marked rectangular areas in the slices and show the traces of controlled PNN degradation. Scale bars: 100 μm in main images, 10 μm in inset images.

Notes

1. In Procedures B and C, bath temperature is crucial to maintain at 32-33 °C for reliable PNN degradation.

2. In Procedure B, the incubation time should not exceed 45 min otherwise; PNNs will be completely degraded making it difficult to find the traces of the degraded PNNs.
3. In Procedure C, recirculating the ChABC solutions into the recording setup is recommended to minimize the quantity of the enzyme.
4. In Procedure C, the total length of perfusion tubing for recirculation of ChABC should be kept minimum to reduce the time lag and the volume of total ChABC solution.
5. For more precise comparison of the change in function upon PNN degradation, brain slices can be cut into 2 halves separating the cerebral hemispheres and one half can be treated with ChABC and other can be used as a control.
6. For PNN's structural integrity analysis in immunohistochemistry (IHC), freely accessible software including ImageJ/Fiji can also be utilized, provided all the experimental groups are analyzed with the same software.
7. The high magnification images for PNNs structural integrity analysis should have the whole range of fluorescence signal with minimal saturation to minimize the variations in WFA intensity due to IHC procedure.

Recipes

1. ChABC
 - a. Reconstitute ChABC from *Proteus vulgaris* in a 0.01% BSA aqueous solution according to the manufacturer's instruction to make 1 U/40 µl stock solution
 - b. Prepare aliquots of 2 U and store at -20 °C until used
 - c. Just before experiment, add appropriate amount directly into the bubbling ACSF to make the working concentration
2. PBS
Dissolve PBS salts mixture in deionized water (DI) to make PBS solution
3. 4% PFA
Dilute the supplied 32% PFA to 1(PFA):7(PBS) to make 4% working solution
4. ACSF
Standard ringer's buffer (125 NaCl, 3 KCl, 1.25 NaH₂PO₄, 25 NaHCO₃, 2 CaCl₂, 1.3 MgSO₄, 25 glucose (all in mM); pH 7.3; 310 ± 5 mOsm) used for acute slice recordings (Tewari, Chaunsali *et al.*, 2018)
5. DAPI stock
Dissolve DAPI in DMSO to make 10 mg/ml stock and store at -20 °C until use

Acknowledgments

This work was supported by NIHRO1-NS036692, NIH-RO1-NS082851, and NIH-RO1-NS052634.

Competing interests

The authors declare no competing interests

Ethics

All animal procedures were approved and performed in accordance with the ethical guidelines set by Virginia Tech Institutional Animal Care and Use Committee (IACUC) under protocols 15-241 (02/11/2016-02/09/2019), 15-106 (07/31/2015-07/30/2018), and 18-126 (07/18/2018-07/15/2021).

References

1. Balmer, T. S. (2016). [Perineuronal nets enhance the excitability of fast-spiking neurons.](#) *eNeuro* 3(4): ENEURO.0112-16.2016.
2. Deepa, S. S., Carulli, D., Galtrey, C., Rhodes, K., Fukuda, J., Mikami, T., Sugahara, K. and Fawcett, J. W. (2006). [Composition of perineuronal net extracellular matrix in rat brain: a different disaccharide composition for the net-associated proteoglycans.](#) *J Biol Chem* 281(26): 17789-17800.
3. Dubey, D., McRae, P. A., Rankin-Gee, E. K., Baranov, E., Wandrey, L., Rogers, S. and Porter, B. E. (2017). [Increased metalloproteinase activity in the hippocampus following status epilepticus.](#) *Epilepsy Res* 132: 50-58.
4. Dityatev, A., Bruckner, G., Dityateva, G., Grosche, J., Kleene, R. and Schachner, M. (2007). [Activity-dependent formation and functions of chondroitin sulfate-rich extracellular matrix of perineuronal nets.](#) *Dev Neurobiol* 67(5): 570-588.
5. Favuzzi, E., Marques-Smith, A., Deogracias, R., Winterflood, C. M., Sanchez-Aguilera, A., Mantoan, L., Maeso, P., Fernandes, C., Ewers, H. and Rico, B. (2017). [Activity-dependent gating of parvalbumin interneuron function by the perineuronal net protein brevican.](#) *Neuron* 95(3): 639-655 e610.
6. Härtig, W., Derouiche, A., Welt, K., Brauer, K., Grosche, J., Mader, M., Reichenbach, A. and Bruckner, G. (1999). [Cortical neurons immunoreactive for the potassium channel Kv3.1b subunit are predominantly surrounded by perineuronal nets presumed as a buffering system for cations.](#) *Brain Res* 842(1): 15-29.
7. Lensjø, K. K., Christensen, A. C., Tennoe, S., Fyhn, M. and Hafting, T. (2017). [Differential expression and cell-type specificity of perineuronal nets in hippocampus, medial entorhinal cortex, and visual cortex examined in the rat and mouse.](#) *eNeuro* 4(3): ENEURO.0379-16.2017.
8. McRae, P. A., Baranov, E., Rogers, S. L. and Porter, B. E. (2012). [Persistent decrease in multiple components of the perineuronal net following status epilepticus.](#) *Eur J Neurosci* 36(11):

- 3471-3482.
9. Morawski, M., Reinert, T., Meyer-Klaucke, W., Wagner, F. E., Troger, W., Reinert, A., Jager, C., Bruckner, G. and Arendt, T. (2015). [Ion exchanger in the brain: Quantitative analysis of perineuronally fixed anionic binding sites suggests diffusion barriers with ion sorting properties.](#) *Sci Rep* 5: 16471.
 10. Papouin, T. and Haydon, P. G. (2018). [Obtaining acute brain slices.](#) *Bio Protoc* 8(2): e2699.
 11. Patel, D. C., Tewari, B. P., Chaunsali, L. and Sontheimer, H. (2019). [Neuron-glia interactions in the pathophysiology of epilepsy.](#) *Nat Rev Neurosci*. DOI: 10.1038/s41583-019-0126-4.
 12. Pizzorusso, T., Medini, P., Berardi, N., Chierzi, S., Fawcett, J. W. and Maffei, L. (2002). [Reactivation of ocular dominance plasticity in the adult visual cortex.](#) *Science* 298(5596): 1248-1251.
 13. Rankin-Gee, E. K., McRae, P. A., Baranov, E., Rogers, S., Wandrey, L. and Porter, B. E. (2015). [Perineuronal net degradation in epilepsy.](#) *Epilepsia* 56(7): 1124-1133.
 14. Slaker, M. L., Harkness, J. H. and Sorg, B. A. (2016). [A standardized and automated method of perineuronal net analysis using Wisteria floribunda agglutinin staining intensity.](#) *IBRO Rep* 1: 54-60.
 15. Slaker, M. L., Churchill, L., Todd, R. P., Blacktop, J. M., Zuloaga, D. G., Raber, J., Darling, R. A., Brown, T. E. and Sorg, B. A. (2015). [Removal of perineuronal nets in the medial prefrontal cortex impairs the acquisition and reconsolidation of a cocaine-induced conditioned place preference memory.](#) *J Neurosci* 35(10): 4190-4202.
 16. Testa, D., Prochiantz, A. and Di Nardo, A. A. (2019). [Perineuronal nets in brain physiology and disease.](#) *Semin Cell Dev Biol* 89: 125-135.
 17. Tewari, B. P., Chaunsali, L., Campbell, S. L., Patel, D. C., Goode, A. E. and Sontheimer, H. (2018). [Perineuronal nets decrease membrane capacitance of peritumoral fast spiking interneurons in a model of epilepsy.](#) *Nat Commun* 9(1): 4724.
 18. Ueno, H., Suemitsu, S., Murakami, S., Kitamura, N., Wani, K., Matsumoto, Y., Okamoto, M., Aoki, S. and Ishihara, T. (2018). [Juvenile stress induces behavioral change and affects perineuronal net formation in juvenile mice.](#) *BMC Neurosci* 19(1): 41.

Construction of Viral Vectors for Cell Type-specific CRISPR Gene Editing in the Adult Mouse Brain

Hiroshi Yamaguchi and Luis de Lecea*

Department of Psychiatry and Behavioral Sciences, Stanford University, Stanford, CA, 94305, USA

*For correspondence: llecea@stanford.edu



[Abstract] Recently developed gene editing technologies based on engineered CRISPR/Cas9 systems enables researchers to disrupt genes in a cell type-specific manner in the adult mouse brain. Using these technologies, we recently showed that the dopamine beta-hydroxylase gene in Locus Coeruleus (LC) norepinephrine neurons plays a vital role in the maintenance of wakefulness. Our method consists of four steps, (1) crossing Cre-dependent spCas9 knockin mice with a Cre-driver mouse line to express spCas9 in the target neural populations, (2) cloning of sgRNA, (3) construction of an AAV (adeno associated virus) vector expressing dual sgRNA, and (4) virus packaging and stereotaxic injection of the virus into the target brain area. Here, we describe a detailed protocol of AAV vector construction for cell type-specific CRISPR gene editing in the adult mouse brain. The method adopts a dual-sgRNA strategy for efficient disruption of the target gene. At first, a few different sgRNAs targeting the same gene are cloned into a plasmid expressing spCas9. After evaluation of the sgRNAs by a T7 endonuclease assay, the two most efficient sgRNAs are cloned in tandem into an AAV vector using the Gibson Assembly method.

Keywords: CRISPR/Cas9, AAV, Adult mouse brain, Gibson Assembly, dual-sgRNA

[Background] Interrogation of gene functions in specific cell subtypes in the brain remains a challenge. The conventional techniques such as RNAi-based methods lack cellular specificity and efficiency. On the other hand, recently developed gene editing techniques using the CRISPR/Cas9 system allows researchers efficient gene disruption in a cell type-specific manner. A research group led by Feng Zhang showed the disruption of multiple genes in the adult mouse brain by AAV-mediated delivery of sgRNA (Swiech *et al.*, 2015). Also, the group established cre-dependent spCas9 knockin mice (Platt *et al.*, 2014). In a recent study, we used an AAV vector carrying dual sgRNA to improve the efficiency of bi-allelic gene targeting (Yamaguchi *et al.*, 2018). We here describe a protocol for the construction of dual sgRNA AAV vector (Figure 1).

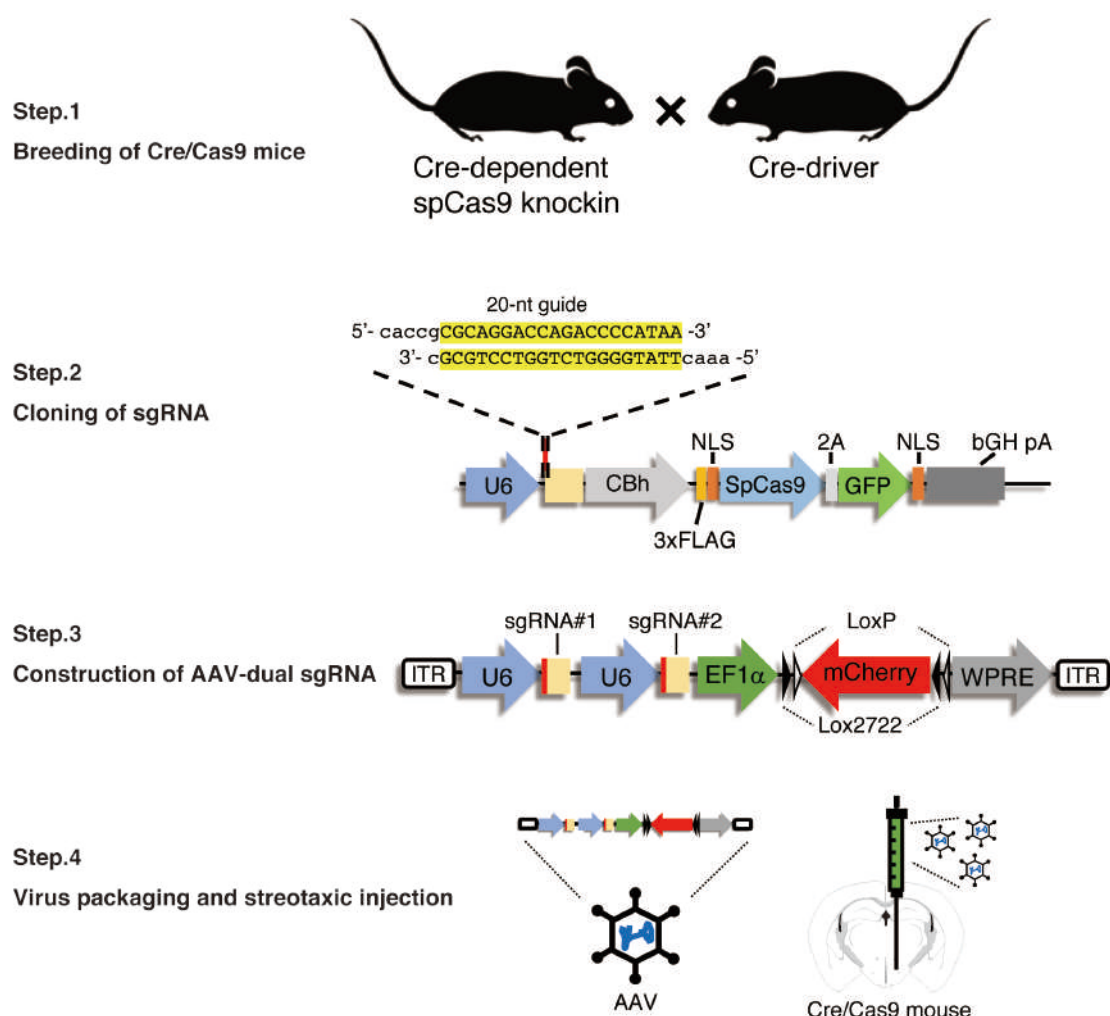


Figure 1. Schematic representation of all the procedure. Our method consists of four steps: (1) crossing Cre-dependent spCas9 knockin mice with a Cre-driver mouse line to express spCas9 in the target neural populations, (2) cloning of sgRNA into the spCas9 expressing plasmid, (3) construction of an AAV vector tandemly expressing dual sgRNA, and (4) AAV packaging and stereotaxic viral injection into the target brain area.

Materials and Reagents

1. Pipette tips
2. 24-well plate (coated) (Thermo Fisher Scientific, catalog number: 142475)
3. 1 ml plastic tube
4. NEB10-beta Competent *E. coli* (New England Biolabs, catalog number: C3019)
5. pX458 (Addgene, catalog number: 48138)
6. pAAV EF1 α DIO mCherry (Addgene, catalog number: 20299)
7. BbsI-HF (New England Biolabs, catalog number: R3539)
8. MluI-HF (New England Biolabs, catalog number: R3198)
9. DpnI (New England Biolabs, catalog number: R0176)

10. Alkaline Phosphatase, Calf Intestinal (CIP) (New England Biolabs, catalog number: M0290)
11. Guide oligonucleotides (see Procedure A)
12. Quick ligation kit (New England Biolabs, catalog number: M2200)
13. Gibson Assembly Master Mix (New England Biolabs, catalog number: E2611)
14. PrimeSTAR HS DNA polymerase (Takara, catalog number: R010)
15. dNTP Mix 10 mM each (the mix of 10 mM of dTTP, dCTP, dGTP and dATP) (GenScript, catalog number: C01689)
16. QIAquick Gel Extraction kit (QIAGEN, catalog number: 28704)
17. QIAprep Spin Miniprep kit (QIAGEN, catalog number: 27104)
18. Tris-EDTA, (1x Solution) (Fisher BioReagents, catalog number: BP2473)
19. LB Broth EZMix Powder (Sigma, catalog number: L7658)
20. LB Agar (Fisher BioReagents, catalog number: BP1425)
21. Ampicillin (Gemini Bio-Products, catalog number: 400-130P)
22. Primer to verify the cloning of sgRNA into pX458: 5'-gactatcatatgcttaccgt-3'
23. Primer to verify the tandem cloning of sgRNAs into pAAV: 5'-actgacgggcaccggagcca-3'
24. Primers for Gibson Assembly:
Primer S1: 5'-taggggttcctgcggccgcacgcgtgagggcatttc-3'
Primer AS1: 5'-ataggccctctctagaaaaaaagcaccgactc-3'
Primer S2: 5'-ttttcttagagagggcatttcccattg-3'
Primer AS2: 5'-atccatttgcaaagcttacgcgtaaaaaagcaccgac-3'

Optional (see Procedure C)

25. NIH3T3 cell (ATCC, catalog number: CRL-1658)
26. AAV vector (pX458-sgRNA or pX458 empty as negative control)
27. Primers: You can design the primers to amplify the target exons by CHOPCHOP (see Procedure C)
28. PrimeSTAR HS DNA polymerase
29. FuGENE6 Transfection Reagent (Promega, catalog number: E2693)
30. DMEM (1x) (Gibco, catalog number: 11995-065)
31. Fetal Bovine Serum (Corning, catalog number: 35-015-CV)
32. Penicillin/Streptomycin (Gibco, catalog number: 15070-063)
33. PBS, pH 7.4 (Gibco, catalog number: 10010-023)
34. TrypLE Select (1x) (Gibco, catalog number: 12563-011)
35. QuickExtract DNA Extraction Solution (Epicentre, catalog number: QE0905T)
36. T7 Endonuclease I (New England Biolabs, catalog number: M0302)

Equipment

1. Pipettes (Gilson, Pipetman classic P10, P20, P200)
2. Centrifuge (Eppendorf, Centrifuge 5424)
3. Incubator (VWR, incubating 5000IR orbital shaker)
4. Thermocycler (Applied Biosystems, GeneAmp PCR system 2700)
5. Electrophoresis chamber (Labnet, ENDURO GEL XL)
6. (Optional) CO₂ Incubator (Binder, CB 170)
7. (Optional) Clean bench (Labconco, Purifier classII biosafety cabinet)
8. (Optional) Centrifugation (Thermo Scientific, Soryall legend XTR)

Procedure

A. Design of sgRNA

Single guide RNAs (sgRNAs) with high efficiency and specificity can be designed by using gRNA design webtools. We recommend CHOPCHOP (<http://chopchop.cbu.uib.no>) because of its user-friendly interface (Labun *et al.*, 2016). Also, you may find the guide design resources on the website of Feng Zhang's lab (<https://zlab.bio/guide-design-resources>). The sgRNA should target early exons (near transcriptional start site) or essential exons of gene function. We usually choose 4 to 6 target sites on early exons which do not have the start codon because frameshift mutations near the start codon can lead to translation from other in-frame ATGs, resulting in the expression of a functional protein. If the target sequence is 5'-CGCAGGACCAGACCCATAATGG-3' [Protospacer adjacent motif (PAM) is labeled in blue], synthesize 5'-caccgCGCAGGACCAGACCCATAA-3' (sense) and 5'-aaacTTATGGGTCTGGTCCTGCGc-3' (anti-sense) to clone the guide sequence into pX458 (Ran *et al.*, 2013) sgRNA scaffold (Figure 3A). cacc (lower case) in the first oligo and aaac (lower case) in the second oligo are overhangs for cloning into BbsI-site in pX458. We also add "g" between cacc and the target sequence in the first oligo because the human U6 promoter prefers "g" at the transcription start site for strong expression. Also, you may design primers using CHOPCHOP to amplify the target site for further evaluation of sgRNAs using the T7 endonuclease I assay (see Procedure C).

B. Cloning of sgRNAs into the spCas9 expressing plasmid (pX458)

1. Digestion of pX458 with BbsI:

X µl	pX458 (10 µg)
5 µl	10x NEB cut smart
1 µl	BbsI-HF
24 - X µl	MilliQ water
30 µl	in total

2. Incubate at 37 °C overnight.

3. Gel purify the plasmid using QIAquick Gel extraction kit. Elute the plasmid with 50 μ l of 1x Tris-EDTA buffer.
 4. Annealing of oligonucleotides encoding sgRNAs:

1 μ l	oligonucleotide, sense (100 μ M)
1 μ l	oligonucleotide, antisense (100 μ M)
8 μ l	1x Tris-EDTA buffer
10 μ l	in total
 5. Incubate at 95 °C for 5 min. Then cool down to room temperature by switching off the thermocycler (30 min).
 6. Prepare the ligation reaction as following:

1 μ l	diluted (1:100 with 1x Tris-EDTA buffer) annealed oligonucleotides
1 μ l	BbsI-digested pX458 (50 ng/ μ l)
5 μ l	2x ligation buffer
1 μ l	Quick ligase
2 μ l	MilliQ water
10 μ l	in total
 7. Incubate at room temperature for 10 min.
 8. Add 5 μ l of the ligation reaction to 50 μ l of NEB10-beta.
 9. Next place on ice for 10 min.
 10. Heat shock at 42 °C for 30 s.
 11. Transfer onto ice for 3 min.
 12. Plate the reaction on an LB-Agar plate containing ampicillin (50 μ g/ml).
 13. Incubate at 37 °C overnight.
 14. Inoculate 2 ml LB broth containing ampicillin (50 μ g/ml) from a single colony and incubate at 37 °C overnight with agitation.
- Note: 60-70% of colonies have a correct insertion in our experience.*
15. Purify the plasmid from 1 ml of the overnight culture using QIAprep Spin Miniprep kit.
Elute the plasmid with 50 μ l of buffer EB and determine the concentration
 16. Verify the plasmid by sequencing with a primer (5'-gactatcatatgcttaccgt-3').

C. (Optional) Evaluation of sgRNA by T7 endonuclease I assay

1. Plate NIH3T3 cells at the density of 2.5×10^4 cells (500 μ l/well, DMEM/10% FBS/1% Penicillin /1% Streptomycin) onto a well of 24-well plate.
2. Incubate in a 37 °C CO₂ incubator overnight.
3. Transfection
 - a. Add 1.5 μ l of FuGENE6 reagent to 50 μ l of serum-free DMEM in a 1 ml plastic tube and mix by vortexing.
 - b. Incubate the mixture for 5 min at room temperature.
 - c. Add 0.5 μ g of pX458-sgRNA or control vector to the mixture and mix by vortexing.

- d. Incubate the mixture for 30 min at room temperature.
- e. Add the mixture to each well of a 24-well plate containing cells.
- f. Incubate in a 37 °C CO₂ incubator for 24 h.
- g. Replace the cell culture media with fresh one (DMEM/10% FBS/1% Penicillin /1% Streptomycin).
- h. Repeat Steps C3d-C3e.

Note: Repeated transfection is essential for high expression of Cas9 and sgRNA to edit the target gene in NIH3T3 cells.

- i. Incubate in a 37 °C CO₂ incubator for 48 h.
4. Remove the supernatant of cells by pipetting and wash cells with 500 µl of 1x PBS.
5. Add 100 µl of QuickExtract to each well and collect the lysate containing genomic DNA to a 1 ml plastic tube.
6. Incubate at 65 °C for 15 min and then at 98 °C for 10 min.
7. Centrifuge at 20,000 × g for 10 min.
8. Collect 60 µl of the supernatant (can be stored at -20 °C).
9. PCR to amplify 200-300 bp fragments around the CRISPR binding site. The primers can be designed by CHOPCHOP.

6 µl	lysate
1.5 µl	dNTP (the mixture of dTTP, dCTP, dGTP and dATP, each at a final concentration of 10 mM)
12 µl	5x buffer
1.5 µl	primer S (10 µM)
1.5 µl	primer AS (10 µM)
1 µl	PrimeSTAR HS DNA polymerase
36.5 µl	MilliQ water
60 µl	in total

10. Start PCR with the following settings:
 - a. Denaturation at 95 °C for 2 min.
 - b. 35 cycles of
 - 95 °C for 10 s
 - 55 °C for 5 s
 - 72 °C for 45 s
 - c. Final elongation at 72 °C for 2 min.
 - d. Store at 4 °C.
11. Gel purify PCR product using QIAquick Gel extraction kit. Elute PCR product with 50 µl of buffer EB.
 - a. Denaturarion and annealing of PCR product:

5 µl	PCR product (200 ng)
2 µl	10x NEB buffer 2

- 12 μ l MilliQ water
19 μ l in total
b 95 °C for 5 min.
c Cool down to room temperature by switching off the thermocycler (30 min).
12. Add 1 μ l of diluted (1:5) T7 endonuclease I (2.5 U/ μ l).
- Note: Dilution of T7 endonuclease I is essential because an excess amount of the enzyme will result in non-specific cleavage of DNA.*
13. Incubate at 37 °C for 30 min.
14. Run on 2% agarose gel and verify bands in sgRNA transfected-wells compared with control wells (Figure 2).

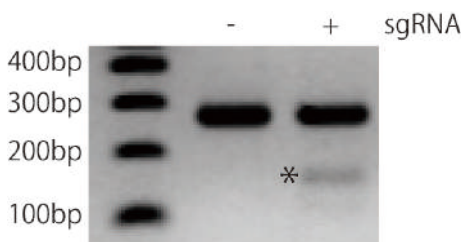


Figure 2. Agarose gel electrophoresis of T7 endonuclease I-digested PCR products derived from NIH3T3 cells transfected with sgRNA and Cas9. The target exon was PCR-amplified and gel purified. After the denaturation and annealing, the PCR product was digested by T7 endonuclease I and run on 2% agarose gel. The asterisk indicates cleaved DNA fragment. In this experiment, we found only one shorter fragment. However, you may find bands of two different sizes after the cleavage if you carefully design the primers. It can be useful to design PCR primers such that the indel resulting from genome editing is not in the middle of the amplicon, ultimately resulting in two cleaved bands of different sizes.

You can quantify the efficiency of gene modification based on the result of T7 endonuclease I assay. The percentage of cleavage on a gel could be converted to the percentage of gene modification by using an equation below.

$$\% \text{ gene modification} = 100 \times (1 - (1 - \text{fraction cleaved})^{1/2}) \text{ (Guschin et al., 2010)}$$

Also, you may evaluate the efficiency of gene editing by a webtool called Synthego's ICE (<https://ice.synthego.com/#/>). Target exons from edited or unedited (control) cells are PCR-amplified and Sanger sequenced. You may submit the results of sequencing to the webtool and ICE compares these sequence traces to give a detailed analysis of gene editing.

D. Tandem cloning of two sgRNAs into pAAV EF1 α DIO mCherry

In Procedure A, you clone several sgRNAs targeting the same gene. For the efficient gene disruption, you tandemly clone two different sgRNAs driven by independent human U6 promoters into an AAV vector (Figures 3B and 3C) using the Gibson Assembly method.

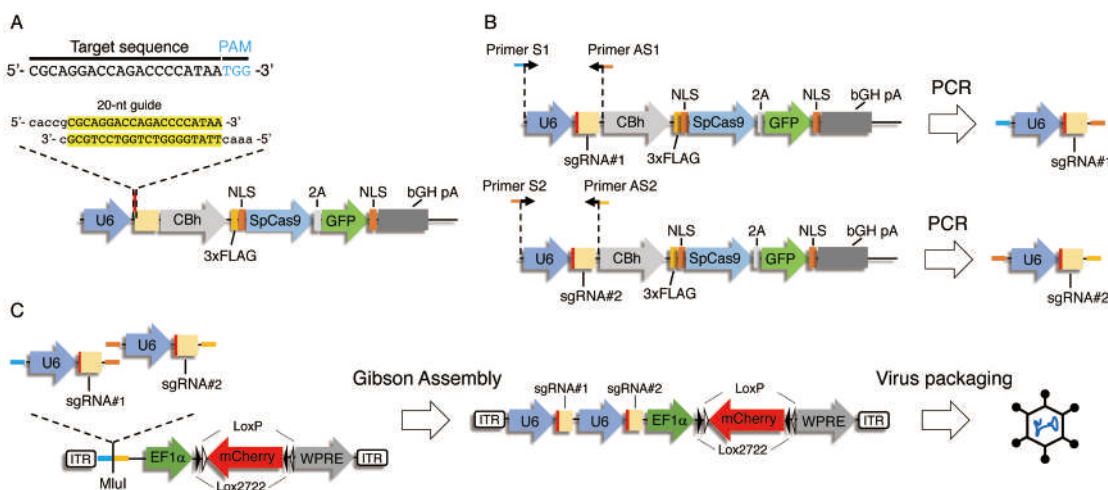


Figure 3. Construction strategy of a dual sgRNA viral vector. A. Cloning of guide oligonucleotides. Oligonucleotides with 20-nt guide sequence and overhangs for cloning into BbsI site in pX458 were annealed and cloned into BbsI-digested pX458. B. Cloning of U6 promoter-driven sgRNAs. U6 promoter followed by sgRNA1 or sgRNA2 were PCR amplified, respectively, by using primers with overhangs for Gibson Assembly. C. Gibson Assembly of the dual sgRNA virus vector. U6-gRNA1 and U6-gRNA2 were cloned into MluI-digested pAAV EF1 α DIO mCherry using Gibson Assembly.

1. Digestion, dephosphorylation and purification of pAAV EF1 α DIO mCherry with MluI.

a. Digestion:

X μ l	pAAV EF1 α DIO mCherry (10 μ g)
5 μ l	10x NEB cut smart
1 μ l	MluI-HF
24 - X μ l	MilliQ water
30 μ l	in total

b. Incubate at 37 °C overnight.

c. Add 1 μ l of CIP, and then incubate at 37 °C for 60 min.

d. Gel purify the plasmid using QIAquick Gel extraction kit.

e. Elute the plasmid with 50 μ l of buffer EB.

2. Amplification of U6 promoter plus sgRNA#1 or sgRNA#2.

a. PCR reaction#1 (Expected size is 393 bp):

3 μ l	pX458-sgRNA#1 (10 ng/ μ l)
1.5 μ l	dNTP, 10 mM each
12 μ l	5x buffer

- 1.5 µl primer S1 (10 µM); 5'- taggggttcctgcggccgacgcgtgagggcctattc -3'
1.5 µl primer AS1 (10 µM); 5'- ataggccctctagaaaaaaagcaccgactc -3'
1 µl PrimeSTAR HS DNA polymerase
39.5 µl MilliQ water
60 µl in total
- b. PCR reaction#2 (Expected size is 388 bp):
- 3 µl pX458-sgRNA#2 (10 ng/µl)
1.5 µl dNTP, 10 mM
12 µl 5x buffer
1.5 µl primer S2 (10 µM); 5'- ttttcttagagagggcctattccatg -3'
1.5 µl primer AS2 (10 µM); 5'- atccatcttgcaaagctacgcgtaaaaaagcaccgac -3'
1 µl PrimeSTAR HS DNA polymerase
39.5 µl MilliQ water
60 µl in total
3. Start PCR with the following settings.
- Denaturation at 95 °C for 2 min.
 - 35 cycles of
 - 95 °C for 10 s
 - 62 °C for 5 s
 - 72 °C for 45 s
 - Final elongatation at 72 °C for 2 min.
 - Store at 4 °C.
4. Run on a 2% agarose gel.
5. Gel purify the PCR product using QIAquick Gel extraction kit. Elute the PCR product with 50 µl of MilliQ water.
6. Digestion of the residual template plasmid:
- 45 µl PCR amplicon#1 or #2
5 µl 10x NEB cut smart
1 µl DpnI
51 µl in total
7. Incubate at 37 °C for 30 min, 80 °C for 30 min.
8. Gibson assembly:
- 1 µl CIP-treated MluI-digested pAAV EF1α DIO mCherry (100 ng/µl)
3 µl PCR amplicon#1
3 µl PCR amplicon#2
3 µl MilliQ water
10 µl Gibson Assembly mix
20 µl in total
9. Incubate at 50 °C for 15 min.

10. Add 2 µl of ligation reaction to 50 µl of NEB10-beta.
11. Follow Steps B9-B15.
12. Verify the plasmid by sequencing with a primer (e.g., 5'-actgacgggcaccggagcca-3').
13. Proceed to virus packaging.
Note: We usually request virus packaging services from [Stanford Neuroscience Gene Vector and Virus core](#).
14. Keep the virus stock at -80 °C.
Note: This strategy can disrupt genes in a cell type-specific manner. You can use the virus not only for adult mouse brain but also other organs.

Recipes

All materials and reagents are commercially available.

Acknowledgments

H.Y. was supported by Uehara memorial foundation research fellowship. L.d.L was supported by National Institute of Health Grants AG047671, MH087592, MH102638. This protocol was adapted from Yamaguchi *et al.* (2018) and includes a recent improvement of the method of our lab.

Competing interests

The authors declare no competing financial interests.

References

1. Labun, K., Montague, T. G., Gagnon, J. A., Thyme, S. B. and Valen, E. (2016). [CHOPCHOP v2: a web tool for the next generation of CRISPR genome engineering](#). *Nucleic Acids Res* 44(W1): W272-276.
2. Platt, R. J., Chen, S., Zhou, Y., Yim, M. J., Swiech, L., Kempton, H. R., Dahlman, J. E., Parnas, O., Eisenhaure, T. M., Jovanovic, M., Graham, D. B., Jhunjhunwala, S., Heidenreich, M., Xavier, R. J., Langer, R., Anderson, D. G., Hacohen, N., Regev, A., Feng, G., Sharp, P. A. and Zhang, F. (2014). [CRISPR-Cas9 knockin mice for genome editing and cancer modeling](#). *Cell* 159(2): 440-455.
3. Ran, F. A., Hsu, P. D., Wright, J., Agarwala, V., Scott, D. A. and Zhang, F. (2013). [Genome engineering using the CRISPR-Cas9 system](#). *Nat Protoc* 8(11): 2281-2308.
4. Swiech, L., Heidenreich, M., Banerjee, A., Habib, N., Li, Y., Trombetta, J., Sur, M. and Zhang, F. (2015). [In vivo interrogation of gene function in the mammalian brain using CRISPR-Cas9](#). *Nat Biotechnol* 33(1): 102-106.

5. Yamaguchi, H., Hopf, F. W., Li, S. B. and de Lecea, L. (2018). [*In vivo* cell type-specific CRISPR knockdown of dopamine beta hydroxylase reduces locus coeruleus evoked wakefulness.](#) *Nat Commun* 9(1): 5211.
6. Guschin, D. Y., Waite, A. J., Katibah, G. E., Miller, J. C., Holmes, M. C. and Rebar, E. J. (2010). [A rapid and general assay for monitoring endogenous gene modification.](#) *Methods Mol Biol* 649: 247-256.

Explant Culture of the Embryonic Mouse Spinal Cord and Gene Transfer by *ex vivo* Electroporation

Mariko Kinoshita-Kawada^{1, 2, 3}, Hiroshi Hasegawa^{4, 5}, Tsunaki Hongu^{4, 6}, Shigeru Yanagi⁷, Yasunori Kanaho⁴, Ichiro Masai², Takayasu Mishima¹, Xiaoping Chen³, Yoshio Tsuboi¹, Yi Rao^{8, 9}, Junichi Yuasa-Kawada^{1, 2, 3, 10, *} and Jane Y. Wu^{3, *}

¹Department of Neurology, Faculty of Medicine, Fukuoka University, Fukuoka, Japan; ²Developmental Neurobiology Unit, Okinawa Institute of Science and Technology Graduate University, Onna, Okinawa, Japan; ³Department of Neurology, Lurie Comprehensive Cancer Center, Northwestern University Feinberg School of Medicine, Chicago, IL, USA; ⁴Department of Physiological Chemistry, Faculty of Medicine and Graduate School of Comprehensive Human Sciences, University of Tsukuba, Tsukuba, Ibaraki, Japan; ⁵Department of Hygienic Sciences, Kobe Pharmaceutical University, Kobe, Japan; ⁶Heidelberg Institute for Stem Cell Technology and Experimental Medicine, German Cancer Research Center, Heidelberg, Germany; ⁷Laboratory of Molecular Biochemistry, School of Life Sciences, Tokyo University of Pharmacy and Life Sciences, Hachioji, Tokyo, Japan; ⁸Peking-Tsinghua Center for Life Sciences, PKU-IDG/McGovern Institute for Brain Research, Peking University School of Life Sciences, Beijing, China; ⁹Chinese Institute for Brain Research, Beijing, China; ¹⁰Center for Advanced Medical Innovation, Kyushu University, Fukuoka, Japan

*For correspondence: jkawada@fukuoka-u.ac.jp; jane-wu@northwestern.edu



[Abstract] Developing axons change responsiveness to guidance cues during the journey to synapse with target cells. Axon crossing at the ventral midline serves as a model for studying how axons accomplish such a switch in their response. Although primary neuron culture has been a versatile technique for elucidating various developmental mechanisms, many *in vivo* characteristics of neurons, such as long axon-extending abilities and axonal compartments, are not thoroughly preserved. In explant cultures, such properties of differentiated neurons and tissue architecture are maintained. To examine how the midline repellent Slit regulated the distribution of the Robo receptor in spinal cord commissural axons upon midline crossing and whether Robo trafficking machinery was a determinant of midline crossing, novel explant culture systems were developed. We have combined an “open-book” spinal cord explant method with that devised for flat-mount retinae. Here we present our protocol for explant culture of embryonic mouse spinal cords, which allows flexible manipulation of experimental conditions, immunostaining of extending axons and quantitative analysis of individual axons. In addition, we present a modified method that combines *ex vivo* electroporation and “closed-book” spinal cord explant culture. These culture systems provide new platforms for detailed analysis of axon guidance, by adapting gene knockdown, knockout and genome editing.

Keywords: Explant culture, Spinal cord, Mouse embryos, Midline, Floor plate, Commissural axons, Axon guidance, Gene knockdown

[Background] Growing axons sense numerous extracellular cues to reach their final target cells (Stoeckli, 2018). At intermediate targets on the way to the destination, axons timely switch on/off responses to guidance cues. Molecular mechanisms underlying this switch have been a hot topic in neurobiology (Guan and Rao, 2003; Sabatier *et al.*, 2004; Dickson and Zou, 2010; Kolodkin and Tessier-Lavigne, 2011; Stoeckli, 2018; Yang *et al.*, 2018; Duccing *et al.*, 2019).

The ventral midline of the central nervous system is an important intermediate target for different types of axons. Floor plate (FP) cells at the ventral midline secrete short- and long-range guidance cues, which act as attractants or repellents, and spatiotemporally organize the formation of neural circuits. Commissural axons project across the midline, connect the left and right sides of the nervous system and play roles in information transfer between both sides (Figures 1A and 1B). Commissural axons are initially guided to the midline by attractants derived from the FP and ventricular zones, such as netrin-1 and Sonic hedgehog (Dominici *et al.*, 2017; Varadarajan *et al.*, 2017; Moreno-Bravo *et al.*, 2019; Wu *et al.*, 2019). At the midline, commissural axons lose their responsiveness to the attractants and acquire responsiveness to repellents, such as Slit and semaphorins (Shirasaki *et al.*, 1998; Zou *et al.*, 2000). Thus, the midline is initially an attractive target for commissural axons, but becomes an unfavorable place upon their arrival, so that commissural axons exit the midline and never re-cross it. What mechanism ensures that commissural axons cross the midline only once? One key is the molecular basis by which commissural axons increase Slit sensitivity upon midline crossing.

Here we will summarize how spinal cord explant cultures have contributed to our understanding of axon guidance. The landmark research using explants showed that FP cells produce chemoattractant activity for commissural axons (Tessier-Lavigne *et al.*, 1988). Two-dimensional co-culture assays using explants of commissural neurons and the FP revealed the presence of unknown midline repellent activity, which is unmasked by inhibiting either axonin-1/TAG-1 (a cell adhesion molecule [CAM] expressed in commissural axons) or NrCAM (expressed in FP cells) (Stoeckli *et al.*, 1997). When Slit was identified as a ligand for Robo receptor and a long-awaited midline repellent (Brose *et al.*, 1999; Kidd *et al.*, 1999; Li *et al.*, 1999), its repellent activity for vertebrate commissural axons was not clarified. But soon later, ingenious assay systems using FP-containing and FP-lacking spinal cord explants embedded in collagen gel revealed that Slit inhibits outgrowth of commissural axons that have crossed the midline (post-crossing axons), but not pre-crossing axons (Zou *et al.*, 2000). This was the first demonstration that Slit is an evolutionarily conserved midline repellent.

To examine how Slit sensitivity of commissural axons was regulated, we established a primary culture system (Kinoshita-Kawada *et al.*, 2019; Yuasa-Kawada *et al.*, 2009). Commissural neurons dissociated from dorsal spinal cords of mouse embryos at post-crossing stages (embryonic day [E]11.5-12.5) exhibit growth cone collapse and the increase in axonal Robo1 levels in response to Slit. In contrast, commissural neurons harvested from pre-crossing stage embryos show neither collapse responses to Slit nor the Slit-induced increase in axonal Robo1. Therefore, even without FP cells, dissociated commissural neurons recapitulate *in vivo* behaviors, with respect to the acquisition of Slit responsiveness. We then sought to develop an explant assay to examine Slit-induced Robo redistribution and growth cone responses in individual axons (or small fascicles) in a more

physiological context, with subcellular resolution. Unfortunately, it was difficult to use so far developed explant assays for such purposes, because axons tended to form vigorous bundles in collagen gel.

To study retinotectal topography, Drs. Friedrich Bonhoeffer, Uli Schwarz and colleagues developed retinal explant culture systems; a large mass of embryonic retinae were flat-mounted onto nitrocellulose (NC) filters and placed on the tectal cell membrane carpets, allowing robust extension of retinal axons (Halfter *et al.*, 1981 and 1983; Bonhoeffer and Huf, 1982; Walter *et al.*, 1987a and 1987b; Ichijo and Bonhoeffer, 1998; Yuasa-Kawada *et al.*, 2003). By combining these protocols with spinal cord explant techniques (Zou *et al.*, 2000), we prepared FP-lacking dorsal spinal cord [dSC (-FP)] and FP-containing hemisected spinal cord [SC (+FP)] explants (from cervical to lumbar levels) from E11.5 embryos and spread them on NC filters. Such explants were cultured on the Matrigel-coated substratum (Figures 1C-1G). Under these conditions, individual axons robustly extended from explants onto the two-dimensional surface, even without netrin-1, a stimulator of commissural axon growth. In both explant types, the extending axons were negative for TAG-1, a pre-crossing commissural axon marker but positive for L1, a post-crossing commissural axon marker (Dodd *et al.*, 1988), maintaining the characteristics of post-crossing axons (Figure 3). These explant cultures allow simple immunostaining protocols and testing effects of Slit alone on Robo distribution (Kinoshita-Kawada *et al.*, 2019).

Furthermore, to perform RNA interference (RNAi) against transducers of Slit-Robo signals, Arf6 GTPase and cytohesin Arf-guanine nucleotide exchange factors (Arf-GEFs), we modified an RNAi-based assay that combines *ex utero* electroporation with spinal cord explant culture (Wolf *et al.*, 2008; Parra and Zou, 2010). Because the spinal cord, especially the FP region, becomes too fragile to prepare open-book explants after electroporation, we developed a new culture system of intact, "closed-book" spinal cords embedded in collagen gel (Kinoshita-Kawada *et al.*, 2019) (Figures 2A-2D). The combination of these culture systems with RNAi-mediated knockdown or clustered regularly interspaced short palindromic repeats (CRISPR)-based genome editing, introduced by electroporation, virus or nanocomplex (e.g., Mikuni *et al.*, 2016; Nishiyama *et al.*, 2017; Park *et al.*, 2019), will allow more flexibility to manipulate experimental conditions and to tag endogenous proteins. Such techniques will contribute to the elucidation of molecular mechanisms of axon guidance.

Materials and Reagents

A. Animals

Pregnant ICR or C57BL/6J strain mice with embryonic day [E]~11.5 embryos

Note: We usually use 1-2 pregnant mice for each experiment. We assume an average of 6-12 embryos per ICR mouse and 4-8 embryos per C57BL/6J mouse. For timed-pregnancy mating, the day of vaginal plug was dated as E0.5, and embryos were staged according to EMAP (<http://www.emouseatlas.org/emap/ema/home.php>). In our hands, in terms of axon growth onto the Matrigel-coated substratum and the ease of handling, the best results have been obtained with embryos between E11.0 and E11.5, in order to prepare dSC (-FP) and SC (+FP) explants. At least, it is better to use embryos before E12.0 than later stages. For use of knockout mice, we prepare

explants from littermate embryos, in parallel with genotyping. Image acquisition and analysis can be performed in a blinded manner. For ex vivo electroporation and closed-book explant culture, we recommend using ICR mouse embryos just before E11.5, with respect to the efficient introduction of axon-tracer plasmid/shRNA to commissural neurons prior to axon midline crossing and the maintenance of tissue integrity.

B. Surgical instruments and materials

1. Scissors, large
2. Scissors, medium
3. Ophthalmic scissors (option) (Natsume Seisakusho, catalog number: MB-50-7)
4. Forceps (7) (Dumont, No. 5 Inox)

Note: We use relatively blunt forceps (a total of 5; 1 for handling coverslips, 2 for mouse surgery and 2 for spinal cord dissection) and sharpened forceps for fine dissection (2).

5. Straight metal spatula, with polished edges
6. Disposable scalpel (Feather, No. 11)
7. Sharpened tungsten needles, bent at a right angle (tungsten wire, diameter: 0.20 mm; Nilaco, catalog number: W-461267) and needle holders (Fine Science Tools, catalog number: 26016-12) (see Figure 1H).

Note: At the tip, the diameter should be approximately 20 µm. The needles can be sharpened in a 1 N NaOH bath by putting the negative electrode of a power supply (low voltage should be set) into the bath and the positive electrode (alligator clip) onto the end of needle holder. Dip in/out the needle tip to make a pointed, tapered tip. See the Recipe “Sharpened tungsten needles” in Cold Spring Harb Protoc (doi:10.1101/pdb.rec069468).

8. Disposable transfer pipettes, 3.5 ml (Sarstedt, catalog number: 86.1171.001) or equivalent (approximately 15 cm in length, with an inner diameter of 2 mm)

Note: When handling whole spinal cords, use cut pipettes, which have opening of approximately 4-5 mm. When handling excised, tiny spinal cord explants, we usually use un-cut pipettes.

9. Acid-washed, sterilized, round coverslips (18 mm in diameter; Matsunami, thickness: No. 1; for preparing the coverslips, see Recipe 1)
10. Black nitrocellulose (NC) membrane filter (gridded on one surface, single-packed and sterile) (Sartorius, Cellulose nitrate filter, catalog number: 13006--47---CAN)
11. Glass slides (Matsunami, Superfrost, catalog number: S2443)
12. 70% Ethanol

C. Culture products

1. 35-mm sterile tissue culture dishes (Corning, Falcon, catalog number: 353001)
2. 60-mm sterile tissue culture dishes (Corning, Falcon, catalog number: 353004)
3. 100-mm sterile tissue culture dishes (Corning, Falcon, catalog number: 353003)

4. 15-ml conical centrifuge tubes (Thermo Fisher Scientific, catalog number: 14-959-70C)
5. 50-ml conical centrifuge tubes (Eppendorf, catalog number: 0030122178)
6. 1.5-ml safe-lock microcentrifuge tubes (Eppendorf, catalog number: 0030120086)
7. Metal weights (stainless steel; made by a local machine shop)

Note: Before use, wash the weights at least three times with distilled water (washing with sonication for 5-10 min is preferable) and with 100% ethanol overnight, air-dry and sterilize them by baking at 180 °C for 3 h or by UV irradiation (when hurrying). It is convenient to have many metal weights of various sizes, although we usually use the 3 x 3 x 14 mm-size weights (see Figure 1M). After use, wash them three times with distilled water (and perform sonication) and with 100% ethanol overnight. Follow the above sterilization procedure for the next round of use. Avoid using detergent for washing and do not autoclave them.

8. Matrigel matrix (Corning, catalog number: 354234)

Note: Thaw a bottle of Matrigel overnight on ice. Make aliquots (0.2 ml per 1.5 ml tube) and store at -80 °C.

9. Concanavalin A (ConA; Type IV, lyophilized powder; Sigma-Aldrich, catalog number: C2010-25MG)
10. ConA stock solution (see Recipe 2)

D. Culture media

1. Hanks' balanced salt solution, no calcium, no magnesium (HCMF; Thermo Fisher Scientific, catalog number: 14170112)
2. Dulbecco's modified Eagle's medium (DMEM), high glucose (Thermo Fisher Scientific, catalog number: 11965092)
3. L-Glutamine, 200 mM solution (Thermo Fisher Scientific, catalog number: 25030081)
4. Fetal bovine serum (FBS) (Thermo Fisher Scientific, Gibco, catalog number: 10270106 or Hyclone, catalog number: SH30910.03)

Note: Heat-inactivation of FBS at 56 °C for 30 min is not essential in this culture protocol.

5. Neurobasal medium (Thermo Fisher Scientific, catalog number: 21103049)
6. B-27 supplement (50x), serum-free (Thermo Fisher Scientific, catalog number: 17504044)
7. Opti-MEM I reduced serum medium (Thermo Fisher Scientific, catalog number: 31985062)
8. Penicillin-streptomycin, liquid (designated Pen/Strep; used as 100x solution; 10,000 units/ml each) (Thermo Fisher Scientific, catalog number: 15140122)
9. HEPES (1 M) (Thermo Fisher Scientific, catalog number: 15630080)
10. Purified human recombinant Slit2 (option: used in our experiment; store aliquots at -80 °C)

Note: Recombinant Slit2 proteins were purified from conditioned media from HEK293 cells stably expressing human Slit2-myc (Li et al., 1999) by ion-exchange chromatography using SP Sepharose Fast Flow (GE Healthcare) (Guan et al., 2007). Control purified preparations, made from parental HEK293 cells by employing the same procedure as for Slit purification, were used for explant assays in parallel. Our detailed protocol for Slit purification is available upon

request to the authors.

11. Medium 1 (see Recipe 3)
 12. Medium 2 (see Recipe 4)
 13. Medium 3 (see Recipe 5)
- E. Materials for *ex vivo* electroporation and closed-book spinal cord explant culture
1. Glass capillaries (Narishige, catalog number: GD-1)
Note: To prepare injection pipettes, pull glass capillaries using a vertical puller and break the capillary tip with fine forceps; if possible, cut it diagonally (tip diameter: approximately 30 µm).
 2. Vertical puller (Narishige, current model: PC-100)
 3. Mouthpiece and pipette joints (for injection before electroporation, we use an apparatus available from Suisaku, Japan (model: slim tube), to which an appropriate length of silicon tube can be attached)
 4. DPBS, no calcium, no magnesium (Thermo Fisher Scientific, catalog number: 14190144)
 5. Leibovitz's L-15 (Thermo Fisher Scientific, catalog number: 11415064)
 6. Horse serum, heat-inactivated (Thermo Fisher Scientific, catalog number: 26050070)
 7. Axon tracer (EGFP/vYFP plasmid)
Note: We have compared among pCAG-EGFP (available from Nepa Gene), pCAG-vYFP (Venus), pCAG-GAP43-EGFP and pCAG-GAP43-vYFP for axon labeling. In our study, pCAG-vYFP showed the best performance in mouse spinal cords. We usually obtain midi-prep grade DNAs by using NucleoBond Xtra Midi EF kit (Macherey-Nagel). We then clean up the DNAs by conventional phenol-chloroform extraction and ethanol precipitation, and obtain a high-purity DNA stock by dissolving in sterile, endotoxin-free TE buffer at a concentration of 8-10 µg/µl. Store at -30 °C (avoid thawing/refreezing cycles of the stock too many times).
 8. Appropriate short-hairpin RNAs (shRNAs; in this paper, we used shRNA against Arf6 [shArf6] cloned in pRS shRNA vector; Origene) and control shRNA (shControl) for RNAi-mediated knockdown (the DNAs are purified as described above and dissolved at an appropriate concentration; see Kinoshita-Kawada *et al.*, 2019)
 9. 0.5-1% Fast Green (10x) (Sigma-Aldrich, catalog number: F7252)
Note: After dissolving in DPBS, sterilize by filtration (0.22 µm). Make aliquots and store them at -30 °C.
 10. Native collagen acidic solution I-AC (3 mg/ml, pH3.0) (Koken, catalog number: IAC-30)
 11. DMEM/F-12, powder (Thermo Fisher Scientific, catalog number: 12500062)
 12. 5x concentrated DMEM/F-12 medium (Recipe 6)
 13. Reconstitution buffer (used for gelatinization of collagen; see Recipe 7)
 14. Medium 4 (see Recipe 8)

F. Fixation

1. PBS (Phosphate-buffered saline) tablets (Takara, catalog number: T900)

Note: Sterility is not required, although the above DPBS can also be used.

2. PBS + 0.025% NaN₃
3. Paraformaldehyde (PFA) (Fuji film/Wako, catalog number: 162-16065)
4. 4% PFA in PBS supplemented with 10% sucrose (~0.3 M sucrose; Walter *et al.*, 1987a; for fixing cultured explants without electroporation)
Note: Prepare a stock in a concentration of 4% PFA in PBS, make aliquots (approximately 30 ml per 50 ml tube) and store at -30 °C. For use in fixation, thaw 4% PFA in PBS and add sucrose to approximately 10 %.
5. 4% PFA in PBS (for fixing cultured explants of electroporated spinal cords)

G. Immunostaining and observation

1. 24 x 60 mm No. 1 Micro cover glass (Matsunami, catalog number: C024601)
Note: This coverslip is used for mounting spinal cord explants that are electroporated and cultured.
2. Sylgard-coated dissection dishes (for preparation, see page 275 of Banker and Goslin, 1998)
3. 0.2% Triton X-100 in PBS
Note: We freshly dilute Triton X-100 (Sigma-Aldrich, catalog number: T8787) on the day of immunostaining.
4. Bovine serum albumin (BSA) (Sigma-Aldrich, catalog number: A2153)
5. Goat serum (Sigma-Aldrich, catalog number: G6767)
6. Skim milk (BD/Difco, catalog number: 232100)
7. Rabbit primary antibodies of interest (in our study, we use anti-Robo antibodies)
8. Anti-L1CAM (mouse monoclonal IgG1; clone 2C2; Abcam, catalog number: ab24345)
9. Anti-TAG-1 (mouse monoclonal IgM; clone 4D7; Developmental Studies Hybridoma Bank)
10. Alexa Fluor 647 mouse anti-β-tubulin, class III (clone TuJ1; BD, catalog number: 560394)
11. Goat anti-mouse IgG (H+L) highly cross-adsorbed secondary antibody, Alexa Fluor 555 (Thermo Fisher Scientific, catalog number: A32727)
12. Goat anti-mouse IgM (heavy chain) cross-adsorbed secondary antibody, Alexa Fluor 555 (Thermo Fisher Scientific, catalog number: A21426)
13. Goat anti-rabbit IgG (H+L) highly cross-adsorbed secondary antibody, Alexa Fluor 488 (Thermo Fisher Scientific, catalog number: A11034)
14. PermaFluor aqueous mounting medium (Thermo Fisher Scientific, catalog number: TA-030-FM)

Equipment

1. CO₂ tank
2. CO₂ incubator (ASTEC, water-jacket type)
3. CO₂ single-stage flowmeter regulator

4. Dissecting microscope (Carl Zeiss, model: Stemi 2000-C; current models: Stemi 305/508)
5. Cold light source (FOSTEC, model: DCRII)
6. Phase contrast microscope (Olympus, model: CKX31; current model: CKX53)
7. Millipore Milli-Q ultrapure water system
8. Laminar flow hood
9. 4 °C refrigerator
10. -30 °C freezer
11. -80 °C freezer
12. Electroporator (Nepa Gene, model: NEPA21)

Note: NEPA21 is a versatile electroporator, which is highly programmable and reproducible with many variables controlled and measurable.

13. Forceps-type electrodes (to electroporate mouse spinal cords, we preferably use CUY665P9-6-2-5, with the tip diameter of 2.5 mm, Nepa Gene)
Note: The shape of electrode tips remarkably affects the efficiency and pattern of gene transfer into the spinal cord.
14. Confocal laser-scanning microscope (Carl Zeiss, model: LSM780 or LSM880) or all-in-one fluorescence microscope (Keyence, model: BZ-X700)
Note: If possible, use an appropriate confocal microscope with image-tiling functions (see Figure 3A). Although laborious, montage images can also be assembled manually. In our initial studies, we used a wide-field BX61I microscope (Olympus) equipped with a CoolSNAP HQ or ES CCD camera (Roper Industries). We manually assembled images that were processed with AutoQuant X3 deconvolution software (Media Cybernetics; see Figure 3C).

Software

1. MetaMorph (version 7.7 and 7.10; Molecular Devices)
2. Photoshop CS5 Extended (Adobe)
3. Illustrator CS5 (Adobe)
4. Excel (Microsoft)
5. Prism 6 (GraphPad)

Procedure

A. Coating of coverslips and black NC filters

Notes:

- a. *Prepare in advance of experiment.*
 - b. *The following steps should be performed inside the laminar flow hood.*
1. Dilute 200 µl of Matrigel (before use, slowly thaw a tube containing aliquoted Matrigel on ice) with 2 ml of HCMF (finally, 1:10 dilution). In our experience, the diluted solution can be stored

at 4 °C for a week, but we usually use a freshly diluted stock. It is important to avoid the formation of Matrigel aggregates in the diluted solution. First, pour 2 ml of HCMF into a 15 ml tube placed on ice and wait for a while. Second, transfer approximately 900 µl of the HCMF into the 200 µl Matrigel-containing tube, immediately mix by pipetting and return the mixture to the initial 15 ml tube placed on ice. Mix well again.

2. Coat sterile, round 18 mm coverslips using the above Matrigel solution. First, transfer 120 µl of the Matrigel solution onto a 35 mm dish and then cover the solutions with a coverslip (Figure 1I). We handle the coverslips with forceps (their tips should be immersed into 70% ethanol and air-dried before use). Incubate the coverslips at 37 °C in the CO₂ incubator for 3-5 h (or more).
3. Coat black NC filter(s) with ConA. Dilute 0.5 ml of ConA (before use, slowly thaw a tube containing aliquoted ConA on ice; 2 mg/ml) into 8 ml of HCMF in a 60-mm dish (the resultant working concentration is 0.125 mg/ml). Slowly place one side of the NC filter onto 5 ml of HCMF (without ConA) in another dish. When the whole surface of the filter becomes wet, immerse it completely and transfer the filter into the ConA-containing HCMF (Figure 1I). Incubate at 37 °C in the CO₂ incubator for 3-5 h (or more).
4. After coating of the coverslips, rinse them with 2 ml of plain DMEM or Medium 3 once (residual Matrigel does not affect axon outgrowth). Place the coverslips, with the coated side up, in new dishes containing 2 ml of Medium 3. Keep them in the CO₂ incubator until use. Do not let them dry anytime.
5. After coating of the NC filter(s), wash it five times each with 8 ml of HCMF (note again that ConA is toxic). Sterilize both sides of the NC filter, in the immersed condition in HCMF, with UV irradiation in the laminar flow hood (5-10 min/side, twice) (use of a UV-sterilizing box is preferable). Keep them in the HCMF at 37 °C in the CO₂ incubator until use. Do not let it dry anytime.

Note: Too long exposure with UV can destroy ConA on the NC filter.

6. For explant-spreading, cut the coated black NC filer with a disposable scalpel to obtain narrow strips (the width of approximately 0.5-1 scale on the filter, 4-5 scales in length) (Figure 1J).

B. Dissecting out spinal cords from mouse embryos and mounting the spinal cord explants onto the NC filter

1. Preparation for dissection

Cool the dissecting medium HCMF on ice. Sterilize dissection instruments with 70% ethanol. The following procedure can be performed outside the laminar flow hood. However, to prevent contamination of explant cultures with fungi, bacteria or yeasts, use sterile solutions, sterile dissecting tools and aseptic techniques. Sterilize the dissection instruments frequently with 70% ethanol during manipulation. A caution should also be taken to exclude the inclusion of fur into the dishes, which may be a major source of contamination in the cultures.

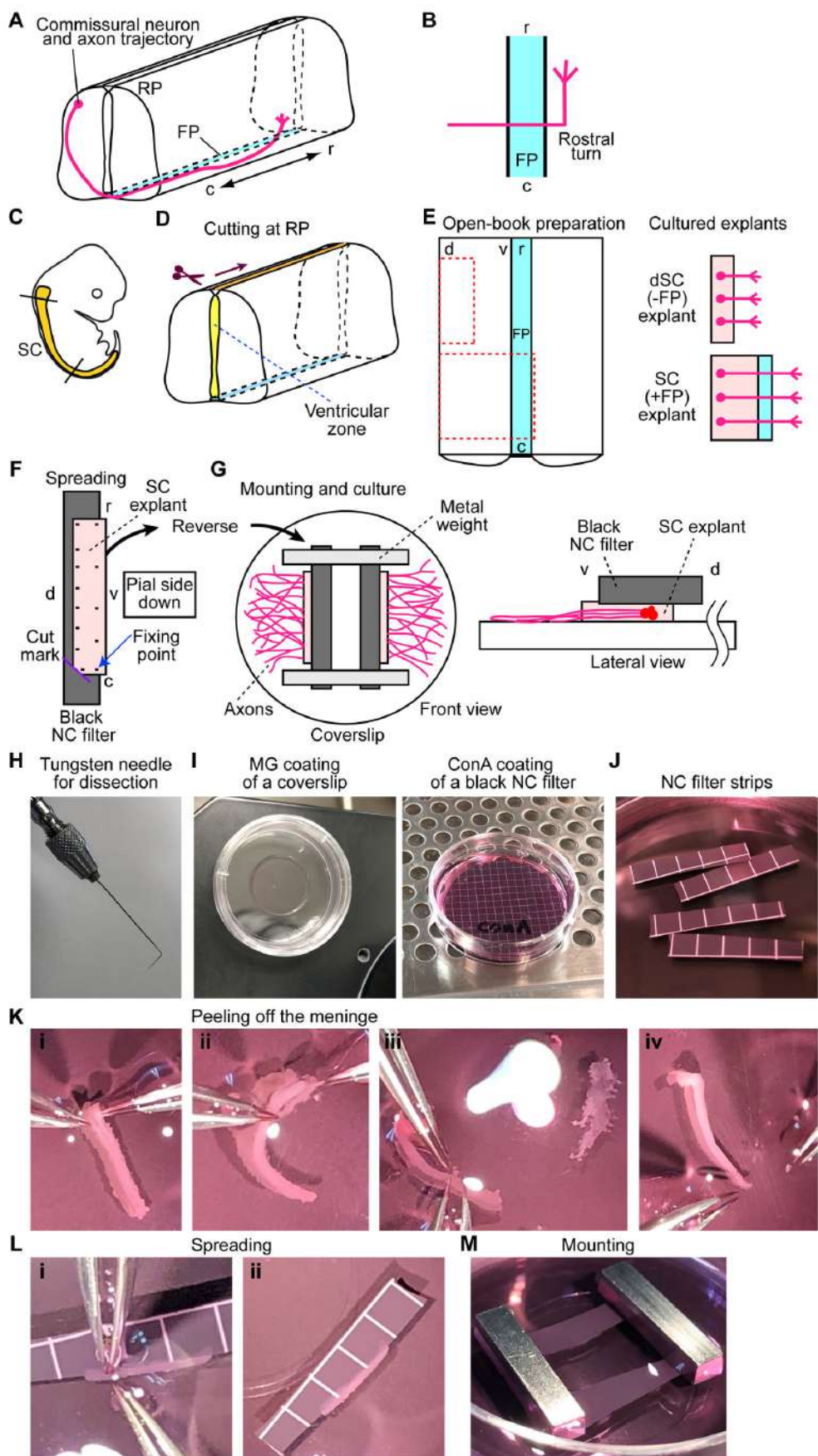


Figure 1. Procedure for spinal cord explant culture. A. The typical axon trajectory of dorsal

commissural neurons in the spinal cord. RP: roof plate; FP: floor plate; r: rostral; c: caudal. B. Dorsal view of the commissural axon trajectory. C-G. Schematic illustration of the procedure: C. Diagram of an E11.5 embryo. The spinal cord (SC) from cervical to lumbar levels is used for explant culture. D. Cutting the spinal cord at the RP. E. Cutting lines to prepare FP-lacking dorsal spinal cord [dSC (-FP)] and FP-containing spinal cord [SC (+FP)] explants. F. Spreading and nailing of spinal cord explants onto the black NC filter. d: dorsal; v: ventral. G. Mounting and culturing of spinal cord explants on the Matrigel-coated coverslip. H. Sharpened tungsten needle used in cutting the explants. I. Matrigel (MG) coating of a coverslip (left) and ConA coating of a NC filter (right). J. Strips of the ConA-coated NC filter. K. An example of peeling off the meninges from the spinal cord. i: Cutting the spinal cord at the RP to prepare an open-book preparation. ii: Peeling off the meninges from the open-book spinal cord in the rostral-to-caudal direction. iii: The meninges are now completely removed. iv: The spinal cord is ready for cutting out dSC (-FP) and SC (+FP) explants. L. An example of spreading and nailing of an explant with forceps onto the NC filter (i). The spinal cord explant fixed on the filter is ready for mounting (ii). M. Setting up and mounting two explants on the coverslip with two metal weights.

2. Removal of uterus

- a. Euthanize the pregnant mouse by CO₂ inhalation, followed by cervical dislocation. Lay the mouse on its back onto a paper towel, and wipe the abdominal area thoroughly with 70% ethanol.
- b. Using blunt forceps, grasp the skin above the genitalia, and cut the skin and then muscles with large scissors to open the entire peritoneal cavity.
- c. Remove the uteri, using forceps and medium-size scissors, and transfer them into a 100 mm dish containing ice-cold HCMF. Care should be taken so that the uteri do not touch the body surface of the mouse.
- d. To reduce the possibility of contamination, wash uteri at least once, twice if possible, by transferring them to HCMF-containing 100 mm dish(es).

3. Dissecting out embryos from the uterus

Note: The following procedure can be performed outside the laminar flow hood.

- a. Place a dish containing the uteri under a dissecting microscope (We performed all subsequent procedures under a dissecting microscope). Using two pairs of blunt No. 5 Inox forceps, tear the uterine horn of each uterus carefully and isolate the embryos from their placentas and amniotic membranes. To avoid damages of embryos, we do not separate the uterus during isolation (keep the state of “peas in a pod”). By using a spatula, transfer the embryos into new HCMF-containing dishes. Take care not to damage embryonic bodies, especially the spinal cord. Frequently wipe forceps and other tools with 70% ethanol. These procedures, from isolating embryos to mounting explants before cultivation, can be performed outside the laminar flow hood, but keep the environment and your tools clean. For isolation of E11.5 mouse embryos from the uterus, see also Elhendawi and

Davies, 2018.

- b. Check the pooled embryos, and discard those that appear damaged, malformed, abnormal, or too small and too large. By staging the embryos with the EMAP system (mentioned above), select appropriate embryos at E11.5 or earlier stages.
4. Isolation of spinal cords
 - a. Dissection should be performed as quickly as possible, and the dishes containing the remaining embryos should be kept on ice. Transfer 3-4 embryos per 60 mm HCMF-containing dish. First, remove almost all of the ventral organs from the embryo body by using two blunt No. 5 Inox forceps. At this step, we do not use scissors. We obtain the brain and spinal cords together with the surrounding tissues. Next, make an incision at the hindbrain-rostral spinal cord region by using blunt forceps. Dissect out the hindbrain and spinal cord regions from the vertebra, in the rostral-to-caudal direction. Do not peel off the meninges yet; the dorsal root ganglion (DRG) may also be attached. Using a cut pipette (cut the tip of the transfer pipettes with opening of approximately 4-5 mm), transfer the spinal cords (with the meninges) into new HCMF-containing dishes. It is better to quickly proceed to the step of mounting the spinal cords onto ConA-coated black NC filters. In our experience, the shorter period between dissecting out spinal cords and mounting them on NC filters results in better axon growth.
 - b. By using two pairs of sharpened No. 5 Inox forceps (alternatively, ophthalmic scissors), tear (or cut) the dorsal midline (roof plate [RP]) of the spinal cord that is still covered with the meninges (Figure 1D), and open up the entire length of spinal cord like a book (we usually tear the RP by grabbing the adjacent meninges, but not spinal cord proper, with forceps) (see Figure 1K). Next, peel off the meninges from the spinal cord in the rostral-to-caudal direction, by sweeping between the outer surface of spinal cords and meninges, with the forceps. As shown in Figure 1C, at this point, we obtain the spinal cords from the cervical to lumbar levels (by cutting the open-book spinal cord with forceps).
5. Preparation of spinal cord explant culture
 - a. For dSC (-FP) explants: immediately dissect out the dorsal half of the spinal cords (see the cutting lines shown in Figure 1E) with a tungsten needle (Figure 1H).
 - b. For SC (+FP) explants: immediately cut the spinal cord at the opposite edge of the FP (Figure 1E) with a tungsten needle.

Note: Do not pool open-book spinal cords or the dSC (-FP)/SC (+FP) explants. If pooled, they will become curled and very difficult to mount onto the NC filter. When one explant is ready, start the Step B5c.
 - c. We usually mark the dorso-caudal corner of the explants by cutting diagonally (Figure 1F). Using a wet pipette (it should be noted that explants can easily adhere to dry surfaces and be damaged), immediately transfer the dSC (-FP) or SC (+FP) explant into a coverslip- and Medium 3-containing dish. Spread the explant on a strip of the ConA-coated black NC filter (Figures 1F, 1J and 1L). To fix the position of the explant, nail the explant on the NC filter

by using blunt forceps, without using real “nails”, and with the pial side downward (Figure 1L (i)). For dSC (-FP) explants, an extra care not to include any piece of FP tissues into the dish should be taken. We strongly recommend mounting the spinal cord one by one, and immediately after the meninges are peeled off.

Notes:

- i. *Use un-cut pipettes for transferring the excised spinal cord explant ready for mounting. The un-cut pipettes, rather than cut pipettes, are suitable for handling small pieces of neural tissues.*
- ii. *For preparing retinal explants, researchers usually “blot” retinal tissues that are spread on the NC filter, further onto a dry filter paper, so that the retina becomes firmly attached to the NC filter (e.g., see Bonhoeffer and Huf, 1982). However, we found that this procedure does not improve axon growth in spinal cord explants and may even compromise tissue integrity. Thus, we do not perform the blotting procedure to prepare spinal cord explants.*
- d. Have two spinal cords mounted on the NC filters. Using forceps, place them in parallel on the Matrigel-coated coverslips in the Medium 3-containing 35 mm dish. Reverse the spinal cord explant-mounted filter strips, and hold them with a pair of stainless metal weights (from right above, gently place the weights to stabilize the two NC strips) (Figures 1G and 1M). Now the ventricular side of the spinal cord is contacting the Matrigel-coated surface of the coverslip. Incubate the dish at 5% CO₂ at 37 °C for 48 h. In our experiments, the cultures were treated with Slit ligand (see Materials and Reagents D.10.). Usually, we do not replace media during 48 h cultivation, before performing ligand stimulation and fixation.

Notes:

- i. *During the flipping step, do not put out the explant on the medium.*
- ii. *Although netrin-1 has been used to promote axon growth in dSC (-FP) explants (e.g., Zou et al., 2000), we do not use netrin-1, irrespective of dSC (-FP) and SC (+FP) explant cultures. Thus, we have examined effects of Slit alone on Robo1 receptor expression (Kinoshita-Kawada et al., 2019).*
- e. Examine axon outgrowth in the explant culture under a phase-contrast microscope. Much more axons should extend from the ventral side of the explants. Under the conditions used, the axonal front should reach a distance of 500 µm or more from the explant after 48 h in culture.
- f. For ligand stimulation, we usually remove the half volume (1 ml) of the culture medium and add 1 ml of the ligand-containing fresh medium. After ligand stimulation, perform fixation of the explant cultures at room temperature for 1 h, by adding 4% PFA plus 10% sucrose in PBS. Immediately before fixation, remove the metal weights carefully. Wash the fixed explants three times with PBS each for 30-60 min, and finally add PBS + 0.025% NaN₃ for storage. The explants can be subjected to immunostaining. Handle with extra care not to detach the explants from the coverslip during fixation, washing and immunostaining steps.

6. Immunostaining

We usually perform immunostaining of the cultured explants 1 day or later after fixation, which gives better results of immunostaining for Robo receptors and L1.

- a. Permeabilize the cultured explants with 0.2% Triton X-100 in PBS for 2 min at room temperature.
- b. Wash three times with PBS for 5 min each.
- c. Block the samples with blocking buffer 1 containing 3% BSA, 0.1% skim milk and 0.05% Triton X-100 in PBS for 30 min at room temperature.
- d. Incubate the explants with the primary antibodies that are diluted in blocking buffer 1 at 4 °C overnight (for approximately 18-20 h). In our experiments, we usually use anti-Robo rabbit polyclonal antibody and anti-L1 (2C2) or anti-TAG-1 (4D7).
- e. Wash three times with PBS (30-60 min each).
- f. Block the samples with blocking buffer 2 containing 3% BSA, 3% goat serum, 0.1% skim milk and 0.05% Triton X-100 in PBS for 10 min at room temperature.
- g. Incubate the explants with the secondary antibodies that are diluted in blocking buffer 2 for 2 h at room temperature. In our experiments, we used Alexa488-conjugated anti-rabbit secondary antibodies and Alexa555-conjugated anti-mouse IgG (or IgM) secondary antibodies.
- h. Wash three times with PBS (30-60 min each).
- i. Incubate the explants with Alexa647-conjugated anti-β-tubulin, class III antibody (TuJ1) that is diluted in blocking buffer 2 for 2 h at room temperature.
- j. Wash three times with PBS (30-60 min each).
- k. Mount the samples onto glass slides with PermaFluor, usually on the day of observation. The mounted samples are not well maintained for a long time. They should be photographed soon.

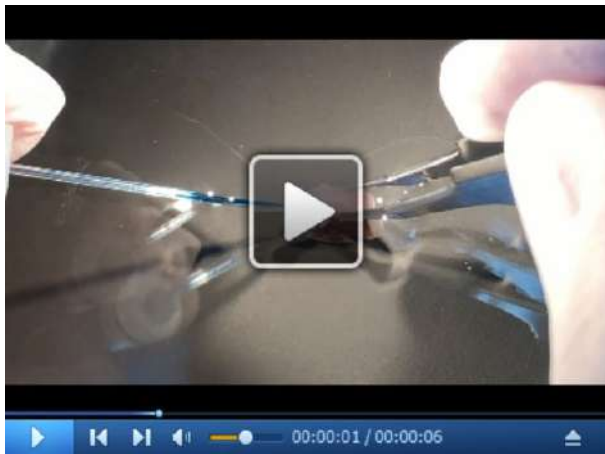
C. Ex vivo electroporation (EP) and spinal cord explant culture

The following procedure can be performed outside the laminar flow hood. Spinal cords are dissected from mouse embryos after DNA injection and EP, and are cultured as “closed-book” explants in collagen matrix at 37 °C at 5% CO₂ for 4 days (Figures 2A-2H). During this culture period, vYFP-expressing commissural axons reach, cross the ventral midline and turn longitudinally in control spinal cord preparations (Figure 2I). The effects of gene knockdown and knockout can be evaluated in terms of midline axon guidance.

1. Dissect out E11.5 mouse embryos into HCMF, as described above. Select the embryos appropriate for EP by performing accurate staging of mouse embryos.

Note: It is important that the curving morphology of the neural tube of the embryos matches the shape of the electrode. In our hands, the stages just before E11.5 are appropriate for introduction of plasmids/shRNAs to pre-crossing neurons by EP and axon midline crossing in situ. E10.5-11.0 spinal cords are difficult to electroporate efficiently and to prepare the explants

in subsequent steps, resulting in insufficient labeling of midline-crossing axons.



Video 1. Injection of an axon-tracer plasmid into the neural tube of a mouse embryo. This video shows an experiment of DNA injection into E11.5 mouse spinal cord before EP under a dissecting microscope. (This video was made at Fukuoka Univ., according to guidelines from the Fukuoka Univ. on Animal Care and approved by the Animal Research Ethics Board of Fukuoka University under protocol # 1815122.)

2. To perform *ex utero* EP, place an embryo in a new 100 mm dish containing an enough volume of cold sterile DPBS under a dissecting microscope. Manually inject spinal cords of E11.5 embryos with a solution containing shRNA constructs (2 µg/µl) and pCAG-vYFP (0.4 µg/µl) supplemented with 0.05-0.1% Fast Green and diluted in DPBS (Video 1). Immediately thereafter, electroporate embryos unilaterally with three 50-ms pulses of 20 V at 50-ms intervals (for E11.5 ICR embryos) by using the NEPA21 electroporator (Nepa Gene) and forceps-type electrodes (CUY665P9-6-2-5, Nepa Gene) (Figures 2E and 2F). Just before performing EP, sandwich the injected embryo gently between two electrodes (we set the cathode left-side and the anode right-side) and press the foot switch of the NEPA21 machine. Wait until EP is finished. Do not sandwich the embryo with the electrodes too tightly during EP. If too tightly sandwiched, the injected DNA solution will leak out, and the embryo may be damaged during EP.

Notes:

- a. *If different types of PBS are used, the actual electric conditions for EP of embryos may become dramatically different. We recommend testing several kinds of PBS for EP, in terms of gene transfer efficiency and tissue integrity. In addition, if we continue to use the same DPBS for EP of many embryos, the current flowed and electric energy tend to increase remarkably, which also affects tissue integrity. We use fresh DPBS in a new dish for every 3 embryos.*
- b. *Inject a sufficient volume of DNA solution into the cavity of the neural tube (two approaches are presented in Figure 2A), but too much volume does not increase the efficiency of gene*

transfer into the spinal cord, because the DNA tends to leak from the embryo after a blowout of the neural tube. EP pulses make the embryonic tissues, especially FP regions fragile. For getting the best results in EP, in terms of the location and efficiency of gene transfer, sufficient practice will be required. If the EP efficiency is too low even after practice, consider whether the shape of your electrodes matches the curving morphology of spinal cords of the embryos, and the electric condition of EP may have to be modified (efficient EP depends on the types of electrodes, pulse voltage, width, numbers and intervals as well as damping factors).

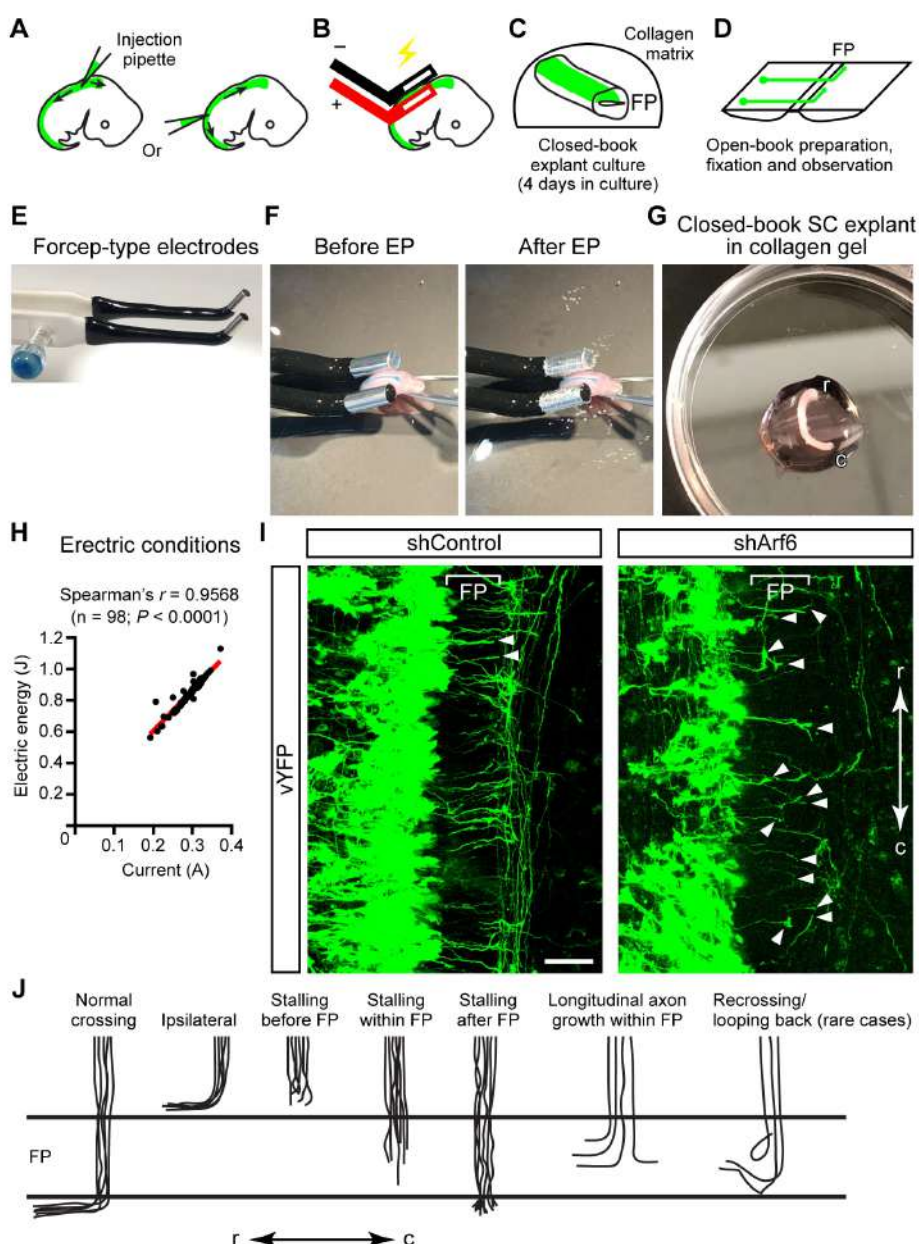


Figure 2. Ex vivo electroporation and closed-book spinal cord explant culture. A-D. Schematic illustration of ex vivo electroporation (EP) and explant culture: A. Two approaches for DNA injection. B. EP of the spinal cord region. C. Explant embedding into collagen matrix, D. Open-book preparation, fixation, and observation. E. Forceps-type electrodes. F. Spinal cord explant before and after EP. G. Closed-book SC explant in collagen gel. H. Scatter plot of Electric energy (J) vs Current (A). Spearman's $r = 0.9568$ ($n = 98$; $P < 0.0001$). I. Fluorescence microscopy images of shControl and shArf6 spinal cord explants. J. Schematic diagrams of axon growth patterns: normal crossing, ipsilateral, stalling before FP, stalling within FP, stalling after FP, longitudinal axon growth within FP, and recrossing/looping back (rare cases).

followed by 4-days culture. D. Open-book preparation and observation of axon trajectories. E. CUY665P9-6-2-5 electrodes (Nepa Gene) used for EP of spinal cords. F. An example of the EP experiment. G. An example of a spinal cord explant embedded in collagen gel, before adding the medium. r: rostral; c: caudal. H. The significant Spearman's correlation between the current and electric energy measured during EP (in case of three 50 ms pulses of 20 V at 50 ms intervals). I. Midline axon trajectories of vYFP/shRNA-coelectroporated spinal cord neurons in open-book preparations. Axons stalling within the FP (marked by brackets) or at the contralateral edge of the FP are indicated by arrowheads. shRNA-mediated Arf6 knockdown in commissural neurons causes axon stalling at the midline. Scale bar: 50 μ m. J. Summary of representative axon trajectories at the midline in shControl- and shRNA-electroporated spinal cords.

3. Immediately after EP, transfer the embryo into numbered 35 mm dishes containing L-15 media. Keep them on ice for recovery. After performing EP of each embryo, gently wipe the electrodes with 70% ethanol.

Note: We found that the tissue integrity of electroporated spinal cords is better when keeping in L-15 than in HCMF. After finishing all the EP steps, clean up the electrodes, brush them softly using a toothbrush (or a cotton swab) and toothpaste. Wash them with distilled water and finally with 70% ethanol, and let them air-dry.

4. After EP of all the embryos are finished, transfer the embryos to fresh HCMF-containing dishes and dissect out spinal cords carefully, one-by-one. When isolating the electroporated spinal cord from the embryo, we usually start dissection from the regions near the roof plate, to avoid damaging the FP. Do not remove the meninges from the spinal cord. Prepare the closed-book explant, with the meninges attached.

Note: We recover the electroporated spinal cords from the cervical to lumbar levels for explant culture. In our hands, successful vYFP expression in the spinal cord, robust axon extension toward the ventral region and axon midline crossing were observed usually from the upper-limbs to lower-limbs levels.

5. Embed each isolated spinal cord in collagen gel. Before starting embedding, have acid collagen solution, 5x concentrated medium (DMEM/F12) and reconstruction buffer, and keep them on ice. Mix 7 volumes of acid collagen solution (for example, 350 μ l/tube, in our experiments) and 2 volumes of 5x concentrated medium (DMEM/F12) (for example, 100 μ l/tube) and keep on ice until use. Just before use, add approximately 0.9-1 volume of reconstruction buffer (for example, 45 μ l/tube) to the above mixture, mix well by pipetting and if needed, adjust pH to ~7.4 by referring to the color of phenol red included in the mixture. When kept on ice or at 4 °C, the collagen mixture can be maintained in the sol state for a while. When kept at 37 °C in a CO₂ incubator, the mixture will gelatinize.

6. Place one spinal cord per 35 mm dish (we usually keep the FP the right side [Figure 2G], so that the electroplated side of the spinal cord is located upward). Cover a “closed-book”

preparation of the explant with 120 μ l of the sol-state collagen mixture and incubate in a CO₂ incubator to gelatinize collagen for 15-30 min (not too long). When the collagen has gelatinized, add 2-2.5 ml of Medium 4 to the dish slowly.

7. Culture at 37 °C for 4 days (exchange daily the half volume, ~1 ml, of the medium).
8. After 4 days of culture, dissect out spinal cords from collagen gel. Transfer them into PBS or HCMF. Remove the meninges, cut the roof plate and prepare open-book preparations. Fix the spinal cord with 4% PFA in PBS on Sylgard-coated dissection dishes for 15 min at room temperature (for this fixation step, Sylgard-coated dishes appear to be much better than usual culture dishes). Continue fixation as immersion fixation of the spinal cord at 4 °C overnight. Wash the spinal cords twice with PBS and finally replace with PBS + 0.025% NaN₃ for storage.

Notes:

- a. *When recovering the spinal cords from the gel, their appearance should be similar to those before cultivation, without remarkable swelling. If so different, consider the milder EP condition (e.g., try fewer pulses, lower voltages). Use 4% PFA in PBS without sucrose for fixation. In the presence of sucrose in the fixative, spinal cords will be floating and damaged due to surface tension.*
- b. *We do not use collagenase to recover the spinal cords from the gel.*
9. Mount the electroprorated spinal cords for observation. Transfer the open-book spinal cord explant, together with PBS, onto a 24 x 60 mm rectangular coverslip, remove most of PBS, add PermaFluor and cover the explant with another coverslip (same size) to make a sandwich. Visualize them under a confocal microscope. We acquire confocal stacks of green-channel images for visualizing vYFP signals and DIC images to show the accurate FP position. We usually observe the spinal cord explant first from the ventricular side and then from the pial side, when necessary.

Data analysis

- A. Quantification of neuronal guidance receptor expression in commissural axons extending from spinal cord explants (in our cases, we analyze the distribution of Robo receptors; see Figure 3).
 1. Take images of immunostained explants by using appropriate tiling functions on a laser-scanning microscope or Keyence all-in-one fluorescence microscope. Alternatively, take images of the explant by manual-hand acquisition using a conventional confocal microscope. Obtain the merged images by assembling maximal-intensity projection images.
 2. Measure signal intensity in the individual axons (or small axon fascicles) by using MetaMorph (or ImageJ) software. We usually quantify the immunosignal intensity in the most distal part and shaft (30 μ m length) of L1-positive commissural axons, which is normalized to TuJ1 immunoreactivity (these signals reflect axon density). We usually prepare 3-8 spinal cord explants for each experimental group, thus from the same numbers of mouse embryos (one explant per embryo), and analyze more than 100 imaging fields for axons per experimental

group (30 images per explant). For statistical analysis, we perform the nonparametric Mann-Whitney test (see Kinoshita-Kawada *et al.*, 2019; Figures 1 and 4).

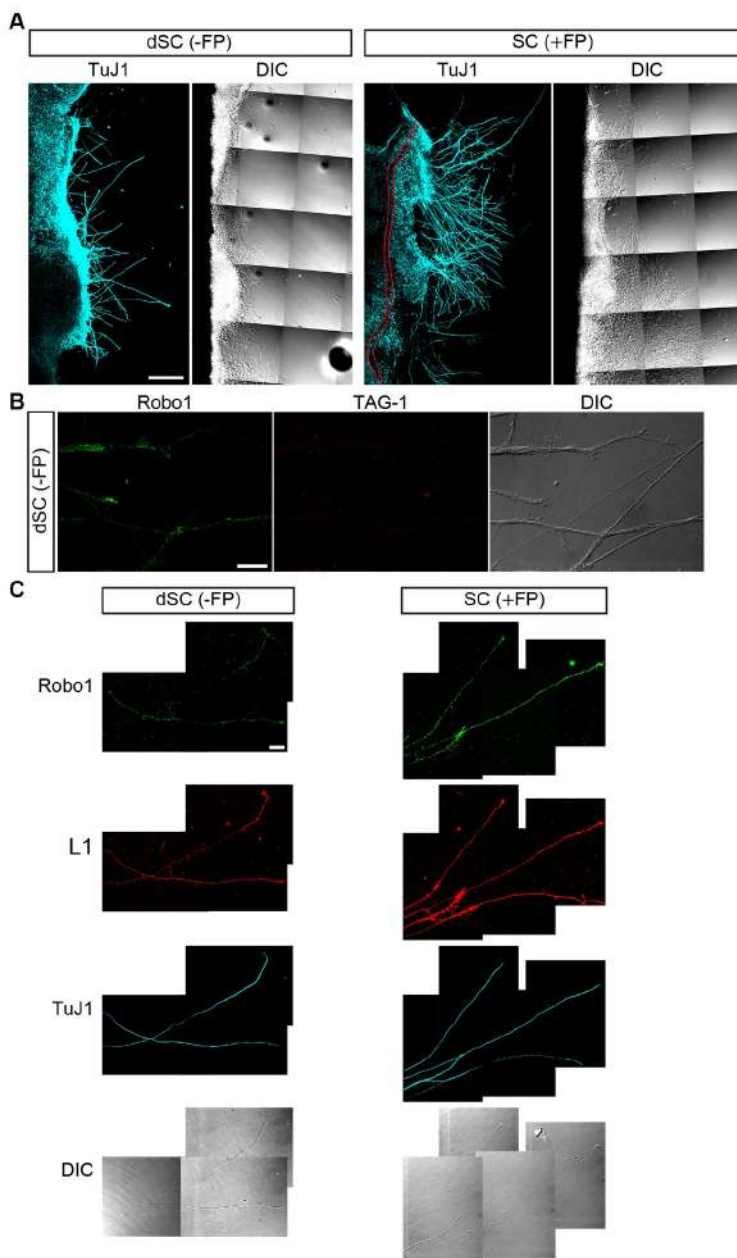


Figure 3. Immunocytochemical characterizaion of commissural axons growing from spinal cord explants. A. axon growth from dSC (-FP) and SC (+FP) explants prepared from E11.5 embryos and cultured on Matrigel-coated coverslips. The explants were immunostained for TuJ1. Differential interference contact (DIC) images are also shown. The FP is marked with red lines. B. Axons extending from dSC are positive for Robo1 but negative for TAG-1, indicating that they do not have characteristics of pre-crossing commissural axons. C. Triple immunostaining of dSC (-FP) and SC (+FP) explants for Robo1, L1 and TuJ1. Axons extending from dSC (-FP) and SC (+FP) explants are double positive for Robo1 and for L1, a

post-crossing commissural axon marker. Scale bars: 250 µm in A; 20 µm in B and C.

- B. Quantification of midline-crossing by commissural axons in electroporated and cultured spinal cord explants.
1. Mount spinal cord explants between two coverslips on the day of observation.
 2. Take images by an LSM confocal microscope (at least green and DIC channels of images should be obtained).
 3. For quantification, count the number of vYFP-positive axons that exhibited turning contralaterally (crossing) or ipsilaterally, stalling (before reaching the FP, within the FP [we include longitudinal axon growth within the FP] or after crossing the FP) or re-crossing/looping back in each imaging field, and present the data as the percentage of the total number of vYFP-positive axons (for categorization of the axon trajectories, see Figure 2J). We usually analyze the axonal trajectories in at least 4 embryos for each experimental group (tracing approximately 200-3000 labeled axons) and perform Kruskal-Wallis test with Dunn's post-hoc test for statistical analysis. In these analyses, no data for vYFP-positive axons were excluded, with exceptions of over-shooting axons (see below; see also Kinoshita-Kawada *et al.*, 2019; Figure 7). We found that axonal phenotypes in commissural neurons vary markedly along the rostrocaudal axis, even within the same embryo. Therefore, we have been analyzing values quantified in electroporated spinal cords at different rostrocaudal levels of individual embryos as distinct data points and as biological replicates.

Note: In our study, midline-overshooting phenotypes of the vYFP-labeled axons were excluded from analysis, because we detected such overshooting phenotypes in the tissue areas damaged during EP and/or manipulation, even in control-electroporated mouse embryos.

Notes

1. All experimental procedures involving animals should be approved by your institutional animal care committee.
2. When working with Matrigel or collagen, keep the original bottle and solution on ice, as much as possible, to prevent solidifying or forming aggregates, which may affect axon growth from explants.

Recipes

1. Acid washing of coverslips
 - a. Wash coverslips with enough amounts of distilled water, with sonication (if available), three times for 5 min
 - b. Wash the coverslips with 70% ethanol for 10 min and wash with distilled water for 10 min, while shaking

- c. Wash the coverslips with 1 N HCl, while occasionally shaking for more than 1 h
- d. Wash the coverslips with distilled water, while shaking, five times for 10 min, and then three times for 30 min
- e. Air-dry the coverslips on KimWipe papers

Note: Place one by one. Separate them with each other at this step. After baking, it is almost impossible to separate them.

- f. Transfer them to a 100 ml beaker and sterilize by baking at 180 °C for 3 h
2. 2 mg/ml ConA stock solution

- a. Dissolve 25 mg of ConA in 12.5 ml of HCMF
- b. Dispense 0.5 ml/1.5 ml tube and store at -80 °C

Note: We do not perform sterilization of ConA stocks by filtration. Instead, we sterilize a ConA-coated NC filter by UV irradiation on the day of experiment. Handle with care and wear a mask; do not inhale the powder because ConA is toxic.

3. Medium 1

DMEM

10% FBS

2 mM L-Glutamine

100 units/ml Pen/100 units/ml Strep

Store at 4 °C

4. Medium 2

Neurobasal + B-27

10 mM HEPES

2 mM L-Glutamine

100 units/ml Pen/100 units/ml Strep

Store at 4 °C

5. Medium 3

1:1 mixture of Medium 1 and Medium 2 (store at 4 °C)

6. 5x concentrated DMEM/F-12 medium

- a. Prepare 5x concentrated medium and add Pen/Strep, but not NaHCO₃

- b. Sterilize by filtration (0.22 µm) and store at 4 °C. This medium contains phenol red

7. Reconstitution buffer (used for gelatinization of collagen)

- a. Dissolve 0.05 N NaOH (0.2 g), 0.26 M NaHCO₃ (2.2 g) and 0.18 M HEPES (4.8 g) per 100 ml of distilled water

- b. Sterilize by filtration (0.22 µm) and store at 4 °C

8. Medium 4 (Sabatier *et al.*, 2004)

45% Opti-MEM I

50% F-12

5% Heat-inactivated horse serum

2 mM Glutamine

40 mM Glucose
100 units/ml Pen/100 units/ml Strep
Store at 4 °C

Acknowledgments

This work was supported by grants from the National Institutes of Health and the Japan Society for the Promotion of Science. We thank all of present and previous members of the Wu and Rao labs for advice, Drs. Fujio Murakami and Atsushi Tamada for generously providing anti-Robo antibodies, Dr. Chen-bing Guan for generously providing his Slit2 purification protocol, Animal/Biology Resources Sections at OIST, Yasutomo Kubota (Molecular Devices) and Nepa Gene for their valuable support. We are grateful to Dr. Hiroyuki Ichijo for introducing us retinal explant culture techniques that were originally developed by Dr. Friedrich Bonhoeffer and colleagues. Our dSC (-FP)/SC (+FP) explant culture protocols were adapted from the previously published protocols (Bonhoeffer and Huf, 1982; Halfter *et al.*, 1981 and 1983; Ichijo and Bonhoeffer, 1998; Walter *et al.*, 1987a and 1987b; Zou *et al.*, 2000). Our *ex vivo* RNAi assay system was adapted based on the previously published protocols (Parra and Zou, 2010; Wolf *et al.*, 2008). Finally, we would like to thank Dr. Zhao Chen for her kind invitation to publish our protocols here.

Competing interests

The authors have no conflicts of interest to disclose.

Ethics

All animal procedures were approved by the Institutional Animal Care and Use Committee at Northwestern University, OIST, Kyushu University and Fukuoka University.

References

1. Banker, G. and Goslin, K. (Eds.) (1998). [Culturing nerve cells](#). 2nd edition. The MIT Press.
2. Bonhoeffer, F. and Huf, J. (1982). [In vitro experiments on axon guidance demonstrating an anterior-posterior gradient on the tectum](#). *EMBO J* 1(4): 427-431.
3. Brose, K., Bland, K. S., Wang, K. H., Arnott, D., Henzel, W., Goodman, C. S., Tessier-Lavigne, M. and Kidd, T. (1999). [Slit proteins bind Robo receptors and have an evolutionarily conserved role in repulsive axon guidance](#). *Cell* 96(6): 795-806.
4. Dickson, B. J. and Zou, Y. (2010). [Navigating intermediate targets: the nervous system midline](#). *Cold Spring Harb Perspect Biol* 2(8): a002055.
5. Dodd, J., Morton, S. B., Karagogeos, D., Yamamoto, M. and Jessell, T. M. (1988). [Spatial](#)

- [regulation of axonal glycoprotein expression on subsets of embryonic spinal neurons.](#) *Neuron* 1(2): 105-116.
6. Dominici, C., Moreno-Bravo, J. A., Puiggros, S. R., Rappeneau, Q., Rama, N., Vieugue, P., Bernet, A., Mehlen, P. and Chedotal, A. (2017). [Floor-plate-derived netrin-1 is dispensable for commissural axon guidance.](#) *Nature* 545(7654): 350-354.
7. Ducuing, H., Gardette, T., Pignata, A., Tauszig-Delamasure, S. and Castellani, V. (2019). [Commissural axon navigation in the spinal cord: A repertoire of repulsive forces is in command.](#) *Semin Cell Dev Biol* 85: 3-12.
8. Elhendawi, M. and Davies, J. A. (2018). [Sebinger Culture: A System Optimized for Morphological Maturation and Imaging of Cultured Mouse Metanephric Primordia.](#) *Bio-protocol* 8(4): e2730.
9. Guan, C. B., Xu, H. T., Jin, M., Yuan, X. B. and Poo, M. M. (2007). [Long-range Ca²⁺ signaling from growth cone to soma mediates reversal of neuronal migration induced by slit-2.](#) *Cell* 129(2): 385-395.
10. Guan, K. L. and Rao, Y. (2003). [Signalling mechanisms mediating neuronal responses to guidance cues.](#) *Nat Rev Neurosci* 4(12): 941-956.
11. Halfter, W., Claviez, M. and Schwarz, U. (1981). [Preferential adhesion of tectal membranes to anterior embryonic chick retina neurites.](#) *Nature* 292(5818): 67-70.
12. Halfter, W., Newgreen, D. F., Sauter, J. and Schwarz, U. (1983). [Oriented axon outgrowth from avian embryonic retinae in culture.](#) *Dev Biol* 95(1): 56-64.
13. Ichijo, H. and Bonhoeffer, F. (1998). [Differential withdrawal of retinal axons induced by a secreted factor.](#) *J Neurosci* 18(13): 5008-5018.
14. Kidd, T., Bland, K. S. and Goodman, C. S. (1999). [Slit is the midline repellent for the Robo receptor in *Drosophila*.](#) *Cell* 96(6): 785-794.
15. Kinoshita-Kawada, M., Hasegawa, H., Hongu, T., Yanagi, S., Kanaho, Y., Masai, I., Mishima, T., Chen, X., Tsuboi, Y., Rao, Y., Yuasa-Kawada, J. and Wu, J. Y. (2019). [A crucial role for Arf6 in the response of commissural axons to Slit.](#) *Development* 146(3): pii: dev172106.
16. Kolodkin, A. L. and Tessier-Lavigne, M. (2011). [Mechanisms and molecules of neuronal wiring: a primer.](#) *Cold Spring Harb Perspect Biol* 3(6): a001727.
17. Li, H. S., Chen, J. H., Wu, W., Fagaly, T., Zhou, L., Yuan, W., Dupuis, S., Jiang, Z. H., Nash, W., Gick, C., Ornitz, D. M., Wu, J. Y. and Rao, Y. (1999). [Vertebrate slit, a secreted ligand for the transmembrane protein roundabout, is a repellent for olfactory bulb axons.](#) *Cell* 96(6): 807-818.
18. Mikuni, T., Nishiyama, J., Sun, Y., Kamasawa, N. and Yasuda, R. (2016). [High-throughput, high-resolution mapping of protein localization in mammalian brain by *in vivo* genome editing.](#) *Cell* 165(7): 1803-1817.
19. Moreno-Bravo, J. A., Roig Puiggros, S., Mehlen, P. and Chedotal, A. (2019). [Synergistic activity of floor-plate- and ventricular-zone-derived netrin-1 in spinal cord commissural axon guidance.](#) *Neuron* 101(4): 625-634 e3.

20. Nishiyama, J., Mikuni, T. and Yasuda, R. (2017). [Virus-mediated genome editing via homology-directed repair in mitotic and postmitotic cells in mammalian brain](#). *Neuron* 96(4): 755-768 e5.
21. Park, H., Oh, J., Shim, G., Cho, B., Chang, Y., Kim, S., Baek, S., Kim, H., Shin, J., Choi, H., Yoo, J., Kim, J., Jun, W., Lee, M., Lengner, C. J., Oh, Y. K. and Kim, J. (2019). [In vivo neuronal gene editing via CRISPR-Cas9 amphiphilic nanocomplexes alleviates deficits in mouse models of Alzheimer's disease](#). *Nat Neurosci* 22(4): 524-528.
22. Parra, L. M. and Zou, Y. (2010). [Sonic hedgehog induces response of commissural axons to Semaphorin repulsion during midline crossing](#). *Nat Neurosci* 13(1): 29-35.
23. Sabatier, C., Plump, A. S., Le, M., Brose, K., Tamada, A., Murakami, F., Lee, E. Y. and Tessier-Lavigne, M. (2004). [The divergent Robo family protein rig-1/Robo3 is a negative regulator of slit responsiveness required for midline crossing by commissural axons](#). *Cell* 117(2): 157-169.
24. Shirasaki, R., Katsumata, R. and Murakami, F. (1998). [Change in chemoattractant responsiveness of developing axons at an intermediate target](#). *Science* 279(5347): 105-107.
25. Stoeckli, E. T. (2018). [Understanding axon guidance: are we nearly there yet?](#) *Development* 145(10): pii: dev151415.
26. Stoeckli, E. T., Sonderegger, P., Pollerberg, G. E. and Landmesser, L. T. (1997). [Interference with axonin-1 and NrCAM interactions unmasks a floor-plate activity inhibitory for commissural axons](#). *Neuron* 18(2): 209-221.
27. Tessier-Lavigne, M., Placzek, M., Lumsden, A. G., Dodd, J. and Jessell, T. M. (1988). [Chemotropic guidance of developing axons in the mammalian central nervous system](#). *Nature* 336(6201): 775-778.
28. Varadarajan, S. G., Kong, J. H., Phan, K. D., Kao, T. J., Panaitof, S. C., Cardin, J., Eltzschig, H., Kania, A., Novitch, B. G. and Butler, S. J. (2017). [Netrin1 produced by neural progenitors, not floor plate cells, is required for axon guidance in the spinal cord](#). *Neuron* 94(4): 790-799 e3.
29. Walter, J., Kern-Veits, B., Huf, J., Stolze, B. and Bonhoeffer, F. (1987a). [Recognition of position-specific properties of tectal cell membranes by retinal axons *in vitro*](#). *Development* 101(4): 685-696.
30. Walter, J., Henke-Fahle, S. and Bonhoeffer, F. (1987b). [Avoidance of posterior tectal membranes by temporal retinal axons](#). *Development* 101(4): 909-913.
31. Wolf, A. M., Lyuksyutova, A. I., Fenstermaker, A. G., Shafer, B., Lo, C. G. and Zou, Y. (2008). [Phosphatidylinositol-3-kinase-atypical protein kinase C signaling is required for Wnt attraction and anterior-posterior axon guidance](#). *J Neurosci* 28(13): 3456-3467.
32. Wu, Z., Makihara, S., Yam, P. T., Teo, S., Renier, N., Balekoglu, N., Moreno-Bravo, J. A., Olsen, O., Chedotal, A., Charron, F. and Tessier-Lavigne, M. (2019). [Long-range guidance of spinal commissural axons by Netrin1 and sonic hedgehog from midline floor plate cells](#). *Neuron* 101(4): 635-647 e4.
33. Yang, T., Huang, H., Shao, Q., Yee, S., Majumder, T. and Liu, G. (2018). [miR-92 suppresses](#)

- [Robo1 translation to modulate Slit sensitivity in commissural axon guidance.](#) *Cell Rep* 24(10): 2694-2708 e6.
34. Yuasa-Kawada, J., Kinoshita-Kawada, M., Wu, G., Rao, Y. and Wu, J. Y. (2009). [Midline crossing and Slit responsiveness of commissural axons require USP33.](#) *Nat Neurosci* 12(9): 1087-1089.
35. Yuasa-Kawada, J., Suzuki, R., Kano, F., Ohkawara, T., Murata, M. and Noda, M. (2003). [Axonal morphogenesis controlled by antagonistic roles of two CRMP subtypes in microtubule organization.](#) *Eur J Neurosci* 17(11): 2329-2343.
36. Zou, Y., Stoeckli, E., Chen, H. and Tessier-Lavigne, M. (2000). [Squeezing axons out of the gray matter: a role for slit and semaphorin proteins from midline and ventral spinal cord.](#) *Cell* 102(3): 363-375.

A blue-themed promotional banner for Bio-protocol. At the top left is the Bio-protocol logo with the tagline "Improve Research Reproducibility". Below the logo, the text "Free access to ~4000 high-quality protocols" is displayed in white. A bulleted list of features follows: "Contributed by 10,000+ scientists (including Nobel Laureates)", "Validated in a primary research paper", ">91% reproducibility (survey of 2165 Bio-protocol users)", and "~1000 videos of key procedural steps". At the bottom of the banner is a blue button containing the text "Sign up at: www.bio-protocol.org".

Free access to ~4000 high-quality protocols

- Contributed by 10,000+ scientists (including Nobel Laureates)
- Validated in a primary research paper
- >91% reproducibility (survey of 2165 Bio-protocol users)
- ~1000 videos of key procedural steps

Sign up at: www.bio-protocol.org